

Computationally efficient analysis & design of optimally compact gear pairs and assessment of gear compliance

Amani, Amin

DOI

[10.4233/uuid:9b46e18b-1fa3-4517-a666-660e4a50f18e](https://doi.org/10.4233/uuid:9b46e18b-1fa3-4517-a666-660e4a50f18e)

Publication date

2016

Document Version

Final published version

Citation (APA)

Amani, A. (2016). *Computationally efficient analysis & design of optimally compact gear pairs and assessment of gear compliance*. [Dissertation (TU Delft), Delft University of Technology]. <https://doi.org/10.4233/uuid:9b46e18b-1fa3-4517-a666-660e4a50f18e>

Important note

To cite this publication, please use the final published version (if applicable). Please check the document version above.

Copyright

Other than for strictly personal use, it is not permitted to download, forward or distribute the text or part of it, without the consent of the author(s) and/or copyright holder(s), unless the work is under an open content license such as Creative Commons.

Takedown policy

Please contact us and provide details if you believe this document breaches copyrights. We will remove access to the work immediately and investigate your claim.

Computationally efficient analysis & design of optimally compact gear pairs and assessment of gear compliance

Proefschrift

ter verkrijging van de graad van doctor
aan de Technische Universiteit Delft,
op gezag van de Rector Magnificus prof.ir. K.C.A.M. Luyben;
voorzitter van het College voor Promoties,
in het openbaar te verdedigen op
dinsdag 15 november 2016 om 15:00.

door

Amin AMANI

Master of Science in Mechanical Engineering
Imam Hossein University (IHU)
geboren te Amol, Iran

This dissertation has been approved by the:

Promotors: Prof. dr. ir. C. Spitas and Prof. dr. ir. V. Spitas

Composition of the doctoral committee:

Rector Magnificus	Chairman
Prof. dr. ir. C. Spitas	Delft University of Technology, promotor
Prof. dr. ir. V. Spitas	National Technical University of Athens, promotor

Independent members:

Prof.dr.ir. K.M.B. Jansen	Industrial Design engineering Faculty, TUDelft
Prof.dr.ir. J. L. Herder	Mechanical, Maritime and Materials Engineering Faculty, TUDelft
Prof.dr.ir. M. Lech Kaminski	Mechanical, Maritime and Materials Engineering Faculty, TUDelft
Prof.dr.ir. H. G. Lemu	Stavanger University, Norway
Dr.ir. U. Lekic	Segula Technologies Nederland B.V.

ISBN: 978-94-6186-739-1

Copyright © 2016 by Amin Amani

amin.amani81@gmail.com

All rights reserved. No part of the material protected by this copy right notice maybe reproduced or utilized in any from or by any means, electronically or mechanically, including photocopying, recording or by any information storage and retrieval system, without written permission from the author.

An electronic version of this dissertation is available at

<http://repository.tudelft.nl/>

Summary

Achieving difficult goals in the design of powertrains regarding performance and reliability are more and more dependent on advanced computational models. Innovative frameworks for computational modelling make possible smart structural design (also: design of smart structures), to address simultaneously seemingly incompatible goals and objectives.

Computational models in the design of powertrains need to be improved by extra methodologies such as non-dimensional analytical formulation and multi scale modelling. These methods increase the competence of inverse engineering solutions in different aspects of the design. The best way to implement these extra needs is to design them smarter. That makes them compact and low-vibration.

Compactness in regard with efficiency, dependability and serviceability; leads us to reduce the space and increase the strength and load capacity. Design of a compact gear drive needs a high-precision modelling of gear meshing. One way to achieve the best robustness performances regarding the modelling is to minimise the clearance between gear teeth. For this purpose, structurally well-defined meshing gear needs to be studied. In geometrical point of view, the structurally well-defined model means a pair of gear without interference. The current analytical formulation for interference presents a design guideline for studying interference along the line of action only for standard gears. In the case of non-standard gear geometry, a new model has to be investigated. Interference for non-standard gears happens because of the penetration of the tip of the driven gear at the tooth root of the driving gear. The new interference model has to cover this area of penetration that occurs at the corner-to-root contact region.

Design of powertrains involving compact, high-power-density and/or high precision gear transmissions need precise computational modelling of dynamics and compliance, over numerous calculation-intensive iterations. Another main concern, with regard to low-vibration systems in particular, is how to tailor the whole stiffness of a gear pair for limiting the amount of vibration in the gear system. However, current analytical/empirical methods for calculating gear compliance become inaccurate outside of the standard geometries for which they have been derived, whereas numerical methods rely on complex finite element models, which are very resource intensive in order to be accurate.

Prediction of the vibration is the main problem for the design of low-vibration gear drives. Unpredictability and complexity of the tooth structure is large challenging to control the vibration of the gear systems. The variations in meshing gears make vibration and eventually create gear noise. This vibration could be transmitted structurally into the auto form, and other components as

sound waves. Low-vibration gear systems have to be controlled by tailoring the stiffness of the meshing gears. Modelling of the gear mesh compliance is the way to approach for the gear stiffness. Investigation in this field without considering a structurally well-defined model for a gear pair is not possible.

With regard to the interference and gear mesh compliance in this research, non-dimensionalisation methodology used to reduce the number of independent parameters and quantify the influence of design parameters of gear geometry on interference risk and the precision of gear mesh compliance.

This methodology permits the simultaneous modelling of entire families of gears and leads wider generality to the results of the numerical solutions. With the combined effect of the cutter radius and the dedendum on the clearance and the resulting tooth bending strength, the exact tooth geometry in search of stronger tooth forms has been determined.

A new high-precision generalised analytical model for interference as non-conjugate corner contact-and-penetration at the tooth root has been presented according to the relation between rack-cutter tip radius coefficient and dedendum coefficient considering the number of teeth and contact ratio for a combination of standard and non-standard gear.

This model overcame inaccuracies in previous form-circle-based analytical models and admitted simpler and faster solutions than competitive numerical simulations for interference. A guideline for the tolerance design of a gear pair has been proposed with regard to the gear design parameters and centre distance deviation for a structurally well-defined gear mesh model.

Compact tooth meshes and lower tensile bending stresses at the root have been produced by minimizing the unused radial clearance, while at the same time avoiding detrimental corner contact at the tooth root, thus leading to optimal solutions for compact gears and allowing the identification of a global optimum. The safety for optimum design of compact gear geometry has been achieved with a design tool (chart).

The analytical formula for the influence of cutter tip radius on maximum root bending stress has been used as a design guideline for the next version of standards, which is also applicable for non-standard design for involute gears. This formula could replace the calculation inside the current standards while leaving the rest of the standards unchanged improving the validity of the standards without need for excessive revision.

A generalised non-dimensional multi-parametric model (meta-model) for involute spur gear design serves to provide a complete analytical overview of the multi-parametric design space and is suitable for the fast assessment of existing designs, for implicit or explicit (direct) gear design, for extracting design guidelines, and for design optimisation. The meta-model for involute spur gear design has been used to identify and explore highly promising under-used

subspaces of the parametric design space, which are currently of significant interest to, for instance, the automotive and aerospace industries.

A versatile hybrid analytical-numerical method has been used for accurately calculating gear mesh compliance of arbitrary (including non-standard) tooth geometries which will be particularly well-suited for complex iterative tasks, such as dynamical simulation and gear design. Finite element analysis in conjunction with Saint-Venant's Principle have been used for accurate and fast numerical calculation of bending & foundational compliance. By means of cubic Hermitian interpolation, the results of the hybrid analytical-numerical method have been mapped to a multi-parametric compliance function of the instantaneous position of two mating gears along the line of action and a large array of design parameters.

The obtained compliance functions can be applied directly to gear dynamical simulations, parametric design and optimisation algorithms etc. The same functions can also provide powerful inverse solutions, which can be used for direct compliance-based gear design, for instance, to obtain optimised low-vibration powertrains.

SAMENVATTING

Het bereiken van moeilijke doelen in het ontwerp van powertrains omtrent de prestaties en betrouwbaarheid zijn meer en meer afhankelijk van geavanceerde rekenmodellen. Innovatieve kaders voor computationeel modelleren mogelijk maken slim constructief ontwerp (ook: ontwerp van slimme constructies), schijnbaar onverenigbare doelstellingen tegelijk aan te pakken.

Computationele modellen in het ontwerp van aandrijflijnen moeten worden verbeterd door extra methodieken zoals niet-dimensionale analytische formulering en multischaalmodel. Deze methoden verhogen van de competentie van inverse technische oplossingen in de verschillende aspecten van het ontwerp. De beste manier om deze extra eisen implementeren is om ze slimmer ontwerpen. Dat maakt ze compact en trillingsarm.

Compactheid in verband met efficiëntie, betrouwbaarheid en bruikbaarheid; leidt ons naar de ruimte te verminderen en de kracht en de belastbaarheid. Ontwerp van een compacte tandwiel drive heeft een hoge precisie-modellering van het vistuig meshing. Een manier om de beste prestaties robuustheid betreffende het modelleren bereiken is de speling tussen tandwiel tanden minimaliseren. Daartoe structureel goed gedefinieerde meshing tandwiel moet worden bestudeerd. In geometrische oogpunt, de structureel goed gedefinieerde model betekent een paar spullen zonder inmenging. De huidige analytische formulering voor interferentie presenteert een ontwerp van richtlijn voor het bestuderen van interferentie langs de lijn van de actie alleen voor standaard versnellingen. Bij afwijkende tandwielgeometrie, een nieuw model moet worden onderzocht. Interferentie voor niet-standaard apparatuur gebeurt omdat de penetratie van de punt van het tandwiel nummer 2 op de tandwortel van het tandwiel nummer 1. De nieuwe storingsmodel moet dit gebied dringen die betrekking optreedt bij de hoek-tot-root contact regio.

Het ontwerp van de aandrijflijnen met compacte, high-power-dichtheid en/of hoge precisie tandwieloverbrengingen nodig precieze computationeel modelleren van de dynamiek en compliance, over tal van rekenintensieve iteraties. Een andere belangrijke zorg met betrekking tot trillingsarme systemen in het bijzonder, hoe de gehele stijfheid van een tandwielpaar maat voor het beperken van de hoeveelheid trilling in het overbrengingssysteem. Echter, de huidige analytische/empirische methoden voor de berekening van versnelling naleving onnauwkeurig worden buiten de standaard geometrieën waarvoor ze zijn afgeleid, terwijl numerieke methoden rekenen op complexe eindige elementen modellen, die heel zijn resource-intensieve, om nauwkeurig te zijn. Voorspelling van de trillingen is het grootste probleem voor het ontwerp van trillingsarme tandwiel ontleent. Onvoorspelbaarheid en complexiteit van tandweefsel grote uitdaging om de trilling van het tandwiel te reguleren. De

variëaties in meshing versnellingen maken trillingen en uiteindelijk geluiden van de transmissie te maken. Deze trilling kan structureel worden overgebracht op de automatische vorm, en andere componenten zoals geluidsgolven. Trillingsarme overbrengingssysteemen moet geregeld door afstemmen van de stijfheid van de tandwielen meshing. Modellering van het vistuig maas naleving is de manier te benaderen voor de versnelling stijfheid. Onderzoek op dit gebied zonder daarbij een structureel goed gedefinieerde model voor een tandwielenpaar niet mogelijk.

Met betrekking tot de interferentie en versnelling mesh naleving in dit onderzoek, niet-dimensionalisation methode gebruikt om het aantal onafhankelijke parameters te verminderen en de invloed van het ontwerp parameters van het vistuig geometrie van interferentie risico en de precisie van het vistuig mesh naleving kwantificeren. Deze methode maakt het gelijktijdig modelleren van hele families versnellingen en leidt breder algemeenheid de resultaten van de numerieke oplossingen. Met het gecombineerde effect van de freesradius en dedendum van de klaring en de resulterende tand buigsterkte De precieze tandgeometrie op zoek sterkere tandvormen bepaald. Een nieuwe high-precision gegeneraliseerde analytisch model voor interferentie als niet-conjugaat hoek contact-en-penetratie in de tandwortel is gepresenteerd op basis van de relatie tussen rack-cutter tip radius coëfficiënt en dedendum coëfficiënt gezien het aantal tanden en contact ratio voor een combinatie van standaard en niet-standaard uitrusting. Dit model overwon onnauwkeurigheden in voorgaande form-circle-gebaseerde analytische modellen en toegelaten eenvoudiger en sneller dan concurrerende oplossingen numerieke simulaties voor interferentie. Een richtlijn voor de tolerantie ontwerp van een versnelling pair is voorgesteld met betrekking tot het ontwerp van het vistuig parameters en het centrum afstand afwijking voor een structureel goed gedefinieerde tandwiel mesh model. Compact tand mazen en onderste buigtrekspanningen de oorzaak zijn geproduceerd door het minimaliseren van de ongebruikte radiale speling, terwijl het vermijden van nadelige hoek contact aan de tandwortel, hetgeen leidt tot een optimale keuze van compact tandwielen en waardoor de identificatie van een globale optimum. De veiligheid voor de optimale vormgeving van compacte tandwiel geometrie is bereikt met een design tool (grafiek). De analytische formule voor de invloed van snijtip radius maximale buigspanning wortel is gebruikt als een ontwerp richtlijn voor de volgende versie van standaarden, die van toepassing voor niet-standaard ontwerp voor spiraalvormige tandwielen is. Deze formule kan worden vervangen door de berekening in de huidige normen terwijl de rest van de standaarden onveranderd verbetering van de geldigheid van de normen zonder dat overmatige herzien. Een algemene dimensieloze multi-parametrisch model (metamodel) voor evolvente tandwiel ontwerp gepresenteerd een volledig analytisch overzicht van de multi-parametrisch ontwerpruimte te bieden en is geschikt voor het snel beoordelen van bestaande

ontwerpen voor impliciete of expliciete (rechtstreekse) ontwerp van het vistuig, voor de extractie van ontwerprichtlijnen, en voor het ontwerp optimalisatie. De meta-model voor evolvente tandwiel ontwerp is gebruikt om veelbelovende onderbenut deelruimten van het parametrisch ontwerpen ruimte, die op dit moment van groot belang zijn dat wil zeggen de automobiel- en luchtvaartindustrie te identificeren en te verkennen. Een veelzijdige hybride analytische-numerieke methode is gebruikt voor het nauwkeurig berekenen tandwielschade naleving van willekeurige (met inbegrip van niet-standaard) tand geometrieën die bijzonder goed geschikt voor complexe iteratieve taken, zoals dynamische simulatie en ontwerp van het vistuig zal zijn. Eindige elementen analyse in combinatie met Saint-Venant het principe zijn gebruikt voor nauwkeurige en snelle numerieke berekening van buigen en fundamentele compliance. Via hermitische kubieke interpolatie zijn de resultaten van de hybride analytische-numerieke methode toegewezen aan een multi-parametrische compliance functie van de momentane positie van twee paren tandwielen langs de werklijn en een groot scala aan ontwerpparameters. De verkregen naleving functies kunnen direct naar versnelling dynamische simulaties, parametrisch ontwerpen en optimalisatie algoritmes etc. Dezelfde functies kunnen ook zorgen voor een krachtige inverse oplossingen, die kunnen worden gebruikt voor direct-naleving gebaseerde ontwerp van het vistuig, dat wil zeggen te verkrijgen geoptimaliseerd trillingsarme aandrijflijnen worden toegepast.

Propositions

- 1) A new high-precision generalised analytical model for interference as non-conjugate corner contact-and-penetration at the tooth root can overcome inaccuracies in previous form-circle-based analytical models and admit simpler and faster solutions than competitive numerical simulations for interference (Chapter 4).
- 2) A guideline for stronger tooth forms (Chapter 3) and the tolerance design of a gear pair (Chapter 5) can be proposed with regard to the gear design parameters and centre distance deviation for a structurally well-defined gear mesh model, respectively.
- 3) A generalised non-dimensional multi-parametric model (meta-model) for involute spur gear design can serve to provide a complete analytical overview of the multi-parametric design space and will be suitable for the fast assessment of existing designs, for implicit or explicit (direct) gear design, for extracting design guidelines, and for design optimisation which are currently of significant interest to i.e. the automotive and aerospace industries (Chapter 8).
- 4) A versatile hybrid analytical-numerical method in conjunction with cubic Hermitian interpolation can be used for accurately fast calculating of direct gear mesh compliance of tooth geometries which will be applied directly to gear dynamical simulations, parametric design and optimisation algorithms etc. The same functions can also provide powerful inverse solutions, which can be used for direct compliance-based gear design, i.e. to obtain optimised low-vibration powertrains (Chapter 9).
- 5) The complexity and unpredictability of gear geometries can be considered a 'black art'.
- 6) Mechanical gears in nature (i.e. jumping insects) are not designed; they are evolved for synchronisation in the animal world.
- 7) Non-dimensionalisation methodology which lends wider generality to the results of the numerical solutions can be used to reduce the number of independent parameters and quantify the influence of design parameters, in general.
- 8) Pretending to know is much easier than actually knowing.
- 9) Only the people who cannot use Mathematics say that it is useless.
- 10) Less interference and more compliance lead to an easier but less interesting life.

These propositions are considered opposable and defensible and as such have been approved by the Promoters: Prof. dr. ir. C. Spitas and Prof. dr. ir. V. Spitas

Contents

1- Introduction	1
1.1. Background of compact gear	1
1.1.1. Interference.....	2
1.1.2. Compliance.....	2
1.2. Objectives of the research	3
1.3. Outline of the thesis.....	4
References.....	8
2-Literature review.....	9
2.1. Interference.....	9
2.2. Gear mesh compliance.....	12
References.....	22
3- Parametric investigation of gear teeth bending strength.....	27
3.1. Introduction.....	27
3.2. Modelling.....	29
3.2.1. Gear tooth modelling	31
3.2.2. Calculation of cutter tip radius limitations.....	33
3.3. Results and discussion.....	35
3.3.1. Interference.....	36
3.3.2. Stress modelling using FEA.....	38
3.4. Conclusion	41
References.....	41
4- Multi-parametric investigation of interference	45
4.1. Introduction.....	45
4.2. State of the art models for interference	47
4.2.1. Analytical model: Form circle interference (Litvin).....	47
4.2.2. Numerical models: Interference simulation	51
4.3. Generalised corner contact-and-penetration model of interference...	53
4.3.1. Corner contact and penetration.....	53
4.3.2. Negative backlash and tooth seizure	59

4.4. Geometrical constraints of the model rack cutter	60
4.5. Multi-parametric tooth modelling	60
4.6. Results and discussion	62
4.6.1. Analytical results	62
4.6.2. Contact simulation	66
4.6.3. Design guidelines.....	68
4.7. Conclusion	71
References.....	71
5- Influence of centre distance deviation on the interference	73
5.1. Introduction.....	73
5.2. Geometrical constraints imposed by manufacturing process.....	75
5.3. Assembly and centre distance.....	75
5.4. Modelling of interference	76
5.5. Results and discussion.....	77
5.5.1. Multi-parametric tooth modelling	77
5.5.2. Interference limit curves	78
5.5.3. Tooth thickness limitation.....	78
5.5.4. Centre distance deviation	79
5.5.5. Implication on gear tolerancing	80
5.6. Conclusion	81
References.....	82
6-Design to maximise compactness and bending strength	85
6.1. Introduction.....	85
6.2. Modelling.....	88
6.2.1. Non-dimensional functional definition of compact gearing	88
6.2.2. Interference analysis	88
6.2.3. Undercutting analysis.....	88
6.2.4. Tooth thickness analysis.....	89
6.2.5. Non-dimensional stress analysis: Root bending.....	89
6.3. Results and discussion.....	89
6.3.1. Geometrical feasibility.....	89

6.3.2. Bending strength and standards benchmark	91
6.4. Design guidelines.....	93
6.5. Conclusion	96
References.....	96
7-Effect of cutter tip radius on the maximum root bending stress.....	101
7.1. Introduction.....	101
7.1.1 Different standards	102
7.1.2. Commercial software	102
7.1.3. Literature review	102
7.1.4. Gear parametric design with regard to the root strength	104
7.1.5. Current study.....	105
7.2. Existing models.....	105
7.3. FEA of root stress (Vs. ISO 6336).....	108
7.4. Comparison method: current approach (at HPST with FEA) and ISO 6336 Method B.....	110
7.5. Results and discussion.....	111
7.6. Design recommendation	115
7.7. Conclusion	115
Reference	116
8- Multi-parametric design model considering manufacturability and geometrical compatibility	119
8.1. Introduction.....	119
8.1.1. General framing of the problem	119
8.1.2. Manufacturability and geometrical compatibility as two considerations of gear design	124
8.1.3. Standards and computational resources for implicit and explicit/ direct gear design	129
8.1.4. Current study.....	129
8.2. Manufacturability modelling.....	130
8.2.1. Tip pointing.....	130
8.2.2. Undercutting	134
8.2.3. Tooth thickness analysis.....	136

8.2.4. Form radius analysis.....	137
8.3. Geometrical compatibility (interference) modelling.....	137
8.3.1. Pitch compatibility.....	137
8.3.2. Thickness-wise interference: Seizure	139
8.3.3. Radial interference	139
8.3.4. Corner contact and penetration.....	140
8.3.5. Addendum and dedendum analysis.....	141
8.4. Parametric couplings and synthesis of generalised model	142
8.4.1. Parametric couplings.....	142
8.4.2. Design parameters	143
8.4.3. Generalised model	147
8.5. Results and discussion.....	147
8.5.1. Multi-parametric gear design maps and limit curves	147
8.5.2. Compact and high contact ratio tooth forms.....	157
8.5.3. Implications of the choice of pressure angle	158
8.6. Conclusion	159
References.....	159
9- Engineering gear tooth compliance	168
8.1. Introduction.....	168
9.2. Non-dimensionalisation of geometry.....	172
9.3. GenEralised non-dimensional modelling of gear mesh compliance ...	173
9.3.1. Bending-Foundational Compliance	173
9.3.2. Hertzian compliance.....	178
9.4. Multi-parametric tooth modelling	181
9.5. Results and discussion.....	182
9.5.1. Model validation, sensitivity analysis and benchmarking.....	182
9.5.2. Influence of Loads on Gear Mesh Compliance.....	187
9.5.3. Influence of design parameters on gear mesh compliance	195
9.6. Cubic Hermitian interpolation (CHI).....	201
9.7. Conclusion	206
Reference	207

10- Conclusion and recommendation	212
Nomenclature.....	217
List of Figures.....	218
List of Tables.....	224
Curriculum Vitae.....	226
List of Publications.....	227

1- Introduction

1.1. BACKGROUND OF COMPACT GEAR

A normal transmission drivetrain system includes shafts, housings, bearings, and gears. Gears in particular are key, complex and dynamically self-exciting elements of these systems, with critical influences to vibration, loading, strength and efficiency of the system and therefore obvious implications in terms of design. Gears are everywhere: in watches, bicycles, domestic appliances, cars, ships, airplanes, wind turbines, factories etc. Wherever we need to transmit consistent rotational motion and/ or power definitely we need power transmission systems including gears, as they remain unparalleled in terms of combined accuracy, efficiency and power density.

Due to increasing requirements for flexible design methodologies able to use adaptively different parameters and assumptions, computational models in power transmission system design need to be improved by extra methodologies such as non-dimensional analytical formulation and multi-scale modelling (local meshing geometry/physics versus drivetrain-scale system response). These methods increase the capability of innovative non-standard (out-of-the-box) solutions in different aspects of the design. For strong, compact, efficient, vibration-free gears, the key challenge is to overcome the uncertainties imposed by a host of (chaotic and semi-chaotic) errors, external excitations and self-excitations. Ultimately, the sensitivity to each of these factors must be understood well, modelled, and then beyond-the-state-of-the-art techno-economically appealing design solutions, guidelines and architectures to minimise or eliminate such sensitivities must be formulated.

For example, compactness is closely coupled in regard with vibration, efficiency, reliability and serviceability; it leads us to reduce the space/ backlash and increase the strength and load capacity and potentially improve other performance aspects, such as dynamics (for example by reduction or elimination of chaotic contact reversal/ rattling). For instance in wind turbine the drive train as the main component of wind turbine, has a significant influence on these aforementioned parameters, with several (system-level) failures traced back to these as root causes. A similar case can be made for all high-power transmissions, but also for motion transmissions, where vibration, noise and lack of positional accuracy are a serious concern even if structural failure is not a risk. Hence the aforementioned aspects have to be taken into account specifically in the design of smart drive trains.

1.1.1. Interference

Design of a compact gear drive needs a high-precision modelling of gear meshing. Compactness requires to minimise the clearance between gear teeth, while still avoiding interference. For this purpose, structurally well-defined meshing gear models need to be studied, where 'well defined' in this context is used to signify the enabling of conjugate tooth action without interference. The prevailing analytical formulation for interference has been suggested by Litvin [1]. The solution presents a design guideline for studying interference along the line of action, but actually fails to address true meshing conditions prevailing in a host of geometries besides those of standard gears. Thus in the case of non-standard and compact gear geometry, a new model has to be developed. Interference for non-standard gears happens because of the penetration of the tip of the driven gear (gear number 2) at the tooth root of the driving gear (gear number 1). The new interference model has to cover this area of penetrating that occurs at the corner-to-root contact region.

1.1.2. Compliance

Prediction of positional accuracy and vibration is the main problem for the design of high-accuracy low-vibration gear drives. The unpredictability of the operating loads and the complexity of the tooth structure and resulting dynamic variability of the mechanical system properties presents a strong challenge to predicting (or even controlling) the instantaneous position and vibration of gear drivetrain systems. There are numerous conceivable explanations for gear vibration produced from the tooth contact strengths [2]. The transfer of the load from the driving gear to the driven gear happens across a varying number of simultaneous moving tooth contacts. The resulting changes in stiffness as well as external excitations can and do cause the direction and amplitude of the contact forces to change rapidly, producing vibration. While little can be done to alter this fundamental phenomenon, a host of solutions present themselves:

- Gear configuration design can be employed to simultaneously consider the effects of a host of parameters of the gear and drivetrain topology and geometry with the purpose of achieving desired low-vibration responses predictably and robustly. Of course, such configuration design requires to obtain a model for the prediction of gear vibration and an investigation of gear dynamics is needed.
- Low-vibration gear systems have to be controlled by tailoring the stiffness of the meshing gears. Modelling of the gear mesh compliance is the way to approach for the gear stiffness. Investigation in this field without considering a structurally well-defined model for a gear pair is not possible.

Compliance mechanisms are flexible mechanisms that transfer an input force or displacement to another point through elastic body deformation [3]. Investigations of the magnitudes of elastic tooth deformations and also their effects on gear performance have been starting for many years since 1970's. There are some advantages in studying of the elastic deformations on gear tooth

such as (1) evaluating the compliance of mating gears in high precision control systems, (2) calculating the gear mesh stiffness for dynamic analyses of compact gear systems, (3) optimising the profile modification in heavily loaded compact gears, for instance wind turbine gearing, and (4) recognising the performance of new type of gears as non-metallic gears, which nowadays are being used in manufacturing uses [4].

Two mating gears are contacting in the direction of the line of action and the displacements of the tooth happen along the line of action. The best definition of tooth compliance is the elastic deflection characteristics of an individual gear tooth. The compliance of one tooth is calculated from deflections due to bending (Bending compliance), foundation deflections (Foundation compliance) and contact deflection (Hertzian compliance).

With regard to the optimised compact gear pairs a structurally well-defined gear has to be designed and for gear mesh compliance the stiffness tailoring has to be assessed.

1.2. OBJECTIVES OF THE RESEARCH

The principal objective of this research is to provide a parametric solution for design of high precision of compliance gear mechanisms which has the ability to control the gear system. To obtain this goal we need to investigate the influence of design parameters of gear geometry on gear compliance and then finding the analytical relations between design parameters and compliance as a design tool. The main research question is how the gear compliance can be assessed by means of computationally efficient analysis and design of optimally compact gear pairs? In order to answer the research question, we performed a versatile hybrid analytical-numerical method for accurately calculating gear mesh compliance. The objectives of this thesis are as follows:

- To find a methodology which permits the simultaneous modelling of entire families of gears and lends wider generality to the results of the numerical solutions.
- To determine the exact tooth geometry in search of stronger tooth forms resulting tooth bending strength.
- To develop a new high-precision generalised analytical model for interference to admit simpler and faster solutions than competitive numerical simulations for interference.
- To propose a guideline for the tolerance design of a gear pair with regard to the gear design parameters and centre distance deviation for a structurally well-defined gear mesh model.
- To produce compact tooth meshes and lower tensile bending stresses at the tooth root leading to optimal solutions for compact gears and allowing the identification of a global optimum.

- To achieve the safety for optimum design of compact gear geometry with a design tool.
- To propose an analytical formula for the influence of cutter tip radius on maximum root bending stress as a design guideline for the next version of standards, which will be also applicable for non-standard design for involute gears.
- To develop a generalised multi-parametric model (meta-model) for involute spur gear design to provide a complete analytical overview of the multi-parametric design space and will be suitable for the fast assessment of existing designs, for implicit or explicit (direct) gear design, for extracting design guidelines, and for design optimisation.
- To find a calculation method for accurately calculating gear mesh compliance of arbitrary (including non-standard) tooth geometries which will be particularly well-suited for complex iterative tasks, such as dynamical simulation and gear design.
- To develop an accurate and fast numerical calculation of bending & foundational compliance.
- To obtain compliance functions to be applied directly to gear dynamical simulations, parametric design and optimisation algorithms etc.

1.3. OUTLINE OF THE THESIS

To address the computationally efficient analysis & design of optimally compact gear pairs and assessment of gear compliance, this thesis has been accomplished based on ten analytical and numerical research papers at TU Delft.

In this research, new formulation for interference limitation was presented according to the relation between the gear design parameters. The number of teeth and contact ratio for a combination of standard and non-standard gear were considered. Interference model was applied for a structurally well-defined gear meshing system. Non-dimensional analytical modelling was used to obtain results for entire gear families. This methodology increased the ability of the power of inverse engineering solutions in different aspects of the powertrain design. The results of interference occurrence were compared, according to formulations of gear geometry as per Litvin's known model of the theory of gearing. The modelling of tooth compliance with the combinations of analytical and numerical (FE) method were introduced. Bending, fillet-foundation and Hertzian compliance were studied. The results showed us that the design parameters and the position of two mating gears along the line of action both had influences on the total gear mesh compliance.

In particular, a comprehensive literature review with regard to the interference phenomena and gear mesh compliance was presented in Chapter 2. Different methodologies for interference and gear mesh compliance calculation with different applications were studied.

Parametric investigation of the combined effect of whole depth and cutter tip radius on tooth strength and compliance for the 20° involute gear system were presented in Chapter 3 [5]. This chapter performed a parametric investigation of the combined effect of the cutter radius and the dedendum on the clearance and the resulting tooth bending strength using analytical calculations, computerised generation and finite element simulations to determine the exact tooth geometry in search of stronger tooth forms.

Multi-parametric investigation of interference in non-standard spur gear teeth were studied in Chapter 4 [6]. This work proposed a general and fast mathematical model for calculating corner penetration at the tooth root, which is applicable to both analytically expressed and discretised tooth geometries. Based thereupon a non-dimensional multi-parametric investigation was carried out to quantify the effect of addendum and dedendum length, cutter tip radius, number of teeth and contact ratio on the interference risk and on this basis generalised guidelines were produced for the design of non-standard large fillet short dedendum 20° involute gears, including a method using standard cutters with indexing offsets. The present model effectively supplanted prior analytical and numerical interference models in the literature, which were proven to be limited subcases of this model.

Influence of centre distance deviation on the interference of a spur gear pair were investigated in Chapter 5 [7]. Gear design generally considers global geometry like tooth profile shape and centre distance, however it needs also to consider the tolerances introduced in the manufacturing and assembly of two mating gears. The influence of these tolerances can be predicted better by understanding the behaviour of such manufacturing and assembly errors in conjunction with the gear geometry design process. To address this, the influence of the centre distance deviation and of the design parameters (i.e. cutter tip radius, dedendum, and tooth thickness) of the tooth profiles on interference were investigated. An analytical modelling framework for interference of a gear pair was developed, which was used to characterise a structurally well-defined gear meshing system. The tolerance zone was evaluated, with regard to cutter tip radius, dedendum, tooth thickness and centre distance deviation for a structurally well-defined gear mesh model. Different gear transmission ratio, contact ratio and a pressure angle of 20° have been considered.

In Chapter 6 [8], the design of profile-generated involute gears was studied to maximise compactness and bending strength using non-standard equivalent rack dedendum and tip radius. A methodology was developed to design non-standard involute gear geometries generated by cutting tools with standard and non-standard proportions, such as to produce compact tooth meshes by minimising the unused radial clearance, while at the same time avoiding detrimental corner contact at the tooth root. It was shown under which parametric combinations of

addendum and tip radius of the equivalent rack (cutter) the feasible design solutions for different tooth numbers and transmission ratios produced lower tensile bending stresses at the root, thus leading to optimal solutions for compact gears and allowing the identification of a global optimum. The analysis led to a comprehensive mapping of the four-parametric design space in consideration of interference and undercutting and the discovered optima were compared to the design solutions found in current ISO, AGMA, GOST and JIS standards.

The effect of cutter tip radius coefficient on the maximum root bending stress of spur involute gears considering comparative evaluation of different standards was studied in Chapter 7 [9]. This chapter performed a parametric investigation of the cutter radius coefficient on the maximum bending stress at the root for spur involute gears. The approach of this chapter was to apply unitary force at the highest point of single tooth contact (HPSTC) and then calculate the stress at the root using finite element analysis (FEA). FEM results were compared with stresses calculated based on the ISO 6336-Method B. A comprehensive comparison with the popular existing gear standards such as DIN, AGMA, ANSI, JIS and GOST was performed. It was shown under which value of the cutter tip radius, the feasible design solutions for different tooth numbers and transmission ratios produced lower bending stresses at the root, consequently leading to design a stronger gear. The analysis led to the analytical relation between the cutter tip radius and maximum bending stress at the root as a function of the number of teeth (for gear 1) and gear transmission ratios, which can be used to design non-standard involute gears as well.

A generalised non-dimensional multi-parametric model for involute spur gear design was presented in Chapter 8 [10], considering manufacturability and geometrical compatibility, where the latter considered various models of interference and accounted for the combined effects of the module, pressure angle, tooth addendum, dedendum, cutter tip radius, and the numbers of teeth of a pair of mating gears. The effect of the same parameters together with tooth thickness on the manufacturability of the individual gear teeth was also modelled in terms of pointing and undercutting. The full range of parameter values, including non-standard ones, was considered. The resulting combined model served to provide a complete analytical overview of the multi-parametric design space and was suitable for the fast assessment of existing designs, for implicit or explicit (direct) gear design, for extracting design guidelines, and for design optimisation. The model can be used to identify and explore highly promising under-used subspaces of the parametric design space, which are currently of significant interest to i.e. the automotive and aerospace industries

In Chapter 9 [11-13], we developed a versatile hybrid analytical-numerical method and non-dimensional modelling framework for accurately calculating gear mesh compliance of arbitrary (including non-standard) tooth geometries

[11, 12]. Finite element analysis was used for the calculation of bending & foundational compliance in conjunction with Saint-Venant's Principle, which has been used to allow accurate and fast numerical calculation whereas Hertzian compliance was calculated analytically with high accuracy for curved elastic body contact. The influence of different combinations of cutter tip radius, dedendum, number of teeth and gear transmission ratio on gear mesh compliance was investigated. By means of cubic Hermitian interpolation, the results of the hybrid analytical-numerical method have been mapped to a multi-parametric compliance function of the instantaneous position of two mating gears along the line of action and a large array of design parameters [11, 13]. The obtained compliance functions can be applied directly to gear dynamical simulations, parametric design and optimisation algorithms etc. The same functions can also provide powerful inverse solutions, which can be used for direct compliance-based gear design, i.e. to obtain optimised low-vibration powertrains. Figure 1.1 presents the relation between the contents of this work as the relations between interference and compliance of a gear pair in order to the design of high-tech powertrains.

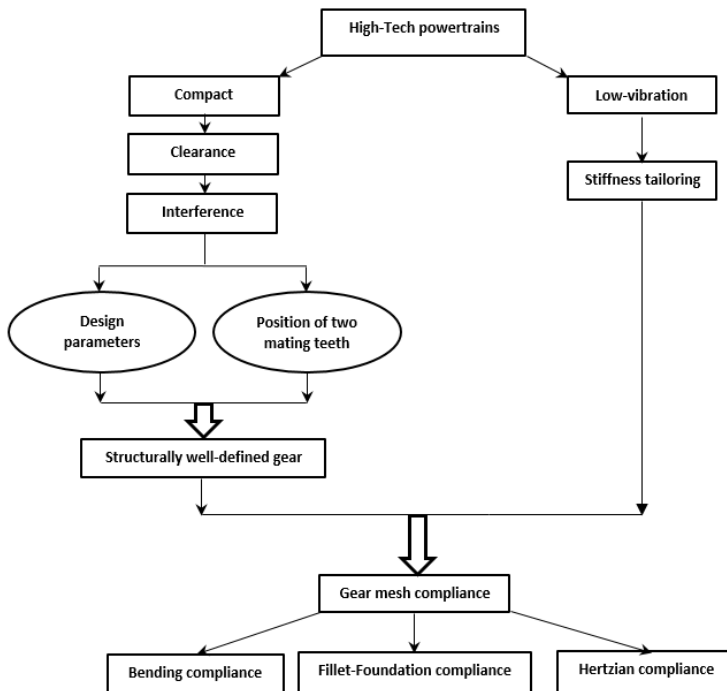


Figure 1.1: The layout of the thesis

REFERENCES

1. Litvin, F. L., 1994, Gear geometry and applied theory, *Prentice Hall*
2. Nevzat Özgüven, H., Houser, D. R., 1988, Mathematical models used in gear dynamics-A review, *Journal of Sound and Vibration*, 121(3):383-411
3. http://en.wikipedia.org/wiki/Compliant_mechanism
4. Arafa, M. H., Megahed, M. M., 1999, Evaluation of spur gear mesh compliance using the finite element method, *Proceedings of the Institution of Mechanical Engineers, Part C: Journal of Mechanical Engineering*, 213(6):569-579
5. Spitas, C., Spitas, V., Amani, A., Rajabalinejad, M., 2014, Parametric investigation of the combined effect of whole depth and cutter tip radius on tooth strength and compliance for the 20° involute gear system, *Acta Mechanica*, 225(2):361-371
6. Spitas, C., Spitas, V., Amani, A., 2015, Multi-parametric investigation of interference in non-standard spur gear teeth, *Mechanism and Machine Theory*, 88:105–124
7. Amani, A., Spitas, C., Spitas, V., Influence of centre distance deviation on the interference of a spur gear pair, *International Journal of Powertrains*, 4(4):315-337
8. Spitas, C., Spitas, V., Amani, A., 2016, Design of profile-generated involute gears to maximise compactness and bending strength using non-standard equivalent rack dedendum and tip radius, Submitted
9. Spitas, C., Spitas, V., Amani, A., 2016, Effect of cutter tip radius coefficient on the maximum bending stress of spur involute gears : comparative evaluation of different standards, Submitted
10. Amani, A., Spitas, C., Spitas, V., 2016, Generalised non-dimensional multi-parametric involute spur gear design model considering manufacturability and geometrical compatibility, Submitted
11. Amani, A., Spitas, C., 2014, Computational modelling of compact gear drives in consideration of interference and compliance, *The 10th International Conference of Computational Methods in Sciences and Engineering (ICCMSE 2014)*, Athens, Greece
12. Spitas, C., Spitas, V., Amani, A., 2016, A versatile analytical- numerical method for accurate calculation of instantaneous gear mesh compliance in real time, Submitted
13. A. Amani, C. Spitas, V. Spitas, Engineering gear tooth compliance using an interpolated multi-parametric cubic Hermitian function map based on a hybrid analytical-numerical contact mechanics model, Submitted

2-Literature review

2.1. INTERFERENCE

The probability of interference occurrence will be decreased when a small gear meshes with a large gear. In general, interference is an undesirable and unwanted property for gear meshing. Interference may result to reduce the length of the action line [1]. Moreover, even if the gears should be compliant enough to survive such an interfering without excessive wear or brakeage for a period, it is too difficult to obtain high-precision [2].

Interference weakens the gear teeth, and it is detrimental to gear meshing. There are some solutions to eliminate interference, for instance, by means of larger gear with more teeth (longer addendum for one gear and shorter for another one), interference will be resolved. Nevertheless with large gears, other problems will be unveiled, for example: increased pitch-line velocity, noise, vibration, wear, reduced power transmission. Moreover, the results of using long and short addendum for meshed gear are in non-standard and non-interchangeable gear. Because of the influences of the addendum on interference, some researcher investigated the relation between addendum modification on gear geometry and effect of the changes on interference [3-7].

Another solution is that interference can be eliminated using a generation process, but this method is not a satisfactory solution because of the effect of tooth weakening [8]. Increasing the number of teeth for small gear can be another option to solve this problem. On the other hand this solution causes to increase the gear size and pitch line velocity. In this case, designers must consider undercutting phenomena to find the optimum number of teeth. Undercutting, although not generally desirable, can indeed remove material that would cause interference. This is the reason that some researchers investigated the optimum number of teeth, to avoid interference and undercutting on gear meshing [9-11]. One of the further effects of interference on the gear is vibration. Currently, the applied methodology to fabricate gear is cutting by basic working principle in industry. This method can be introduced into two parts that are from generating and cutting method [12]. The method of generating applies the principle of shape tooth profile more than the form cutting. It can be divided into pinion cutter and rack cutter [13].

In particular, Komori et al. [14] investigated the failures due to contact of side edge and tip edge of tooth as trochoidal interference in detail: Plastic flow and wear of tooth flank of several micron meters were observe in the interference zone in dedendum. The damage was clearer near tooth root of driving gear, compared with that of driven one. On the other hand, interfering tip edge was not damaged severely. Corner rounding of tip edge softened the failure condition

due to trochoidal interference, but the effect was limited. Simulation method for contacting state of helical gear teeth with tooth form modification considering trochoidal interference was developed.

Lin et al. [15] studied the effect of extended tooth contact on the modelling of spur gear transmissions. This study compared the static transmission error and dynamic load of heavily loaded, low-contact-ratio spur gears when the effect of tooth flexibility has been considered and when it has been ignored. Neglecting the effect yielded an underestimate of resonance speeds and an overestimate of the dynamic load.

Seager [16] studied the separation of gear teeth in approach and recess, with particular reference to scoring failure. It was shown that the ideal separation might be very small over an appreciable internal beyond tip contact, and, therefore, severe corner contact, which was conducive to scoring, might occur, unless there was sufficient tip relief. The dependence of ideal separation on pressure angle and tooth pitch was investigated. Increasing the pressure angle would usually, but not always, reduce the susceptibility to corner contact: a high pressure angle was generally recommended because it was consistent also with low sliding speed and high tooth strength. Reducing the tooth pitch reduced both the tip sliding speed and the ideal separation, and, therefore, a balance should be sought in designing against scoring. The results of scoring tests should be reviewed to take into account the possible effects of corner contact. Realistic rating of gears for scoring resistance must include a measure of the severity of corner contact.

Munro et al. [17] devoted to a phenomenon known as corner contact, or contact outside the normal path of contact, which could occur in spur and helical gear transmission systems under certain conditions. In this case, a change in position of the driven gear with respect to its theoretical position took place, thus inducing a transmission error referred to here as the transmission error outside the normal path of contact. The research dealt with spur gears only, but the results were directly applicable to helical gears. It systematized previous knowledge on this subject, suggested some further developments of the theory and introduces the novel phenomenon of top contact. The theoretical results were compared with experimental measurements using a single flank tester and a back-to-back dynamic test rig for spur and helical gears, and they were in good agreement. Convenient approximate equations for calculation of transmission error suggested here were important for analysis of experimental data. This would make possible the calculation of tooth stiffness values needed for use in theoretical models for spur and helical gear transmission systems.

Eritenel et al. [18] presented an evaluation of tooth deflections and the effect of load on the backlash of these gears using a finite element program that had an accurate contact deflection analysis embedded within it. In addition to deflection analysis, the effect of tip modification on the contact regime and loads along the

edges of the plastic gears was presented. An example spur gear pair and an example helical gear pair were used to demonstrate the analysis methodology. The results of the analysis showed that backside tooth contact did not occur as tooth deflections in plastic gears increase with increasing load. In fact, the backside gap actually increased with increasing load.

It has been shown in this research that backside contact due to tooth deflections would not occur in meshing involute gear pairs. In fact, the backside gap actually increased as load was increased. The addition of tip relief also increased this backside gap. It has been also shown for these examples other derivatives of the analysis, namely, the significance of corner contact and the application of tip relief to minimize this contact.

Chen et al. [19] presented the simulation on gear backlash and interference check of harmonic drive with circular-arc teeth profile. To ensure uniqueness, geometry invariability and continuity of tooth profile expression, a representation for circular-arc tooth profile based on arc length coordinate was proposed, and Heaviside function was used to present common tangent double circular-arc tooth profile. Assembly models of harmonic drive with circular-arc tooth profile were built under different wave generators. In these models, flex spline tooth could reflect the real working state of deformed flex spline. Using coordinate transformation, meshing simulation was executed by determining the relative position of engaged teeth profile. Then, gear backlash distribution of engaged teeth profile during assembly was obtained. And interference check was carried out according to the backlash. Experimental results showed that harmonic drive with double circular-arc tooth profile had wider meshing range and uniform backlash distribution. The change of maximum radial displacement of flex spline would lead to larger influence on backlash distribution, even cause teeth profile interference.

Zhou and Chen [20] presented new modelling and calculation of impact friction caused by corner contact in gear transmission. Based on the mechanism of corner contact, the process of corner contact was divided into two stages of impact and scratch, and the calculation model including gear equivalent error-combined deformation was established along the line of action. According to the distributive law, gear equivalent error was synthesized by base pitch error, normal backlash and tooth profile modification on the line of action. The combined tooth compliance of the first point lying in corner contact before the normal path was inversed along the line of action, on basis of the theory of engagement and the curve of tooth synthetic compliance & load-history. Then the impact positions and forces, from the beginning to the end during corner contact before the normal path, were calculated accurately. Due to the aforementioned results, the backlash model during corner contact was founded, and the impact force and frictional coefficient were quantified. A numerical example was performed and the averaged impact friction coefficient based on

the presented calculation method was validated. This research obtained the results which could be referenced to understand the complex mechanism of teeth impact friction and quantitative calculation of the friction force and coefficient, and to gear exact design for tribology.

Tang et al. [21] established precise three-dimensional model of spur gear based on hob-shaving process with virtual manufacturing approach. Carried out dynamic simulation analysis based on corner contact. Obtained the dynamic stress variation rule for the gear under impact loads. The simulation results shown that the position of maximum dynamic stress at root of tooth under different conditions appeared on both sides symmetrically. The dynamic stress was bigger than the theoretic static strength under impact loads in ISO standard, and the position of maximum dynamic stress was on the higher side of the dangerous section determined according to ISO standard. The dynamic stress caused by the engaging-in impact was the maximum under different conditions, and the shorter the impact time was, the larger the dynamic stress was.

It can be concluded that each solution in interference on gear geometry has its own consequence. Sometimes giving rise to a new problem such as noise, vibration and wear is related to the other parameters in gear geometry. A new solution in gear geometry must be found, according to parametric design with some limitations. It will be able to use the new restrictions to remove interference occurrence and further problems which are related to it.

2.2. GEAR MESH COMPLIANCE

There are a very large number of studies which include only the tooth stiffness as the potential energy storing element in the system. The flexibility (torsional and/or transverse) of shafts, bearings, etc., are all neglected in these works. The basic characteristic of the models in this group is that the only compliance considered is due to the gear tooth and that all other elements are assumed to be perfectly rigid. The resulting models are either translational or torsional. Many researches have been investigated about finding the accurate compliance coefficient. One of the reasons of using compliance instead of stiffness is to simplify the calculations and modelling of gear dynamic behaviours regarding series or parallel spring in mathematical modelling of spring-mass system. Some different techniques have been investigated in the stiffness of spur gear teeth. These approaches might be categorized in three main groups such as analytical method, finite element method and experimental method [24].

Early experimental investigations on gear tooth deflection were conducted by Walker [25-26], who described an apparatus featuring a pivoted lever capable of carrying weights at one end and having at its opposite end a flat, ground and polished surface bearing against the gear tooth under investigation. Load was applied at different points along the tooth profile and the actual deflection at the

point of load application was measured with a dial indicator reading up to 0.0001 in.

A large amount of both experimental and theoretical work has been published on spur gear compliance. Weber and Banaschek [27] obtained 2D analytical expressions for the tooth compliance and have provided a basis for much of the subsequent experimental and theoretical research. The existing European gear design standards (BS, ISO, DIN) use 2D tooth compliance data based on research carried out by Winter and Podlesnik [28]. This work provides an industrial datum for gear tooth compliance.

In 1949, Weber [29] presented a theoretical investigation on spur gear tooth deformation, in which the mesh deflection of various gears mating with a rack was calculated. The tooth deformations due to bending moment, transverse shear and normal force were obtained by calculating the corresponding elastic strain energies and equating them to the work done, whereas the tooth local deflection was calculated by applying the Hertzian elastic contact theory. Weber has carried out a complete analysis about the occurrence of deflection due to bending-, direct compression-, direct shearing- of tooth and bending, shearing and direct compression of the rim material considered as an elastic deformation. Energy methods, the two-dimensional theory of elasticity for simple shape, and simple beam theory were employed to compute the various component deflections due to load.

Richardson [30] introduced compliance model for single and multiple tooth pair regarding the model of gear action to predict the contact load and significant stress that exist between mating gear teeth under operational condition to initiate careful investigation of dynamic loads.

Aida [31] presented other examples of studies in this area. He modelled the vibration characteristics of gears by considering tooth profile errors and pitch errors, and by including the variation of teeth mesh stiffness.

Chabert et al. [32] used FE method for spur gears of different ratios with 20-deg pressure angle and standard addendum proportions to evaluate stresses and strains in spur gear teeth subjected to a static load that was applied at three different points along the tooth profile.

Premilhat et al. [33] applied a complex analytic transformation method to evaluate the combined mesh stiffness characteristics of spur gears acted upon by a concentrated load. The contribution of tooth local contact deformation to overall tooth deflection was separately obtained from the Hertzian elastic contact theory.

Cornell and Westervelt [34] obtained a relationship between compliance and stress sensitivity of spur gear teeth. The variation of tooth pair compliance with position along the line of action is defined quite adequately by five term power series. The magnitude and variation of the tooth pair compliance with load position affects the dynamics and loading significantly. The tooth root stresses

along with their evaluation using tests, finite element analysis, and analytic transformation results, which indicated good agreement.

Terauchi and Nagamura [35] presented an evaluation of the deflection of spur gear teeth subjected to a distributed load based on the Hertzian contact pressure distribution resulting from contact between the tooth profiles and a straight edge.

Cornell [36] applied the materials properties in the behaviour of root stresses and tooth deformation considering the effects of bending, shear, Hertzian contact deformation and foundation flexibility. He developed analytical model for the total deflection of gear tooth at the point of load application and in the direction of load into the effects of three main components as basic, foundation and Hertzian deflection.

Coy and Chao [37] introduced the mesh size selection method for the FE analysis of gear tooth deflection based on a finite element study of two cylinders in contact including the effect of Hertzian deformations. The method has been used to calculate spur gear tooth deflection.

Vedmar [38] determined 3D gear tooth influence coefficients for use in a similar elastic model. No published work has been found reporting experimental results for a complete spur gear.

Savage et al. [39] constructed a computer model to simulate the compliance and load sharing in a spur gear mesh. The effects of deflections on mesh compliance and load sharing are investigated. The model includes deflection contributions from the bending and shears in the teeth, the Hertzian contact deformations. The model shows that rimmed gears increase mesh compliance and, in some cases, improve load sharing.

Tavakoli and Houser [40] used compliance calculation in order to find optimum profile modifications to minimize the static transmission errors of spur gears for dynamic behaviour. It has been assumed that the compliance will be aimed in three parts as:

1. Cantilever beam deflection due to both bending and shear;
2. Rigid body tooth rotation at its base; and
3. Contactor Hertzian deflection.

Choy [41] defined the variation of tooth pair compliance with position along the line of action by analytical modelling of a five-term power series for dynamic analysis of a 2240-kW (3000-hp) helicopter planetary system. The results of analytical approach compared with some experimental studies which have showed a good correlation in gear-tooth loads.

Steward [42] found the tooth contact compliance can contribute up to 30 percent towards the total contact line compliance. For a non-uniform load distribution and near the tip/root/ends of the tooth flank there is a complicated 3D contact stress field that cannot be readily modelled. The accuracy of the deflection (and root bending stress) results has been verified by applying point

loads to a spur gear. The test gear was chosen to be as large as practicable (18 mm module, 18 teeth) to give the biggest possible deflection.

Choi and David [43] studied the combined mesh stiffness characteristics of involute spur and helical gears and their transmission errors due to tooth deflections under load were evaluated. The bending and shear deflections on the contact line of a gear tooth were obtained by the finite element method (using isoparametric plate elements), and the contact deflections were obtained using Hertzian contact theory and the equation of Weber & Banaschek [27]. With these deflections, under the assumption of mathematically exact geometry, the mesh stiffness and compliance of a tooth pair were found using the so called flexibility method. Then using the mesh contact ratio and load sharing ratio, the combined mesh stiffness characteristics of a gear pair and their transmission errors due to the tooth deflections along the line of action were evaluated.

Lee et al. [44] presented a computer simulation for the dynamic response of high-contact ratio spur gear transmission. He implemented analytical approach of gear mesh stiffness with tooth profile modification for gear dynamic motion to investigate the influence of linear profile modification and loading conditions on the dynamic tooth load and stress of high-contact-ratio spur gears.

Costopoulos and Spyropoulou [45] introduced three kinds of compliance such as bending, foundational and Hertzian compliance and also developed an algorithm for the calculation of compliance of the teeth of spur gears and also for the evaluation of the load Distribution among the teeth as the gears are in mesh.

Lin and Liou [46] investigated the elastic deflection -base on Webers's investigation- in five categories as: A) bending deflection, B) shear deformation, C) axial compression, D) flexibility of the fillet and foundation, E) local contact deflection, to introduce an analytical model to measure the tooth stiffness for gear dynamics.

Vinayak and Singh [47] extended the multi-body dynamics modelling strategy for rigid gears to include compliant gear bodies in multi-mesh transmissions. Only external, fixed centre, helical or spur gears were considered. This formulation combined distributed gear mesh stiffness and gear blank compliance models in a multi-body dynamics framework resulting in a set of non-linear differential equations with time-varying coefficients. Linearization and other simplifications were applied to yield the resulting linear time-invariant equations of motion. Several solution techniques were used to determine eigensolutions and forced harmonic responses. The resulting normal mode solutions were compared to those obtained by the finite element analysis for several examples of transmission containing flexible gears. A parametric study has been performed to assess the effect of gear orientation on the dynamics of transmissions. Finally analytical predictions were compared to the results of a laboratory experiment.

Arafa and Megahed [24] used finite element modelling technique to evaluate the mesh compliance of spur gears and also load sharing between the meshing gear

teeth Contact between the engaging teeth is simulated through the use of contact elements. Results are compared with earlier predictions based on analytical, numerical and experimental methods.

Pimsarn and Kazerounian [48] introduced pseudo-interference stiffness estimation (PISE) method which is as accurate as finite element contact analysis for determination of the contact force and the equivalent mesh stiffness for geared system. This method is based on the approximation of local contact deformation to be equal to geometric interference of assumedly rigid bodies and combines the finite element analysis to analyse the singular stiffness at the contact region. The difference between the corresponding results of PISE and finite element contact model is within 8%.

Sainsot et al. [49] presented a new analytical bidimensional formula for fillet/foundation compliance analysis based on Muskhelishvili's theory applied to elastic rings. The results of this new approach shown that they are in very good agreement with the results of finite element models and can directly account integrated into gear computer codes for tooth and body-induced deflections.

Fonseca et al. [50] used mesh compliance analysis of the gear pair to develop an objective function for optimization for prediction of gear vibration. Based on a mathematical formulation for computing static transmission error and load sharing for low-contact-ratio external spur gears The GA algorithm was designed to minimize the weighted sum of the magnitudes of gear mesh frequency components.

Chaari et al. [51] presented an analytical formulation of gear compliance for modelling of pitting and crack. Their influence on the gear mesh stiffness is analysed. A planetary gear set is presented as a case study to implement the tooth fault modelling.

Zouari et al. [52] studied the effect of crack dimension and the direction of crack propagation, in the teeth foot, on the mesh stiffness using a finite element method with a three-dimensional survey. For spur gears, the mesh stiffness was affected in a meaningful manner by the presence of a foot crack of one or more teeth. This study was an attempt to estimate the effect of crack size, position, and direction on the spectrum of the gear mesh stiffness.

He et al. [53] studied gear dynamic models with time-varying mesh stiffness, viscous mesh damping, and sliding friction forces and moments. Semi-analytical single-and multi term harmonic balance methods were developed for an efficient construction of the frequency responses. First, an analytical single-degree-of-freedom, linear time-varying system model was developed for a spur gear pair in terms of the dynamic transmission error. Harmonic solutions were then derived and validated by comparing with numerical integration results. Harmonic solutions were extended to a six-degree-of-freedom system model for the prediction of (normal) mesh loads, friction forces, and pinion/gear displacements (in both line-of-action and off-line-of-action directions). Semi-analytical

predictions compared well with numerical simulations under non-resonant conditions and provided insights into the interaction between sliding friction and mesh stiffness.

Chaari et al. [54] reported how the stiffness of one tooth can be calculated from deflections by bending, fillet-foundation deflections and contact deflection and how tooth crack is effecting on this stiffness. This was important to know how these factors effect on the stiffness of one tooth. A comparison with finite element model was presented in order to validate the analytical formulation.

Wu et al. [55] presented the results of a detailed three-dimensional analysis of the torsional mesh stiffness of spur gears, through applying finite element methods were presented. In this research, tooth contact of a pair of spur gears system was analysed as body contact in a three-dimensional coordinate. The gears torsional deformation including three main components which were the body torsional deformation, tooth bending deformation and tooth surface contact deformation, the three components determined the torsional mesh stiffness of gears. The torsional mesh deformation and stiffness under different torque case were analysed in mesh. FEM were used to conduct the difference of one pair teeth and two pairs teeth torsional mesh stiffness, and the different gear torsional mesh deformation and stiffness in different contact position were analysed, it was found that the stiffness compensation exist when contrasting the two different mesh case.

Li and Kahraman [56] incorporated a gear load distribution model that considers the total gear mesh compliance caused by the Hertzian contact, tooth bending, base rotation, and shear deformation into a transient elasto-hydrodynamic lubrication model.

Meagher et al. [57] used compliance for numerical modelling of gear dynamic based on lumped parameter model. Lumped method used for quick calculation of gear stiffness. This model created based upon the modifications for torsion of the gear body and Hertzian contact. The numerical method compared with finite element modelling and rigid multi-body kinematic modelling.

Thirumurugan and Muthuveerappan [58] did a great job regarding normalised mesh compliance. They used finite element analysis to find the influence of finite-element modelling, boundary conditions, gear ratio, teeth number, module, pressure angle at pitch circle, backup ratio, generating rack cutter tip radius, and addendum modification factor on the load-sharing ratio and in turn in the maximum fillet stress on gear compliance. Through an approach based on the load-sharing ratio, that calculates the tooth load, an optimum design can be achieved. But this research couldn't be able to find the relation between all these parameters with compliance. And it means we need individual investigation for the influence of parameter design on optimised gear geometry.

Bouchaala et al. [59] applied an analytical model for gear mesh stiffness to find the equation of motion for investigation of non-linear dynamic behaviour of a

single stage spur gear. Also the influence of the Hertzian stiffness on the dynamic behaviour of the system especially in the transient regime has been investigated. Liu and Parker [60] studied the nonlinear, parametrically excited dynamics of two spur gear pairs in a two-stage counter-shaft configuration. The dynamic model included parametric excitations and contact loss of both tooth meshes with two different mesh frequencies. The time-varying mesh stiffness and nonlinear tooth separation functions were reformulated into forms suitable for perturbation analysis. The periodic steady-state solutions were obtained by the method of multiple scales and compared against a semi-analytical harmonic balance method as well as numerical integration for fundamental and subharmonic resonances for ranges of system parameters. The interaction of the two meshes was found to depend strongly on the relation of the two mesh periods. The dynamic influences of design parameters, such as shaft stiffness, mesh stiffness variations, contact ratios, and mesh phasing, were discussed. The closed-form solutions provided design guidelines in terms of the system parameters.

Liu et al. [61] presented the spur gear lubrication analysis with dynamic loads. The influence of speed on lubrication performance was investigated through its direct influence on lubrication and indirect influence by affecting dynamic loads of the gear pair. The effect of dynamic loads on film thickness, pressure distribution, and temperature field were studied. In this work, the potential energy-based method is applied to model the effective mesh stiffness analytically. The effects of Hertzian energy, bending energy, axial compressive energy, as well as shear energy are taken into account for dynamic model.

Pandya and Parey [62] revisited the technique of conventional photoelasticity to explore the possibility of using it as a supplementary technique to experimentally measure the variation of gear mesh stiffness. An attempt has been made to calculate the variation of mesh stiffness for a pinion having a cracked tooth and a gear tooth with no crack of a spur gear pair. An analytical methodology based on elastic strain energy method in conjunction with total potential energy model has been adopted and implemented within the mesh stiffness calculations. To visualize the state of stress in a structure using finite element and other currently available methods, photoelasticity was considered to be one of the oldest and most developed experimental technique. An experimental methodology based on conventional photo-elasticity technique for computing stress intensity factor for cracked spur gear tooth was presented for different single tooth contact position and crack length. The relation between contact position, crack length, crack configuration, stress intensity factor (SIF) and the variation of total effective mesh stiffness have been quantified. Finally, a comparison has been made and the results obtained from finite element method based on linear elastic fracture mechanics, analytical method and proposed experimental method has been outlined.

Chen and Shao [63] proposed a general analytical mesh stiffness model to include the effect of the gear tooth errors. This proposed model established the relationship between the gear tooth errors and the total mesh stiffness, load sharing among different tooth pairs in mesh and loaded static transmission errors (LSTE). It was suitable for not only the gear pairs with low contact ratio (LCR), but also the gear pairs with high contact ratio (HCR). Two spur gear pair models, namely one with LCR between 1 and 2 and the other one with HCR between 2 and 3, were used to demonstrate the effectiveness of the proposed mesh stiffness model. Influences of the tooth profile modification, applied torque and gear tooth root crack on the mesh stiffness, load sharing and loaded static transmission errors were also investigated.

Pandya and Parey [64] used linear elastic fracture mechanics based finite element method to perform the crack propagation path studies of high contact ratio spur gear having tooth root crack for two gear parameters namely backup ratio and pressure angle. A total potential energy model has been adopted to analytically estimate the mesh stiffness variation. The percentage change in mesh stiffness with increasing crack length was an important parameter in fault diagnosis of geared transmission. Two gear parameters as back-up ratio and pressure angle have been studied and the effect of crack length on mesh stiffness have been outlined. With the increase of deterioration level gears having lower back-up ratio fault could be detected at an early stage, similarly, chances for early fault detection was more for gears having higher pressure angle

Li et al. [65] constructed a solution for the calculation of mesh stiffness considering the sliding friction effect, and the influence of the sliding friction on mesh stiffness was analysed. Further, the analytical results indicate mesh stiffness was sensitive to the sliding friction in poorly lubricating conditions specially. These contributions would not only simplify the calculation of mesh stiffness associated with the sliding friction but also be good for assessing the dynamic behaviours of spur gear drives in some special operating conditions.

Ma et al. [66] proposed the misalignment consideration of gear root circle and base circle and accurate transition curve, an improved mesh stiffness model for a healthy gear pair and validated by the finite element method (FEM). Based on the improved method, three mesh stiffness calculation methods for cracked gear pair were presented and compared with FEM. These methods are;

1. Straight lines for crack path and limiting line;
2. Straight line for crack path and parabolic curve for limiting line; and
3. Parabolic curves for crack path and limiting line.

The results shown that there was a significant difference between method 1 and FEM under large crack condition and the results of methods 2 and 3 were quite close to FEM result, which has also showed that the parabolic curve as a limiting line was appropriate. Mesh stiffness of method 2 was very close to that of

method 3 and showed that it was acceptable to assume the crack path to be a straight line.

Raghuwanshi and Parey [67] applied photoelasticity technique for measuring the stress intensity factor (SIF) for cracked gear tooth. Subsequently SIF has been used to calculate the gear mesh stiffness. The variations in the SIF and mesh stiffness have been quantified with angular displacements of the gears. Photoelasticity experiments have been performed for different crack lengths at the tooth root of the spur gear pair. Experimental results of mesh stiffness variation were compared with one of the analytical methods for example potential energy method, which was widely used by researchers to calculate gear mesh stiffness.

Ma et al. [68] presented an improved analytical model (IAM) for the time-varying mesh stiffness (TVMS) calculation of cracked spur gears. In the improved analytical model, the calculation error of TVMS under double-tooth engagement due to repeatedly considering the stiffness of the fillet-foundation was revised, and the effects of reduction of fillet-foundation stiffness of cracked gears and extended tooth contact (ETC) were also considered, which had a great influence on TVMS, especially under the condition of large torques and crack levels. Moreover, the comparisons among the IAM, traditional analytical model (TAM) and finite element model were also carried out under different torques and crack depths. IAM was also verified by comparing TVMS and vibration responses obtained by FE model, which could be considered as a gauge to evaluate the calculation error. The results shown that the maximum error of IAM was about 12.04%, however, that of TAM could be up to 32.73%.

Li et al. [69] constructed a calculation solution of mesh stiffness of face gear drives with a spur gear, which was based on the proposed equivalent face gear teeth and Ishikawa model, and the influence of contact effects on mesh stiffness of face gear drives was investigated. The results indicated the mesh stiffness of face gear drives was sensitive to contact effects under heavy loaded operating conditions, specially.

The most powerful method for determining accurate stress and deflection information is the finite element method [70]. Although the FE method may be rather expensive to use in an everyday gear design situation, considerable research employing this technique is being performed, with research results being used to supply application factors and stress modifying factors in gear rating standards. With modern development in high speed computing, finite element analysis has been utilized to accurately and efficiently determine the gear teeth deformation and stresses. It is generally accepted by research community that in estimating the stiffness of gear teeth in mesh, finite element analysis of the contact model is more accurate than other methods. However, finite element contact modelling is computationally expensive and very difficult to model. Table 2.1 presents the summary of literature review as follow:

Table 2.1: Summary of literature review

Year	Researcher	Method			Application				
		Analytical	FE	Experimental	Elastic deformation	Stress	Dynamic/ Vibration	Lubrication	Crack
1938	Walker			*	*				
1940	Walker			*	*				
1949	Weber	*			*				
1955	Richardson	*				*	*		
1969	Aida	*					*		
1974	Chabert		*			*			
1974	Premilhat	*			*				
1981	Cornell	*				*			
1981	Terauchi	*			*	*			
1982	Coy		*		*				
1985	Vedmar	*			*				
1986	Savage	*			*				
1986	Tavakoli	*					*		
1989	Choy	*					*		
1990	Steward	*		*	*				
1990	Choi	*	*		*				
1991	Lee	*				*	*		
1994	Costopoulos	*			*				
1998	Lin	*					*		
1998	Vinayak	*	*	*			*		
1999	Arafa		*		*				
2002	Pimsarn		*		*				
2004	Sainsot	*			*				
2005	Fonseca	*					*		
2006	Chaari	*					*		
2007	Zouari		*						*
2008	He	*					*		
2009	Chaari	*					*		
2009	Wu		*		*				
2010	Li		*					*	
2010	Meagher	*					*		
2010	Thirumurugan	*				*			
2011	Bouchaala	*					*		
2012	Liu & Parker	*					*		
2013	Liu	*						*	
2013	Pandya	*		*					*
2013	Chen & Shao	*					*		*
2013	Pandya		*						*
2014	Li		*					*	
2014	Ma		*						*
2015	Raghuwanshi	*		*					*
2015	Ma	*	*						*
2015	Li	*					*		

Table 2.1 indicates that most researchers use analytical method for gear mesh compliance calculation and the dynamic/vibration is the most common application. Recently the crack propagation is going to be an interesting topic for gear researchers.

REFERENCES

1. Litvin, F. L., 1994, Gear geometry and applied theory, *Prentice Hall*
2. Spiegelberg, C., Christie, M., 2003, Torque loss in spur gears with interference, *Proceedings of the Institution of Mechanical Engineers, Part J: Journal of Engineering Tribology*, 217:385-395
3. Baglioni, S., Cianetti, F., Landi, L., 2012, Influence of the addendum modification on spur gear efficiency, *Mechanism and Machine Theory*, 49:216-233
4. Chen, T., Sun, W., Zhang, X., 2011, An analytical method to determine the addendum modification parameters of involute helical gears, *Proceedings of the Institution of Mechanical Engineers, Part C: Journal of Mechanical Engineering Science*, 225(11):2516-2524
5. Atanasiu, V., Iacob, M. R., 2010, Tooth wear effects on dynamic transmission error of spur gears with addendum modifications, *International Review of Mechanical Engineering*, 4(6):638-644
6. Li, S., 2008, Effect of addendum on contact strength, bending strength and basic performance parameters of a pair of spur gears, *Mechanism and Machine Theory*, 43(12):1557-1584
7. Spitas, C., Spitas, V., 2006, Non-linear dynamical simulation of spur gears with indexing errors and profile modifications, *Proceedings of the 25th IASTED International Conference on Modelling, Identification, and Control*, Lanzarote, Canary Islands, 354-359
8. Maitra, G. M., 2001, Handbook of gear design, *Tata McGraw-Hill Education*
9. Chen, C. F., Tsay, C. B., 2005, Tooth profile design for the manufacture of helical gear sets with small numbers of teeth, *International Journal of Machine Tools and Manufacture*, 45(12-13):531-1541
10. Guilbault, R., 2011, Tooth influence on flexural and torsional flexibility, and model tooth number prediction for optimum dynamic simulation of wide-faced spur gears, *ASME Journal of Mechanical Design*, 128(3):626-633
11. Vantsevich, V. V., 2000, Spur bevel gear differentials: Designing involute tooth numbers for the pinion and side gear, *Proc. of the Institution of Mechanical Engineers, Part D: Journal of Automobile Engineering*, 214(7), 719-730
12. Spitas, C., Spitas, V. 2006, Can non-standard involute gears of different modules mesh?, *Journal of Mechanical Engineering Science*, 220(8):1305-1313
13. Spitas, V., Costopoulos, T., Spitas C., 2007, Fast modelling of conjugate gear tooth profiles using discrete presentation by involute segments, *Mechanism and Machine Theory*, 42(6):751-762

14. Komori, M. , Kubo, A., Takahashi, T., Tanaka, T., Ichihara, Y., Takeda, K., 2004, Failures of involute gears due to contact of side edge and tip edge of tooth (4th report, failure caused by trochoidal interference due to elastic deformation of tooth) , *Journal of the Japan society of mechanical engineers*, (Chapter C), 700(70):219-225
15. Lin, H. H., Wang, J., Oswald, F. B., Coy, J. J., 1994, Effect of extended tooth contact on the modeling of spur gear transmissions, *Gear Technology*, 11(4):18-25
16. Seager, D. L., 1976, Separation of gear teeth in approach and recess, and the likelihood of corner contact, *ASLE Transactions*, 19(2):164-170
17. Munro, R. G., Morrish, L., Palmer, D., 1999, Gear transmission error outside the normal path of contact due to corner and top contact, *Proceedings of the Institution of Mechanical Engineers, Part C: Journal of Mechanical Engineering*, 213(4):319-400
18. Eritenel, T., Vijayakar, S. M., Houser, D. R., Casella, J. M., 2003, Effect of tooth deflection and corner contact on backside separation (backlash) of gear pairs, *ASME International Design Engineering Technical Conferences and Computers and Information in Engineering Conference*, DETC2003/PTG-48014:103-110
19. Chen, X.-X. , Lin, S.-Z., Xing, J.-Z., Liu, Y.-S., 2011, Simulation on gear backlash and interference check of harmonic drive with circular-arc teeth profile, *Jisuanji Jicheng Zhizao Xitong/Computer Integrated Manufacturing Systems*, 17(3):643-648
20. Zhou, C., Chen, S., 2014, Modeling and calculation of impact friction caused by corner contact in gear transmission, *Chinese Journal of Mechanical Engineering (English Edition)*, 27(5):958-964
21. Tang, J.-Y., Peng, F.-J., Huang, Y.-F., 2009, Numerical analysis of dynamic stress variation in spur gear under impact loads , *Zhendong yu Chongji/Journal of Vibration and Shock*, 28(8):138-143
22. Nevzat Özgüven, H., Houser, D. R., 1988, Mathematical models used in gear dynamics-A review, *Journal of Sound and Vibration*, 121(3):383-411
23. http://en.wikipedia.org/wiki/Compliant_mechanism
24. Arafa, M. H., Megahed, M. M., 1999, Evaluation of spur gear mesh compliance using the finite element method, *Proceedings of the Institution of Mechanical Engineers, Part C: Journal of Mechanical Engineering*, 213(6):569-579
25. Walker, H., 1938, Gear tooth deflection and profile modification, Part I., *The Engineer*, 166:409-412
26. Walker, H., 1938, Gear tooth deflection and profile modification, Part II., *The Engineer*, 166:434-436
27. Weber, C., Banascheck, K., 1950, The deformation of loaded gears and the effect on their load carrying capacity, Part5, *Sponsored Research (Germany), British Scientific and Industrial Research*, London, Report No.6.
28. Winter, H., Podlesnik, B., 1980, Quoted as reference for stiffness work for ISO 6336/DP design standard

29. Weber, C., 1949, The deformation of loaded gears and the effect on their load carrying capacity, Part I, *Sponsored Research (Germany), British Scientific and Industrial Research*, London, Report No. 3
30. Richardson, H. H., 1955, Static and dynamic load, stress and deflection cycles in spur gears system, PhD thesis, MIT
31. Aida, T., 1969, Fundamental research on gear noise and vibration, *Transaction of the Japanese Society of Mechanical Engineering*, 35:2113-2119
32. Chabert, G., Tran, T. D., Mathis, R., 1974, An evaluation of stresses and deflection of spur gear teeth under strain, *Journal of Engineering for Industry*, 96(1):85-93
33. Premilhat, A., Tordion, G. V., Baronet, C. N., 1974, An improved determination of the elastic compliance of a spur gear tooth acted on by a concentrated load, *Journal of Engineering for Industry*, 96(2):382-384
34. Cornell, R. W., Westervelt, W. W., 1978, Dynamic tooth loads and stressing for high contact ratio spur gears, *ASME Journal of Mechanical Design*, 100(1):69-76
35. Terauchi, Y., Nagamura, K., 1981, On tooth deflection calculation and profile modification of spur gear teeth, *Proceedings of International Symposium on Gearing and Power Transmission*, 2(C-27):159-164
36. Cornell, R. W., 1981, Compliance and stress sensitivity of spur gear teeth, *ASME Journal of Mechanical Design*, 103(2):447-459
37. Coy, J. J., Chao, C. H., 1982, A method of selecting grid size to account for Hertz deformation in finite element analysis of spur gears, *ASME Journal of Mechanical Design*, 104(4):759-764
38. Vedmar, L., 1985, On the Design of External Involute Helical Gears, PhD thesis, *Transactions of Machine Elements Division/Lund Technical University*, Lund, Sweden
39. Savage, M., Caldwell, R. J., Wisor, J. W., Lewicki, D. G., 1986, Gear mesh compliance modelling, *NASA technical report TM-88843*, Presented at the Rotary Wing Propulsion System Specialist's Meeting of the American Helicopter Society, Williamsburg, VA, USA.
40. Tavakoli, M. S., Houser, D. R., 1986, Optimum profile modifications for the minimization of static transmission errors of spur gears, *Journal of Mechanisms, Transmissions and Automation in Design*, 108(1):86-94
41. Choy, F. K., 1989, Experimental and analytical evaluation of dynamic load and vibration of a 2240-kw (3000-hp) rotorcraft transmission, *Journal of the Franklin Institute*, 326(5):721-735
42. Steward, J. H., 1990, The compliance of solid, wide-faced spur gears, *ASME Journal of Mechanical Design*, 112(4):590-595
43. Choi, M., David, J. W., 1990, Mesh stiffness and transmission error of spur and helical gears, *SAE Technical Papers*, ID: 901764
44. Lee, C., Oswald, F. B., Townsend, D. P., Lin, H. H., 1991, Influence of linear profile modification and loading conditions on the dynamic tooth load and stress of high-contact-ratio spur gears, *ASME Journal of Mechanical Design*, 113(4):473-480

45. Costopoulos, Th., Spyropoulou, M., 1994, Tooth compliance and load distribution of spur gears, *Modelling, Simulation & Control. B*, 54(3-4):23-30
46. Lin, H. H., Liou, C. H., 1998, A parametric study of spur gear dynamics, *NASA Technical Reports*, NASA/CR-1998-206598:1-90
47. Vinayak, H., Singh, R., 1998, Multi-body dynamics and modal analysis of compliant gear bodies, *Journal of Sound and Vibration*, 210(2):171-212
48. Pimsarn, M., Kazerounian, K., 2002, Efficient evaluation of spur gear tooth mesh load using pseudo-interference stiffness estimation method, *Mechanism and Machine Theory*, 37(8):769-786
49. Sainsot, P., Duverger, O., Velex, P., 2004, Contribution of gear body to tooth deflections-a new bidimensional analytical formula, *ASME Journal of Mechanical Design*, 126(4):748-752
50. Fonseca, D. J., Shishoo, S., Lim, T. C., Chen, D. S., 2005, A genetic algorithm approach to minimize transmission error of automotive spur gear sets, *Applied Artificial Intelligence: An International Journal*, 19(2):153-179
51. Chaari, F., Fakhfakh, T., Haddar, M., 2006, Analytical investigation on the effect of gear teeth faults on the dynamic response of a planetary gear set, *Noise & Vibration Worldwide*, 37(8):9-15
52. Zouari, S., Maatar, M., Fakhfakh, T., Haddar, M., 2007, Three-dimensional analyses by finite element method of a spur gear: Effect of cracks in the teeth foot on the mesh stiffness, *Journal of Failure Analysis and Prevention*, 7(6):475-481
53. He, S., Rook, T., Singh, R., 2008, Construction of semianalytical solutions to spur gear dynamics given periodic mesh stiffness and sliding friction functions, *ASME Journal of Mechanical Design*, 130(12):1226011-1226019
54. Chaari, F., Fakhfakh, T., Had, M., 2009, Analytical modelling of spur gear tooth crack and influence on gear mesh stiffness, *European Journal of Mechanics-A/Solids*, 28(3):461-468
55. Wu, Z., Wang, T., Zhang, R., 2009, A study of spur gear torsional mesh stiffness, *Proceedings of International Technology and Innovation Conference*, October 2009, 4 pages
56. Li, S., Kahraman, A., 2010, A transient mixed elasto-hydrodynamic lubrication model for spur gear pairs, *Journal of Tribology*, 132(1):1-9
57. Meagher, J., Wu, X., Kong, D., Lee, C. H., 2010, A comparison of gear mesh stiffness modelling strategies, *Conference Proceedings of the Society for Experimental Mechanics Series, Structural Dynamics*, 3(PART1):255-263
58. Thirumurugan, R., Muthuveerappan, G., 2010, Maximum fillet stress analysis based on load sharing in normal contact ratio spur gear drives, *Mechanics Based Design of Structures and Machines: An International Journal*, 38(2):204-226
59. Bouchaala, N., Chaari, F., Khabou, M. T., Fakhfakh, T., Haddar, M., 2011, Influence of the non-linear Hertzian stiffness on the dynamics of a spur gear system under transient regime and tooth defects, *International Journal of Vehicle Noise and Vibration*, 7(2):149-177
60. Liu, G., Parker, R. G., 2012, Nonlinear, parametrically excited dynamics of two-stage spur gear trains with mesh stiffness fluctuation, *Proceedings of the*

Institution of Mechanical Engineers, Part C: Journal of Mechanical Engineering Science,226(8):1939-1957

61. Liu, H., Mao, K., Zhu, C., Chen, S., Xu, X., Liu, M., 2013, Spur gear lubrication analysis with dynamic loads, *Tribology Transactions*, 56(1):41-48
62. Pandya, Y., Parey, A., 2013, Experimental investigation of spur gear tooth mesh stiffness in the presence of crack using photoelasticity technique, *Engineering Failure Analysis*, 34:488-500
63. Chen, Z., Shao, Y., 2013, Mesh stiffness calculation of a spur gear pair with tooth profile modification and tooth root crack, *Mechanism and Machine Theory*, 62:63-74
64. Pandya, Y., Parey, A., 2013, Crack behavior in a high contact ratio spur gear tooth and its effect on mesh stiffness, *Engineering Failure Analysis*,34:69-78
65. Li, Z., Chen, H., Chen, J., Zhu, R., 2014, Analytical impact of the sliding friction on mesh stiffness of spur gear drives based on Ishikawa model, *Vibroengineering Procedia*, 4:29-33
66. Ma, H., Song, R., Pang, X., Wen, B., 2014, Time-varying mesh stiffness calculation of cracked spur gears, *Engineering Failure Analysis*, 44:179-194
67. Raghuwanshi, N. K., Parey, A., 2015, Mesh stiffness measurement of cracked spur gear by photoelasticity technique, *Measurement: Journal of the International Measurement Confederation*,73:439-45
68. Ma, H., Pang, X., Feng, R., Zeng, J., Wen, B., 2015, Improved time-varying mesh stiffness model of cracked spur gears, *Engineering Failure Analysis*, 55:271-287
69. Li, Z., Wang, J., Zhu, R., 2015, Influence predictions of contact effects on mesh stiffness of face gear drives with spur gear, *Transactions of Nanjing University of Aeronautics and Astronautics*, 32(5):566-570
70. Rothbart, H. A.,1996, Mechanical design handbook, *McGraw-Hill*

3- Parametric investigation of gear teeth bending strength

Summary

Standard 20° spur gears are typically generated with a whole depth of 2.2 to 2.25 times the module. At the nominal centre distance, this leaves a radial clearance, which is in itself redundant from a functional point of view. However the intrinsic geometry of the cutting process always results in a non-involute root profile (the trochoid), which is even more pronounced in the case of using a rounded cutter tip in order to increase the strength of the cutting edge. Larger tip radii produce stronger tooth fillets, potentially increasing the bending strength, but reducing the involute part of the tooth. Thereby they increase the risk of interference with mating gears. This chapter performs a parametric investigation of the combined effect of the cutter radius and the dedendum on the clearance and the resulting tooth bending strength using analytical calculations, computerised generation and finite element simulations to determine the exact tooth geometry in search of stronger tooth forms. Non-dimensional modelling is used to obtain results applicable to entire gear families.

3.1. INTRODUCTION

High-power mechanical transmissions are dominated by gears and involute spur gears are widely used to transmit motion and power between parallel shafts. The main reason for the popularity of involute spur gears is their simplicity in design, ease of manufacture and maintenance, and relatively low sensitivity to errors [1]. Their design should be balanced between the required performance characteristics and their failure resistance.

The most common causes of failure in spur gears are:

a) pitting, which occurs under repeated loading in all rolling contacts [2], and can be related to the contact pressure, b) scoring, which occurs on the tooth surface due to high speeds, high tooth loading and high sliding velocities under insufficient lubrication conditions, also subject to the influence of geometrical errors [3], and c) tooth breakage, which is mainly because of excessive bending stress and it occurs either during repeated loading or due to an overload, which exceeds the gear material strength. Cracks initiate on the tensile side of the root fillet, consequently tooth breakage can be traced to the maximum tensile bending stress at the tooth fillet [4].

All of the aforementioned factors depend on tooth geometry. However, the additional typical operational requirements to reduce noise, transmission error,

wear, and backlash make more complex the selection of optimal tooth geometry. For instance, increasing the tooth whole depth to achieve higher contact ratio can reduce the load carrying capacity of individual teeth. On the other hand, for high contact ratio spur gears (above two), where one expects the load-sharing between mating teeth to compensate for this reduction [5], a small pitch error or other error could neutralise this effect, making high contact ratio designs applicable only under precise accuracy (and cost) conditions. Gear errors can in fact throw many of the known optimal solutions off-balance [4]. To overcome these problems, there are still some options available, mainly the profile modification (relief) of gear teeth. In the case of tip relief, the removal of a small amount of material near the gear tooth tip can be useful and for producing a more gradual engagement of the tooth profile, although the success of this intervention also depends on the operating conditions [6].

Due to importance of geometry in gear design, many researchers investigated its influence, especially with respect to deflection [7], bending strength [8-12], vibration [13-15] transmission error [16-19], and noise [19-20] and also a number of researchers presented the effects of some parameters in gear geometry such as pressure angle [11, 13, 21-22], addendum [18, 23-24] and module [25-26].

Tooth profiles generated with the usual cutting methods and tools contain an involute part and, near their root, a trochoidal part. The involute part of the tooth is intended for meshing with the teeth of the mating wheel whereas the trochoidal part is a by-product of the generation (cutting) process, which is neither designed nor intended for meshing. Therefore, it is essential that the trochoidal root of one tooth does not interfere with the involute tip of its mating tooth as it comes into and goes out of mesh [27].

The literature covers the geometry of the involute and trochoid quite extensively [11, 24, 28-31], while at the same time alternatives have been suggested and studied for the trochoidal form of the tooth root [31-34]. In addition, on the topic of gear geometry there are several gear standards such as ISO, DIN, AGMA, JIS [35-43], which are used widely for gear design, as production tooling is made more easily available. Among these standards similar parameters are used, but there are differences in coefficients that define the basic design. For instance, for the rack cutter proportions, each standard has its own coefficients and there are different values suggested for the same parameters, for example DIN 867.1 recommends cutter tip radius coefficient (c_c)=0.3 and dedendum coefficient (c_f)=1.25, whereas DIN 867.4 recommends c_c =0.16 and c_f =0.16 and ISO 53.A recommends c_c =0.38 and c_f =1.25 and etc. This alone seems to suggest that there is no identified standard.

In this chapter, the combined effect of the cutter radius and the dedendum on the clearance on the geometry of meshing and resulting tooth clearance is investigated for the 20° system. The results presented here were obtained for pinions with 20 teeth, which is a fairly representative number for many power

transmissions. The same method can be used to extract results for other pinion tooth numbers.

The gear forms under consideration were numerically generated and simulated to find the combinations of cutter tip radius coefficients and dedendum coefficients that do not produce interference. Then, for these valid choices of parameters, finite element analysis (FEA) was used to qualify the designs and find the strongest solutions. A map was produced of this two-parametric design space, where also the standards-compliant solutions were plotted for comparison. In order to reduce the independent geometrical parameters and make the results more generally applicable, non-dimensional modelling was used.

3.2. MODELLING

Figure 3.1 presents on a gear tooth profile two clearly identifiable regions AC and CD , which are produced by a generating method using a rack cutter (or equivalent hob cutter). Region AC is an involute produced by the straight face of the cutter, whereas region CD is a trochoid produced by the rounded tip of the cutter. Point C defines the form radius and is a function of the cutter geometry and its relative position to the workpiece. If the specific gear is made to mesh with another gear at a given centre distance, then point B is defined as the point of the profile that contacts with the tooth tip of the corresponding gear. Obviously, point B delimits the active part of the tooth profile AB , with no contact whatsoever being possible below B . The radius thus defined is termed the limit radius. The location of point B is by definition a function of the geometries of both mating gears as well as of their centre distance, in contrast to point C , which characterises each gear separately.

Functional considerations relating to involute contact demand that point B lie at or above the form radius, hence point C , so that $r_b \geq r_s$, or otherwise, depending also on the presence or not of undercutting, interference may occur resulting in impact, vibration and wear. Apparently, the limiting case where B and C are coincident presents the fullest possible use of the available involute, though in actual practice allowances must be made for manufacturing and assembly errors and tolerances, as well as dynamic deflections during operation.

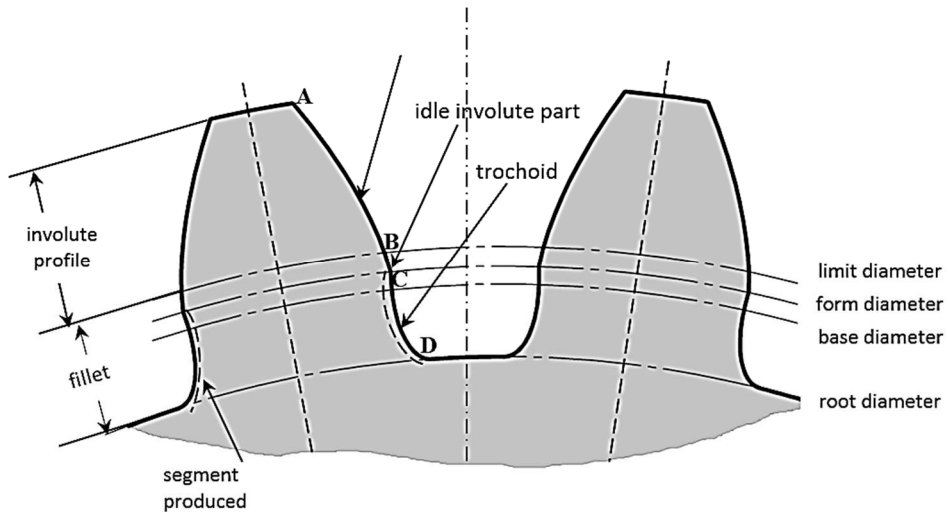


Figure 3.1: Tooth geometry and identification of different functional regions

Point *D*, lying at the inside diameter, is determined by the cutter geometry alone. The locations of points *C* and *D*, being functions of the same parameters, are therefore, interrelated. Clearly, the tooth shape, as dictated by the locations of points *C* and *D*, has a definitive influence on the maximum developed tensile stress, and therefore, on the bending strength. The following observations are relevant here as:

- 1) Increasing the cutter tip radius increases the root cross section and reduces stress concentration, therefore enhancing bending strength.

- 2) Decreasing the whole depth reduces the leverage of the forces acting on the teeth, thereby reducing the bending moments and again enhancing bending strength.

- 3) It is logical to expect that different combinations of the cutter tip radius and of the whole depth will result in different values for bending strength and stiffness, some being more advantageous than others.

- 4) Considering the limitation imposed by point *B* on the form radius (point *C*) that $r_B \geq r_s$, the cutter tip radius and the whole depth cannot be modified in complete independence of each other, as they tend to act antagonistically; in simple terms, there is no room to fit a large fillet in a small whole depth without (unacceptably) sacrificing part of the useful involute.

The analysis steps will be therefore, i) to identify acceptable combinations of the cutter tip radius and the whole depth, and ii) to evaluate and compare the bending strength of the resulting gears.

Additional methodologies employed within the above framework include a) non-dimensional modelling to increase the generality and applicability of results, b) FEA for calculating the bending stresses and hence the strength, and c) two-parametric mapping of the design space. These are examined in the following

sections.

3.2.1. Gear tooth modelling

3.2.1.1. Non-dimensionalisation

Every geometrical feature f on the transverse section of a full-scale gear tooth is connected with the corresponding feature f^* of the transverse section of the non-dimensional gear tooth through the equation:

$$f = mf^* \quad (3.1)$$

Which m is the module. Since the whole depth is simply expressed in a non-dimensional form as addendum coefficient (c_k) + dedendum coefficient (c_f), this formulation concludes the undertaken geometrical analysis. This allows the simultaneous modelling of all module families, lending wide generality to the results. Non-dimensional modelling is also expanded to stress analysis. Tooth bending stress can be calculated in non-dimensional teeth σ^* by assuming unitary tooth width $b = 1$ and unitary normal load $P_N^* = 1$. The non-dimensional stress is related to the actual bending stress σ_F using the following equation:

$$\sigma_F = \sigma_F^* \frac{P_N}{bm} \quad (3.2)$$

3.2.1.2. Establishing an analytical relationship between the cutter tip radius and the form circle radius

The generation of point \hat{C} on the tooth profile by the corresponding point on the cutter is illustrated in Figure 3.2. In those cases where both primary and secondary cuts are made (undercutting), this analysis holds for the primary cutting action; the secondary cutting action that produces the final gear tooth profile will then be studied numerically in a next step.

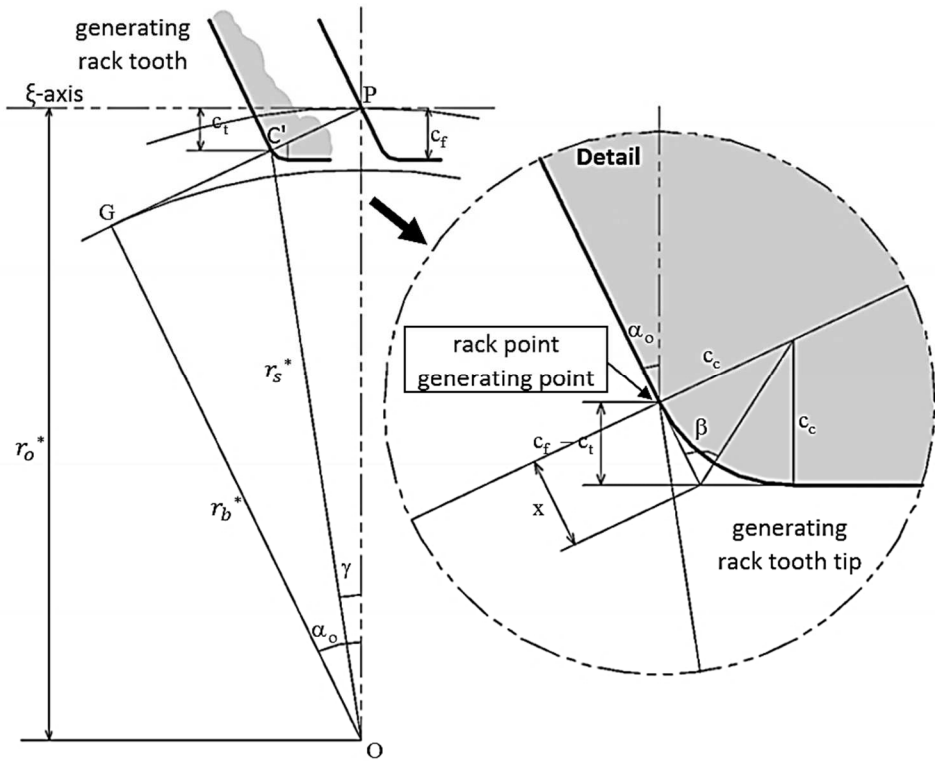


Figure 3.2: Analysis of gear cutting at the tooth fillet (gear not shown, only rack cutter tooth shown for clarity)

By exploiting the symmetry of the rack cutter tooth as shown in Figure 3.2 the following relationship is deduced:

$$\beta = \frac{\pi}{4} + \frac{\alpha_0}{2} \quad (3.3)$$

Also:

$$\tan \beta = \frac{c_c}{x} \quad (3.4)$$

$$c_f - c_t = x \cos \alpha_0$$

And therefore:

$$c_f - c_t = c_c \frac{\cos \alpha_0}{\tan \left(\frac{\pi}{4} + \frac{\alpha_0}{2} \right)} \quad (3.5)$$

Having defined point \hat{C} as the intersection of the line of action GP and the ξ -axis offset by c_t , it is possible to calculate the form radius as:

$$r_s^* = \sqrt{\left(\frac{c_t}{\tan \alpha_0}\right)^2 + (r_o^* - c_t)^2} \quad (3.6)$$

Equation (3.6) is implicit in terms of c_t and is therefore of limited usefulness if r_s^* is known and c_t must be calculated. Then, observing that $\hat{C}P = GP - G\hat{C}$, the following alternative may be derived from the geometry and used instead:

$$\frac{c_t}{\sin \alpha_0} = r_o^* \sin \alpha_0 - \sqrt{(r_s^*)^2 - (r_o^* \cos \alpha_0)^2} \quad (3.7)$$

The system of equations (3.5), (3.6) and (3.7) defines in a non-dimensional form the interrelation between the dedendum c_f , the cutter tip radius c_c and the form radius r_s^* .

3.2.2. Calculation of cutter tip radius limitations

A cross-section of the tooth of a generating rack cutter for various cases of tip radius is represented in Figure 3.3. Zero radius has been known to cause localised tool wear, causing in turn poor surface quality and dimensional inaccuracy of the manufactured gear. The AGMA standard recommendation for 20° involute gears is $c_c = 0.30$ [35], while other radii are also possible.

For a given whole depth, there is a practical limitation on the maximum radius that is obtainable; the larger radii will be incompatible with the designated whole depth for the 20° gear system, i.e. they cannot be realised unless the whole depth is reduced.

Figure 3.3 describes the case of maximum cutter tip radius, where it can be observed that the tip thickness \hat{t}_u of a sharp tooth of the non-dimensional rack cutter relates to the pitch thickness $\pi(1 - c_s)$, the dedendum c_f and the pressure angle according to the formula:

$$\hat{t}^* = \pi(1 - c_s) - 2c_f \tan \alpha_0 \quad (3.8)$$

Obviously, the centre of any fillet must lay on the bisecant δ -axis, therefore the intersection of the bisecant and of the rack tooth centre-line should define the centre of the maximum possible fillet. The radius must be, therefore:

$$\max\{c_c\} = \frac{1}{2} \hat{t}^* \tan \beta \quad (3.9)$$

Substituting with equations (3.3), (3.4) and (3.8) we obtain finally:

$$\max\{c_c\} = \left[\frac{1}{2}\pi(1 - c_s) - c_f \tan \alpha_0 \right] \tan \left(\frac{\pi}{4} + \frac{\alpha_0}{2} \right) \quad (3.10)$$

For standard addendum gears of the 20° system with $c_f = 1.25$ and $c_s = 0.5$, equation (3.10) evaluates to $\max\{c_c\} = 0.47$. Equation (3.10) poses an additional restriction that must be evaluated together with equations (3.5), (3.6), (3.7).

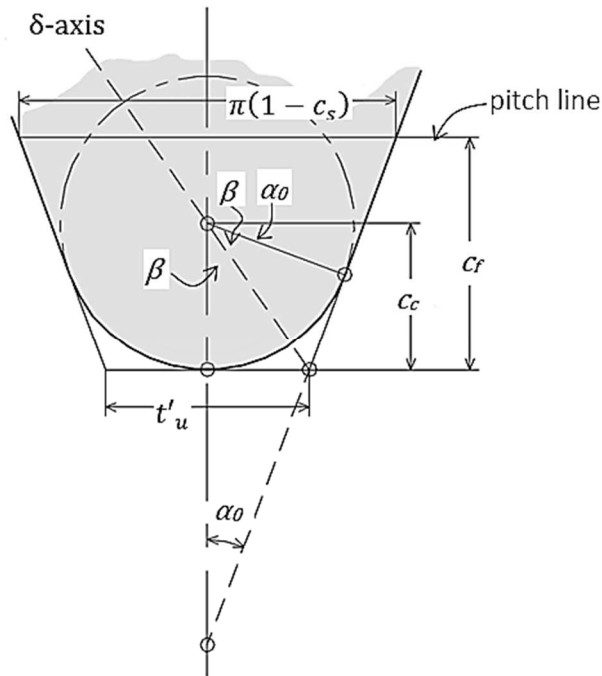


Figure 3.3: Calculation of the maximum cutter tip radius for a given dedendum

For a known value of r_s^* and therefore of c_t and assuming that the maximum cutter tip radius is used, the corresponding dedendum is calculated by combining equations (3.5) and (3.10) as follows:

$$c_f = \frac{\frac{1}{2}\pi(1-c_s) \cos \alpha_0 + c_t}{1 + \sin \alpha_0}, \quad c_c = \max\{c_c\} \quad (3.11)$$

3.3. RESULTS AND DISCUSSION

Firstly the design space was defined by bounding the parameters for the pinion as follows:

$$\begin{aligned} 1 &\leq c_f \leq 1.25 \\ 0 &\leq c_c \leq \max\{c_c\} = 0.47 \end{aligned} \quad (3.12)$$

The main reason for selection of these boundaries, is that the maximum possibility of dedendum coefficient, that most of the standards have been suggested, is 1.25 and with using this number in equation (3.10), the maximum value of cutter tip radius coefficient will be 0.47.

The numbers of pinion and wheel teeth were fixed at $N_1 = N_2 = 20$, the pressure angle at 20° , the addendum coefficient at $c_k = 1$.

Next the gear profiles were generated using an in house computer programme in C++, TFdraw [10].

Using appropriate definitions for the cutter proportions, two-dimensional parametric plots of the tooth profiles have been calculated for the pinion and are shown in Figure 3.4 in non-dimensional coordinates, the coordinate origin being the pinion centre.

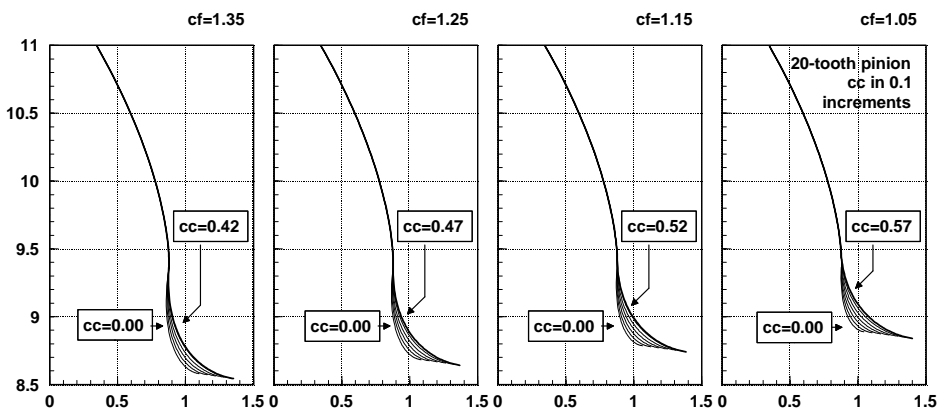


Figure 3.4: Calculated tooth profiles of a 20-tooth pinion for some of the dedendum-cutter tip radius combinations, including maximum tip radius, as calculated by equation (3.10). Notice the shift of the form radius

Two different trends are identified:

- 1) For combinations of relatively large values of dedendum and small values of cutter tip radius, the form radius increases (therefore, the involute part shrinks), suggesting the presence of a secondary cutting action (undercutting).
- 2) For combinations of relatively small values of dedendum and large values of cutter tip radius, the form radius increases also (thus the involute part shrinks),

which, depending on the mating gear geometry and the centre distance, presents an increasing risk of interference. As this is the region that produces the shallowest teeth with the stronger fillets, it is expected that this is the region where strength-wise optimal designs are to be required between these contrary trends.

3.3.1. Interference

The produced gear geometries were checked for interference by means of detailed meshing simulation. Some characteristic control positions for two combinations of gear geometries are plotted in Figure 3.5. The detected interference mode involves a two-point simultaneous contact phenomenon. This is a similar mechanism to undercutting, only there is no cutting action involved here; instead, there is secondary contact action.

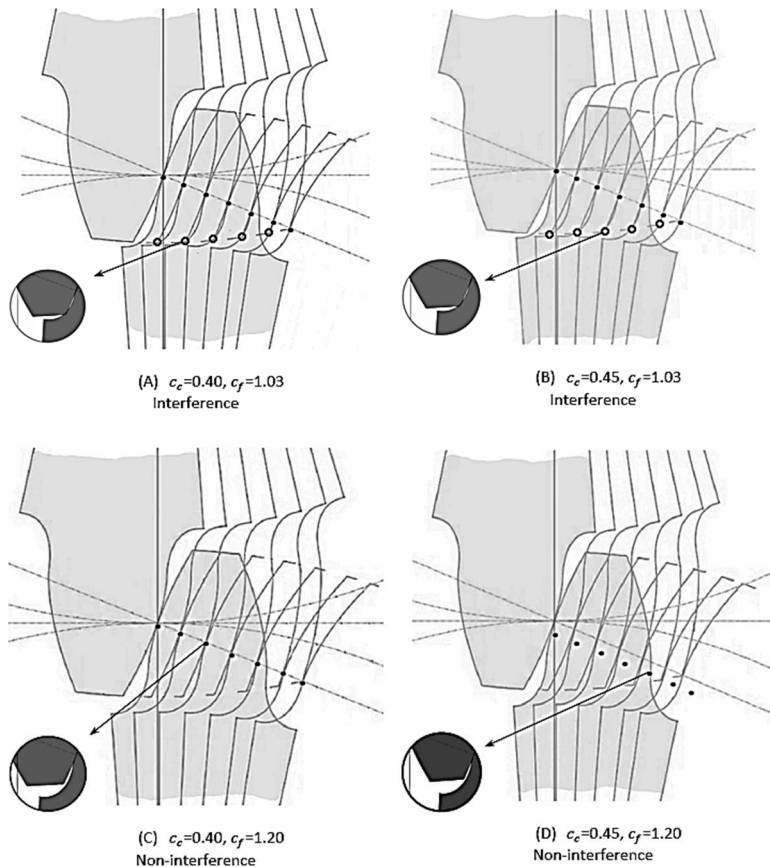


Figure 3.5: Interference simulations a pinion defined by equations (3.4) and (3.11) in mesh with AGMA standard gears

Figure 3.6 presents a map of the considered design space, where regions of interference and non-interference were identified. In this figure the “S” numbers stand for different standards. In the same figure, the tooth geometries produced by various standards are also mapped.

Table 3.1 presents a convenient analytical expression of the boundaries of the locus of non-interference, which corresponds to feasible design solutions. The regression produced from the simulations shows the diagonal boundary segment to be linear.

Table 3.1: The boundaries of non-interference area

Zone	c_f	c_c
1	1.000	0.00 ~ 0.15
2	1.00 ~ 1.25	0.00
3	1.25	0.00 ~ 0.47
4	1.12 ~ 1.25	0.47
5	1.00~1.12	$-9.8402c_f^2 + 23.372c_f - 13.37$

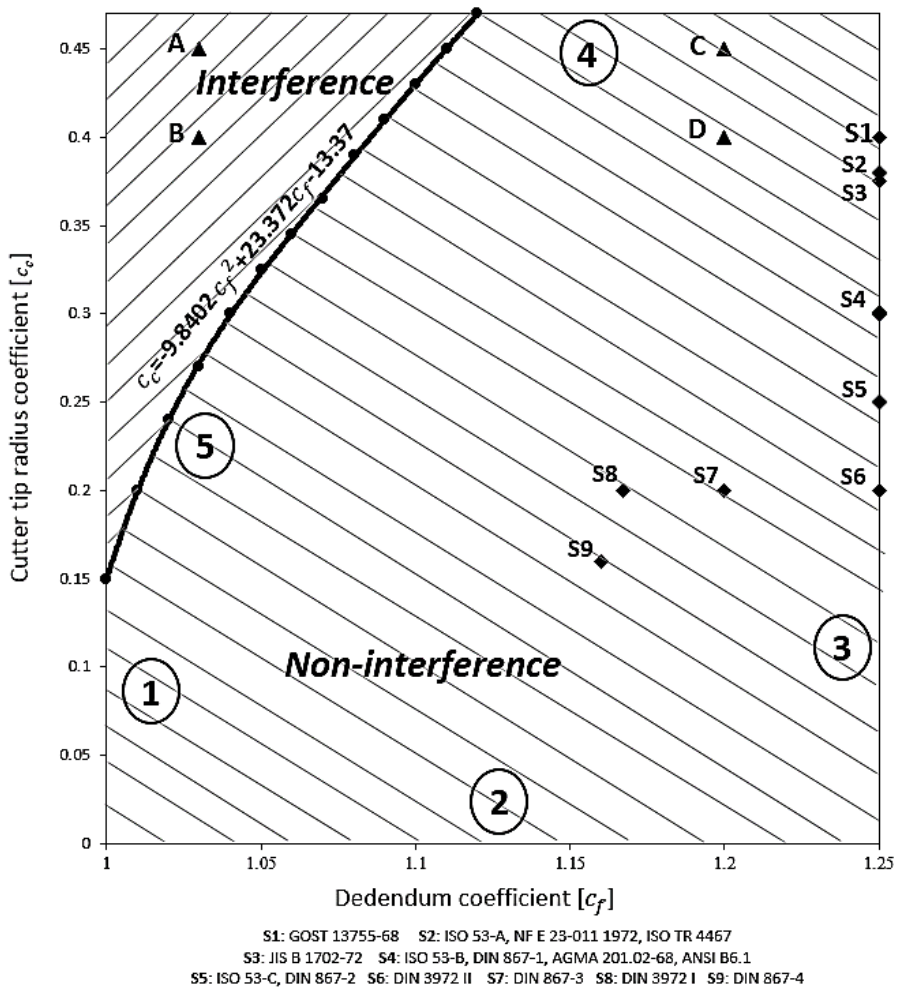


Figure 3.6: Two parametric c_c vs. c_f map of gear tooth proportions into the interference space. The “S” numbers stand for different standards.

3.3.2. Stress modelling using FEA

For the purposes of this investigation ANSYS was used to simulate the loading of different gear pairs with consistent boundary and loading conditions, namely point loading at the Highest Point of Single Tooth Contact considering one-tooth models fixed at their boundary (Figure 3.7), consistent with standard practice [33, 46-48].

The iso-parametric element PLANE82 is used for modelling the gear tooth. This element provides accurate results for mixed (quadrilateral-triangular) automatic meshes and can tolerate shapes well suited to model curved boundaries.

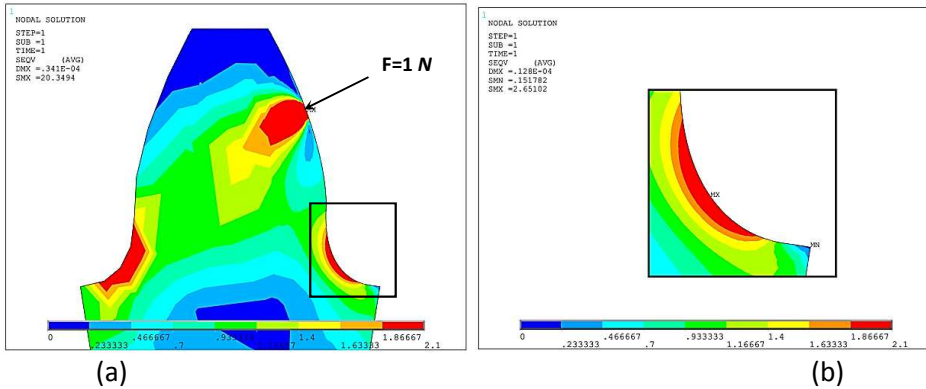
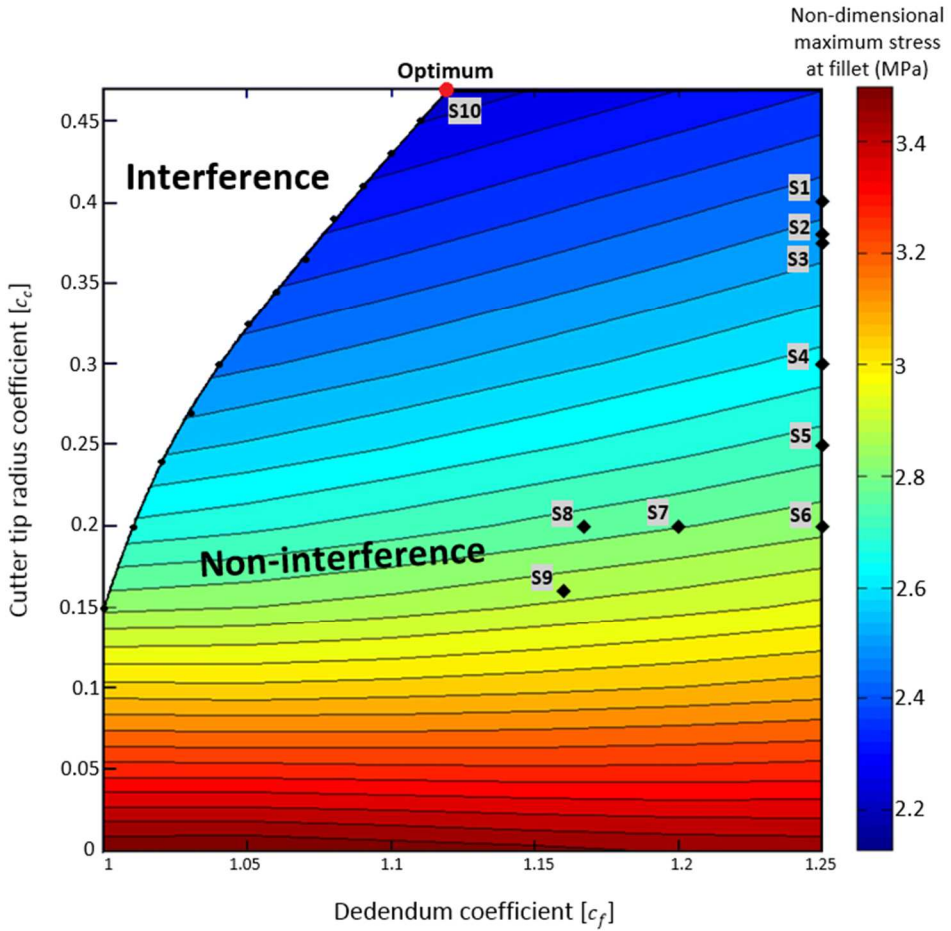


Figure 3.7: Single-tooth finite element model for $c_f=1.25$, $c_c=0.30$ as per AGMA 201.02, a) Non-dimensional bending stress, b) Detail: Maximum non-dimensional bending stress at the critical section

The FEA results were superposed on the map of Figure 3.7, producing the maximum stress map and iso-stress contours in Figure 3.8. Based on these results the following observations are made:

- With increasing dedendum coefficient the leverage of the applied load increases therefore leading to higher fillet stress values.
- Increasing the cutter tip radius results in larger generated root fillet therefore reducing stress concentration.
- It is obvious that existing standard designs **S1** – **S9** do not lead to minimum root stress tooth forms.
- The optimum solution choice **S10** ($c_f=1.12$ and $c_c=0.47$) lies at the top left corner of the non-interference region, verifying the original hypothesis that the optimum would compromise the trends of minimum dedendum, maximum cutter tip radius and the requirement for non-interference.



S1: GOST 13755-68 S2: ISO 53-A, NF E 23-011 1972, ISO TR 4467
 S3: JIS B 1702-72 S4: ISO 53-B, DIN 867-1, AGMA 201.02-68, ANSI B6.1
 S5: ISO 53-C, DIN 867-2 S6: DIN 3972 II S7: DIN 867-3 S8: DIN 3972 I S9: DIN 867-4

Figure 3.8: Topological graph of finite element analysis results for maximum tensile stress at tooth root with different combination of cutter tip radius and dedendum coefficient. The “S” numbers (S1-S9) stand for different standards.

To illustrate the difference between the standards and the optimal design, a comparison is presented in Table 3.2.

Table 3.2: Comparison of different standards and optimal design for rack cutter proportions. Stress related to the non-dimensional maximum tensile stress at tooth root

Standard		c_c	c_f	Stress (MPa)	Stress Reduction (%)
ISO 53	Profile A	0.38	1.25	2.51374	12.07
	Profile B	0.30	1.25	2.65102	18.19
	Profile C	0.25	1.25	2.72502	21.49
DIN 867	1	0.30	1.25	2.65102	18.19
	2	0.25	1.25	2.72502	21.49
	3	0.20	1.20	2.82474	25.94
	4	0.16	1.16	2.88391	28.58
DIN 3972	I	0.20	1.167	2.79332	24.54
	II	0.20	1.25	2.85356	27.22
JIS B 1702-72		0.375	1.25	2.52328	12.50
NF E 23-011 1972		0.38	1.25	2.51374	12.07
AGMA 201.02-68		0.30	1.25	2.65102	18.19
ISO TR 4467		0.38	1.25	2.51374	12.07
GOST 13755-68		0.40	1.25	2.47561	10.37
ANSI B6.1		0.30	1.25	2.65102	18.19
Optimum		0.47	1.12	2.24289	n/a

3.4. CONCLUSION

In this chapter a two-parametric investigation of the effect of the dedendum coefficient and the tip radius coefficient on the interference and strength of spur gears was carried out using non-dimensional geometrical modelling and Finite Element Analysis.

Increasing the dedendum and the tip radius of the cutter were found to produce adverse effects on the generated gear tooth and an optimal solution was sought by scanning the available design space to produce a stronger tooth form without interference.

As expected, the optimum was located at the boundary of the permissible area of non-interference, where the trends for lower dedendum and larger tip radius were compromised. A thorough comparison with the majority of the existing gear standards was performed and the optimum solution was found to outperform all of them in terms of strength by a factor of 10.37% to 28.58%.

REFERENCES

1. Waldron, K. J., Kinzel, G. L., 2004, Kinematics, dynamics, and design of machinery, 2nd Edition, *John Wiley & Sons, INC.*
2. Aslantaş, K., Taşgetiren, S., 2004, A study of spur gear pitting formation and life prediction, *Wear*, 257(11):1167-1175

3. Terauchi, Y., Nadano, H., 1982, Effect of tooth profile modification on the scoring resistance of spur gears, *Wear*, 80(1,2): 27-41
4. Townsend D. P., 1992, Dudley's gear handbook, *McGraw Hill*.
5. Liou C.-H., Lin H. H., Oswald F. B., Townsend D. P., 1996, Effect of contact ratio on spur gear dynamic load with no tooth profile modifications, *Journal of Mechanical Design*, 118(3):439-443
6. Yildirim, N., Munro, R. G., 1999, A systematic approach to profile relief design of low and high contact ratio spur gears, *Proceedings of the Institution of Mechanical Engineers, Part C: Journal of Mechanical Engineering Science*, 213(6):551-562
7. Mahanta, P. K., Kavi, N., 2000, Determination of deflection of spur gear tooth by finite element method, *Journal of the Institution of Engineers (India): Mechanical Engineering Division*, 81(3):105-107
8. Pedersen, N. L., 2010, Improving bending stress in spur gears using asymmetric gears and shape optimization, *Mechanism and Machine Theory*, 45(11):1707-1720
9. Tesfahunegn, Y. A., Rosa, F., Gorla, C., 2010, The effects of the shape of tooth profile modifications on the transmission error, bending, and contact stress of spur gears, *Proceedings of the Institution of Mechanical Engineers, Part C: Journal of Mechanical Engineering Science*, 224(8):1749-1758
10. Spitas, C., Spitas, V., 2007, A FEM study of the bending strength of circular fillet gear teeth compared to trochoidal fillets produced with enlarged cutter tip radius, *Mechanics Based Design of Structures and Machines*, 35(1):59-73
11. Spitas, C., Spitas, V., 2008, Effect of cutter pressure angle on the undercutting risk and bending strength of 20° involute pinions cut with equivalent nonstandard cutters, *Mechanics Based Design of Structures and Machines* 36(2):189-211
12. Spitas, V., Spitas, C., 2007, Four-parametric design study of the bending strength of circular-fillet versus trochoidal-fillet in gear tooth design using BEM, *Mechanics Based Design of Structures and Machines*, 35(2):163-178
13. Li, W., Liu, N., Li, N., Liu, Y.J., Ma, L., 2012, Vibration modal analysis of involute gear with asymmetric tooth profile and double pressure angles, *Advanced Materials Research*, 418-420:1748-1751
14. Su, L., Sun, Y., Wen, J., 2012, Experimental and numerical analysis for two kinds of impact vibration of gear, *Applied Mechanics and Materials*, 141(1):43-48
15. Gill-Jeong, C., 2010, Numerical study on reducing the vibration of spur gear pairs with phasing, *Journal of Sound and Vibration*, 329(19):3915-3927
16. Velez, P., Bruyre, J., Houser, D. R., 2011, Some analytical results on transmission errors in narrow-faced spur and helical gears: Influence of profile modifications, *Journal of Mechanical Design*, 133(3):031010
17. Atanasiu, V., Iacob, M. R., 2010, Tooth wear effects on dynamic transmission error of spur gears with addendum modifications, *International Review of Mechanical Engineering*, 4(6):638-644
18. Mohammadpour, M., Mirzaee, I., Khalilarya, S. A., 2009, Mathematical-numerical model to calculate load distribution, contact stiffness and

- transmission error in involute spur gears, *Proceedings of the ASME International Design Engineering Technical Conferences and Computers and Information in Engineering Conference (DETC2009)*, 6:81-87
19. Davoli, P., Gorla, C., Rosa, F., Rossi, F., Boni, G., 2007, Transmission error and noise emission of spur gears, *Gear Technology*, 24(2):34-38
 20. Litvin, F. L., Lian, Q., Kapelevich, A. L., 2000, Asymmetric modified spur gear drives: Reduction of noise, localization of contact, simulation of meshing and stress analysis, *Computer Methods in Applied Mechanics and Engineering*, 188(1):363-39
 21. Khoshnaw, F. M., Ahmed, N. M., 2009, The pressure angle effects of spur gears on stress concentration factor, *Engineering Computations*, 26(4):360-374
 22. Handschuh, R. F., Zakrajsek, A. J., 2011, High-pressure angle gears: Comparison to typical gear designs, *Journal of Mechanical Design*, 133(11):114501
 23. Baglioni, S., Cianetti, F., Landi, L., 2012, Influence of the addendum modification on spur gear efficiency, *Mechanism and Machine Theory*, 49:216-233
 24. Chen, T., Sun, W., Zhang, X., 2011, An analytical method to determine the addendum modification parameters of involute helical gears, *Proceedings of the Institution of Mechanical Engineers, Part C: Journal of Mechanical Engineering Science*, 225(11):2516-2524
 25. Li, Q., Bian, Y., Zhong, Z.P., Liu, G. H., Chen, Y., 2011, Study on the large module spur gear cold forming process by means of numerical simulation, *Advanced Materials Research*, 189-193:2642-2646
 26. Mendi, F., Başkal, T., Boran, K., Boran, F. E., 2010, Optimization of module, shaft diameter and rolling bearing for spur gear through genetic algorithm, *Expert Systems with Applications*, 37(12):8058-8064
 27. Buckingham E., 1988, Analytical mechanics of gears, *Dover Publications Inc.*
 28. Thirumurugan, R., Muthuveerappan, G., 2011, Critical loading points for maximum fillet and contact stresses in normal and high contact ratio spur gears based on load sharing ratio, *Mechanics Based Design of Structures and Machines*, 39(1):118-141
 29. Thirumurugan, R., Muthuveerappan, G., 2010, Maximum fillet stress analysis based on load sharing in normal contact ratio spur gear drives, *Mechanics Based Design of Structures and Machines*, 38(2):204-226
 30. Math, V. B., Chand, S., 2004, An approach to the determination spur gear tooth root fillet, *Journal of Mechanical Design*, 126(2):336-340
 31. Spitas, C. A., Spitas, V. A., 2006, Generating interchangeable 20° spur gear sets with circular fillets to increase load carrying capacity, *Gear Technology*, 23(4):28-34
 32. Kapelevich, A. L., 2000, Geometry and design of involute spur gears with asymmetric teeth, *Mechanism and Machine Theory*, 35(1):117-130
 33. Sankar, S., Raj, M. S., Nataraj, M., 2010, Profile modification for increasing the tooth strength in spur gear using CAD, *Engineering*, 2(9):740-749

34. Spitas V. A., Costopoulous T. N., Spitas C. A., 2001, Geometrical and structural modeling of novel spur gear teeth of circular fillet, *Proceedings of IASTED International Conference on Applied Simulation and Modeling (ASM 2001)*, 399-403
35. AGMA, 201.02 and 201.02A, 1968, Tooth proportions for coarse pitch involute spur gears. Alexandria VA: Gear Manufacturers Association (AGMA)
36. ISO 53, 1974, Cylindrical gears for general and heavy engineering- Standard basic rack tooth profile
37. DIN 867, 1986, Basic rack tooth profiles for involute teeth of cylindrical gears for general engineering and heavy engineering
38. DIN 3972, 1952, Reference Profiles of Gear-cutting Tools for Involute Tooth Systems according to DIN 867
39. JIS B 1702-72, 1976, Accuracy for spur and helical gears
40. NF E 23-011, 1972, Cylindrical gears for general and heavy engineering - Basic rack and modules (similar to ISO 467 and ISO 53)
41. ISO/TR 4467, 1982, Addendum modification of the teeth of cylindrical gears for speed-reducing and speed increasing gear pairs
42. GOST 13755-81, 1981, Basic requirements for interchangeability. Gearings cylindric evolvent gears. Basic rack ()
43. ANSI B6.1, 1968, Coarse pitch gears
44. Litvin F. L., 1994, Gear geometry and applied theory, *Prentice Hall*
45. Maitra G. M., Prasad L. V., 1995, Handbook of mechanical design, *Tata McGraw-Hill Education*
46. Patel, S., 2010, Finite element analysis of stresses in involute spur & helical gear, Master Thesis, The University of Texas at Arlington
47. Hassan, A. R., 2009, Contact stress analysis of spur gear teeth pair, *World Academy of Science, Engineering and Technology*, 58:611-616
48. Kanber, B., 2006, Analysis of spur gears by coupling finite and boundary element methods, *Mechanics Based Design of Structures and Machines*, 34(3):307-324

4- Multi-parametric investigation of interference

Summary

Tooth interference, normally avoided altogether by adhering to standard design guidelines, becomes a concern when non-standard tooth forms with reduced radial clearance are employed, such as large-fillet short-dedendum gears. These tooth forms have shorter involute working flanks and excess material at the root, which can lead to non-conjugate corner contact and penetration at the tooth root. Existing models for interference are unable to predict this, or rely on calculation-intensive simulations, which make them impractical for design.

This work proposes a general and fast mathematical model for calculating corner penetration at the tooth root, which is applicable to both analytically expressed and discretised tooth geometries. Based thereupon a non-dimensional multi-parametric investigation is carried out to quantify the effect of addendum and dedendum length, cutter tip radius, number of teeth and contact ratio on the interference risk and on this basis generalised guidelines are produced for the design of non-standard large fillet short dedendum 20° involute gears, including a method using standard cutters with indexing offsets. The present model effectively supplants prior analytical and numerical interference models in the literature, which are proven to be limited subcases of this model.

4.1. INTRODUCTION

The design of high performance gears must constantly seek to overcome manufacturing and logistical limitations. I.e. one of the challenges is to make gear sets as compact as possible, with the aim to reduce space, increase strength and potentially improve other performance aspects, such as dynamics. Correspondingly, compact gears may be obtained either by optimising the macro-geometry to minimise the total volume of a gear pair [1], or by minimising specifically part of the clearance between gear teeth, when that is possible [2]. In compact gear tooth forms of the latter type, a number of established design solutions have been categorised in dedicated books [3], standards [4] and gear design software [5-8]. The state-of-the-art, as reflected through these, includes a number of solutions for free-formed as well as generated tooth geometries, which however present a number of limitations:

- Free-form geometries, as i.e. obtainable in injection-moulded plastic gears, use the familiar enveloping principles established already since Reuleaux [9]. The fundamental concept is that it is generally beneficial to use the entire tooth

depth for meshing and therefore eliminate radial clearance and non-meshing parts of the tooth profile [10]. Such compact meshes are at the same time sensitive to geometrical errors and interference under loaded static and dynamic conditions. Due to their relatively high compliance, plastic gears can be forgiving to such errors (to some degree), but the same is not true for the large array of high-torque high-power applications, where steel gears that have significantly higher strength, stiffness and accuracy, must be used.

- Generated geometries, as i.e. produced by material removal, are still the dominant solution. Compared to free-form geometries, they obviously allow less freedom of form, as they must be generated by simple tool geometries reducible to the basic rack cutter model. A number of standards have explored possibilities to reduce the unused part of the whole depth by recommending dedendum coefficients lower than the traditional 1.25 [11, 12] and as low as 1.16 [11]. Moreover, in Chapter 2, it has been demonstrated in a two-parametric study of a gear stage involving two same-size pinions that significant bending strength increase can be obtained by manipulating simultaneously the dedendum and the rack cutter tip radius, whereas Nguyen and Lin [2] attempted the same by modifying the gear dedendum only, in conjunction with the mating addendum. At the same time, in the high torque high power applications special hardened gear steels and other metal alloys are the material of choice, their high stiffness and sensitivity to errors means that too tight meshes can result in high vibration, wear and even seizure. Therefore clearance should be minimised but not eliminated, to compensate for these effects. Furthermore, because not all parts of the meshing teeth are conjugate to one-another, specifically at the tooth fillet regions, minimising clearance at one location requires the risk of inducing interference at another. Such an occurrence typically results in large impacts and vibration, local breakdown of the lubricant oil film and rapid failure [13]. Therefore, predicting interference emerges as the critical challenge in this context.

In the context of detecting interference, a few different methods are in use. For involute profiles, Litvin [14] considers the limiting condition of contact at the form diameter as the condition for interference. Although analytically elegant and fast, this condition is only valid for a subcase of the real phenomenon and generally leads to underestimation of interference risk, producing false negatives, as has been noted in later work [15] and will be demonstrated in the following section.

On the other hand, simulation of tooth contact [5-8, 13, 15] can produce more accurate predictions of interference, but at significant calculation, especially in case of three dimensional models, depending on starting 'guess values' to assure numerical convergence, as has been demonstrated in similar tooth contact analysis studies [16]. In one implementation, Polder and Broekhuisen [15] proposed a distance-based condition for root-tip proximity, which they used to infer interference risk and discuss tooth form tolerance limits. As will be shown in the following section, present implementations of such simulations, if not

supervised closely, can also produce unclear results and false negatives in terms of detecting interference.

In addition, iterations of contact simulations over different points in the design space are generally time-intensive to set up and interpret: Simulations generally lack the analytical insight about the type and cause for interference that they detect and require further human supervision to provide such insight. For these reasons, simulations become especially impractical when tackling multi-parametric design problems, where each parameter adds one additional dimension to the search matrix. Particularly in the context of large fillet short dedendum spur gears, at least eight parameters stand out as potentially significant: the cutter tip radius (radii), the dedendum length(s), the addendum length(s) and the numbers of teeth of the mating gears. A mapping of the design space using conventional tooth contact simulations in this context is obviously unfeasible. Therefore a new model for interference, both accurate and suitable for fast and large parametric sweeps must be sought.

Starting from basic geometrical principles, this chapter proposes a new generalised analytical model for interference as non-conjugate corner contact-and-penetration at the tooth root. From this, a geometrical condition is extracted that admits a simple and explicit mathematical solution for either analytically expressed or discretised tooth profiles.

With the purpose to investigate interference in compact tooth forms, this model is furthermore adapted to the involute geometry and applied to a multi-parametrically defined family of non-standard large-fillet short-dedendum 20° involute gears. The generality of the study is extended by non-dimensionalising all geometrical features in terms of the module. From this study design envelopes are defined to outline interference regions in the multi-parametric space and, based on the results, the order of the problem is reduced to three parameters only, as opposed to the original eight.

Previous theory [14] is shown to introduce significant errors and false negatives in the prediction of interference for the small cutter tip radius and small dedendum configurations, while converging to the predictions of the present model for large cutter tip radius large dedendum configurations. The reasons for this discrepancy are traced back to basic principles. Numerical interference simulations in state of the art software are also inaccurate and shown to produce false negatives in certain cases. The present model for interference can effectively supplant the prior models, both analytical and numerical, which are reduced to limited subcases of this model.

4.2. STATE OF THE ART MODELS FOR INTERFERENCE

4.2.1. Analytical model: Form circle interference (Litvin)

The basic assumption behind this class of models is that two involute teeth in mesh will interfere if and only if the tip of one tooth will mesh with a part of the

mating tooth lying below its form circle, as shown in Figure 4.1b, where Figure 4.1a shows an assumedly non-interfering case. This item can in fact be stated in different but equivalent ways in terms of involute angles [14], lengthwise positions on the line of action (this chapter), radii and potentially any other variable used to describe meshing position. The form circle itself is calculated from the meshing of each tooth with its rack cutter, also shown in Figures 4.1a and 4.1b. Effectively, this model fundamentally assumes as such that interference will occur along the path of contact.

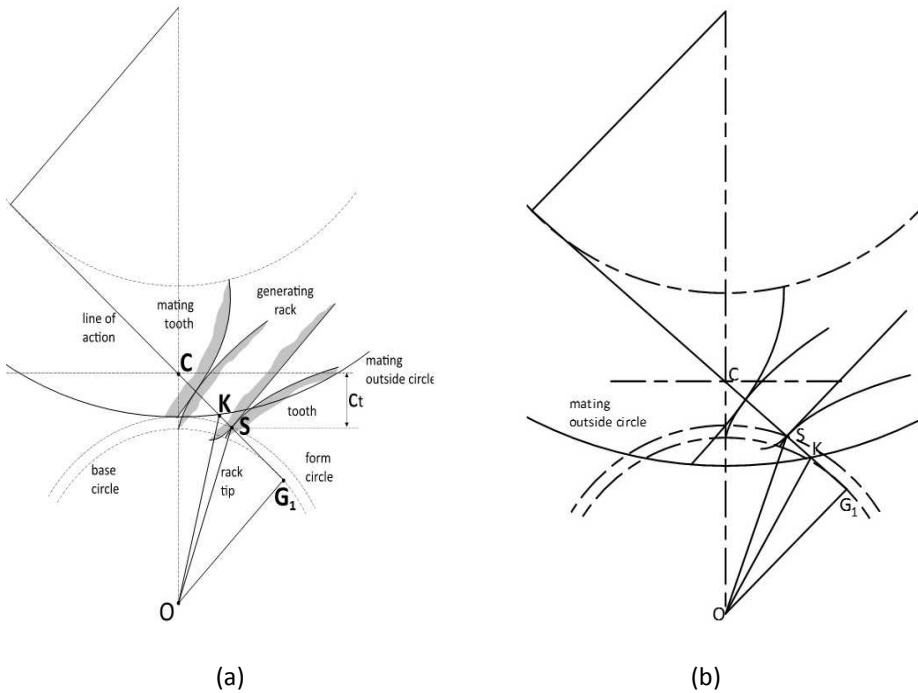


Figure 4.1: Gear tooth (bottom gear) in mesh with generating rack and mating tooth (top gear), showing (a) an assumed noninterfering configuration and (b) an assumed interfering configuration

Using the definitions and notation in Figures 4.1a and 4.1b, the necessary and sufficient condition for non-interference at the root of the reference gear (gear 1) proposed by Litvin [13] is as follows:

$$\widehat{G_1OS} \leq \widehat{G_1OK} \quad (4.1)$$

Given the basic property of the involute that $G_1S = r_{b1}\widehat{G_1OS}$ and $G_1K = r_{b1}\widehat{G_1OK}$, this condition is equivalent to:

$$G_1S \leq G_1K \quad (4.2)$$

And by subtracting both sides of equation (4.2) from G_1C be brought to the simplest form:

$$CK \leq CS \quad (4.3)$$

An analytical expression of either condition in terms of gear design parameters is not provided in the primary source [14] or subsequently the gear design literature that cites it [17-23]. Starting from equation (4.3), we elaborate such an analytical expression hereunder as follows:

$$CK = G_2K - G_2C \quad (4.4)$$

$$= \sqrt{r_{k2}^2 - r_{b2}^2} - r_{b2} \tan \alpha_o \quad (4.5)$$

$$CS = \frac{c_t}{\sin \alpha_o}$$

Where the length c_t is the projection of CS on the centre line of the gear pair and is a property of the generating rack defining the start point of its round tip (point S in Figure 4.1a, 4.1b). For simplicity we omit all the subscripts related to the reference gear (gear 1) and understand instead that any magnitude not designated by the subscript '2' refers to gear 1 or is common to both gears.

Next, substituting equations (4.4) and (4.5) into equation (4.3) we obtain:

$$\sqrt{r_{k2}^2 - r_{b2}^2} - r_{b2} \tan \alpha_o \leq \frac{c_t}{\sin \alpha_o} \quad (4.6)$$

$$c_t \geq \left(\sqrt{r_{k2}^2 - r_{b2}^2} - r_{b2} \tan \alpha_o \right) \sin \alpha_o$$

Substituting equation (3.5) into equation (4.6) we obtain:

$$c_f - c_c \frac{\cos \alpha_o}{\tan \left(\frac{\pi}{4} + \frac{\alpha_o}{2} \right)} \geq \frac{1}{m} \left(\sqrt{r_{k2}^2 - r_{b2}^2} - r_{b2} \tan \alpha_o \right) \sin \alpha_o \quad (4.7)$$

Considering the manufacturing parameters of gear 2 (which need not be the same as the reference gear 1), we alternatively express its outside radius as:

$$r_{k2} = r_{o2} + c_{k2}m \quad (4.8)$$

$$= \frac{1}{2} N_2 m + c_{k2}m$$

Furthermore, we observe that:

$$r_{b2} = \frac{1}{2} t_b N_2 \quad (4.9)$$

Where the base pitch t_b will be common to both gears as is requisite for basic meshing compatibility [24] and is thus not given a subscript.

t_R being the circular pitch, we know that:

$$\begin{aligned} t_R &= \pi m \\ \frac{t_b}{\cos \alpha_o} &= \pi m \\ t_b &= \pi m \cos \alpha_o \end{aligned} \quad (4.10)$$

From equations (4.9) and (4.10) we deduce that:

$$r_{b2} = \frac{1}{2} N_2 \pi m \cos \alpha_o \quad (4.11)$$

Substituting equations (4.8) and (4.11) into equation (4.7) we obtain:

$$\begin{aligned} c_f - c_c \frac{\cos \alpha_o}{\tan \left(\frac{\pi}{4} + \frac{\alpha_o}{2} \right)} & \quad (4.12) \\ & \geq \left(\sqrt{\left(\frac{1}{2} N_2 + c_{k2} \right)^2 - \frac{1}{4} N_2^2 \pi^2 \cos^2 \alpha_o} \right. \\ & \quad \left. - \frac{1}{2} N_2 \pi \sin \alpha_o \right) \sin \alpha_o \end{aligned}$$

This condition defines a mapping from the non-dimensional gear design parameter space $c_f - c_c - N_2 - c_{k2} - \alpha_o$ (recall that no subscript implies subscript '1', or a magnitude common to both gears) to the interference existence space, segregating two half planes in the $c_f - c_c$ plane, as follows:

$$\begin{aligned} c_c \leq c_f \tan \left(\frac{\pi}{4} + \frac{\alpha_o}{2} \right) \sec \alpha_o & \quad (4.13) \\ - \left(\sqrt{\left(\frac{1}{2} N_2 + c_{k2} \right)^2 - \frac{1}{4} N_2^2 \pi^2 \cos^2 \alpha_o} - \frac{1}{2} N_2 \pi \sin \alpha_o \right) \tan \left(\frac{\pi}{4} \right. \\ & \quad \left. + \frac{\alpha_o}{2} \right) \tan \alpha_o \end{aligned}$$

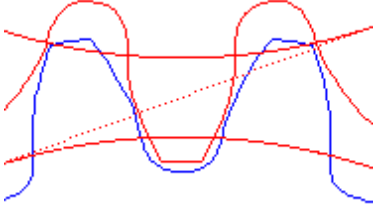
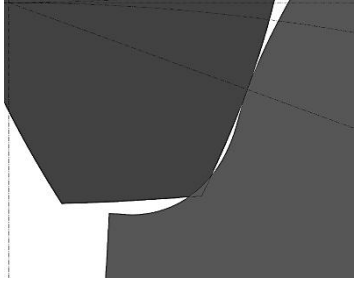
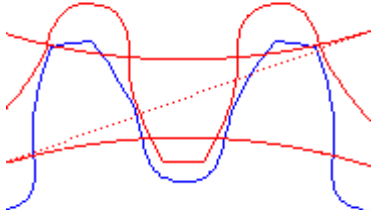
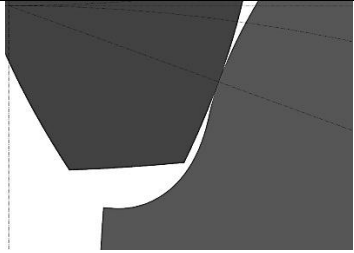
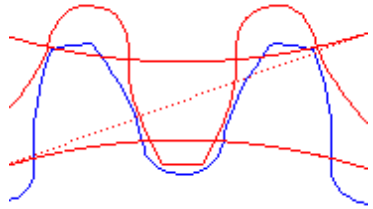
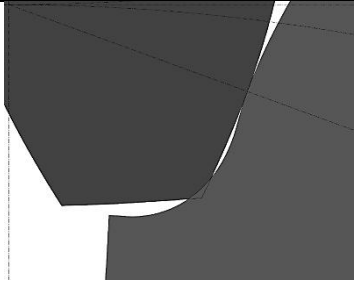
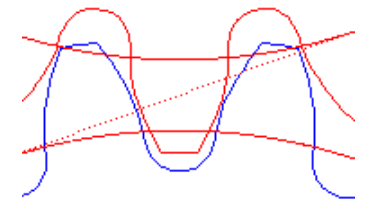
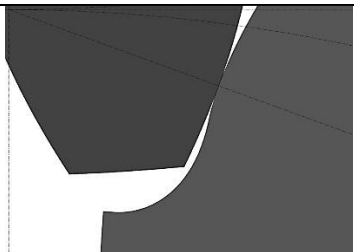
And is the analytical equivalent to Litvin's necessary and sufficient geometrical condition for non-interference. We shall be discussing the applicability and

accuracy of this model and its further implications and utility to gear design in section 3.6.

4.2.2. Numerical models: Interference simulation

This simple class of models works by discretising the mating gear surfaces and rotating them stepwise to simulate a number of finite anticipated meshing positions. If penetration of one discretised surface to the other is detected, then an interference warning is issued. Unlike analytical models, as in section 4.2.1, these models are obviously limited to checking one specific parametric configuration at a time and do not provide analytical insights in the form of a mapping from the design parameter space to the interference existence space. Implementations of this class of models can be found in a number of scientific studies [13, 15] and most commercial gear design and analysis software [5-8]. Remarkably, the large-fillet short-dedendum geometries from Chapter 3, when reproduced with KISSsoft v03-2011 [5] produced inconsistent warnings with regard to interference that were verified by simulation to be incorrect (Table 3.1). These false negatives were shown to be dependent on backlash and were eliminated in the particular software by setting backlash to zero; however, it can easily be understood that backlash can only affect the occurrence of seizure, which is a particular type of interference, but has no effect by itself on corner contact and penetration on the driving side. In fact, seizure will always unveil in a geometrical simulation at some point as penetration, but the opposite is not true. Clearly, an accurate model for corner penetration -and hence generalised interference- that may be used even with non-standard geometries in the examined simulation software is missing.

Table 4.1: Interference calculations by KISSsoft v03-2011 [5] vs. simulation results for two pinions in mesh ($N_1 = N_2 = 20$, $c_{k1} = c_{k2} = 1.0$, $c_{s1} = c_{s2}$ as per DIN3967 cd25 [12])

c_c	c_f	KISSsoft [5]	Chapter 3
0.40	1.03	 <p>No interference warning if backlash (Interference warning if zero backlash)</p>	 <p>Interference</p>
0.40	1.20	 <p>No interference warning</p>	 <p>No interference</p>
0.45	1.03	 <p>No interference warning if backlash (Interference warning if zero backlash)</p>	 <p>Interference</p>
0.45	1.20	 <p>No interference warning</p>	 <p>No interference</p>

4.3. GENERALISED CORNER CONTACT-AND-PENETRATION MODEL OF INTERFERENCE

4.3.1. Corner contact and penetration

Consider two parametric curves $\vec{t}_1(r_1), \vec{t}_2(r_2)$ describing respectively two mating tooth flanks, where r_1, r_2 can be any suitable parameters, for each of which a continuous bijective mapping $T \rightarrow \mathbb{R}^2 : r \rightarrow \vec{t}$ exists and T are continuous intervals in \mathbb{R} (i.e. r can be the distance of each profile point from the centres of the respective gears or the length of each curve up to said point). The same definition can be extended to tooth surfaces, if at least one of $r_1, r_2 \in \mathbb{R}^2$, in which case the mapping will be of the form $T \rightarrow \mathbb{R}^3 : r \rightarrow \vec{t}$, where T must be a continuous segment in \mathbb{R}^2 .

During a mesh cycle, these flanks will engage in conjugate action around the pitch point, and will each rotate according to a known law of the form:

$$i_{12}d\theta_2 - d\theta_1 = 0 \quad (4.14)$$

Where both angular velocities must be of the same sign for compatible rotation. For the sake of simplicity and without loss of generality, we demand that the following condition be true when two teeth mate with their leading sides at the pitch point:

$$\theta_2 = \theta_1 = 0 \quad (4.15)$$

Considering equations (4.14) and (4.15) in the case of constant transmission ratio integrates over time for the leading side to:

$$i_{12}\theta_2 - \theta_1 = 0 \quad (4.16)$$

And for the coast side to:

$$i_{12}(\theta_2 - \varphi_{s2}) - (\theta_1 - \varphi_{s1}) = 0 \quad (3.17)$$

Where φ_s is the angle corresponding to the tooth pitch thickness of each gear, such that:

$$\varphi_s = c_s \frac{2\pi}{N} \quad (4.18)$$

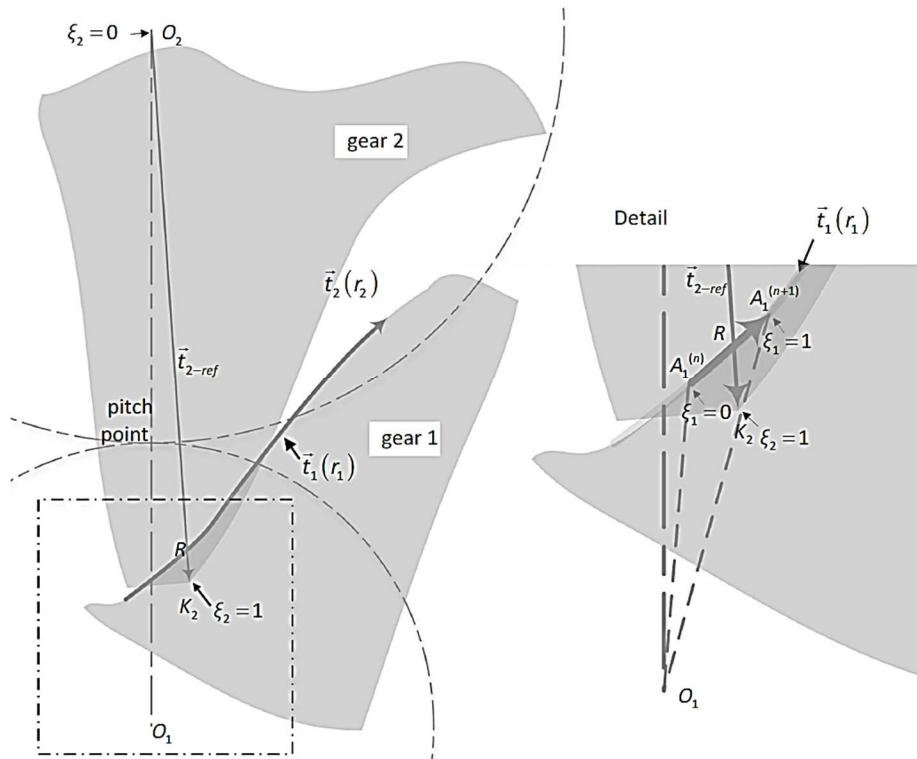


Figure 4.2: Model of gear meshing and corner contact and penetration. Right: Detail showing contact discretisation around point **R**

Depending on their shape the tip of each tooth may (or not) penetrate the other near the vicinity of its root. Such corner penetration is shown in Figure 4.2. It is clearly non-conjugate and must therefore be classified as interference. This model is consistent with all known accounts of interference, including tooth seizure (in which case the corner penetration will occur on the coast side of the teeth) and is different than conjugate-type ‘penetrations’ in compliant teeth models, which are resolved by means of deflection [25]. At this point we make two modelling choices:

- 1) Without harm to generality, hereafter we shall check for corner penetration between the root of gear 1, modelled by tooth flank $\vec{t}_1(r_1)$, and the tip of gear 2, modelled by tooth flank $\vec{t}_2(r_2)$. To check for the opposite effect it is sufficient to switch the indices 1 and 2 in all subsequent calculations.
- 2) The concept of corner penetration affords one more substantial reduction to the complexity of the model: instead of considering the entire flank of gear 2, it is only necessary to concentrate at a single reference point, the corner K_2 . The position parameter r_{2-ref} of this point is typically known, so the location of the point is easily found as:

$$\vec{t}_{2-ref} = \vec{t}_2(r_{2-ref}) \quad (4.19)$$

This reference point can be located at the outside radius, if the tooth is assumed to have a knife edge, or a more relevant point somewhat lower, where the chamfer or tooth rounding may begin, as is customary in gear design [26] or as a result of mild wear. Generally, placing the reference point at the outside radius can be expected to lead to more conservative, safer predictions.

With regard to the tooth flank of gear 1, it is possible to similarly limit the area of interest if it is known beforehand (i.e. through analytical considerations) that certain segments may be excluded: Most especially, the conjugately operating segment of a tooth will by its definition only engage in conjugate action- this excludes the former corner penetration mode that is examined here and thus the corresponding segment can be safely excluded from further analysis.

Turning to Figure 3.2, corner interference can be modelled as follows:

4.3.1.1. Continuous model

Consider for a kinematically compatible gear position (θ_1, θ_2) . There will be corner interference if and only if an intersection point R exists between the curve t_2 and the line O_2K_2 .

Considering the vector descriptions for the curve t_2 and the line O_2K_2 , in mathematical terms this translates to the requirement that two real numbers r_1 and ξ_2 exist such that the following conditions are simultaneously true:

$$\overrightarrow{OO_1} + \vec{t}_1(r_1) = \overrightarrow{OO_2} + \xi_2 \overrightarrow{O_2K_2} \quad (4.20)$$

$$\vec{t}_1(r_1) = \overrightarrow{O_1O_2} + \xi_2 \vec{t}_2(r_{2-ref}) \quad (4.21)$$

$$r_1 \in T_1 \quad (4.21)$$

$$0 \leq \xi_2 \leq 1 \quad (4.22)$$

Where O is the centre of any arbitrary reference coordinate system.

In general equation (4.20) can be expected to yield a set of non-linear equations, depending on the tooth form, which may be solved analytically or numerically for r_1 and ξ_2 and the latter solutions can then be checked against equations (4.21), (4.22).

4.3.1.2. Discrete models of first and higher orders

In the case that the tooth profiles are described as discretised point clouds, the continuous model in section 4.3.1.1 may still be used by creating an interpolating function from the point cloud, i.e. using polynomial interpolation. However, it can be more practical to directly use a discrete model with such discrete data sets. We first develop a first order model of this kind as follows:

Consider for a kinematically compatible gear position (θ_1, θ_2) two neighbouring points $A_1^{(n)}$ and $A_1^{(n+1)}$ on the profile of gear 1 and the reference point K_2 at the corner of gear 2, as shown in the detail of Figure 4.2. There is corner contact or penetration in the vicinity of $A_1^{(n)}$ if and only if the vectors $A_1^{(n)}A_1^{(n+1)}$ and O_2K_2 intersect. In mathematical terms, this translates to the requirement that two real numbers ξ_1 and ξ_2 exist such that the following conditions are simultaneously true:

$$\overrightarrow{OA_1^{(n)}} + \xi_1 \overrightarrow{A_1^{(n)}A_1^{(n+1)}} = \overrightarrow{OO_2} + \xi_2 \overrightarrow{O_2K_2} \quad (4.23)$$

$$0 \leq \xi_1 \leq 1 \quad (4.24)$$

$$0 \leq \xi_2 \leq 1 \quad (4.25)$$

Where O is the centre of any arbitrary reference coordinate system.

This expression is particularly suitable for working with discretised expressions of the tooth profiles, as the index n can be set to follow the sequence of points making up the discrete representation of (a subset of) the profile of gear 1.

Considering the distance between points $A_1^{(n)}$ and $A_1^{(n+1)}$ as infinitesimally small, it is possible to obtain an elegant analytical expression of the intersection clause of equations (4.23), (4.24) and (4.25):

$$\overrightarrow{OA_1(r_1)} + \delta\xi_1 \frac{d}{dr_1} \overrightarrow{OA_1(r_1)} = \overrightarrow{OO_2} + \xi_2 \overrightarrow{O_2K_2} \quad (4.26)$$

$$\overrightarrow{OO_1} + \vec{t}_1(r_1) + \delta\xi_1 \frac{d}{dr_1} \vec{t}_1(r_1) = \overrightarrow{OO_2} + \xi_2 \overrightarrow{O_2K_2}$$

$$\vec{t}_1(r_1) + \delta\xi_1 \frac{d}{dr_1} \vec{t}_1(r_1) = \overrightarrow{O_1O_2} + \xi_2 \overrightarrow{O_2K_2}$$

$$r_1 \in T_1 \quad (4.27)$$

$$|\xi_1| \leq tol \quad (4.28)$$

$$0 \leq \xi_2 \leq 1 \quad (4.29)$$

Where $\delta\xi_1$ can be any very small (positive or negative) real number within a predefined tolerance, which characterises the solution accuracy. This is basically a local linearisation of the continuous model described under equations (4.20), (4.21) and (4.22). To allow for larger tolerances, but at the cost of solution simplicity, equation (4.26) can be further extended as a Taylor series to produce higher order discrete models for corner interference:

$$\vec{t}_1(r_1) + \sum_n \frac{\delta\xi_1^n}{n!} \frac{d^n}{dr_1^n} \vec{t}_1(r_1) = \overrightarrow{O_1O_2} + \xi_2 \overrightarrow{O_2K_2} \quad (4.30)$$

Equation (4.26), or in general equation (4.30), are especially suitable when a parametric analytical expression is known for $\vec{t}_1(r_1)$ but it is also usable with an interpolated function derived from a discrete point cloud; furthermore the nature of the vector derivative allows to neglect the chosen origin O , if the same derivative is known under another coordinate system.

In addition to the above expressions, corner contact and penetration distinguishes itself from conjugate corner contact in that at the point of intersection the tangent vectors of the two tooth profiles are not parallel. This translates into the following necessary condition for corner interference:

$$\frac{d}{dr_1} \vec{t}_1(r_1) \times \frac{d}{dr_2} \vec{t}_2(r_{2-ref}) \neq 0 \quad (4.31)$$

If the entire tooth profile for gear 1 is used for checking interference, equations (4.23), (4.26) and (4.30) can be expected to yield also conjugate contact solutions along the path of contact, which equation (4.31) will identify and filter out. Using equation (4.31) is for the same reason redundant when the conjugate segment of tooth 1 has been excluded in advance, as only interference contact can be expected between non-conjugate profiles.

4.3.1.3. Implementation over the entire mesh cycle

To obtain usable expressions for the points considered in equations (4.23), (4.26) and (4.30), we link the instantaneous positions of the profiles to their known reference positions established in equation (4.15) by introducing the matrix $\langle \theta \rangle$, which affects a planar rotation by an angle $\langle \theta \rangle$:

$$\langle \theta \rangle = \begin{bmatrix} \cos\theta & -\sin\theta \\ \sin\theta & \cos\theta \end{bmatrix} \quad (4.32)$$

The simplest model can be obtained by considering that a) the flank equations $\vec{t}_1(r_1)$ and $\vec{t}_2(r_2)$ refer to their respective local gear-bound coordinate system, such that the x-axis is made to pass through the pitch point, and that b) at the reference position defined in equation (4.15) the leading flank pitch points coincide. The models developed in sections 4.1.1 and 4.1.2 will then be valid for the position $\theta_1 = \theta_2 = 0$. At any other kinematically compatible gear position θ_1, θ_2 any vector \vec{t}_1 fixed on gear 1 must be remapped to:

$$\vec{t}_1 \rightarrow \langle \pm\theta_1 \rangle \vec{t}_1 \quad (4.33)$$

where the top sign case corresponds to a global coordinate system orientation in which gear 1 rotates clockwise when $d\theta_1 > 0$ and the bottom sign case

corresponds to the opposite coordinate system orientation. Both modelling choices are equivalent.

For any vector \vec{t}_2 fixed on gear 2 the corresponding transformation is:

$$\vec{t}_2 \rightarrow \langle \mp \theta_2 \rangle \vec{t}_2 \quad (4.34)$$

In practical terms, implementation of the different meshing positions means that the fixed position interference models developed in sections 4.1.1 and 4.1.2 are transformed using equations (4.33) and (4.34) as follows:

Continuous model:

$$\langle \pm \theta_1 \rangle \vec{t}_1(r_1) = \overrightarrow{O_1 O_2} + \xi_2 \langle \mp \theta_2 \rangle \vec{t}_2(r_{2-ref}) \quad (4.35)$$

$$r_1 \in T_1 \quad (4.36)$$

$$0 \leq \xi_2 \leq 1 \quad (4.37)$$

Discrete model, first order:

$$\langle \pm \theta_1 \rangle \left[\overrightarrow{O_1 A_1^{(n)}} + \xi_1 \overrightarrow{A_1^{(n)} A_1^{(n+1)}} \right] = \overrightarrow{O_1 O_2} + \xi_2 \langle \mp \theta_2 \rangle \overrightarrow{O_2 K_2} \quad (4.38)$$

$$0 \leq \xi_1 \leq 1 \quad (4.39)$$

$$0 \leq \xi_2 \leq 1 \quad (4.40)$$

Approximated continuous model, first order:

$$\langle \pm \theta_1 \rangle \left[\vec{t}_1(r_1) + \delta \xi_1 \frac{d}{dr_1} \vec{t}_1(r_1) \right] = \overrightarrow{O_1 O_2} + \xi_2 \langle \mp \theta_2 \rangle \overrightarrow{O_2 K_2} \quad (4.41)$$

$$r_1 \in T_1 \quad (4.42)$$

$$|\xi_1| \leq tol \quad (4.43)$$

$$0 \leq \xi_2 \leq 1 \quad (4.44)$$

Approximated continuous model, higher order:

$$\langle \pm \theta_1 \rangle \left[\vec{t}_1(r_1) + \sum_n \frac{\delta \xi_1^n}{n!} \frac{d^n}{dr_1^n} \vec{t}_1(r_1) \right] = \overrightarrow{O_1 O_2} + \xi_2 \langle \mp \theta_2 \rangle \overrightarrow{O_2 K_2} \quad (4.45)$$

$$r_1 \in T_1 \quad (4.46)$$

$$|\xi_1| \leq tol \quad (4.47)$$

$$0 \leq \xi_2 \leq 1 \quad (4.48)$$

The condition for non-conjugate contact from equation (4.31) also transforms across different mesh positions and is as follows:

$$\langle \pm\theta_1 \rangle \frac{d}{dr_1} \vec{t}_1(r_1) \times \langle \mp\theta_2 \rangle \frac{d}{dr_2} \vec{t}_2(r_{2-ref}) \neq 0 \quad (4.49)$$

The algorithm used in this work for implementing the first order discrete model, as per equations (4.38), (4.39) and (4.40), is shown in Figure 4.3. The implementation of numerical solutions for the continuous and n -order approximated continuous models is similar, except that equation (4.38) and its corresponding parameters used in the iterative solution loops in Figure 4.3 are replaced by the appropriate formulation as per equations [(4.35), (4.36), (4.37)], [(4.41), (4.42), (4.43), (4.44)] or [(4.45), (4.46), (4.47), (4.48)] respectively.

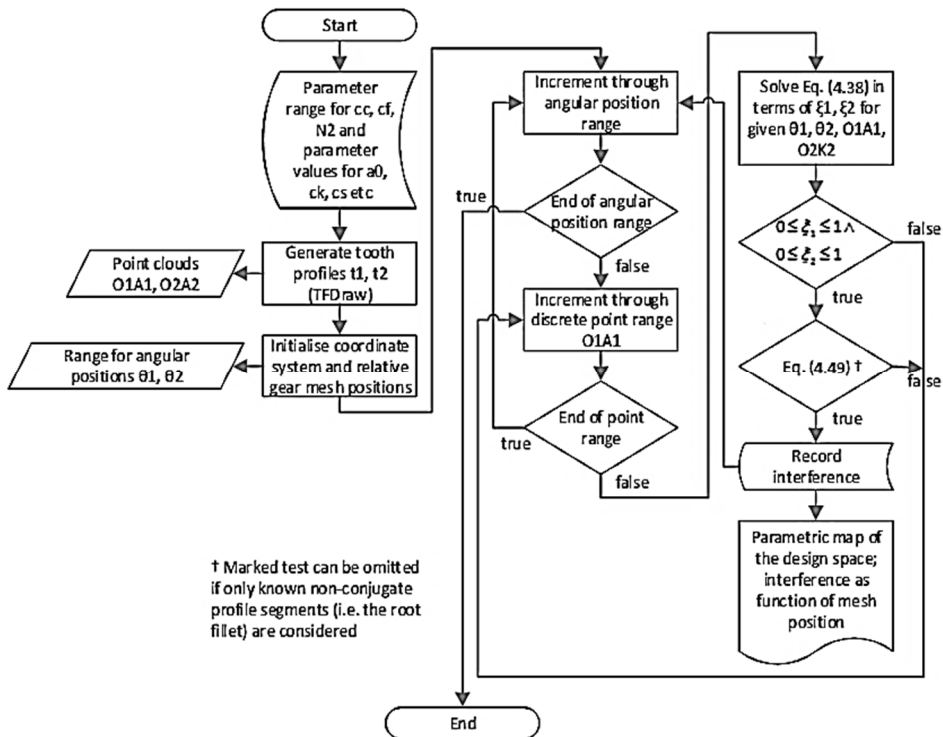


Figure 4.3: Algorithm for the discrete first order model for detecting corner interference

4.3.2. Negative backlash and tooth seizure

Negative backlash, i.e. due to errors in tooth thickness or centre distance, also leads to interference but is essentially different than the phenomenon studied in section 4.3.1. It can be detected by observing only the conjugate parts of the profiles and no corner-to-root contact need take place. Nonetheless, if the leading profiles are positioned in a compatible meshing position, seizure will unveil as corner penetration at the coast sides. Thus, tooth seizure manifests as

a specific case of corner penetration; to test for it, equation (4.17) should be used together with the appropriate expressions for the coast profiles and one of the models in section 4.3.1.3. Note that, unlike corner-to-root contact, equation (4.49) need not be true at the same time.

In the usual case of symmetrical teeth, the symmetry can be used to advantage by inverting the direction of observation of the gear plane. This simple coordinate system transformation allows to use the known lead profile expressions, whereas equation (4.17) remains valid, on the condition that the signs for φ_{s1} and φ_{s2} are reversed.

Special case:

Note that for a special case of zero backlash teeth, where $c_{s1} = c_{s2} = 0.5$, equation (4.18) shows that:

$$\begin{aligned} -i_{12}\varphi_{s2} + \varphi_{s1} &= -i_{12}c_{s2}\frac{2\pi}{N_2} + c_{s1}\frac{2\pi}{N_1} & (4.50) \\ &= (-c_{s2} + c_{s1})\frac{2\pi}{N_1} \\ &= 0 \end{aligned}$$

By applying equation (4.50) to equation (4.17), the latter is reduced to equation (4.16). Therefore for this particular case and provided that the gear teeth are symmetrical, a single-sided interference check using equation (4.17) will be sufficient to detect also tooth seizure. Note that it is otherwise not necessarily the case that tooth seizure can be predicted by single lead-side checks; normally a double-sided check will be required.

4.4. GEOMETRICAL CONSTRAINTS OF THE MODEL RACK CUTTER

The model rack cutter is generally defined as a trapezium with radius applied to its tip, as shown in Figure 3.3. The trapezoidal dimensions impose a limit to the maximum obtainable radius, which can be calculated from the geometrical model of a symmetrical cutter as per equations (3.8) (3.9), (3.10) and (3.11).

Another limiting condition can be obtained by considering the maximum possible dedendum, at which the maximum cutter tip radius is zero. This is the case of a triangular rack ending with a knife edge. The corresponding mathematical condition is simply:

$$\max c_f = \frac{1}{2}\pi(1 - c_s)\cot\alpha_0 \quad (4.51)$$

4.5. MULTI-PARAMETRIC TOOTH MODELLING

For the purposes of this study a set of 13 relevant independent design parameters was considered (dependent ones are shown in parentheses), as shown in Table 4.2. This multi-parametric study focuses on actively varying 6 of

these: the numbers of teeth, dedendum and cutter tip radius coefficients for each gear. The pressure angle, profile shift, addendum and thickness coefficients form another interesting cluster of parameters that will be researched in their own right in a subsequent work and for this study have been assigned constant nominal or customary values. Having decomposed the interference check into two partial checks for each tooth root, as per section 4.3.1, it is furthermore only necessary to consider the root geometry of the reference gear, and therefore reduce the number of parameters from 6 to 4, without loss of generality. These are marked in italics in Table 4.2.

These choices practically allow for a sweep of a significant segment of the design space, which contains the recommendations by many standards for cylindrical gears produced by means of material removal, such as DIN 867 [11], DIN 3972 [12], ISO 53 [27], GOST 13755-81 [28], JIS B 1702-72 [29], AGMA 201.02 and 201.02A [30] etc.

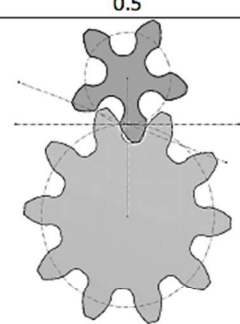
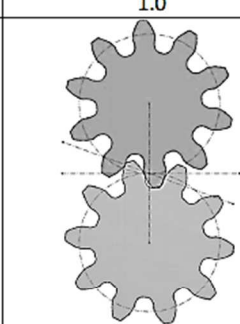
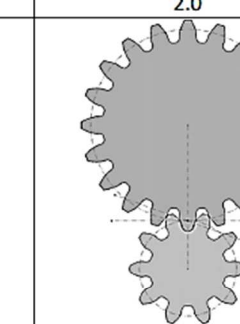
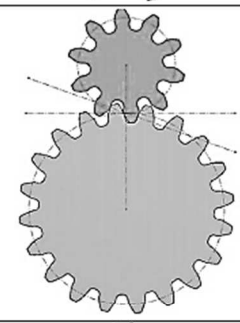
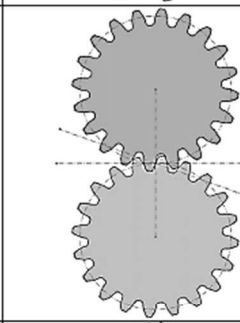
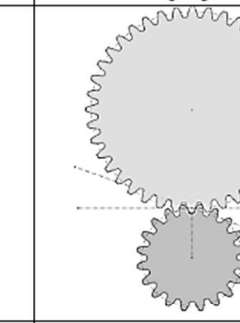
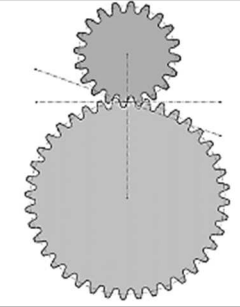
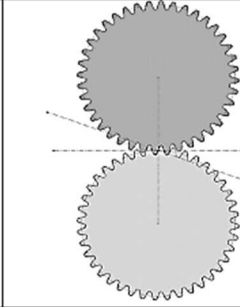
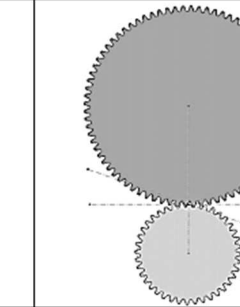
Table 4.2: Design parameters and ranges explored in the study

Gear	α_0	N	i_{12}	c_f	c_c	c_k	c_a	c_m
Ref. (1)	20°	10, 20, 40		1.00-1.25	0.00-0.50	n/a	n/a	0.0
Mating (2)	(20°)	(5, 10, 20, 40, 80)	0.5, 1.0, 2.0	n/a	n/a	1.0	0.5	0.0

For each combination of design parameters N_1, c_{f1}, c_{c1} a discrete model was produced for the reference gear (gear 1), in the form of a sequence of points $\vec{t}_1^{(n)}$ on the gear's reference coordinate system. The in-house programme TFDraw [31, 32] was used for this purpose. To allow for highly accurate solutions, a high point cloud density was used with 300 points per profile. A numerical sensitivity analysis showed that further increasing the density (to up to 1000 points per profile) only results in differences below the 4th significant digit, or less than 0.01%. The reference point \vec{t}_{2-ref} of gear 2 was selected to coincide with the theoretical tooth tip corner and was calculated analytically within TFDraw.

The meshing gear macro-geometries from Table 3.2, omitting the root shape variations due to c_c, c_f , are visualised in Table 4.3

Table 4.3: Gear pair macro-geometries computed in the parametric study, scanning the $N_1 - i_{12}$ space. For clarity the root shape variations due to c_c, c_f are not shown here and nominal values are used ($c_c = 0.30, c_f = 1.25$)

N_1	i_{12}		
	0.5	1.0	2.0
10			
20			
40			

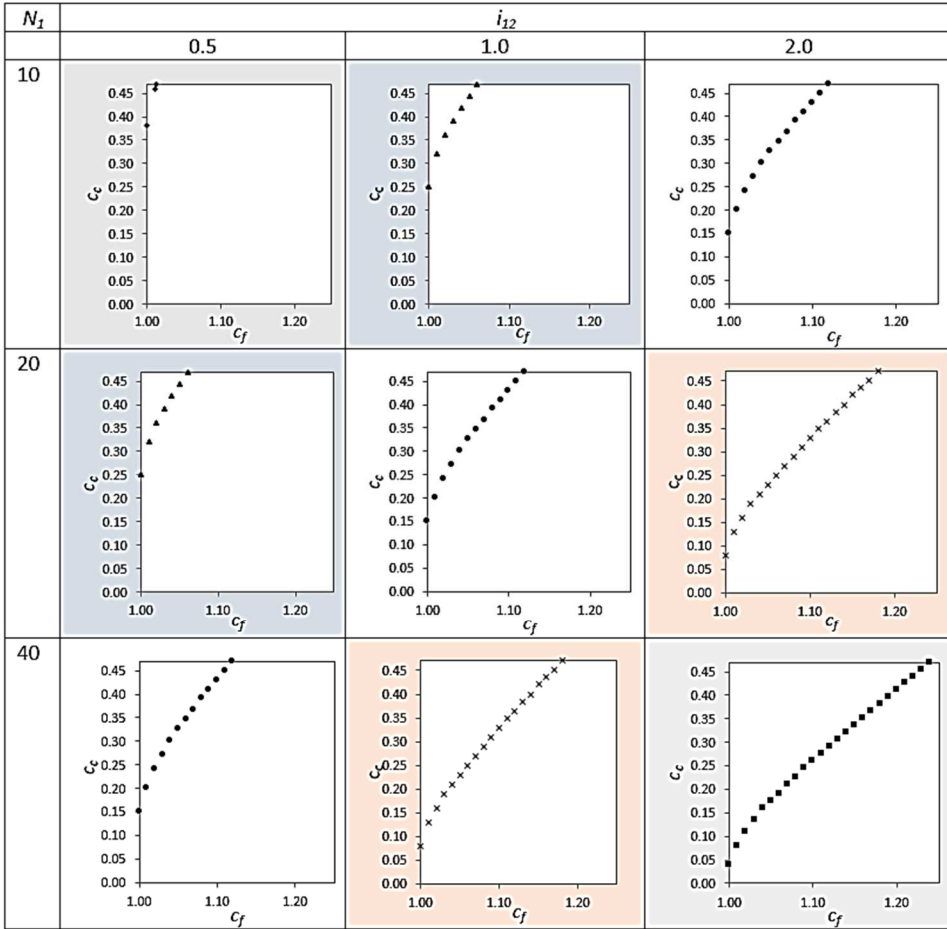
4.6. RESULTS AND DISCUSSION

4.6.1. Analytical results

4.6.1.1. Parametric mapping of the design space: Interference limit curves

The parametric space defined in section 3.5 was input to the interference detection model developed in section 4.3.1.3 using discretised generated profiles in conjunction with equations (4.38), (4.39) and (4.40), as per the implementation shown in Figure 4.3. The limits between interference and non-interference regions in the design space were computed and are plotted in Table 3.4. The results concern interference at the root of the reference gear (gear 1).

Table 4.4: Interference limit curves in the four-parametric design space $c_{f1}, c_{c1}, N_1, i_{12}$. Boundaries on the iso- N_2 combinations are identical. The results in this table correspond 1-1 to the configurations in Table 4.3



The results in Table 4.4 clearly show that the interference limit is not dependent on the number of teeth of the reference gear (gear 1) or the contact ratio, but only on the number of teeth of the mating gear (gear 2). Thus any combination of N_1, i_{12} , where $N_1 i_{12} = N_2$ is constant, produces an identical interference limit curve. This has been further confirmed in additional ‘what-if’ simulations with more random parameter values. This insight allows to reduce by one the dimensions of the parametric space, without loss of generality, and report the results in a simpler diagram in terms of c_{f1}, c_{c1}, N_2 , as shown in Figure 4.4.

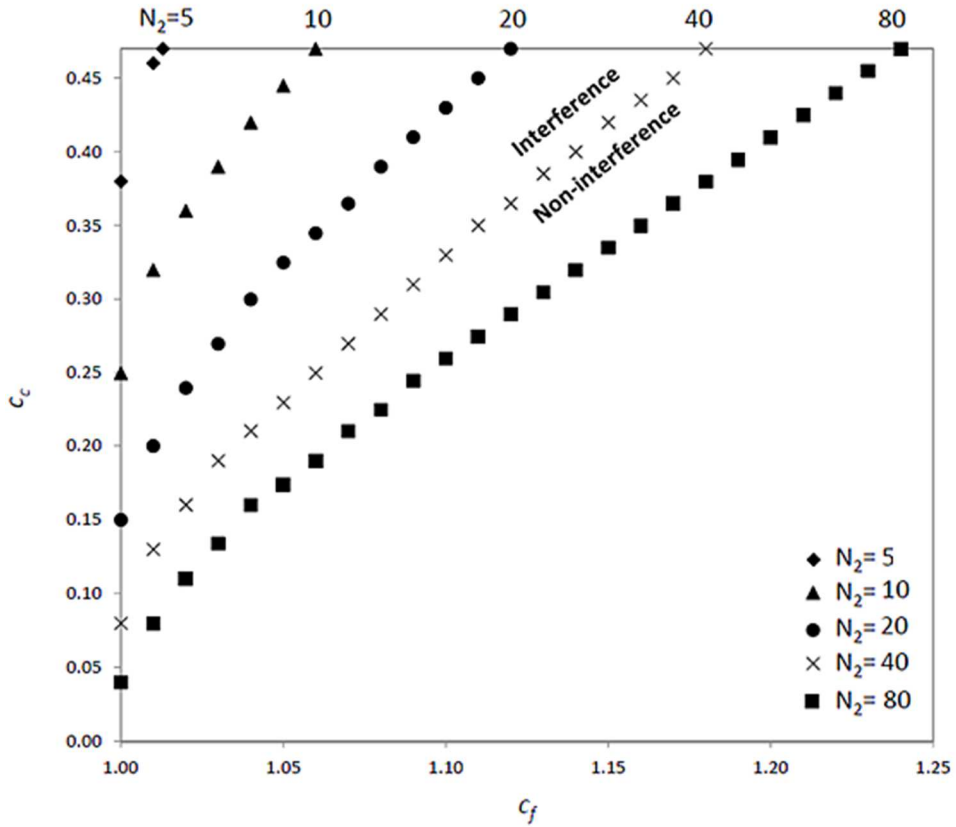


Figure 4.4: Interference limit curves in the three-parametric design space c_{f1}, c_{c1}, N_2 after elimination of parameters N_1, i_{12}

Interestingly, the $c_c - c_f$ curves produced are non-linear, especially near the lower values of c_c, c_f , unlike the linear relationship suggested by equation (4.13), which in turn is based on equation (4.1) and the form circle interference model [14]. We explore this apparent discrepancy in the next subsection.

Next we proceed to plot the predictions of equation (4.13) next to the predictions of the generalised corner penetration model, as per section 4.6.1.1. This is shown in Figure 4.5 for a subset of the results.

For different numbers of teeth equation (4.13) yields a family of parallel straight lines with inclination that is solely the function of the pressure angle, as follows:

$$\frac{dc_c}{dc_f} = \tan\left(\frac{\pi}{4} + \frac{\alpha_o}{2}\right) \sec\alpha_o \quad (4.58)$$

In this case, where $\alpha_o = 20^\circ$, the inclination is $\frac{dc_c}{dc_f} = 1.5198$.

At this point the following observations can be made:

- The form-circle interference model, as per equation (4.13), predicts interference limit lines on the $c_c - c_f$ plane, which are tangent to the exact interference limit curves produced with the generalised corner penetration model.
- At sufficiently high values of c_c, c_f the limit curves coincide with the limit tangents. However, as c_c, c_f decrease the tangents deviate from the exact solutions and thereby predict erroneous interference-safe zones, hence false negatives.
- The error in the case of these false negatives is for 20° involutes of the order of 100% for very shallow dedendum (near $c_f = 1$) irrespective of the number of teeth; in terms of absolute magnitude it is larger at the lower tooth number ranges.
- Conclusively, the form circle interference hypothesis predicts a tangent to the true interference limit curve and is generally not valid, yielding false negatives, except at sufficiently high c_c, c_f values. Nonetheless, it provides a useful limit-tangent to the true interference limit curves calculated by the corner penetration model developed in this chapter.

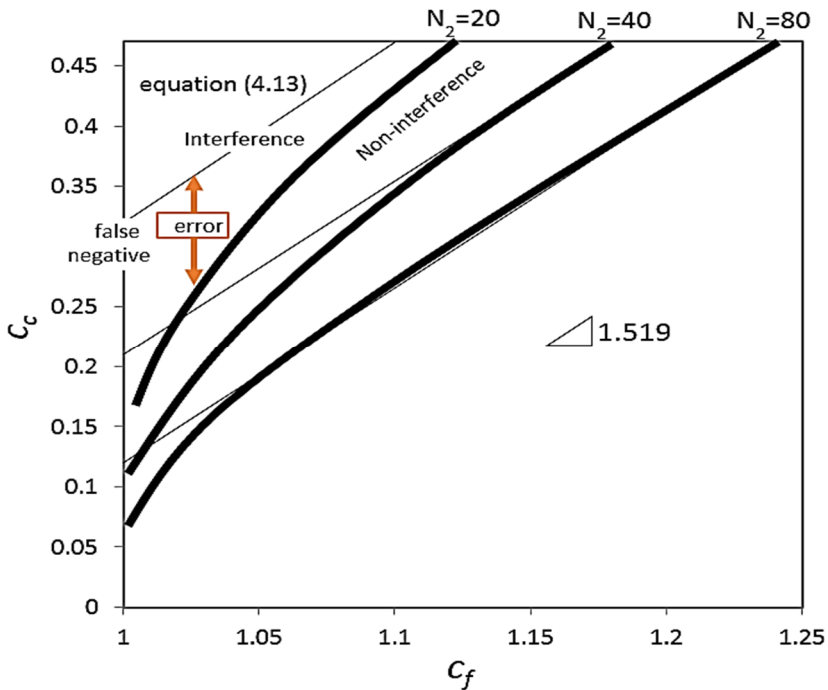


Figure 4.5: Interference limit curves as predicted by equation (4.13) (thin straight lines) versus the corner penetration model (thick lines) on the $c_c - c_f$ plane

4.6.1.2. Speed, accuracy and solution stability

Hereunder we summarise main observations with regard to the speed, accuracy and numerical stability of the solution presented in this chapter:

- The corner contact-and-penetration condition employed in this chapter simplifies the general contact analysis problem by eliminating the profile function of the mating gear $\vec{t}_2(r_2)$ from the contact calculation and substituting it with a single reference point $\vec{t}_2(r_{2-ref})$, typically the tooth corner. This provides a faster and, because of the form of equations (4.35), (4.38), (4.41) and (4.45), which lends itself to explicit calculations, always stable solution. The calculation of the results presented in this chapter over the entire parameter range described in section 4.5 lasted a few seconds in total, not requiring human supervision.
- The presented model for interference, in any of its four variants presented in section 4.3.1.3 (from equation (4.35) to equation (4.49)), is unique in that it introduces directional parameters admitting algebraic values, i.e. ξ_1, ξ_2 , thus allowing exact and explicit solutions, whether analytical or numerical. This is not the case when distance metrics and the corresponding non-linear Euclidean norms are used, as in Polder's approach [15], which by nature increase the calculation overhead.
- The same use of algebraic values allows an immediate assessment not only of the distance from the intersection, which in the direction of the radius of the mating gear is directly calculated as $(\xi_2 - 1)r_{2-ref}$, but also of the penetration versus non-penetration of the two mating profiles. In contrast, considering that a calculation of profile proximity using a Euclidean norm gives no such indication as to the spatial configuration, it is not technically possible for a distance-based solution algorithm to detect penetration without either human supervision, additional assumptions, or additional calculation-intensive algorithms.
- The fast solution times and convergence allow stricter tolerances to be used in the calculation, affording higher accuracy for the same use of computational resources. Furthermore, the clear differentiation between corner contact-and-penetration and negative backlash (seizure) allows for accurate detection of the former mode of interference, which can otherwise be missed by some modern numerical simulation algorithms, as shown in section 4.2.2.

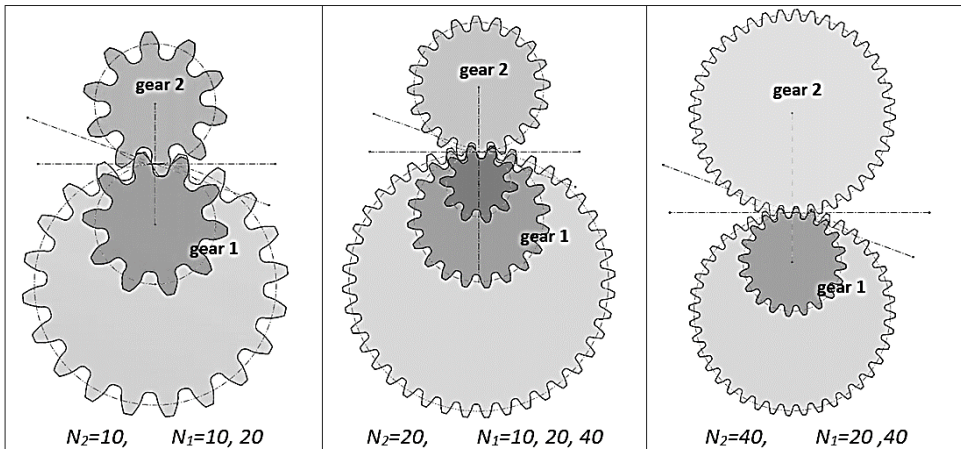
4.6.2. Contact simulation

To verify the results and explain the observed trends, the discretised profile models corresponding to some interesting test cases (at or beyond the limit of interference) were imported into SolidWorks [33] to produce fully detailed models for the reference gear. Mating gear models were also constructed in the same way, where the root geometry was set to a standard definition using $c_f = 1.25$ and $c_c = 0.3$. The meshing was simulated in SolidWorks by rotating the gears in short increments around those positions identified by the corner penetration solution algorithm as having the closest proximity. These contact

simulations confirmed the analytically obtained results predicting marginal interference and non-interference.

Furthermore, these simulations shed some first insight into the accuracy and physical significance of the observation made previously, that the occurrence of corner penetration is not dependent on the number of teeth of the reference gear. Indeed, overlapping simulations of tooth contact were conducted, where reference gears having different numbers of teeth, but with otherwise identical parameters, were placed in mesh with the same mating gear, as shown in Table 4.5. Although each gear has a distinctly different root shape, it has been observed consistently that, as the reference point of the mating gear approaches the roots of the reference gears, the root profiles locally coincide, apparently also in terms of their higher-order derivatives and curvature. To the best knowledge of the authors, this local coincidence has not been previously observed or predicted. This is shown in Figures 4.6 and 4.7 for one case of marginal interference and one case of marginal non-interference respectively and explains sufficiently the simultaneous occurrence (or not) of interference across the different reference gears. Further investigation of this effect must trace the causes to the theoretical geometry of the trochoid and should be addressed in future research.

Table 4.5: Simulated overlays of reference gears (gear 1, bottom) with different numbers of teeth, producing identical interference patterns when meshing with the same gear (gear 2, top)



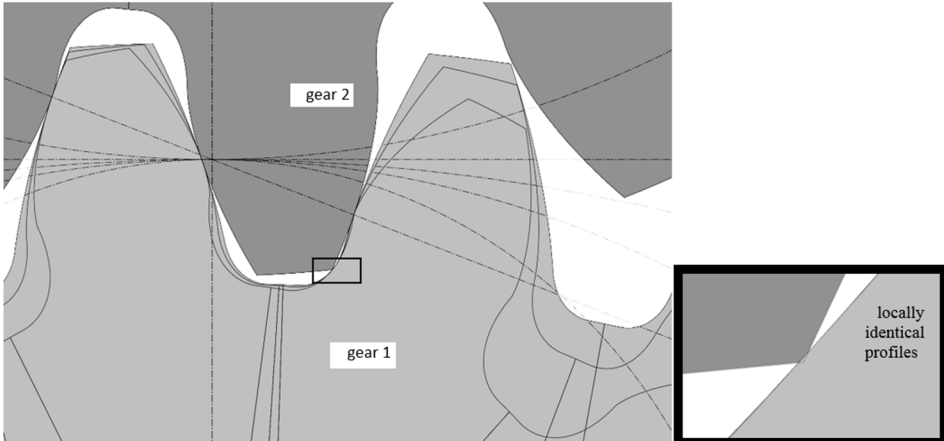


Figure 4.6: Contact simulation showing corner penetration at the tooth root of three reference gears having different numbers of teeth, but otherwise being identical, meshing with the same gear. $N_2=20$, $N_1=10, 20, 40$

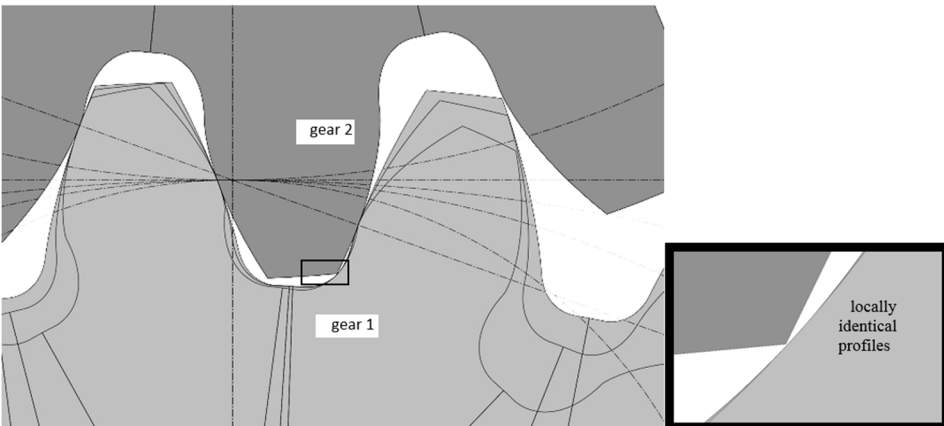


Figure 4.7: Contact simulation showing marginal non-interference at the tooth root of three reference gears having different numbers of teeth, but otherwise being identical, meshing with the same gear. $N_2=20$, $N_1=10, 20, 40$

4.6.3. Design guidelines

4.6.3.1. General insights

The model presented in this chapter was demonstrated for involute gears, but by virtue of the generic form of equations (4.35), (4.38), (4.41) and (4.45), it is applicable to any tooth form, even non-conjugate ones, as in tip-relieved or otherwise modified gears. If the considered profiles are expressed analytically, then also analytical and even potentially explicit solutions can be found to the interference condition.

Focusing now on the involute case study presented, the following design insights emerge:

- The occurrence of interference at the root of a reference gear depends on its dedendum and cutter tip radius and on the number of teeth of the mating gear, on the condition that the latter has a standard addendum. It is independent of the gear module and of the number of teeth of the reference gear, thus allowing entire gear size ranges to be analysed by a single computation.
- The position for interference and non-interference can be determined in the $c_c - c_f - N_2$ design subspace by means of design limit curves, which are bound at high c_c, c_f values by limit tangents.
- The mentioned limit curves represent designs of zero clearance between the root of the reference gear and the tip of its mating gear in at least one position in the mesh cycle. Within the employed parameterisation, no further reduction of clearance is possible. As such, the limit curves represent the gear designs having the most compact tooth forms.
- The farther a design point is from an interference limit curve in the $c_c - c_f - N_2$ non-interference subspace, the larger the root clearance is. Conversely, the farther this point is from an interference limit curve in the $c_c - c_f - N_2$ interference subspace, the more severe the interference if otherwise. Thus, the $c_c - c_f - N_2$ interference mapping may conceivably be used for tolerancing.
- Smaller numbers of teeth in the mating gear make possible the use of larger cutter tip radii and smaller dedendum on the reference gear, irrespective of its own number of teeth). This potentially makes large module-low tooth number gear pairs more viable, if both gears (and especially the more vulnerable pinion) may be strengthened by being made more compact.

4.6.3.2. *Generating compact gears with standard cutters*

It is typically the case in production facilities that the available cutters (i.e. hobs) comply to a single standard, in which case c_c, c_f are practically fixed for the entire size range. Nonetheless, compact gears are obtainable by positive shifting while keeping the outside diameter of the blank the same as in the non-shifted configuration. This will emulate a rack cutter of smaller c_f , while c_c will remain unchanged. The procedure will tend to produce thicker teeth, in which case a second pass with an index offset will be required to obtain the appropriate tooth thickness (and the corresponding clearance) at the pitch circle. In the case of such a procedure, where c_c is fixed in advance, the $c_c - c_f$ plot (Figure 4.6) is not a particularly appropriate chart for selecting the geometry and process parameters. The same results can be plotted instead on the $c_f - N_2$ plane, as shown in Figure 4.8, where the interference limit curves are plotted for tooling-dependent fixed values of c_c .

Lastly, the $N_2 - c_c$ plot, of less technical significance but nonetheless insightful, is shown in Figure 4.9 for completeness.

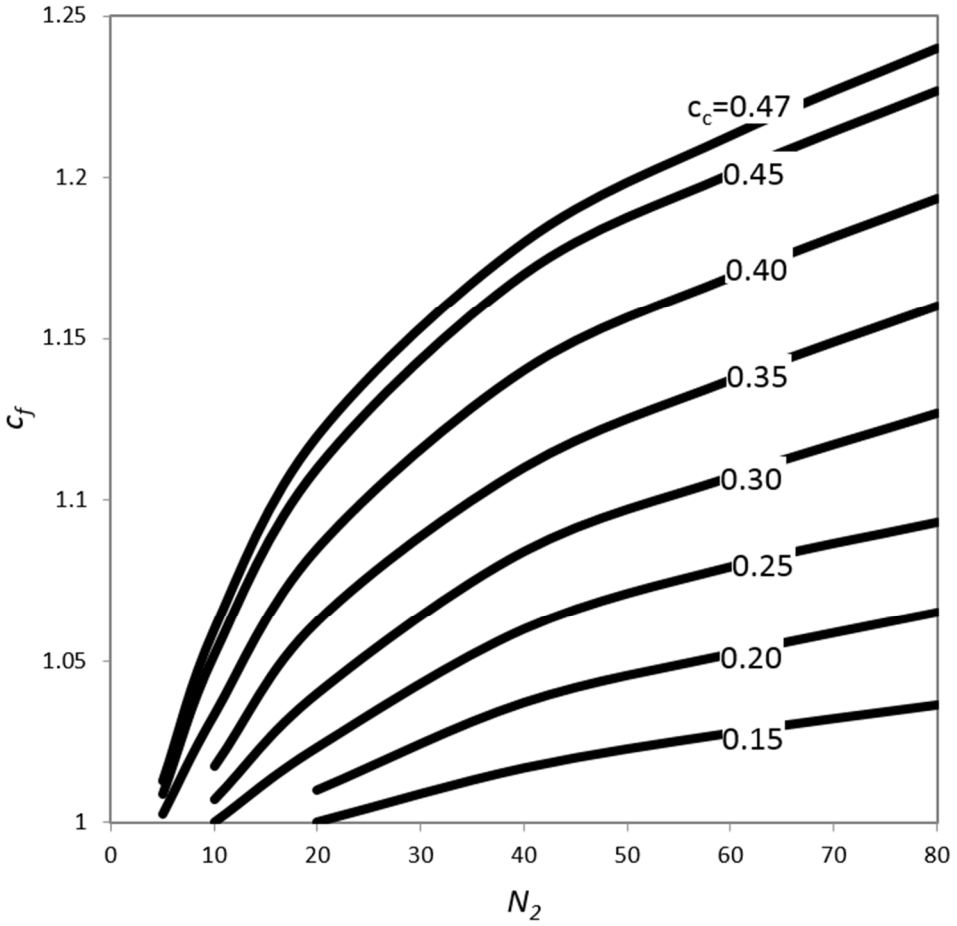


Figure 4.8: Cubic spline approximations of interference limit curves on the $c_f - N_2$ plane

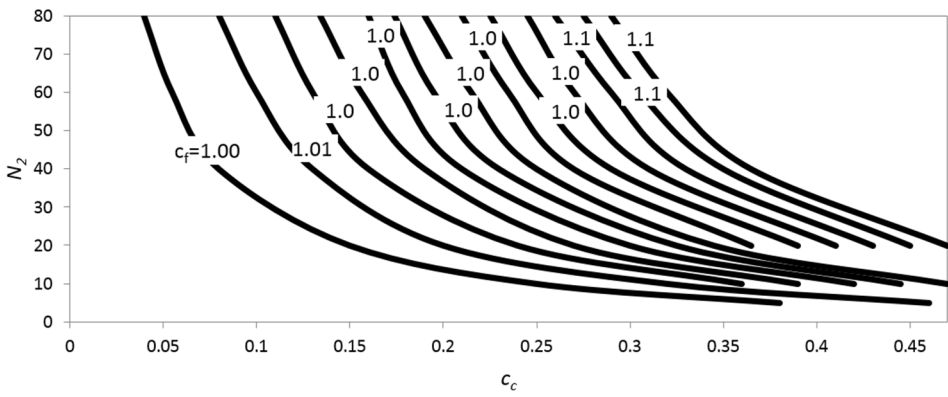


Figure 4.9: Cubic spline approximations of interference limit curves on the $N_2 - c_c$ plane

4.7. CONCLUSION

Starting from basic geometrical principles, this work proposed a new generalised analytical model for interference as non-conjugate corner contact-and-penetration at the tooth root. From this a geometrical condition was extracted that admits a simple and explicit mathematical solution for either analytically expressed or discretised tooth profiles. This condition overcomes inaccuracies in previous form-circle-based analytical models and admits simpler and faster solutions than competitive numerical simulations for interference.

The model was applied to compact involute teeth and was used for the extraction of design guidelines in the form of interference limit curves, which, for a given gear irrespective of its number of teeth, were shown to depend only on its dedendum and cutter tip radius and the number of teeth of the mating gear.

REFERENCES

1. Savage, M., Coy, J. J., Townsend, D. P., 1982, Optimal tooth numbers for compact standard spur gear sets, *Journal of Mechanical Design*, 104:749-758
2. Nguyen, T., Lin, H. H., 2011, Compact design for non-standard spur gears, *Journal of Mechanical, Aerospace and Industrial Engineering*, 2(1):1-15
3. Kapelevich, A. L., 2013, *Direct gear design*, CRC Press
4. ANSI/AGMA 1006-A97, 1997, Tooth proportions for plastic gears, Appendix F: generating gear geometry without racks
5. KISSsoft AG, version 03/2011
6. Gear Design Pro 2011, Dontyne System, V4.5
7. GearTeq 2012, Camnetics Incorporated, version 20.32.341
8. Geartrax 2012, Camnetics Incorporated, version 20.671 for SolidWorks 2012
9. Reuleaux, F., 1894, The constructor: a handbook of machine design with portrait and over 1200 Illustrations, *H.H. Suplee*, Philadelphia
10. Kleiss, R. E., Kapelevich, A. L., Kleiss, N. J., 2001, New opportunities with molded gears, *AGMA Fall Technical Meeting*, Detroit, October 3-5
11. DIN 867, 1986, Basic rack tooth profiles for involute teeth of cylindrical gears for general engineering and heavy engineering
12. DIN 3972, 1952, Reference profiles of gear-cutting tools for involute tooth systems according to DIN 867
13. Smith, J. D., 2003, *Gear Noise and Vibration*, 2nd Ed., CRC Press
14. Litvin, F. L., 1994, *Gear geometry and applied theory*, Prentice Hall
15. Polder, J. W., Broekhuisen, H., 2003, Tip-fillet interference in cylindrical gears, *Proceedings of ASME Design Engineering Technical Conference*, 4 A, Chicago, IL, 473-479
16. Litvin, F. L., Vecchiato, D., Fuentes, A., Gonzalez-Perez, I., 2004, Automatic determination of guess values for simulation of meshing of gear drives, *Computer Methods in Applied Mechanics and Engineering*, 193(33-35):3745-3758

17. Jin, X., Zhang, T., Yang, H., 2012, Research on gear assembly interference check based on virtual technology, *Communications in Computer and Information Science*, 288 CCIS(PART 1):45-52
18. Chen, X.-X., Lin, S.-Z., Xing, J.-Z., Liu, Y.-S., 2011, Simulation on gear backlash and interference check of harmonic drive with circular-arc teeth profile, *Computer Integrated Manufacturing Systems*, 17(3):643-648
19. Zhao, Z.-Q., Zhang, C.-L., Cheng, A.-M. , Du, Q., 2008, Profile overlap interference constraint conditions of internal parallel move gears transmission, *Transaction of Beijing Institute of Technology*, 28(10):856-859
20. Jin, X., Zhang, Z.-J., Ye, X., Li, Z.-X., 2006, Calculating model of interference amount for miniaturized gear and shaft shrink fit, *Journal of Beijing Institute of Technology (English Edition)*, 15(2):138-143
21. Sosa, A. D., Echeverria, M. D., Moncada, O. J., 2005, Analysis of stresses in ADI internal gears mounted with interference: Distortion and residual stresses effects, *Latin American Applied Research*, 35(3):241-246
22. Komori, M., Kubo, A., Takahashi, T., Tanaka, T., Ichihara, Y., Takeda, K., 2004, Failures of involute gears due to contact of side edge and tip edge of tooth (4th report, failure caused by trochoidal interference due to elastic deformation of tooth), *Transactions of the Japan Society of Mechanical Engineers, Part C*, 70(12):3581-3589
23. Sun, Y., Zhang, C., Zhou, L., 2004, Meshing interference for spur gears with profile modification, *Proceedings of the 11th World Congress in Mechanism and Machine Science*, 777-781
24. Spitas, C., Spitas, V., 2006, Can non-standard involute gears of different modules mesh?, *Journal of Mechanical Engineering Science*, 220(8):1305-1313
25. Spitas, C., Spitas, V., 2006, Calculation of overloads induced by indexing errors in spur gearboxes using multi-degree-of-freedom dynamical simulation, *Proceedings of the Institution of Mechanical Engineers, Part K: Journal of Multi-body Dynamics*, 220(4):273-282
26. Townsend, D. P., 1992, *Dudley's gear handbook*, McGraw Hill
27. ISO 53, 1974, Cylindrical gears for general and heavy engineering- Standard basic rack tooth profile
28. GOST 13755-81, 1981, Basic requirements for interchangeability, Gearing cylindrical evolute gears. Basic rack
29. JIS B 1702-72, 1976, Accuracy for spur and helical gears
30. AGMA, 201.02 and 201.02A, 1968, Tooth proportions for coarse pitch involute spur gears Alexandria VA: Gear Manufacturers Association (AGMA)
31. Spitas, V., Costopoulos, T., Spitas, C., 2007, Fast modelling of conjugate gear tooth profiles using discrete presentation by involute segments, *Mechanism and Machine Theory*, 42(6):751-762
32. Spitas, V., Costopoulos, T., Spitas, C., 2002, A quick and efficient algorithm for the calculation of gear profiles based on flank involutization, *Proceedings of the 4th GRACM Congress on Computational Mechanics*, Patra, Greece
33. Dassault Systèmes, SolidWorks 2013, The Digital Product Experience

5- Influence of centre distance deviation on the interference

Summary

Gear design generally considers global geometry like tooth profile shape and centre distance, however it needs also to consider the tolerances introduced in the manufacturing and assembly of two mating gears. The influence of these tolerances can be predicted better by understanding the behaviour of such manufacturing and assembly errors in conjunction with the gear geometry design process. To address this, in the present study the influence of the centre distance deviation and of the design parameters (i.e. cutter tip radius, dedendum, and tooth thickness) of the tooth profiles on interference will be investigated. An analytical modelling framework for interference of a gear pair is developed, which is used to characterise a structurally well-defined gear meshing system. The tolerance zone is evaluated, with regard to cutter tip radius, dedendum, tooth thickness and centre distance deviation for a structurally well-defined gear mesh model. Different gear transmission ratio, contact ratio and a pressure angle of 20° have been considered. The results of the present work can be used as a guideline for the tolerance design of a gear pair.

5.1. INTRODUCTION

A nominal (or perfect) geometry (i.e. one that is following the law of gearing [1-3]) is most typically assumed in the design of gears, as any deviations are expected automatically to be of little significance, as long as good adherence to manufacturing and design standards [4-10] is maintained. In reality, gears are not as perfect as desirable and this matter cannot be ignored in the precision design of (non-standard) gears.

Gears are designed based on global geometry like tooth geometry and centre distance, but it is necessary to consider also the tolerances introduced in assembly [11-17] and manufacturing [17-20] of a gear pair. Knowing the tolerance to such deviation is essential for designers to control manufacturing, assembly and the design process of gears itself.

In particular, the errors in gear transmission systems can be categorised in three parts: I) manufacturing errors like pitch, indexing, profile and distortion errors [16,21-22], II) assembly errors like eccentricity, misalignment and centre distance deviation [16,21] and III) errors in the design of gear geometry with regard to the design parameters [23-24].

With regard to assembly errors, while crowning can be used partly to alleviate the ill-effects of misalignments, errors in the centre distance may not be counteracted in such direct manner: While a larger centre distance will have little effect on an involute transmission, a shorter one may cause seizure if zero-clearance, zero backlash and/or radially compact gears are concerned, and in either case there are well-documented dynamical influences as well [25-29].

In fact, the larger the errors, the larger the risk of interference and vibration, which can result in system-wide catastrophic failure [15]. Operation loads in general, combined with the flexibility of shafts and bearings cause rapid oscillation of the centre distance about its constant as-assembled value, thus increasing the error.

The analytical formulation for tooth interference has been suggested by Litvin [1]. However the solution is valid for studying interference occurring along the line of action only, which is a false premise in most non-standard and compact gear design configurations. Figure 5.1 presents the relations between different parameters of the present study.

The main focus of this work is to investigate the influence of centre distance deviation on the interference of mating gears, in conjunction with other coupled design parameters defining the tooth form (cutter tip radius, dedendum, tooth thickness and number of teeth). Since Litvin's model [1] is generally not applicable in the case of non-standard gear geometry, a new model has to be investigated: Interference for non-standard gears occurs due to the penetration of the tip one gear into the tooth root of the mating gear as has been explained in Chapter 3. The new interference model has to cover this penetration mechanism that takes place at the corner-to-root contact region.

In addition new analytical relations for interference occurrence are presented in terms of rack-cutter tip radius, dedendum and tooth thickness. The number of teeth and contact ratio for a combination of standard and non-standard gears has been considered. Non-dimensional analytical modelling is used to obtain results for entire gear families. The results of interference occurrence are compared, according to formulations of gear geometry as per Litvin's known model [1]. The tolerance zone is evaluated with regard to all considered parameters for a pressure angle of 20 degrees.

The results show that the design parameters of the geometry as well as the centre distance deviation have an important role in the occurrence of interference. The "safe design zone" for the different tolerances is thus extracted. The results of the present study yield a better understanding of the influence of the design parameters and centre distance deviation on interference of two mating gears and the charts can be used directly as design guidelines.

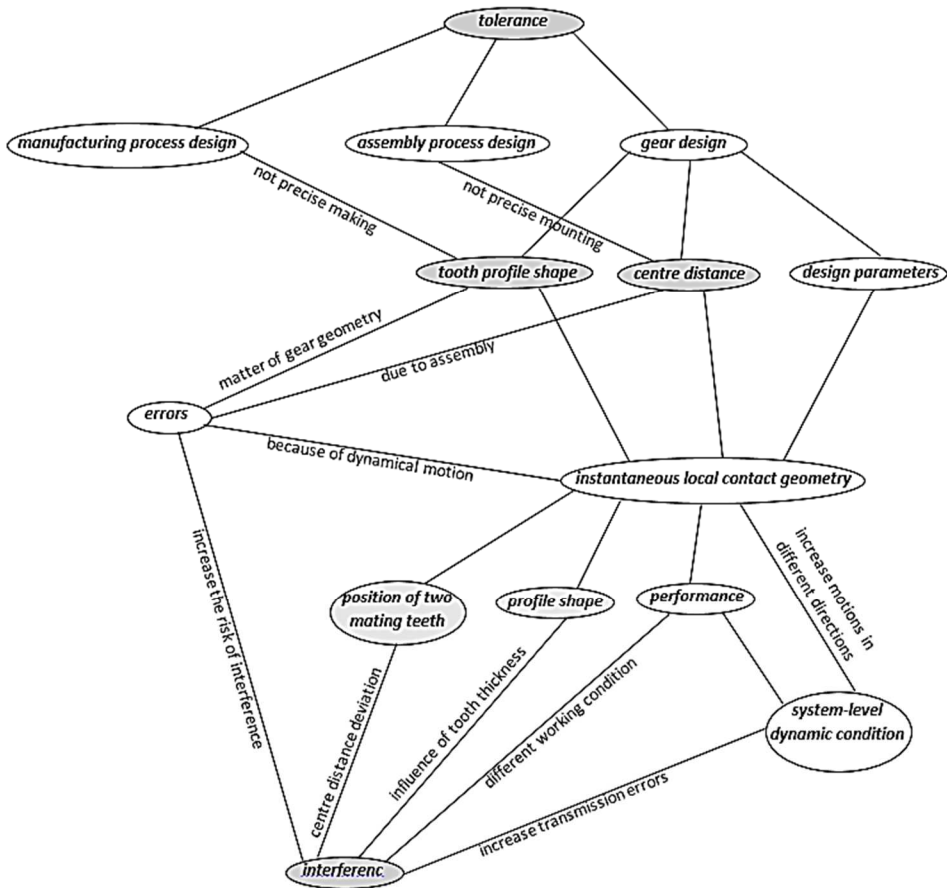


Figure 5.1: Qualitative relations between different parameters on the design of tolerance

5.2. GEOMETRICAL CONSTRAINTS IMPOSED BY MANUFACTURING PROCESS

A cross-section of the tooth of a generating rack cutter for various cases of tip radius is defined as a trapezium with a radius applied to its tip, i.e. as shown in Figure 3.3 [23-39]. There is a practical limitation on the maximum radius for a given whole depth, which can be calculated from the geometrical model of a symmetrical cutter as shown in Figure 3.3

5.3. ASSEMBLY AND CENTRE DISTANCE

The nominal centre distance is determined as follows:

$$a_{12} = m \left(\frac{N_1 + N_2}{2} + c_{m1} + c_{m2} \right) \quad (5.1)$$

Where m is module, N_1 and N_2 are the number of teeth for gear number 1 and 2, respectively, c_{m1} and c_{m2} are the addendum modification of gear number 1 and 2, respectively; that in this work the value for both c_{m1} and c_{m2} are zero. Because of the assembly errors, it is difficult to mount a gear pair in the exact position dictated by the centre distance. In addition, instantaneous local contact geometry deviation due to system dynamics cause deviations in centre distance [27-29]. In fact, a bit larger centre distance is used to improve the operation pressure angle. For instance, if the actual centre distance is made 1.7116% larger, gears cut with 20° hobs or shaper-cutters will run at 22.5° pressure angle [2]. According to the same source, because of the mentioned occurrences, it is possible to have another centre distance, which is called as operating centre distance. The deviations of centre distance can cause further problems such as interference between two mating teeth. The consequence of interference will affect wear, pitting, scoring and tooth breakage. For this study, the influence of centre distance deviation for non-standard tooth geometry is evaluated. The tooth shape profile is changed by changing the design parameters. With the given amount of centre distance deviation, the effects of the design parameters on the interference between a pair of gears are investigated. Non-dimensional centre distance deviations $\delta=0, 0.01, 0.02, 0.03, 0.05, 0.07$ are considered. Gears 1 and 2 are a non-standard and a standard gear, respectively. Different gear transmission ratios $i_{12}=0.25, 0.5, 1, 2$ are considered.

5.4. MODELLING OF INTERFERENCE

Generally, interference is an undesirable occurrence during meshing. Interference destroys the gear teeth, and it is generally detrimental to gear meshing. There are several methods to avoid interference i.e. by using shorter addendum for one or both meshing gears. Nevertheless, other problems will be unveiled, such as: increased vibration, wear and reduced power transmission [40].

Due to the influences of addendum on interference, some researchers investigated the influence of addendum modification on interference [41-44]. Another solution is that to eliminate interference by means of one of the generation processes i.e. using the cutting tool which removes the interfering portion of the flank. This method is not a satisfactory solution because of the effect of tooth weakening that interference is replaced by undercutting [40] and the apparent shortening of the meshing involute portion leading to reduced contact ratio.

Increasing the number of teeth for small gears can be an alternative option to solve this problem. On the other hand this solution causes increase of the gear size and pitch line velocity and an optimum module – number of teeth solution has to be sought for.

Using larger pressure angle is also as a solution which increases sliding velocity and reduces tip thickness, while increasing bearing loads and frictional forces at the same time [40].

Each solution in interference on gear geometry has its own consequence. Sometimes giving rise to a new problem such as noise, vibration and wear which is related to the other parameters in gear geometry. A new solution must be found, according to the parametric design with some limitations. It has to be able to use the new restrictions to remove interference and further problems which are related to it.

In this analysis, the corner contact-and- penetration model of section 4.3 is applied. The occurrence of interference on the path of contact considers two mating tooth flanks, as shown in Figure 4.2. During a mesh cycle, these flanks will engage in conjugate action around the pitch point.

The points of the gear profile were generated using an in house computer programme in *C++*, using the algorithm presented in Figure 4.3.

In the corner contact instant illustrated in Figure 4.2, O_1 is the original point of the gear number 1 and O_2 is the original point of the gear number 2. The algorithm has been used in this study for implementing the corner contact's model, is in accordance with equations (from (4.35) to (4.49)) which have been introduced in section 4.3.1.3.

5.5. RESULTS AND DISCUSSION

5.5.1. Multi-parametric tooth modelling

A non-dimensionalisation scheme is applied, which permits the simultaneous modelling of entire families of gears and lends wider generality to the results of the numerical solutions of this study. This methodology has been introduced in section 3.2.1.1.

For the purposes of this study a set of relevant independent design parameters for a pair of involute gears was considered as follows:

Pressure angle is 20 degrees for both gears. Number of teeth for gear 1 ranges between 10, 20 and 40. Gear transmission ratios have been considered as 0.25, 0.5, 1.0, 2.0 and 4 which means that for gear 2, the number of teeth will be 5, 10, 20, 40 and 80, respectively. The mating gear geometry is kept standard; therefore the value of dedendum, cutter tip radius, addendum and profile shift modification coefficient will be 1.25, 0.3, 1.0 and 0.0, respectively. Tooth thickness for gear 2 is assumed to be compatible to gear 1. For gear 1 as non-standard gear different values for the design parameters are studied as: dedendum: between 1.00~2.20, cutter tip radius: between 0.00~0.62, addendum: 1.0, tooth thickness: between 0.50~0.70, profile shift modification: 0.0. Different centre distance deviations are considered as per section 3.3. ($\delta = 0, 0.01, 0.02, 0.03, 0.05, 0.07$).

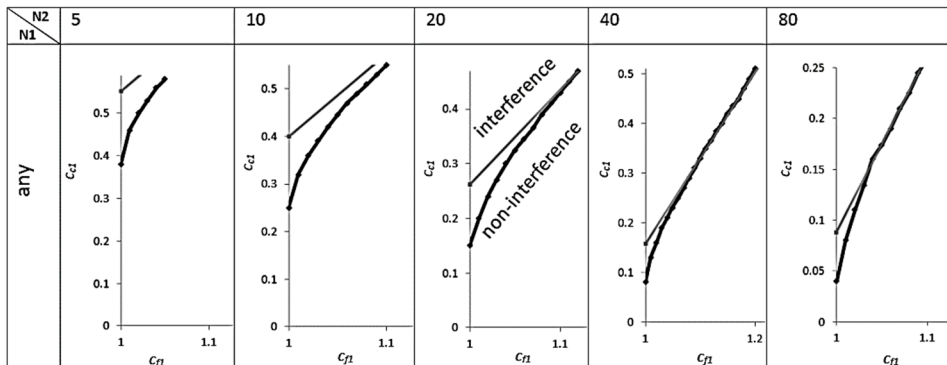
5.5.2. Interference limit curves

The parametric mapping of the design space was conducted by means of the corner contact-and-penetration model of interference which has been developed in section 4.3. The limits between interference and non-interference regions in the design space were computed and are plotted in Table 5.1.

In this table, the straight grey lines are the boundary line between interference and non-interference that has been suggested by Litvin [1] according to equation (4.13). The point & black line curves are the result of using the presented corner contact-and-penetration model. If the selected design parameter combination corresponds to a point will be above each line/curve, it means that the interference will be happened and if it will be below the line, it means that there is no interference and the design will be safe, according to the model corresponding to the particular curve.

The results concern interference at the root of gear 1, therefore the curves are presented mathematically as minimum (root) clearance function $\delta(c_f, c_c)$. This new function is a function of addendum and cutter tip radius for each gear pair. The results of parametric mapping present in Table 5.1. It can be found that the interference limit is independent of the number of teeth of gear 1 or the contact ratio, and only dependent on the number of teeth of gear 2.

Table 5.1: Interference limit curves as predicted by equation (4.13) (grey lines) versus the corner contact-and-penetration model (points & black lines) on the $c_{c1} - c_{f1}$ plane



5.5.3. Tooth thickness limitation

The maximum value of c_{c1} with changing the amount of c_{f1} has been introduced by equation (3.10) while the value of c_s is given. In equation (3.10) different values for tooth thickness (c_{s1}) present some limitations for different combinations of c_{c1} and c_{f1} . Figure 5.2 presents the feasible design space for different $c_{c1} - c_{f1}$ combinations in regard with tooth thickness limitations. With increasing the amount of tooth thickness, it is clear that the tolerance area for different values of c_{c1} , c_{f1} will be decreased.

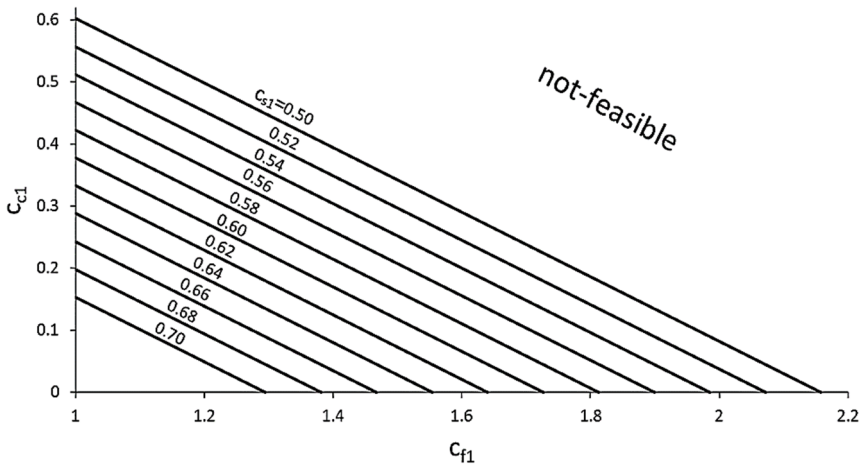


Figure 5.2: The limitation of $c_{c1} - c_{f1}$ combination for different values of tooth thickness (c_{s1}). (c_{s2} assumed to be compatible)

5.5.4. Centre distance deviation

The influence of centre distance deviation for interference of a gear pair with different combinations of cutter tip radius and dedendum coefficient is presented in Figure 5.3.

It is clear that increasing the deviation of centre distance causes a decrease of the interference risk for a gear pair. With decreasing the gear transmission ratio the interference risk will be increased, while the value of centre distance deviation is given. With increasing the value of centre distance deviation and decreasing the value of tooth thickness simultaneously, the risk of interference will be increased.

There is a special result about the centre-distance deviation of larger gears. With increasing the number of teeth of the mating gear ($N_1=20$, $N_2=80$), the gap between the interference curve for nominal centre distance ($\delta=0.00$) and the centre distance with deviation of 0.01 ($\delta=0.01$) will be increased. This means that the sensitivity of occurrence of interference which is expressed mathematically as $\nabla\delta(c_f, c_c)$, and hence the corresponding uncertainty risk are reduced in the case of gears with more teeth, as can be seen in Figure 5.3.

Figure 5.3 only shows results for $N_1=20$, however identical trends appears for $N_1=5$, 10, 40 and 80, because it was shown in Table 3.4 that the corner contact-and-penetration interference at the root of gear 1 is not dependent on N_1 .

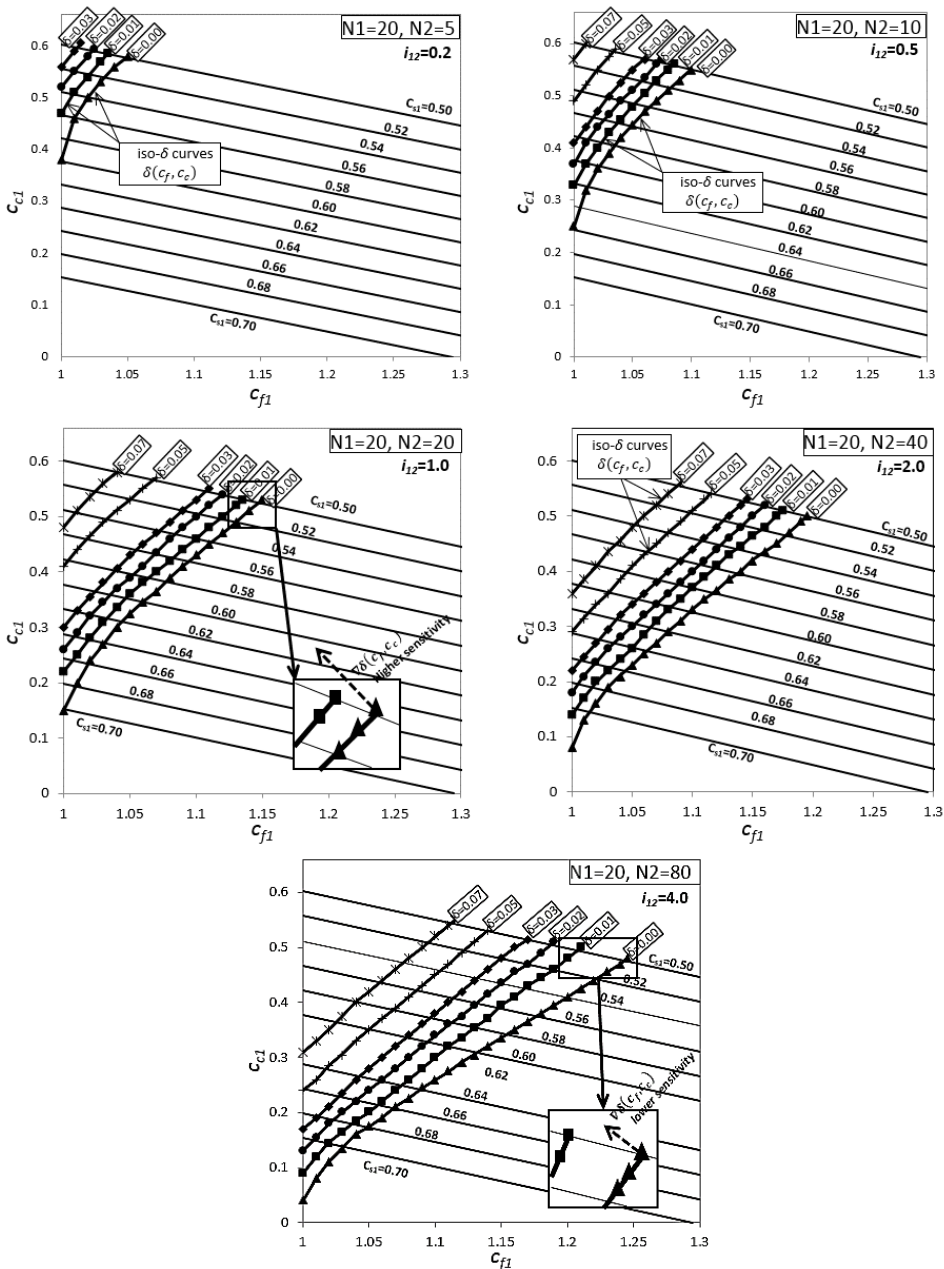


Figure 5.3: Influence of centre distance deviation on interference risk for different gear tooth combinations & transmission ratios

5.5.5. Implication on gear tolerancing

An illustration of the tolerance zone and how it affects design is presented in Figure 5.4. For instance, design at the centre of zone A is within the interference

envelopes (thick lines), but clearly zone A itself exceeds them. Therefore this design presents a high interference risk. Because of centre distance deviation (assembly errors, dynamics), it is wiser to select i.e. zone B (Figure 5.4), which presents a more safely placed tolerance zone.

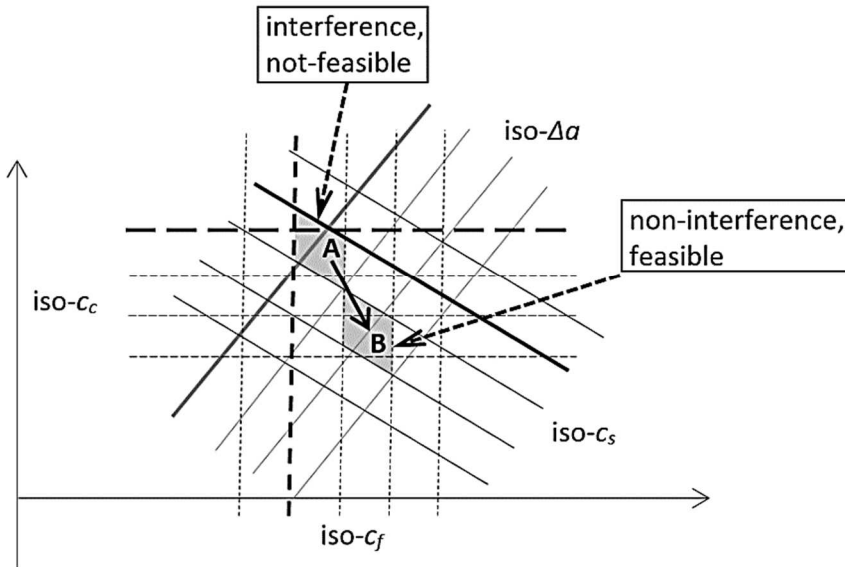


Figure 5.4: Influence of different design parameters on the tolerance zone

5.6. CONCLUSION

In the present work the influence of the design parameters of gear tooth geometry and of the centre distance deviation on interference risk have been investigated, to determine the effect of errors in gear assembly process. A corner contact-and-penetration model for interference has been presented, which allows for minimising the clearance between gear teeth while maintaining interference-free operation. This is applicable to both analytically expressed and numerically discretised tooth profiles. Non-dimensionalisation methodology has been used to quantify the influence of the design parameters of gear geometry on interference risk. The tolerance zone has been evaluated, with regard to cutter tip radius, dedendum, tooth thickness and centre distance deviation. Different gear transmission ratios, contact ratios and a pressure angle of 20 degrees have been considered. The results of the present study introduced a new guideline for the tolerance-based design of gear geometry, incorporating tolerance zones.

REFERENCES

1. Litvin, F. L., 1994, Gear geometry and applied theory, *Prentice Hall*
2. Errichello, R., Townsend, D. P., 1992, Gear tooth calculations, in: D.P. Townsend (Ed.), *Dudley's Gear Handbook*, *Mc-Graw Hill*
3. Buckingham, E., 1988, Analytical Mechanics of Gears, *Dover Publications Inc.*
4. ANSI/AGMA 1006-A97, 1997, Tooth proportions for plastic gears, Appendix F: Generating gear geometry without racks, AGMA, Alexandria, VA.
5. ISO 53, 1974, Cylindrical gears for general and heavy engineering- Standard basic rack tooth profile
6. DIN 867, 1986, Basic rack tooth profiles for involute teeth of cylindrical gears for general engineering and heavy engineering
7. DIN 3972, 1952, Reference profiles of gear-cutting tools for involute tooth systems according to DIN 867
8. AGMA, 201.02 and 201.02A, 1968, Tooth proportions for coarse pitch involute spur gears, Alexandria VA: Gear Manufacturers Association (AGMA)
9. GOST 13755-81, 1981, Basic requirements for interchangeability, Gearings cylindrical evolvent gears, Basic rack
10. JIS B 1702-72, 1976, Accuracy for spur and helical gears
11. Li, S., 2007, Effects of machining errors, assembly errors and tooth modifications on loading capacity, load-sharing ratio and transmission error of a pair of spur gears, *Mechanism and Machine Theory*, 42:698-726
12. Li, S., 2007, Finite element analyses for contact strength and bending strength of a pair of spur gears with machining errors, assembly errors and tooth modifications, *Mechanism and Machine Theory*, 42:88-114
13. Wang, J., Qin, D., Lim, T. C., 2011, Influence of combined assembly error and bearing elasticity on spur gear tooth contact load distribution, *Proceedings of the Institution of Mechanical Engineers, Part C: Journal of Mechanical Engineering Science*, 225:1507-1521
14. Falah, A. H., Alfares, M. A., Elkholy, A. H., 2013, Localised tooth contact analysis of single envelope worm gears with assembly errors, *International Journal of Advanced Manufacturing Technology*, 68:2057-2070
15. Wang, J., Lim, T. C., Yuan, L., 2013, Spur gear multi-tooth contact dynamics under the influence of bearing elasticity and assembly errors, *Proceedings of the Institution of Mechanical Engineers, Part C: Journal of Mechanical Engineering Science*, 227(11):2440-2455
16. Velez, P., Maatar, M., 1996, A mathematical model for analysing the influence of shape deviations and mounting errors on gear dynamic behaviour, *Journal of Sound and Vibration*, 191(5):629-660
17. Nakhatakyan, F. G., 2008, Determining the flexural stress concentration factor for gear teeth taking into account elastic deformations and errors in manufacture and assembly of gearing elements, *Journal of Machinery Manufacture and Reliability*, 37(4):348-351
18. Cheon, G. J., Parker, R. G., 2004, Influence of manufacturing errors on the dynamic characteristics of planetary gear systems, *KSME International Journal*, 18(4):606- 621

19. Ottewill, J. R., Neild, S. A., Wilson, R. E., 2009, Intermittent gear rattle due to interactions between forcing and manufacturing errors, *Journal of Sound and Vibration*, 321:913-935
20. Bonori, G., Pellicano, F., 2007, Non-smooth dynamics of spur gears with manufacturing errors, *Journal of Sound and Vibration*, 306:271-283
21. Ben Amar, M., Maatar, M., Maalej, A., 2006, Experimental and numerical analysis of the effect of gear center distance variation and misalignment error on the dynamic behavior of narrow-faced spur gear drives, *Mecanique et Industries*, 7(1):71-78
22. Spitas, C., Spitas, V., 2006, Non-linear dynamical simulation of spur gears with indexing errors and profile modifications', *Proceedings of the 25th IASTED International Conference on Modelling, Identification, and Control*, Lanzarote, Canary Islands, 354-359
23. Spitas, C., Spitas, V., 2007, Four parametric design study of the bending strength of circular-fillet versus trochoidal-fillet in gear tooth design using BEM, *Mechanics Based Design of Structures and Machines*, 35(2):163-178
24. Spitas, C., Spitas, V., 2008, Effect of cutter pressure angle on the undercutting risk and bending strength of 20° involute pinions cut with equivalent nonstandard cutters, *Mechanics Based Design of Structures and Machines*, 36(2):189-211
25. Lin, H. H., Liou, C. H., Oswald, F. B., Townsend, D. P., 1996, Balancing dynamic strength of spur gears operated at extended center distance, *American Society of Mechanical Engineers, Design Engineering Division (Publication) DE*, 88:23-28
26. Jin, L., Ma, F., Peng, F., 2012, The influence of the center-to-center distance on the accuracy of the serration with the new gear hob, *Applied Mechanics and Materials*, 217-219:1908-1911
27. Skrickij, V., Bogdevičius, M., 2010, Vehicle gearbox dynamics: Centre distance influence on mesh stiffness and spur gear dynamics, *Transport*, 25(3):278-286
28. Han, J., Wang, G., 2006, Study on eccentricity and minimum geometrical center distance of the eccentric involute gears transmission, *Materials Science Forum*, 505-507:985-990
29. Wang, X., Chen, Y., 2012, Study of the mathematic modeling method of the center distance minimum for gear set of spur gear, *Advanced Materials Research*, 430-432:2000-2003
30. Spitas, V., Costopoulos, T., Spitas, C., 2007, Fast modelling of conjugate gear tooth profiles using discrete presentation by involute segments, *Mechanism and Machine Theory*, 42(6):751-762
31. Spitas, V., Costopoulos, T., Spitas, C., 2002, A quick and efficient algorithm for the calculation of gear profiles based on flank involutization, *Proceedings of the 4th GRACM Congress on Computational Mechanics*, Patra, Greece
32. Colbourne, J. R., 1987, *The Geometry of Involute Gears*, Springer-Verlag
33. Wildhaber, E., 1946, Conjugate pitch surfaces, *American Machinist*, 90(13):150-152
34. Yeh, T., Yang, D. C. H., Tong, S., 2001, Design of new tooth profiles for high-load capacity gears, *Mechanism and Machine Theory*, 36:1105-1120

35. Tavakoli, M. S., Houser, D. R., 1986, Optimum profile modifications for the minimization of static transmission errors of spur gears, *Journal of Mechanisms, Transmissions, and Automation in Design*, 108(1):86-95
36. Bonori, G., Barbieri, M., Pellicano, F., 2008, Optimum profile modifications of spur gears by means of genetic algorithms, *Journal of Sound and Vibration*, 313(3-5):603-616
37. Chen, Z., Shao, Y., 2013, Mesh stiffness calculation of a spur gear pair with tooth profile modification and tooth root crack, *Mechanism and Machine Theory*, 62:63-74
38. Sankar, S. and Nataraj, M., 2011, Profile modification-a design approach for increasing the tooth strength in spur gear, *International Journal of Advanced Manufacturing Technology*, 55(1-4):1-10
39. Spitas, C., Spitas, V., 2007, A FEM study of the bending strength of circular fillet gear teeth compared to trochoidal fillets produced with enlarged cutter tip radius, *Mechanics Based Design of Structures and Machines*, 35(1):59-73
40. Maitra, G. M., 2001, Handbook of gear design, *Tata McGraw-Hill Education*
41. Spiegelberg, C., Christie, M., 2003, Torque loss in spur gears with interference, *Proceedings of the Institution of Mechanical Engineers, Part J: Journal of Engineering Tribology*, 217:385-395
42. Baglioni, S., Cianetti, F., Landi, L., 2012, Influence of the addendum modification on spur gear efficiency, *Mechanism and Machine Theory*, 49:216-233
43. Atanasiu, V., Iacob, M. R., 2010, Tooth wear effects on dynamic transmission error of spur gears with addendum modifications, *International Review of Mechanical Engineering*, 4(6):638-644.
44. Li, S., 2008, Effect of addendum on contact strength, bending strength and basic performance parameters of a pair of spur gears, *Mechanism and Machine Theory*, 43(12):1557-1584

6-Design to maximise compactness and bending strength

Summary

A methodology is developed to design non-standard involute gear geometries generated by cutting tools with standard and non-standard proportions, such as to produce compact tooth meshes by minimizing the unused radial clearance, while at the same time avoiding detrimental corner contact at the tooth root. It is shown under which parametric combinations of dedendum and tip radius of the equivalent rack (cutter) the feasible design solutions for different tooth numbers and transmission ratios produce lower tensile bending stresses at the root, thus leading to optimal solutions for compact gears and allowing the identification of a global optimum. The analysis leads to a comprehensive mapping of the four-parametric design space in consideration of interference and undercutting and the discovered optima are compared to the design solutions found in current ISO, AGMA, GOST and JIS standards.

6.1. INTRODUCTION

In spite of the increasing possibilities of using explicit design methods for producing matched gear pairs, as in the case of moulded plastic gears, the large majority of gears used in power transmissions must still be batch-produced by some form of generating process, typically hobbing, milling, shaving, grinding etc. The design of such profile generated gears is subject to several restrictions arising from the need to use practical and therefore generally simple shapes for the generating cutters, which are typically abstracted for the purpose of analysis to an equivalent generating rack. In the case of involute gears, which comprise the large majority of generated gears, the rack profile is a trapezium. The positioning of the rack relative to the centre of the gear blank and its outside radius defines the tooth whole depth and the dedendum- and considering the blank's outside diameter also the addendum. A rounding is typically applied to the rack tip to strengthen the cutter, which at the same time is responsible for producing a different trochoid shape for the tooth root than would otherwise be obtained by an unrounded tip. A larger cutter tip radius results in the removal of less material from the tooth root, producing wider tooth roots with trochoidal shapes characterised by larger radii of curvature. Generally, as follows from basic principles of the mechanics of tooth bending, both shortening the dedendum and enlarging the root fillet leads to stronger gear tooth forms.

However, not all combinations of whole depth/ dedendum and cutter tip radius are viable:

- All other design parameters kept constant, increasing the whole depth will be limited by the tooth thickness, as it will tend to produce pointed teeth at a certain value, beyond which the outside diameter of the gear will be compromised by the cutting of the second tooth flank and the as-produced whole depth will be in fact reduced.
- Reducing the whole depth and/ or increasing the cutter tip radius can conversely lead to interference at the tooth root, where the mating teeth will tend to develop secondary non-conjugate corner contact and penetration with catastrophic results during operation.
- Too low a cutter tip radius and/ or large whole depth may also lead to undercutting during manufacturing. While it is quite possible for undercut gears to function, undercut tooth forms are weaker than non-undercut ones and are usually best avoided for this reason.

Currently a number of models are known in gear theory to predict the geometrical (pointing, undercutting) and kinematical integrity (interference) for any given geometry, which may be used to detect and simulate the problematic conditions described above [1-5]. Based on these models, as well as basic CAD simulations, current commercial-grade software such as KISSsoft [6], Gear Design Pro [7], GearTeq [8] and GearTrax [9] also provide facilities to detect the same problems. However, while these analysis capabilities are competent, no comprehensive model exists to-date that is able to solve the same problem inversely, hence to dictate viable and optimal tooth designs so as to achieve specific performance goals, such as i.e. bending strength. Thus to design using the present models and methods many iterations are needed and it is generally not known where the optimal solutions lie in the design space. This is clearly manifested by polyphony of standards for gear tooth geometry currently in force. Even for the 20° involute system only, ISO [10], AGMA [11], GOST [12], JIS [13] etc offer many alternative rack (and hence tooth) proportions, in some cases also overlapping partly, but there is no evidence that these 'industry best practices' are optimal in terms of some performance index (i.e. strength), or even nearly-so.

Over the years, several scientific models have been proposed to deal with important aspects of the gear design problem. I.e. a number of researchers [14-29] have developed parametric models for bending strength calculation and optimisation. A number of different interference models can be found in [1, 30-37], with Litvin's model [1] probably being the most well-known, although recently found to have limited validity in the case of non-standard gear geometries. Undercutting studies can be found in [1, 4, 38-41].

With regard to gear geometry, different researchers have studied the effects of profile shifting [42-48], addendum [24, 49-56] and tooth thickness [56-60], while

dedendum and tooth root geometry have also been featured in a number of studies [16, 61-66].

Yet the wealth of studies underlying the mentioned highlights remains largely compartmentalised, each study addressing by necessity a limited scope within the design space. In the context of multi-parametric gear design, and especially considering how geometric compatibility and interference impose non-linear constraints on what actually can be achieved, a method is still missing that will allow a multi-parametric overview of how compactness, undercutting and interference affect feasible designs in terms of contact ratio and (resistance to) different failure modes. Hereafter we shall explicitly concern ourselves with bending failure only, noting that inclusion of additional failure modes (i.e. pitting, scoring) can be achieved in the same manner.

In this chapter, we start from basic principles to frame a comprehensive model for the parametric design of profile-generated involute gears. The model simultaneously considers all applicable geometric and kinematical constraints [14] to qualify each point in the design space (hence each combination of geometrical gear design parameters) in terms of geometrical and kinematical integrity. Bending strength is also considered as a relevant performance metric, and, building on prior results by the research team, the design space is characterised in terms of where the highest bending strength can be obtained. The same is done for the contact ratio, which is an important indicator for load sharing and dynamics. Based on each performance metric, a global optimum is thus identified; at the same time, given the multi-parametric nature of the problem, it may be desirable to dictate a-priori or restrict the range of certain parameters, such as the number of teeth and the transmission ratio, and thus loci of optimal solutions are also identified.

The main contribution of this chapter is in synthesising the different compartmentalised state-of-the-art solutions it builds upon into one comprehensive multi-parametric model, with subsequent exploration of the full design space with regard to the considered parameters. While the focus here is on compactness, non-interference, bending strength and contact ratio, the same paradigm is extensible to pitting, scoring etc failure modes. Design guidelines are extracted and multi-dimensional maps of the design space are given in terms of dedendum/ whole depth, cutter tip radius, and numbers of teeth. Benchmarks against standards as well as known non-standard 'best industry practices' reveal significant potential in the less explored parts of the design space, especially with regard to a multitude of low-clearance, compact gear designs. In spite of several works dealing with compartmentalised aspects of the same design problem, neither the presented integral approach nor these findings have been shown previously in the literature.

6.2. MODELLING

6.2.1. Non-dimensional functional definition of compact gearing

We employ the same non-dimensionalisation concept as introduced in section 3.2.1.1, whereby all gear dimensions are expressed as ratios of the gear module m .

Whole depth is the sum of the addendum and dedendum and is readily identifiable from the cutting geometrical setup, unlike the latter two, which depend also on the cutting kinematics, which in turn define the pitch circle. In this study, we consider the gears to be meshed at their nominal centre distances and pitch circles, maintaining thereby the link to the cutting kinematics for convenience.

In the same convention, we consider an addendum coefficient of $c_k = 1$ and therefore manipulate the dedendum and whole depth simultaneously, considering that:

$$c_w = c_k + c_f \quad (6.1)$$

Where c_w is the non-dimensional whole depth and c_f is the dedendum coefficient.

6.2.2. Interference analysis

In this analysis, the corner contact-and-penetration model of section 4.3 is applied. The occurrence of interference on the path of contact considers two mating tooth flanks, as shown in Figure 4.2. During a mesh cycle, these flanks will engage in conjugate action around the pitch point. The points of the gear profile were generated using an in house computer programme in C++, using the algorithm presented in Figure 4.3.

6.2.3. Undercutting analysis

Conditions of non-undercutting tooth by a rack-cutter (Figure 3.2) may be determined by using the general approach presented based on simple geometric considerations, which has been introduced by Litvin [1]. The undercutting limitation is expressed as:

$$\alpha_0 - \gamma \geq 0 \quad (6.2)$$

From Figure 3.2 of section 3.2.1.1, we know however that:

$$\gamma = \tan^{-1} \frac{c_t}{\frac{\tan \alpha_0}{(r_{o,u} - c_t)}} \quad (6.3)$$

Thus from equation (5.3) and substituting some details of Figure 3.2 in equation (6.2) we conclude that:

$$\alpha_0 - \tan^{-1} \frac{c_f \tan(45^\circ + \frac{\alpha_0}{2}) - c_c \cos \alpha_0}{\tan \alpha_0 [(r_{o,u} - c_f) \tan(45^\circ + \frac{\alpha_0}{2}) + c_c \cos \alpha_0]} \geq 0 \quad (6.4)$$

6.2.4. Tooth thickness analysis

Equations (3.10) and (3.11) are used for tooth thickness analysis to find the limitation of tooth thickness with regard to the cutter tip radius and dedendum coefficient.

6.2.5. Non-dimensional stress analysis: Root bending

Tooth bending stress Stresses can be calculated in non-dimensional teeth σ^* by assuming unitary tooth width $b = 1$ and unitary normal load $P_N^* = 1$. The non-dimensional stress is related to the actual bending stress σ_F using equation (3.2) as:

$$\sigma_F = \sigma_F^* \frac{P_N}{bm}$$

as suggested by Townsend [2] and Spitas [15, 23]. The actual stress calculations can be conducted by any suitable FEA.

6.3. RESULTS AND DISCUSSION

6.3.1. Geometrical feasibility

For the purposes of this study a set of relevant independent design parameters was considered, as shown in Table 6.1.

Table 6.1: Design parameters and ranges explored in the study

Gear	α	N	i_{12}	c_f	c_c	c_k
Ref. (1)	20°	10, 20, 40		1.00-2.20	0.00-0.62	1.0
Mating (2)	20°	5, 10, 20, 40, 80	0.5, 1.0, 2.0	1.25	0.30	1.0

6.3.1.1 Interference Limit Curves

Parametric mapping of the design space was conducted by means of corner contact-and-penetration model of interference which has been developed in section 4.3. The limits between interference and non-interference regions in the design space were computed and were presented in Table 5.1. The results concerned interference at the root of gear 1.

The results of parametric mapping as shown in Table 5.1 clearly indicated that the interference limit was independent of the number of teeth of gear 1 (reference gear) or the contact ratio, but only on dependent on the number of teeth of gear 2 (mating gear).

6.3.1.2 Undercutting limitation

Using equation (6.1) for different number of teeth for gear 1 gives us this opportunity to design a gear without undercut as shown in Figure 6.1. With increasing the number of gear teeth and the value of c_f , the safety of the design in the non-undercut part will be increased.

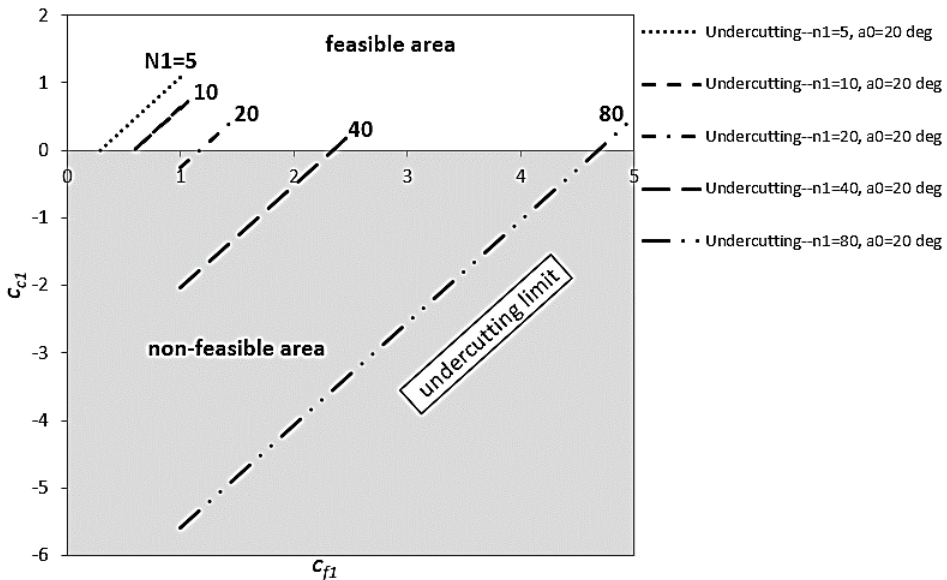


Figure 6.1: Undercutting limitation of $c_{c1} - c_{f1}$ combination for different number of teeth. The grey area is non-feasible design area

6.3.1.3 Tooth thickness limitation

The maximum value of c_c , with changing the amount of c_f while the value of c_s is given was presented by means of equation (3.10). Different value for c_s as tooth thickness coefficient presented the limitation of the combination of c_c and c_f . The limitation of $c_c - c_f$ combination for different value of tooth thickness coefficient (c_s) was presented in Figure 5.2. The design space for different

combination of c_c and c_f will be less with increasing the amount of tooth thickness.

6.3.2. Bending strength and standards benchmark

Four different combinations of c_c and c_f for a nonstandard gear ($N_1=10, 20, 40$) meshing with a standard gear ($N_2=5, 10, 20, 40, 80$) the latter as per ISO53.2 profile B [10]/ DIN867. Different gear transmission ratios are also taken into account, using the listed tooth number combinations. For the purposes of this investigation ANSYS was used to simulate the loading of different gear pairs with consistent boundary and loading conditions. For bending stress calculations point loading at the Highest Point of Single Tooth Contact (HPSTC), which, in consideration of Saint-Venant's principle, produced fast and accurate calculations of the root stress using single tooth models meshed with iso-parametric PLANE82 elements having an increased mesh density at the tooth root. The local mesh density choice was selected based on a sensitivity analysis based on initial trials with increasing density, until no measurable error in the stress prediction was produced.

Based on these results which are shown in Figure 6.2 the following observations can be concluded:

- A) With increasing the value of c_c and c_f , the maximum bending stress (σ_1) will be decreased, due to a reduction of the stress concentration and of the bending moment at the tooth root cross-section;
- B) With increasing the number of teeth for gear 1, while the number of teeth for gear 2 is fixed and the value of c_{c1} and c_{f1} are given; σ_1 will be decreased, due to the increase in contact ratio and corresponding decrease in the bending moment due to the lowering of the HPSTC. This trend is non-linear and becomes less significant with increasing numbers of teeth;
- C) With increasing the gear transmission ratio, σ_1 will be increased (this is in agreement with point B). Furthermore, combining B and C makes it obvious that with decreasing the gear transmission ratio while the value of m_c is increasing, σ_1 will be decreased;
- D) The choice of c_{f1} is limited by the number of teeth, with small tooth numbers allowing only a small variation in c_{f1} ; and
- E) Likewise, small tooth numbers limit the choice of c_{c1} . Obviously, the value of gear contact ratio (m_c) is independent on the values of c_c and c_f .

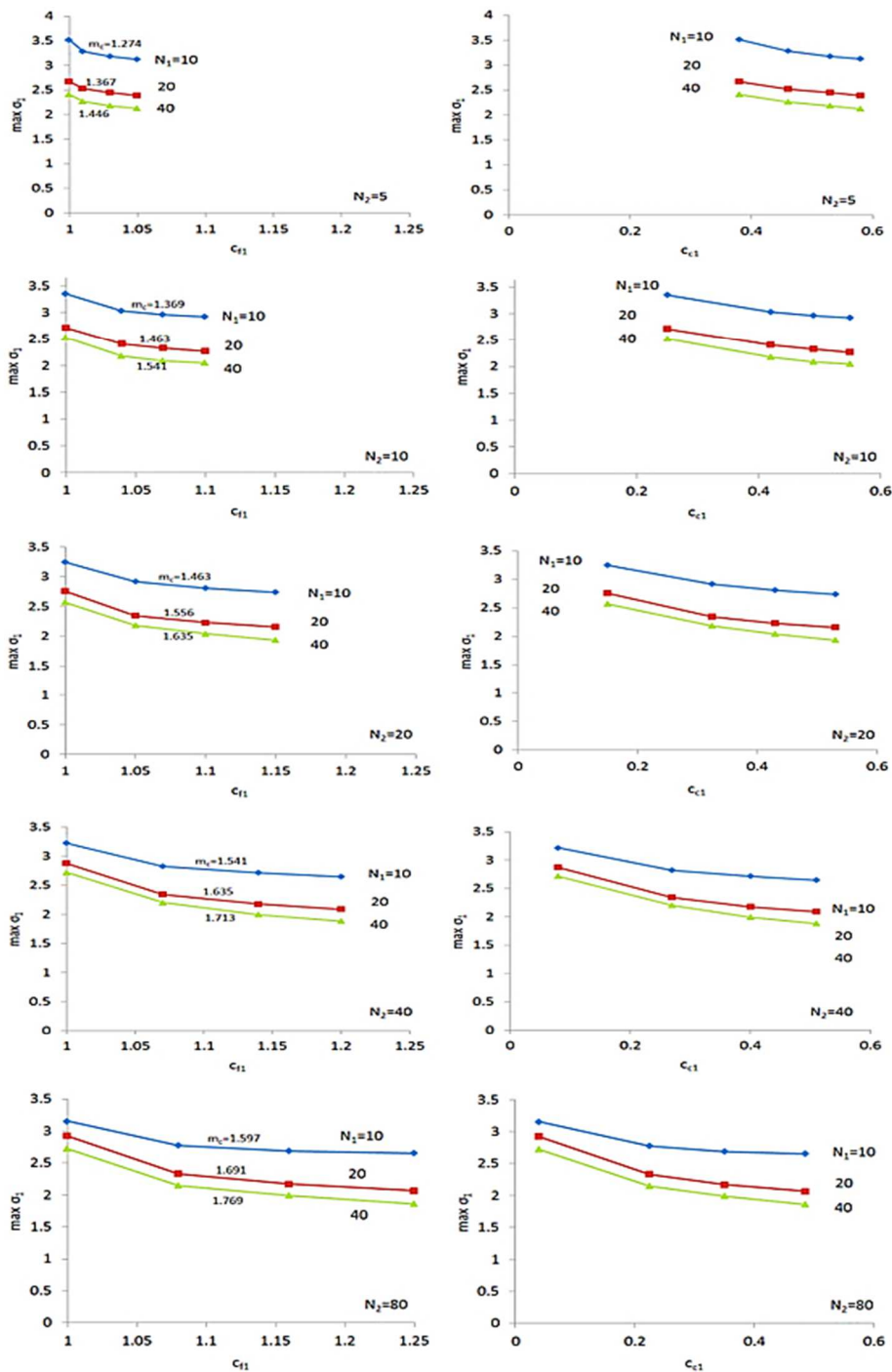


Figure 6.2: Maximum non-dimensional root stress corresponding to the corner contact (CCP) limit curve as a function of c_{f1} (left column) or c_{c1} (right column), N_1 and N_2

6.4. DESIGN GUIDELINES

By gathering all the results of interference (section 6.3.1.1), undercutting (section 6.3.1.2), tooth thickness (section 6.3.1.3), root bending stress (section 6.3.2) analysis, a mapping of the four-dimensional design space including dedendum and cutter tip radius coefficient for gear 1 and number of teeth of gear 1 and 2 and corresponding design guideline can be developed as shown in Figure 6.3.

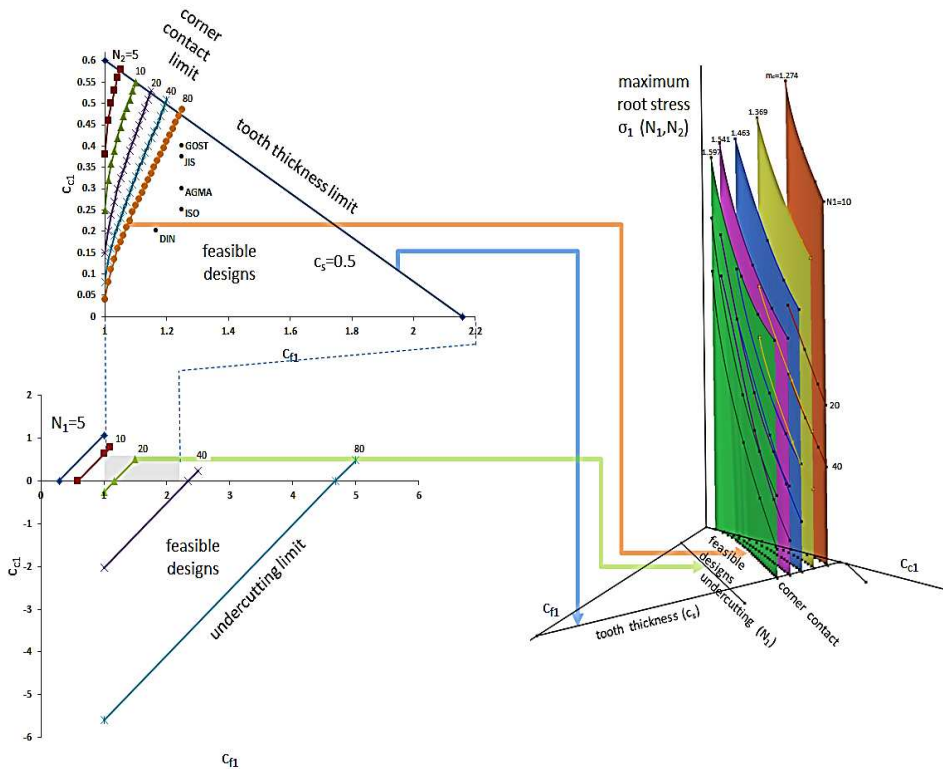


Figure 6.3: Depiction of four-dimensional design space c_{f1}, c_{c1}, N_1, N_2 , showing the locus of feasible designs as bounded by the various interference and undercutting limits, as well as the compact designs that produce the minimal stresses

Figure 6.3 serves as a case study to show the mapping of the four-dimensional design space for $N_1=20$ (non-standard gear), $N_2 = 5, 10, 20, 40, 80$ (standard gear), with $c_s=0.5$ because of the tooth thickness limitation and c_{f1} and c_{c1} between $1 \sim 2.16$ and $0 \sim 0.6$, respectively.

The space of feasible designs is delimited by the tooth thickness and undercutting limit lines. By means of corner contact-and-penetration model we can identify the interference limit lines: The risk of interference will be increased with using decreasing values for c_f and increasing values for c_c . However, these

are the exact designs that have the lowest root stress/ highest root strength. Therefore Figure 6.3 can be used to identify optimal designs and allow an assessment of interference risk (proximity to the interference lines) versus bending strength increase.

In particular, it is already established that the optimum design will be the intersection point of corner contact limit curves and tooth thickness limit lines (Chapter 4). Figure 6.3 reveals that these points are far from the standard points which means that there is promising room for exploration and improvement. It is apparently some of the compact designs (i.e. designs having a near-zero minimum tip-to-root clearance), which are closest to interference, that produce the minimal root stresses.

Table 6.2. shows a comparison of the root stresses for the standard and the identified optimal compact designs. It is evident that by optimally adapting the dedendum and cutter tip radius coefficients to the number of teeth, significant reduction can be achieved in terms of the maximum root bending stress, resulting in higher bending strength. The achieved stress reduction at the reference gear is more prominent in the case of a mating gear with a smaller tooth number, because this affords much larger root radius and smaller dedendum, but remains significant regardless of the tooth number of the mating gear. Depending on the tooth numbers, stress reduction in this case is seen to range between 16%-48% (compared to DIN3972 I), 15%-46% (compared to ISO 53 B), 12%-43% (compared to AGMA 201.02-68), 8%-42% (compared to JIS B 1702-72), 6%-41% (compared to GOST 13755-68).

In comparison with the suggested standard values for c_c and c_f for different standards (i.e. GOST, JIS, AGMA, ISO, DIN), the optimal design solutions revealed in Figure 6.3 and tabulated in Table 6.2 allow a better-informed choice of the relevant tooth design parameters, and the development of gear designs of known strength and safety without trial-and-error iterations, in a first-time-right manner.

Using Figure 6.3 as a nomogram and guideline can serve to explore, compare and select at-a-glance gear designs, standard or otherwise, that possess sufficient bending strength for a given application and that are safe from undercutting and interference when in mesh with another known gear. The limiting influence of the tooth thickness is also considered. Alternatively, different values for c_c and c_f can be selected to achieve the minimum root stress for a given tip-to-root clearance, as per the methodology in a prior limited study (Chapter 3). Gear vibration excitation can further be accounted for and controlled, to a degree, by means of the contact ratio –particularly in the case of integer loaded contact ratio; such a study is omitted here.

Table 6.2: Maximum root stress obtained by different designs

Standard	c_{e1}	c_{f1}	N_2	Maximum bending stress at root (Mpa)
This chapter	0.580	1.05	5	2.39
	0.550	1.10	10	2.26
	0.530	1.15	20	2.15
	0.510	1.20	40	2.09
	0.485	1.25	80	2.06
GOST 13755-68	0.4	1.25	5	4.06
			10	3.81
			20	2.47
			40	2.30
			80	2.18
JIS B 1702-72	0.375	1.25	5	4.12
			10	3.87
			20	2.52
			40	2.35
			80	2.23
AGMA 201.02-68	0.3	1.25	5	4.23
			10	4.04
			20	2.65
			40	2.47
			80	2.35
ISO 53 B	0.25	1.25	5	4.39
			10	4.13
			20	2.72
			40	2.54
			80	2.42
DIN 3972 I	0.2	1.167	5	4.62
			10	4.33
			20	2.79
			40	2.59
			80	2.46

6.5. CONCLUSION

In this chapter, a design guideline for the design of profile-generated involute gears to maximize compactness (i.e. minimise minimum tip-to-root clearance) and bending strength has been developed. It was shown that the bending strength-optimised tooth designs are also compact designs. Non-standard equivalent rack dedendum and cutter tip radius have been considered, as well as the compatibility limitation imposed by tooth thickness and undercutting. For modelling gear interference a corner contact-and-penetration model was used. Non-dimensionalisation methodology has been used to reduce the number of independent parameters and quantify the influence of the latter on interference risk.

The results of the four-parametric design space exploration show that significantly lower root stress can be achieved with certain non-standard designs, resulting in a strength increase of between 6%-48%, depending on the tooth number of the mating gear. A design guideline in the form of a nomogram was produced, which can be used for the direct inverse mapping of design requirements to gear geometry, producing better-informed choice of the relevant tooth design parameters, and the development of gear designs of known strength and safety without trial-and-error iterations, in a first-time-right manner.

REFERENCES

1. Litvin, F. L., 1994, *Gear Geometry and Applied Theory*, Prentice Hall
2. Townsend, D. P., 1992, *Dudley's Gear Handbook*, McGraw Hill
3. Buckingham, E., 1988, *Analytical Mechanics of Gears*, Dover Publications Inc.
4. Spotts, M. F., 1985, *Design of Machine Elements*, 6nd Edition, Prentice hall
5. Merritt, H. E., 1962, *Gears*, 3rd Edition, Pitman
6. KISSsoft AG , version 03/2011
7. Gear Design Pro 2011, Dontyne System, version 4.5
8. GearTeq 2012, Camnetics Incorporated, version 20.32.341, <http://www.camnetics.com>
9. Geartrax 2012, Camnetics Incorporated, version 20.671 for SolidWorks 2012
10. ISO 53, 1974, *Cylindrical gears for general and heavy engineering- Standard basic rack tooth profile*
11. AGMA, 201.02 and 201.02A, 1968, *Tooth proportions for coarse pitch involute spur gears*, Alexandria VA: Gear Manufacturers Association (AGMA)
12. GOST 13755-81, 1981, *Basic requirements for interchangeability. Gearings cylindric evolvent gears, Basic rack*
13. JIS B 1702-72, 1976, *Accuracy for spur and helical gears*

14. Spitas, C., Spitas, V., 2006, Can non-standard involute gears of different modules mesh?, *Proceedings of the Institution of Mechanical Engineers, Part C: Journal of Mechanical Engineering Science*, 220(8):1305-1313
15. Spitas, C., Spitas, V., 2008, Effect of cutter pressure angle on the undercutting risk and bending strength of 20° involute pinions cut with equivalent nonstandard cutters, *Mechanics Based Design of Structures and Machines*, 36(2):189-211
16. Spitas, C., Spitas, V., Costopoulos, T., 2009, Reduction of tooth fillet stresses using novel one-sided involute asymmetric gear design, *Mechanics Based Design of Structures and Machines*, 37(2):157-182
17. Spitas, V., Spitas, C., 2007, Numerical and experimental comparative study of strength-optimised AGMA and FZG spur gears, *Acta Mechanica*, 193(1-2):113-126
18. Spitas, V., Spitas, C., 2007, Four-parametric design study of the bending strength of circular-fillet versus trochoidal-fillet in gear tooth design using BEM, *Mechanics Based Design of Structures and Machines*, 35(2):163-178
19. Spitas, V., Spitas, C., 2007, Optimizing involute gear design for maximum bending strength and equivalent pitting resistance, *Proceedings of the Institution of Mechanical Engineers, Part C: Journal of Mechanical Engineering Science*, 221(4):479-488
20. Spitas, C., Spitas, V., 2007, A FEM study of the bending strength of circular fillet gear teeth compared to trochoidal fillets produced with enlarged cutter tip radius, *Mechanics Based Design of Structures and Machines*, 35(1):59-73
21. Spitas, V., Costopoulos, T., Spitas, C., 2006, Optimum gear tooth geometry for minimum fillet stress using BEM and experimental verification with photoelasticity, *ASME Journal of Mechanical Design*, 128(5):1159-1164
22. Spitas, C., Spitas, V., 2006, Generating standard 20° involute pinions with increased fillet strength by using 25° rack cutters with non-standard module, *Proceedings of the Institution of Mechanical Engineers, Part C: Journal of Mechanical Engineering Science*, 220(8):1297-1304
23. Bretl, N., Schurer, S., Tobie, T., Stahl, K., Höhn, B.-R., 2013, Investigations on tooth root bending strength of case hardened gears in the range of high cycle fatigue, *AGMA Fall Technical Meeting*, 103-118
24. Li, S., 2008, Effect of addendum on contact strength, bending strength and basic performance parameters of a pair of spur gears, *Mechanism and Machine Theory*, 43(12):1557-1584
25. Muni, D. V., Kumar, V. S., Muthuveerappan, G., 2007, Optimization of asymmetric spur gear drives for maximum bending strength using direct gear design method, *Mechanics Based Design of Structures and Machines*, 35(2):127-145
26. Tobie, T., Oster, P., Höhn, B. -R., 2005, Systematic investigations on the influence of case depth on the pitting and bending strength of case carburized gears, *Gear Technology*, 22(4):40-48
27. Masuyama, T., Inoue, K., Yamanaka, M., Kitamura, K., Saito, T., 2004, Evaluation of bending strength of carburized gears, *Gear Technology*, 21(3):30-37

28. Saada, A., Velex, P., 1995, Extended model for the analysis of the dynamic behavior of planetary trains, *ASME Journal of Mechanical Design*, 117(2A):241-247
29. Kapelevich, A. L., Kleiss, R. E., 2002, Direct gear design for spur and helical involute gears, *Gear Technology*, 19(5):29-35
30. Chen, X. -X., Lin, S. -Z., Xing, J. -Z., Liu, Y. -S., 2011, Simulation on gear backlash and interference check of harmonic drive with circular-arc teeth profile, *Computer Integrated Manufacturing System*, 17(3):643-648
31. Komori, M., Kubo, A., Takahashi, T., Tanaka, T., Ichihara, Y., Takeda, K., 2004, Failures of involute gears due to contact of side edge and tip edge of tooth (4th report, failure caused by trochoidal interference due to elastic deformation of tooth), *Transactions of the Japan Society of Mechanical Engineers Series C*, 70(12):3581-3589
32. Jin, X., Zhang, T., Yang, H., 2012, Research on gear assembly interference check based on virtual technology, *Communications in Computer and Information Science*, 288(1):45-52
33. Jin, X., Zhang, Z. -J., Ye, X., Li, Z. -X., 2006, Calculating model of interference amount for miniaturized gear and shaft shrink fit, *Journal of Beijing Institute of Technology (English Edition)*, 15(2):138-143
34. Sosa, A. D., Echeverria, M. D., Moncada, O. J., 2005, Analysis of stresses in ADI internal gears mounted with interference: Distortion and residual stresses effects, *Latin American applied research*, 35(3):241-246
35. Sun, Y., Zhang, C., Zhou, L., 2004, Meshing interference for spur gears with profile modification, *Proceedings of 11th World World Congress in Mechanism and Machine Science*, 2:777-781
36. Zhao, Z. -Q., Zhang, C. -L., Cheng, A. -M., Du, Q., 2008, Profile overlap interference constraint conditions of internal parallel move gears transmission, *Transactions of Beijing Institute of Technology*, 28(10):856-859
37. Maitra, G. M. , 2001, Handbook of Gear Design, *Tata McGraw-Hill Education*
38. Brauer, J., 2002, Analytical geometry of straight conical involute gears, *Mechanism and Machine Theory*, 37:127-141
39. Maitra, G. M., Prasad, L. V. , 1995, Handbook of Mechanical Design, *Tata McGraw-Hill Education*
40. Alipiev, O., Antonov, S., Grozeva, T., 2013, Generalized model of undercutting of involute spur gears generated by rack-cutters, *Mechanism and Machine Theory*, 64:39-52
41. Tseng, R. T., Tsay, C. B., 2001, Mathematical model and undercutting of cylindrical gears with curvilinear shaped teeth, *Mechanism and Machine Theory*, 36:1189-1202
42. Rockwell, P. D., 2001, Profile shift in external parallel-axis cylindrical involute gears, *Gear Technology*, 18(6):18-25
43. Wang, C., Liu, H., Xiang, C. -L., 2014, Influences of profile modification on dynamic characteristics of involute spur gears under a fluctuating torque, *Journal of Vibration and Shock*, 33(24):32-38

44. Barone, S., Borgianni, L., Forte, P., 2004, Evaluation of the effect of misalignment and profile modification in face gear drive by a finite element meshing simulation, *ASME Journal of Mechanical Design*, 126(5):916-924
45. Chen, Z., Shao, Y., 2013, Mesh stiffness calculation of a spur gear pair with tooth profile modification and tooth root crack, *Mechanism and Machine Theory*, 62:63-74
46. Bonori, G., Barbieri, M., Pellicano, F., 2008, Optimum profile modifications of spur gears by means of genetic algorithms, *Journal of Sound and Vibration*, 313(3-5):603-616
47. Hsi Lin, H., Oswald, F. B., Townsend, D. P., 1994, Dynamic loading of spur gears with linear or parabolic tooth profile modifications, *Mechanism and Machine Theory*, 29(8):1115-1129
48. Sankar, S., Nataraj, M., 2001, Profile modification-a design approach for increasing the tooth strength in spur gear, *International Journal of Advanced Manufacturing Technology*, 55(1-4):1-10
49. Baglioni, S., Cianetti, F., Landi, L., 2012, Influence of the addendum modification on spur gear efficiency, *Mechanism and Machine Theory*, 49:216-233
50. Chen, T., Sun, W., Zhang, X., 2011, An analytical method to determine the addendum modification parameters of involute helical gears, *Proceedings of the Institution of Mechanical Engineers, Part C: Journal of Mechanical Engineering Science*, 225(11):2516-2524
51. Atanasiu, V., Iacob, M. R., 2010, Tooth wear effects on dynamic transmission error of spur gears with addendum modifications, *International Review of Mechanical Engineering*, 4(6):638-644
52. Antal, T. A., 2009, A new algorithm for helical gear design with addendum modification, *Mechanika*, 77(3):53-57
53. Imrek, H., Unuvar, A., 2009, Investigation of influence of load and velocity on scoring of addendum modified gear tooth profiles, *Mechanism and Machine Theory*, 44(5):938-948
54. Arikan, M. A. S., 2003, Determination of addendum modification coefficients for spur gears operating at non-standard center distances, *ASME Design Engineering Technical Conferences and Computers and Inf. in Engineering Conference*, DOI: 10.1115/DETC2003/PTG-48063
55. Pedrero, J. I., Artés, M., 1996, Approximate equation for the addendum modification factors for tooth gears with balanced specific sliding, *Mechanism and Machine Theory*, 31(7):925-935
56. Hsu, R.-H. , Su, H.-H., 2014, Tooth contact analysis for helical gear pairs generated by a modified hob with variable tooth thickness, *Mechanism and Machine Theory*, 71:40-51
57. Sharif, K. J., Evans, H. P., Snidle, R. W., 2006, Wear modelling in worm gears, *Solid Mechanics and Its Applications*, 134: 371-383
58. Litvin, F. L., Hsiao, C. -L., Ziskind, M. D., 1998, Computerized overwire (ball) measurement of tooth thickness of worms, screws and gears, *Mechanism and Machine Theory*, 33 (6):851-877

59. Li, S., Kahraman, A., 2010, Prediction of spur gear mechanical power losses using a transient elastohydrodynamic lubrication model, *Tribology Transactions*, 53(4):554-563
60. Höhn, B. R., Oster, P., Schrade, U., 2005, Studies on the micropitting resistance of case-carburised gears - Industrial application of the new calculation method, *VDI Berichte (1904 II)*:1287-1307
61. Hu, Y., Zhang, X.-C., Yang, Z.-J. , Zhang, J., 2011, Precision cutting of spiral bevel gear with spherical involute tooth profile, *Beijing Gongye Daxue Xuebao/Journal of Beijing University of Technology*, 37(5):641-647
62. Brown, F. W., Davidson, S. R., Hanes, D. B., Weires, D. J., Kapelevich, A. 2010, Analysis and testing of gears with asymmetric involute tooth form and optimized fillet form for potential application in helicopter main drives, *AGMA Fall Technical Meeting*, 172-186
63. Sanders, A., Houser, D. R., Kahraman, A., Harianto, J., Shon, S., 2011, An experimental investigation of the effect of tooth asymmetry and tooth root shape on root stresses and single tooth bending fatigue life of gear teeth, *ASME Proceedings of 11th International Power Transmission and Gearing Conference*, IDETC/CIE, 8:297-305
64. Costopoulos, Th., Spitas, V., 2009, Reduction of gear fillet stresses by using one-sided involute asymmetric teeth, *Mechanism and Machine Theory*, 44(8):1524-1534
65. Chaphalkar, N., Hyatt, G., Bylund, N., 2013, Analysis of gear root forms: A review of designs, standards and manufacturing methods for root forms in cylindrical gears, *AGMA Fall Technical Meeting*, 33-39
66. Brown, F. W., Davidson, S. R., Hanes, D. B., Weires, D. J., Kapelevich, A., 2010, Analysis and testing of gears with asymmetric involute tooth form and optimized fillet form for potential application in helicopter main drives, *AGMA Fall Technical Meeting*, 172-186

7-Effect of cutter tip radius on the maximum root bending stress

Summary

This chapter performs a parametric investigation of the cutter radius coefficient on the maximum bending stress at the root for spur involute gears. The approach of this chapter is to apply unitary force at the highest point of single tooth contact (HPSTC) and then calculation of the root stress using FEA. Non-dimensional modelling is used to obtain results applicable to entire gear families. FEM results are compared with stresses calculated based on the ISO 6336-Method B. A comprehensive comparison with the popular existing gear standards such as DIN, AGAM, ANSI, JIS and GOST is performed. It is shown under which value of the cutter tip radius, the feasible design solutions for different tooth numbers and transmission ratios produce lower bending stresses at the root, consequently leading to design a stronger gear. The analysis leads to the analytical relation between the cutter tip radius and maximum bending stress at the root as a function of the number of teeth (for gear 1) and gear transmission ratios, which can be used non-standard involute gears as well.

7.1. INTRODUCTION

Gear is one of the most critical components in mechanical power transmission systems. The design of gearing is one of the classical topics of machine design [1-5]. Spur gear is one kind of gear that widely used in power transmission between parallel shafts. Designing highly loaded spur gears for powertrain systems that are both strong and quiet requires analysis methods that can easily be implemented and also provide information on contact and bending stresses along transmission errors. The objective of the powertrain is to transmit power with lower weight, lower vibration, and higher load-carrying. Nevertheless, the gear load capacity may be limited by the bending strength [6].

Three main models of gear tooth failure have been stated in AGMA 2001 [7] Standard as: bending fatigue leading to the tooth crack, surface contact fatigue leading to flank pitting, and lubrication break down leading to scuffing. Hence, the prediction the bending stress at the tooth root is very important [8]. If the bending stress is too high, larger module has to be used to decrease it, but this will increase the tooth size.

7.1.1 Different standards

Gear standards suggest some analytical formulas for the strength calculation of gears. BS 436(Part 3):1986 [9] provides methods for the calculation of contact and root bending stresses for metal involute gears. This standard is similar to the ANSI/AGMA (ANSI B6.1-1968, R1974) Standard [10] for stress calculation in pairs of involute spur or helical gears. For general gear design, ISO Standard provides a complex method similar to British Standard with less complexity. Some standards like ISO 6336 [11], DIN 3990 [12], and AGMA 908-B89 [13] use practically the same methods with different ranges for the factors in the calculation of load capacity, and eventually the gear strength calculations. AGMA 6004-F88 [14], AGMA 6014-A06 [15], and AGMA 6011-I03 [16] are used for the strength calculation of open gear rims for the special applications. In recent years, the established standard of almost universal use is the ANSI (ANSI B6.1-1968, R1974) [10] 20-degree standard spur gear form. It provides a gear with good strength and without fillet undercut for gears with more than seventeen teeth.

7.1.2. Commercial software

Gear design software use Standards and 2D FEA for the strength calculation. KISSsoft [17] provides the calculating according to the all well-known standards such as ISO, DIN, AGMA for plastic and metal gears with different applications i.e. naval ship, turbo drives, etc. Gear Design Pro [18] uses ISO and AGMA standards for this kind of calculation. HyGEARS [19] uses Finite Strips method [20], which is a 2D subset of the Finite Element Analysis to calculate tooth deformation and bending stresses instantly without having to resort to an external solver, a real time saver.

7.1.3. Literature review

Gear researchers have proposed some solutions to overcome the failure problem that bending stress causes. The equation for calculation of bending stress in a gear tooth was developed by Lewis in 1892 [21]. This equation applies as a foundation for a modern version of the bending strength equation defined by different standards such as AGMA. The new added factors in the standards in Lewis equation made it more accurate for the bending stress calculation.

Spitas and Spitas [22] studied the bending strength of circular fillet gear teeth compared to trochoidal fillets produced with enlarged cutter tip radius based on 2D FEA for the 20° involute gear system. The bending strength of the circular fillet gears surpasses that of trochoidal fillet gears irrelevant of the tip radius used for tooth numbers less than 17. In the case of higher tooth numbers, the solutions were equivalent.

Zhao et al. [6] investigated the increasing of bending strength in spur gears using shape optimization of cutting tool profile with introducing quadratic rational Bezier curve to describe the cutter tip based on FEA.

Aziz and Chassapis [23] reported a comparative analysis of tooth-root strength using stress–strength interference (SSI) theory with FEM-based verification. In this research, a reliable algorithm was developed to evaluate the gear tooth reliability by the bending strength criterion and integrated into the developed gear program as a probabilistic design tool.

Li [24] presented 3D FEM to conduct surface contact stress and root bending stress calculations of a pair of spur gears with machining errors, assembly errors, and tooth modifications. The results also compared with ISO and JGMA standards. In another research [25], he studied the effect of addendum on contact strength, bending strength and basic performance parameters of a pair of spur gears

Pedrero et al. [26] calculated the tooth bending strength of high transverse contact ratio (between 2 and 2.5) for spur and helical gear drives. The determinant load conditions have been calculated and the nominal contact stress and the nominal tooth-root stress have been computed.

Yamanaka et al. [27] experimentally investigated the influence of manufacturing methods (hobbed and forged gears) on bending strength and obtained the relationship between the strength and the manufacturing cost.

Spitas et al. [28] performed a parametric investigation of the combined effect of whole depth and cutter tip radius on the bending strength of 20 involute gear teeth. The results of the tooth bending strength computerised by means of analytical calculations, and finite element simulations applied to determine the exact tooth geometry in search of stronger tooth form.

Biernacki analysed of the material and design modifications influence on strength of the cycloidal gear system [29]. In this research, the influence of the plastic-steel combination on the stress and deformation distributions in the operation of the cycloidal gears was verified.

Spitas and Spitas [30] studied four-parametric design of the bending strength of circular-fillet versus trochoidal-fillet in gear tooth design using Boundary Element Method (BEM). The set of geometrical and operational design parameters considered comprised the number of pinion teeth, contact ratio, tooth thickness coefficient, and profile shifting coefficient.

Kapelevich and Shekhtman [31] applied FEA for bending stress evaluation of Direct Gear Design for non-standard gear tooth profiles. Optimization of the fillet profile allowed reducing the maximum bending stress in the gear tooth root area by 10-30%.

Tesfahunegn et al. [32] studied the effects of the shape of linear and non-linear tooth profile modifications on the transmission error, bending, and contact stress of spur gears. The results of these comparisons showed that the optimal

amount of profile modifications was not independent of profile modifications shape; hence, the procedures used to design linear PMs could not be directly applied to the design of non-linear profile modifications.

Pedersen [33] studies on the minimization of tooth bending stress in spur gears with simplified shapes of fillet and tool shape determination. A simple but sufficiently flexible root parameterization was applied and emphasis was put on the importance of separating the shape parameterization from the finite element analysis of stresses.

Kawalec et al. [34] presented a comparative analysis of tooth-root strength evaluation methods used within ISO and AGMA standards and verified them with developed models and simulations using FEA. The influence of helix angle, pressure angle, and addendum modification coefficient on tooth-root strength has been investigated. The tooth-root stress will be decreased with increasing the macro design parameters such as module, the number of teeth, pressure angle, helix angle and addendum modification coefficient. The results were compared with loading at the tip point and the highest point of single tooth contact (HPSTC). The results for ISO standard and FEA were close to each other with large difference from AGMA standard. For example, if the number of teeth for gear 1 is $N_1=80$, the result of tooth-root stress according to AGMA, FEA and ISO is 400, 500 and 535 MPa, respectively. Using the accurate result of FEA as a reference, it means that the difference between the result of FEA and ISO is 7%, nevertheless, the difference is 20% in comparison with AGMA.

With this comprehensive research on different standards, software and literatures, it can be observe that no study exists for effect of cutter tip radius on maximum bending stress at root which would be applicable for gear design. Even the gear software cannot provide such a design guideline for the influence of cutter tip radius on root bending stress and there is no way of assessing accurately the effect of different choices of cutter tip radius on gear strength.

7.1.4. Gear parametric design with regard to the root strength

Gear analyses in the past were performed using analytical methods, which required a number of assumptions and simplifications. In general, gear analyses are multidisciplinary, including calculations related to the tooth stresses and the failures. In this study bending stress analyses are performed, with the main aim of designing spur gears to resist bending failure.

The gear root stress can be reduced by optimizing the macro design parameters (module, number of teeth, pressure angle, diameters, helix angle, face width, addendum, dedendum, fillet radius, addendum modification, clearance, backlash) and micro design parameters (tip relief, root relief, profile modification, lead crown modification, roll angles of profile modification).

Each one of the micro and macro design parameters has own influence on the tooth bending strength. The tooth-root stress will be decreased with increasing

the macro design parameters [34]. With increasing the addendum coefficient, the maximum root tensile stress will be increased [25]. The maximum bending stress at the root will be decreased with increasing cutter tip radius or with decreasing the amount of dedendum coefficient, while the other design parameters are given [28].

7.1.5. Current study

In this study, the effect of the cutter radius on the root bending stress is investigated for the 20° gear system while trying to design spur gears to resist bending failure of the teeth. Non-dimensional modelling is used in order to reduce the independent geometrical parameters and make the results more generally applicable. The results presented here were obtained for pinions with 10, 20, 40 and 80 teeth. The mating gears is standard gear with 20 teeth and $c_c=0.3$, $c_f=1.25$. These gear forms that were numerically generated and simulated do not produce interference [35]. Bending strength which is considered as a relevant performance metric, was built on prior results by the research team [28]. Bending stress calculated in two ways. The first one is according to the standard formulas of ISO 6336, which are kind of modified Lewis equation, and the second one is based on the point loading at the Highest Point of Single Tooth Contact (HPSTC) using 2D FEA and both ways are plotted for comparison. Design guideline for maximum bending stress at the tooth root is produced and two-dimensional map of the design area is given in terms of cutter tip radius and number of teeth.

7.2. EXISTING MODELS

All standard methods depend on the calculation of the nominal tensile bending stress at the fillet of the loaded spur gear tooth. The stress concentration compensates by applying a factor which derived by either empirical or semi-empirical methods [36].

There are different method for calculation of maximum bending stress at the tooth root. The first one was introduced by Lewis [20], considering the tooth as a fixed beam at its root with the transmitted load. He used a parabola tangent to the dedendum of the tooth flank for determination of the critical section. AGMA standard [13] uses the modified version of Lewis formula for calculation of maximum bending root stress (Figure 7.1). The Local tooth-root stress σ_F can be calculated as:

$$\sigma_F = F_t K_o K_v K_s \frac{1}{b m_t} \frac{K_H K_B}{Y_J} \quad (7.1)$$

where F_t is transmitted tangential load at the operating pitch diameter, K_o is overload factor, K_v is dynamic factor for bending strength, K_s is size factor, b is net face width of narrowed member, m_t is transverse metric module, K_H is load-distribution factor, K_B is rim-thickness factor and Y_j is bending strength geometry factor.

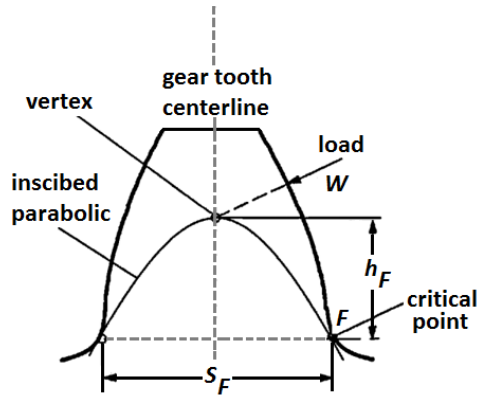


Figure 7.1: Determination of the critical section location according to the AGMA standard [13]

ISO (ISO 6336) [11] and DIN (DIN 3990) [12] uses “30 degrees tangent” method - called as Niemann formula [37]- for the bending stress calculation (Figure 7.2). This method is approximate and the stressed point is independent of the load location, located at a specific point at the tooth root. The applicability of this method is only for the design of low loaded gears [38]. The disadvantage of this method is not to consider the position changing of the critical section due to the displacement of the load along the active tooth profile [36].

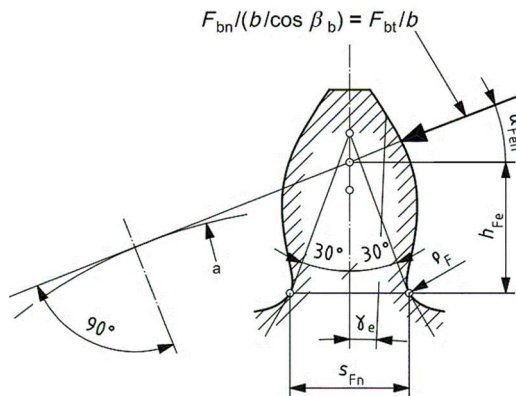


Figure 7.2: Determination of normal chordal dimensions of tooth root critical section according the ISO standard (ISO 6336-3 Method B) [11]

In this standard the Nominal tooth-root stress is calculated as:

$$\sigma_{F0} = \frac{F_t}{bm_t} Y_F Y_S Y_\beta \quad (7.2)$$

And the Local tooth-root stress σ_F was introduced as:

$$\sigma_F = \sigma_{F0} K_A K_V K_{F\alpha} K_{F\beta} \quad (7.3)$$

Whereas, F_t is transmitted tangential load at the pitch diameter, b is effective face width, m_t is transverse module, Y_F is tooth form factor, Y_S is stress correction factor, Y_β is helix angle factor, K_A is application factor for bending strength, K_V is dynamic factor for bending strength, $K_{F\alpha}$ is transverse load distribution factor root stress and $K_{F\beta}$ is face load distribution factor root stress. The semi-empirical method named as Heywood's method [39], is utilised for the determination of maximum real stress at critically stressed point at the root of a stubby beam with constant width (Figure 7.3) [40]. This method was later modified in order to make more precise prediction of the critical point. Heywood equation is based on photo-elasticity experiment with various fillet geometries of tooth. Tooth and root geometry are considered simultaneously.

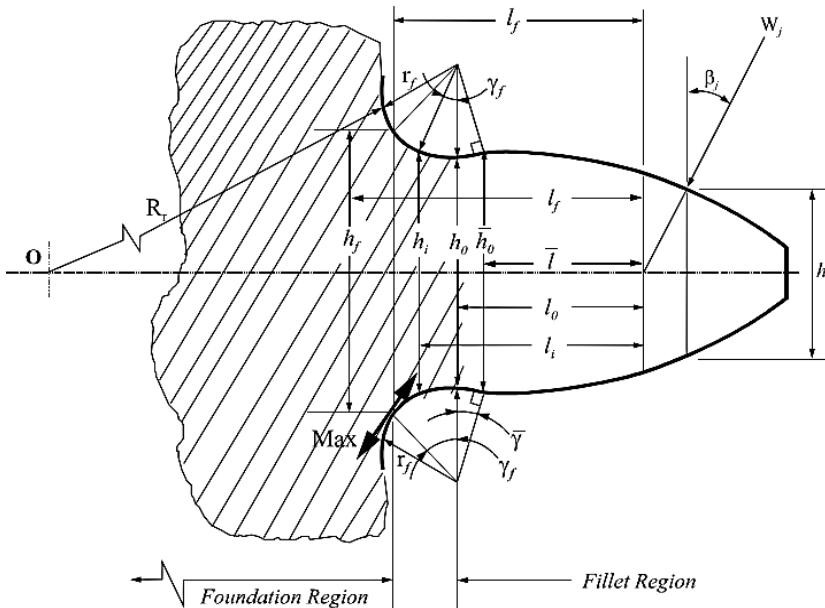


Figure 7.3: Tooth geometry for stress calculations using modified Heywood formula [40]

$$\sigma_j = \frac{W_j \cos \beta_j}{F} \left[1 + 0.26 \left(\frac{h_f}{2r_f} \right)^{0.7} \right] \left[\frac{6l_f}{h_f^2} + \sqrt{\frac{0.72}{h_f l_f}} \left(1 - \frac{h_L}{h_f} v \tan \beta_j \right) - \frac{\tan \beta_j}{h_f} \right] \quad (7.4)$$

Whereas σ_j is root bending stress at loading position j , W_j is transmitted load at loading position j , β_j is load angle, h_f is Tooth thickness at critical section, F is face width of gear tooth, v is approximately 1/4, according to Heywood [38], r_f is fillet radius, l_s is bending moment arm.

The Heywood formula concentration of the equivalent straight-sided projection shape did not lend itself to all generated gear design variation. However this method is more accurate than the modified Lewis method for normal gear design. This formula correlates well with the experimental data and finite element analysis results [41, 42].

An empirical formula for calculation the maximum root bending stress has been introduced by Dolan and Broghamer [43] based on a photo-elastic study of stress in gear tooth fillets. In addition, the same methodology has been done by Kelly and Pederson [42] based on photo-elastic work, combining the best features of two existing methods. Some data from actual gear test run were shown verifying the accuracy of the new solutions.

In addition to the aforementioned methods some commercial software like KISSsoft [17] use a method named as Static Calculation. In this method, each coefficient (application factor, face load factor, transverse coefficient, dynamic factor) is set to 1.0. The load at the tooth root is calculated with the tooth form factor according to ISO 6336-Method B and the helix angle (without the stress correction factor).

Nevertheless, in all the methods the loaded gear tooth is treated as a simple cantilever beam bending theory. The calculated stress is multiplied by different factors to produce the real bending stress with varying accuracies due to parameters included.

In this chapter the 30 degrees tangent method (Niemann formula) according to ISO 3663-Method B [11] is used for the calculation of maximum root bending stress, as most of the commercial gear design software use [17-19]. The results compared with the results of Finite Element Method applying the load at the highest point of single tooth contact (HPSTC) according to Spitas [44].

7.3. FEA OF ROOT STRESS (VS. ISO 6336)

For the purposes of this investigation ANSYS was used to simulate the loading of different gear pairs with consistent boundary and loading conditions, namely

point loading at the Highest Point of Single Tooth Contact considering one-tooth models fixed at their boundary (Figure 3.7), consistent with standard practice [34].

The iso-parametric element PLANE82 is used for modelling the gear tooth. This element provides accurate results for mixed (quadrilateral-triangular) automatic meshes and can tolerate shapes well suited to model curved boundaries.

Highest Point of Single Tooth Contact

The choice of load point is an important criteria in designing the gear. It is proven that the normal load P_N on a gear tooth is not maximum when applied at the addendum circle [46]. Generally, the load is assumed to have acting at the tip of the gear tooth. The load can act lower down the tip along the tooth profile. Nevertheless, for maximum nominal bending stress, assuming perfection in gear tooth, the load is assumed to be acting at the highest point of single tooth contact (HPSTC) [22, 44]. This point can be defined as the point along the tooth profile which is distant one the base pitch from the tip circle when measured along the line of action as presented in Figure 7.4 [22, 44]. Point B' in Figure 7.4, is the highest point of single tooth contact (HPSTC) for gear 1 and its position, defining the radius $r_{B'}$, is [22, 44]:

$$r_{B'} = O_1B' = \sqrt{r_{k1}^2 + (\varepsilon - 1)t_g[(\varepsilon - 1)t_g] - 2\sqrt{r_{k1}^2 + r_{g1}^2}} \quad (7.5)$$

Dividing by the module of the pair, the above equation yields its equivalent in terms of non-dimensional values:

$$r_{B'u} = \frac{r_{B'}}{m} = \sqrt{r_{k1u}^2 + (\varepsilon - 1)t_{gu}[(\varepsilon - 1)t_{gu}] - 2\sqrt{r_{k1u}^2 + r_{g1u}^2}} \quad (7.6)$$

The HPSTC is unique for different gear transmission ratios and tooth geometries.

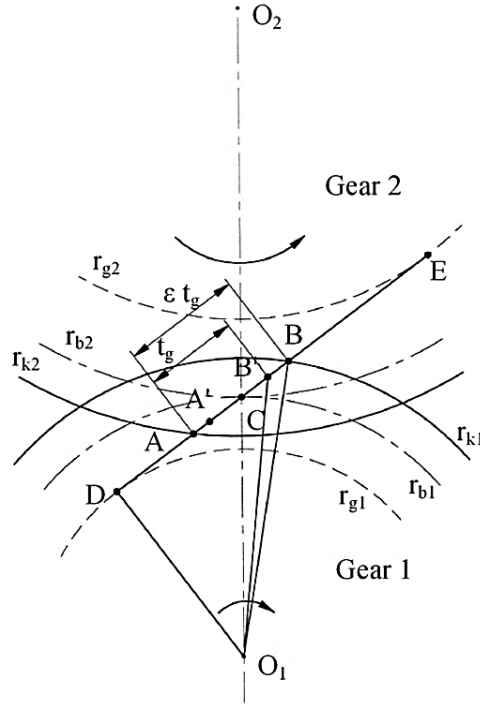


Figure 7.4: Non-dimensional gear modelling of a single teeth contact, Point B' is the highest point of single tooth contact (HPSTC) for gear 1 [22, 44]

7.4. COMPARISON METHOD: CURRENT APPROACH (AT HPST WITH FEA) AND ISO 6336 METHOD B

Gear strength and durability relate to the power and forces to be transmitted. Thus, the equations that relate tangential force at the pitch circle (F_t), power (P), and torque (T) are basic to the calculations. Because of the static calculation, the power is not applicable ($P = 0$).

We use the applied load as $P_N^* = 1$ at HPSTC (equation 6.6) with FEA for different combination of a gear pair. The gear number one is standard gear with different amount of cutter tip radius coefficient according to the different standards and the amount of dedendum coefficient is given ($c_f=1.25$). The pressure angle for both gears is 20 degree. The mating gear (gear number 2) is standard gear according to AGMA, 201.02 [44] ($N_2=20$, $c_c=0.30$, $c_f=1.25$). The comparison between the amount of cutter tip radius coefficient (c_c) for different standards ($c_f=1.25$, $c_k=1.00$) is presented in Table 7.1.

Table 7.1: Comparison of different standards; different cutter tip radius (c_c) and given dedendum ($c_f = 1.25$). The addendum coefficient is constant ($c_k = 1.0$)

Standard		c_c	c_f
ISO 53 [46]	Profile A	0.38	1.25
	Profile B	0.30	1.25
	Profile C	0.25	1.25
DIN 867 [47]	1	0.30	1.25
	2	0.25	1.25
	3	0.20	1.20
DIN 3972 :1952 II [48], DIN 58412:1987 [49]		0.20	1.25
JIS B 1702-72 [50]		0.375	1.25
NF E 23-011 1972 [51]		0.38	1.25
AGMA 201.02-68 [52]		0.30	1.25
ISO TR 4467 [53]		0.38	1.25
GOST 13755-68 [54]		0.40	1.25
ANSI B6.1 [55]		0.30	1.25

The static calculation according to ISO 6336-Method B [11] is used as the analytical results for the result comparison. We make a comparison with using the same created torque as follows:

- 1) Finding the HPST for the tooth of gear one,
- 2) Apply normal force as $P_N^* = 1$ at HPST using equation (7.6),
- 3) Calculating the created torque according to equation (3.2),
- 4) find the result of maximum bending stress σ_F^* from ANSYS,
- 5) Applying equation (3.2) to the non-dimension result.

Then, for ISO 6336-Method B:

- A) Applying the created torque from the current approach to find F_t (the nominal tangential load, the transverse load tangential to the reference cylinder),
- B) Using equation (7.2) to find the Nominal tooth-root stress σ_{F0} ,
- C) Calculation the local tooth-root stress σ_F according to equation (7.3).

7.5. RESULTS AND DISCUSSION

Six different sizes of cutter tip radius coefficient ($c_c = 0.20, 0.25, 0.30, 0.375, 0.38, 0.40$) are considered, while the size of dedendum and addendum are given as $c_c=1.25$, $c_k=1.00$, respectively. Four distinct cases are examined for unshifted teeth with $N_1=10, 20, 40$, and 80 teeth. These teeth are considered to be

dimensionless and loaded at their HPSTC according to equation (7.6). The number of teeth, cutter tip radius, dedendum and addendum coefficient for the mating gear (gear 2) is given ($N_2=20$, $c_c=0.30$, $c_c=1.25$, $c_k=1.00$).

Based on these results which are shown in Figures 6.5 and 6.6, observed findings can be summarized:

A) With increasing the value of c_c , the amount maximum bending stress will be decreased,

B) With increasing the number of teeth for gear 1, while the number of teeth for gear 2 is fixed and the value of c_c and c_f are given; σ_F will be decreased,

C) With increasing the gear transmission ratio, σ_F will be increased,

D) The value of gear contact ratio is independent on the value of c_c and c_f . As it is obvious with decreasing the gear transmission ratio while the value of gear contact ratio is increasing, σ_F will be decreased.

E) The difference between the results of the current approach and ISO standard will be decreased with increasing the amount of c_c , while the gear transmission ratio is given.

F) The difference between current approach and ISO standard will be increased with increasing the number for teeth for gear 1, while the value of c_c is given. For example, from 1.77% for $c_c=0.40$, $N_1=10$ up to 43.2% for $c_c=0.40$, $N_1=80$.

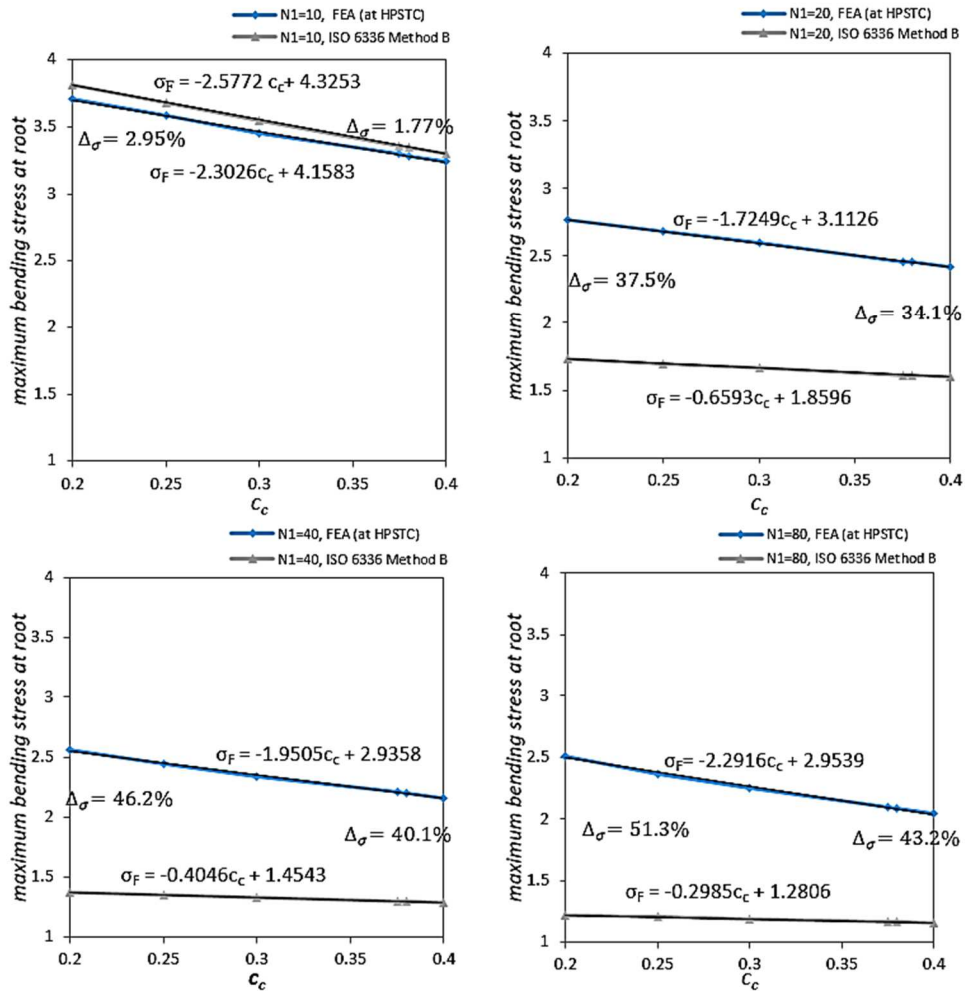


Figure 7.5: The maximum bending stress at tooth root with different amount of cutter tip radius and gear contact ratio

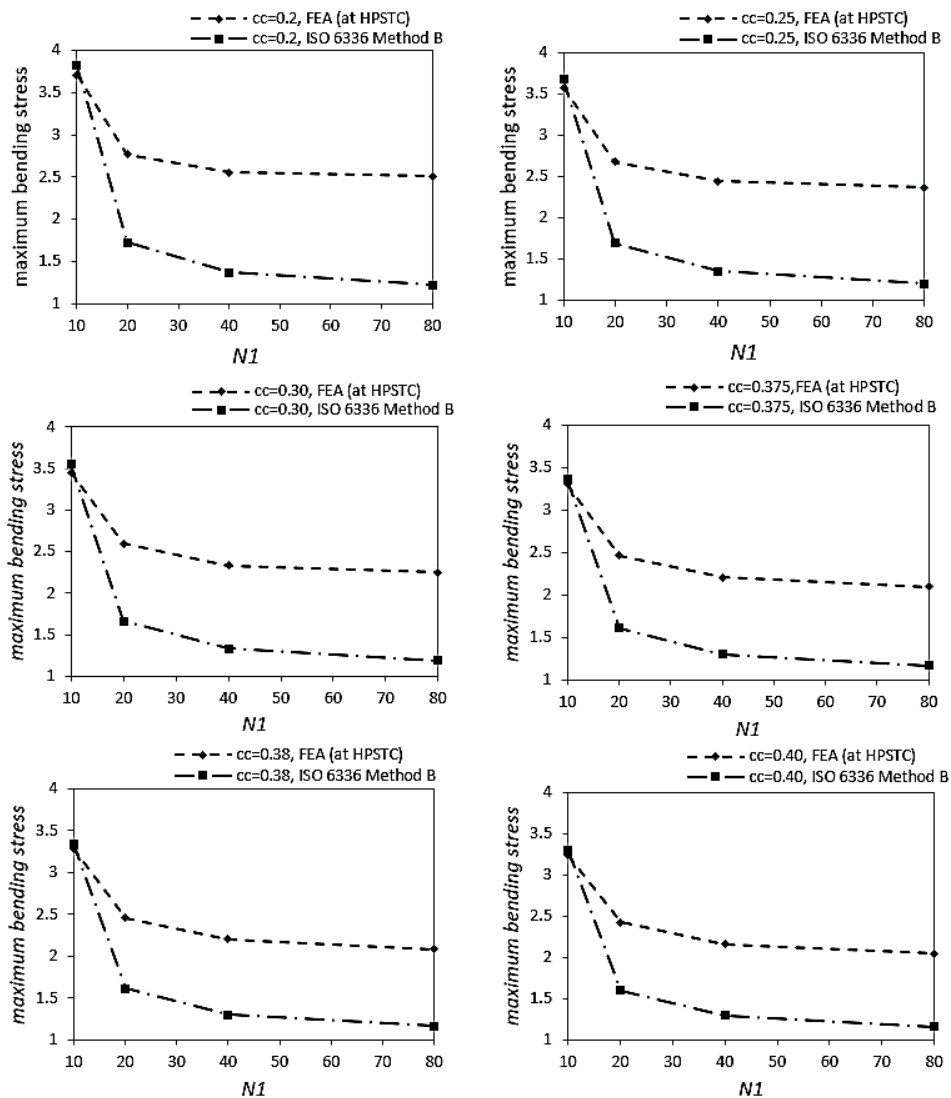


Figure 7.6: Influence of the number of teeth for gear 1, while the value of cutter tip radius is given

The difference between the current approach and ISO standard can be explained in two ways: first is the position of the critical section for calculation the maximum bending stress at the root, and the second one is the position of the load at the tooth.

In FEA, the maximum stress at root area can be easily found (Figure 3.6), however in ISO standard there is special point, which is found with 30 degrees tangent method as the calculation point for obtaining the maximum bending stress at the root.

7.6. DESIGN RECOMMENDATION

In Figure 7.5 the analytical formula for maximum bending stress at the root as function of cutter tip radius, the number of teeth and gear transmission ratio ($\sigma_F(c_c, N1, i_{1,2})$) was presented for each graph.

For the next version of standards, this analytical formula can be used as a design guideline for the influence of cutter tip radius as on the design parameters on maximum root bending stress of spur involute gears which is also applicable for non-standard design for involute gears. Using this design guideline can decrease the amount of time and cost of analyses and leading us to obtain better results to achieve maximum root stress for the design of stronger gears with selecting the non-standard value for cutter tip radius. Clearly, the same approach can be used for the influence of other design parameters on the gear strength. This formula can replace the calculation inside the current standards while leaving the rest of the standards unchanged improving the validity of the standards without need for excessive revision.

7.7. CONCLUSION

In the present study, a parametric investigation of the effect of the cutter tip radius coefficient on the maximum root bending stress of spur involute gears was carried out using Finite Element Analysis conducted on non-dimensionalised tooth geometries and loading conditions considering loading at the highest point of single tooth contact (HPSTC).

The results of maximum bending stress at the root from the current approach were compared with the Method B of ISO 6336 (30 degrees method). A thorough comparison with the popular gear standards such as AGMA, DIN, JIS and GOST was presented. The differences ranged from 1.77% ($N_1=10, N_2=20, c_c=0.40$) up to 51.3% ($N_1=80, N_2=20, c_c=0.20$) which can be seen in Figure 7.6, revealing significant inaccuracies inherent to the ISO 6336-Method B. These inaccuracies were also explained from the point of view of the basic principles.

Based on the accurate finite element analysis results, a parametric investigation was used to produce analytical formulas for maximum bending stress at the root as function of the cutter tip radius, the number of teeth and the gear transmission ratio, hence of the form $\sigma_F(c_c, N1, i_{1,2})$. The formula can be used as a design guideline for the selection of the cutter tip radius to maximise the gear strength for standard and non-standard involute gears. Furthermore the same formula can replace the corresponding calculation in ISO 6336 for root bending strength as well as in the software that use this standard, resulting in increased accuracy and better informed designs with minimal change to the standards overall.

REFERENCE

1. Litvin, F. L., 1994, Gear geometry and applied theory, *Prentice Hall*
2. Townsend, D. P., 1992, Dudley's gear handbook, *McGraw Hill*
3. Buckingham, E., 1988, Analytical mechanics of gears, *Dover Publications Inc.*
4. Spotts, M. F., 1985, Design of machine elements, 6nd Edition, *Prentice hall*
5. Merritt, H. E., 1954, Gears, 3rd Edition, *Isaac Pitman & Sons*
6. Zhao, X., 2014, Increasing bending strength in spur gears using shape optimization of cutting tool profile, *Australian Journal of Mechanical Engineering*, 12(2):208-216
7. ANSI/AGMA 2001-D04, 2004, Fundamental rating factors and calculation methods for involute spur and helical gear teeth
8. Hossan, M. R., 2008, Strength evaluation of polymer composite spur gear by finite element analysis, Thesis, Master of Science Major in Mechanical Engineering, South Dakota State University
9. BS 436-3, 1986, Spur and helical gears, Method for calculation of contact and root bending stress limitations for metallic involute gears
10. ANSI B6.1, 1968, Coarse pitch spur gear tooth forms
11. ISO 6336, 2006, Calculation of load capacity of spur and helical gears - Part 1: Basic principles, introduction and general influence factors
12. DIN 3990-1, 1987, Calculation of load capacity of cylindrical gears; introduction and general influence factors, Deutsches Institut fur Normung E.V.
13. AGMA 908-B89, 1989, Geometry factors for determining the pitting resistance and bending strength of spur, helical and herringbone gear teeth
14. AGMA-6004-F88, 1988, Gear power rating for cylindrical grinding mills, kilns, coolers, and dryers
15. ANSI/AGMA 6014-A06, 2006, Gear power rating for cylindrical shell and trunnion supported equipment (mill gears)
16. ANSI/AGMA 6011-I03, 2004, Specification for high speed helical gear units
17. KISSsoft AG, version 03/2011
18. Gear Design Pro 2011, Dontyne System, Version 4.5
19. HyGEARS 2004, Involute Simulation Softwares Inc., Version 4.0
20. Lewis, W., 1893, Investigation of the strength of gear teeth, *Proceedings of the Engineering Club*, 1(FC' 82):16-23
21. Gosselin, C., Gagnon, P., Cloutier, L., 1998, Accurate tooth stiffness of spiral bevel gear teeth by the finite strip method, *Journal of Mechanical Design, Transactions of the ASME*, 120(4):599-605
22. Spitas, C., Spitas, V., 2007, A FEM study of the bending strength of circular fillet gear teeth compared to trochoidal fillets produced with enlarged cutter tip radius, *Mechanics Based Design of Structures and Machines: An International Journal*, 35(1):59-73
23. Aziz, E. S., Chassapis, C., 2014, Comparative analysis of tooth-root strength using stress–strength interference (SSI) theory with FEM-based verification,

- International Journal on Interactive Design and Manufacturing*, 8(3):3159-170
24. Li, S., 2007, Finite element analyses for contact strength and bending strength of a pair of spur gears with machining errors, assembly errors and tooth modifications, *Mechanism and Machine Theory*, 42:88-114
 25. Li, S., 2008, Effect of addendum on contact strength, bending strength and basic performance parameters of a pair of spur gears, *Mechanism and Machine Theory*, 43(12):1557-1584
 26. Pedrero, J. I., Vallejo, I. I., Pleguezuelos, M., 2007, Calculation of tooth bending strength and surface durability of high transverse contact ratio spur and helical gear drives, *Journal of Mechanical Design, Transactions of the ASME*, 129(1):69-74
 27. Yamanaka, M., Matsushima, Y., Miwa, S., Narita, Y., Inoue, K., Kawasaki, Y., 2010, Comparison of bending fatigue strength among spur gears manufactured by various methods, *Journal of Advanced Mechanical Design, Systems and Manufacturing*, 4(2):480-491
 28. Spitas, C., Spitas, V., Amani, A., Rajabalinejad, M., 2014, Parametric investigation of the combined effect of whole depth and cutter tip radius on the bending strength of 20° involute gear teeth, *Acta Mechanica*, 225(2):361-371
 29. Biernacki, K., 2015, Analysis of the material and design modifications influence on strength of the cycloidal gear system, *International Journal of Precision Engineering and Manufacturing*, 16(3):537-546
 30. Spitas, V., Spitas, C., 2007, Four-Parametric design study of the bending strength of circular-fillet versus trochoidal-fillet in gear tooth design using BEM, *Mechanics Based Design of Structures and Machines*, 35(2):163-178
 31. Kapelevich, A. L., Shekhtman, Y. V., 2003, Direct gear design: Bending stress minimization, *Gear Technology*, 20(5):44-47
 32. Tesfahunegn, Y. A., Rosa, F., Gorla, C., 2010, The effects of the shape of tooth profile modifications on the transmission error, bending, and contact stress of spur gears, *Proceedings of the Institution of Mechanical Engineers, Part C: Journal of Mechanical Engineering Science*, 224(8):1749-1758
 33. Pedersen, N. L., 2014, Minimizing tooth bending stress in spur gears with simplified shapes of fillet and tool shape determination, *Engineering Optimization*, 47(6):1-20
 34. Kawalec, A., Wiktor, J., Ceglarek, D., 2006, Comparative analysis of tooth-root strength using ISO and AGMA standards in spur and helical gears with FEM-based verification, *Journal of Mechanical Design, Transactions of the ASME*, 128(3):1141-1158
 35. Spitas, C., Spitas, V., Amani, A., 2015, Multi-parametric investigation of interference in non-standard spur gear teeth, *Mechanism and Machine Theory*, 88:105-124
 36. Spitas, V., Spitas, C., 2007, Numerical and experimental comparative study of strength-optimised AGMA and FZG spur gears, *Acta Mechanica*, 193(1-2):113-126

37. Niemann, G., Winter, H., 1985, *Maschinelemente, Band 2: Getriebe allgemein, Zahnradgetriebe, Grundlagen and Stirnradgetriebe*. 2nd Edn., Springer, Berlin, ISBN-10: 3540111492, pp: 376.
38. Raptis, K. G., Costopoulos, Th. N., Tsolakis, A. D., 2012, Comparison between Niemann's and finite element method for the estimation of maximum allowable stress of meshing spur gear teeth at highest point of single tooth contact, *American Journal of Engineering & Applied Sciences*, 5(2):205-216
39. Heywood, R. B., 1962, Designing against fatigue of metals, 1st Edn., *Reinhold*
40. Nguyen, T., Lin, H. H., 2011, Compact Design for Non-Standard Spur Gears, *International Journal of Mechanical, Aerospace, and Industrial Engineering*, 2(1):1-15
41. Cornell, R. W., 1981, Compliance and stress sensitivity of spur gear teeth, *ASME Journal of Mechanical Design, Transactions of the ASME*, 103:447-459
42. Kelley, B., Pederson, W., 1958, The Beam Strength of Modern Gear Tooth Design, SAE Technical Paper, DOI:10.4271/580017
43. Dolan, T. J., Broghamer, E. L., 1942, A photo-elastic study of stress in gear tooth fillets, *University of Illinois at Urbana-Champaign*, Bulletin series No. 335
44. Spitas, V., Costopoulos, T. H., Spitas, C., 2005, Increasing the strength of standard involute gear teeth with novel circular root fillet design, *American Journal of Applied Sciences*, 2:1058-1064
45. AGMA, 201.02 and 201.02A, 1968, Tooth proportions for coarse pitch involute spur gears. Alexandria, VA: Gear Manufacturers Association (AGMA)
46. ISO 53, 1974, Cylindrical gears for general and heavy engineering- Standard basic rack tooth profile
47. DIN 867, 1986, Basic rack tooth profiles for involute teeth of cylindrical gears for general engineering and heavy engineering
48. DIN 3972, 1952, Reference Profiles of Gear-cutting Tools for Involute Tooth Systems according to DIN 867
49. DIN 58412, 1987, Basic rack tooth profile for gear tools for fine mechanics; involute gears according DIN 58400 and DIN 867
50. JIS B 1702-72, 1976, Accuracy for spur and helical gears
51. NF E 23-011, 1972, Cylindrical gears for general and heavy engineering - Basic rack and modules (similar to ISO 467 and ISO 53)
52. ISO/TR 4467, 1982, Addendum modification of the teeth of cylindrical gears for speed-reducing and speed increasing gear pairs
53. GOST 13755, 1981, Basic requirements for interchangeability. Gearings cylindrical evolute gears. Basic rack
54. ANSI B6.1, 1968, Coarse pitch gears

8- Multi-parametric design model considering manufacturability and geometrical compatibility

Summary

A generalised non-dimensional multi-parametric model for involute spur gear design is presented, considering manufacturability and geometrical compatibility, where the latter considers various modes of interference and accounts for the combined effects of the module, pressure angle, tooth addendum, dedendum, cutter tip radius, and the numbers of teeth of a pair of mating gears. The effect of the same parameters together with tooth thickness on the manufacturability of the individual gear teeth is also modelled in terms of pointing and undercutting. The full range of parameter values, including non-standard ones, is considered. The resulting combined model serves to provide a complete analytical overview of the multi-parametric design space and is suitable for the fast assessment of existing designs, for implicit or explicit (direct) gear design, for extracting design guidelines, and for design optimisation. The model can be used to identify and explore highly promising under-used subspaces of the parametric design space, which are currently of significant interest to i.e. the automotive and aerospace industries.

8.1. INTRODUCTION

8.1.1. General framing of the problem

In almost all kinds of industrial applications for motion and power transmission such as automotive, aerospace, robotics, machinery etc., gears - and involute gears in particular- are indispensable and mission critical elements of the design. Gear design itself is a complex process that, in spite of much accumulated knowledge and supporting standards, computational models [1-7] and software [8-12], still critically depends on the experience of the designer, especially if time constraints prohibit an exhaustive iterative multi-parametric search. In fact, the possible independent design parameters that must be studied even in the case of a 'simple' spur gear configuration comprise i.e. module, addendum, profile shift, tooth thickness, dedendum, cutter tip radius, pressure angle, face width etc, thus already numbering 8 parameters. The study is further complicated by the possibility to adjust each parameter for each gear separately. More crucially, it is important to consider the choice of these parameters in the early stage of

the design, and in full consideration of the couplings (and constraints) that govern their feasible choices. The part of the design space that is not excluded because of aforementioned constraints can then be subject to parameter selection and possibly a design optimisation study. Already, in the automotive and aerospace industry every major company is developing and exploring its own class of non-standard designs and continuous improvements are being sought to achieve higher compactness, higher strength and load carrying capacity, improved dynamics with reduced noise and vibration signatures, in particular with regard to performance under partial or reversing loads, whining, rattling etc.

Several but limited studies and supporting models exist for this kind of design space exploration: Dedicated studies exist i.e. for the influence of module [7, 13], addendum [14-22], profile modification [23-29] tooth thickness [30-36], dedendum [37-42], cutter tip radius [43-46], pressure angle [47-54], etc, but without considering the simultaneous manipulation of other design parameters as well, typically assigning standard values to the latter. Additionally, many researchers have investigated the influences of each design parameter for different applications such as contact analysis [55-63], stress [64-71], vibration [72-78], dynamics [79-88], cracking [89-93], lubrication [94-101], etc, but with similar limitations to their scope of the design space. Furthermore, the knowledge present in industrial publications/ technical reports is on the other hand very specific to given machine applications and not easily generalizable or verifiable.

Hereunder we provide some selective examples of the aforementioned limitations in scope, which, while justified or necessary in the context of the respective studies, mean that the possibility to generalise the results without additional modelling is likewise limited:

8.1.1.1. Dedicated parametric studies

Module: for example, with regard to the influence of the module, Nonaka et al [13] studied the strength of spur gear teeth with small modules of the order of 0.1 to 1.0 mm by using a specially designed gear test rig. The failure mode of gear teeth was observed for both tempered and soft nitrided gears. A sign of uneven contact along face width was found only for very small gears of modules 0.1 and 0.2 mm, which was very unlikely for such high precision in alignments of gear axes. Influences of the choice of pressure angle or tooth proportions were not considered, limiting the scope of the study.

Addendum: With regard to the effect of addendum, for example, Li [15] investigated its influence on tooth contact strength, bending strength of spur gears. Finite element analysis, the method of mathematical programming and teeth contact model were utilized to lead the contact analyses of the loaded teeth, calculation of stress and deformation of spur gears with not the same

contact ratios and addendums. Load-sharing rate, root bending stress, contact stress, mesh stiffness and also the transmission error of the spur gears were analysed. It was detected that the number of contact teeth can be increased with increasing the amount of addendum, in addition, the contact & root bending stresses can be reduced with this kind of increasing. The effects of cutter tip radius (hence fillet radius), pressure angle etc parameters were not accounted for in this study.

Profile modification: for instance, Lin et al [28] investigated the influence of parabolic and linear profile modification on low contact ratio of spur gears tooth with regard to the dynamic response. The influence of the modification zone's length and the whole modification were calculated at different speeds and loads for obtaining the optimum amount of profile modification with regard to the minimum dynamic loading. A novel design charts were presented that have been included the non-dimension maximum dynamic load curves. The charts were applied at several loads using various profile modification. Minimisation of the dynamic loads can be defined from the charts taking into the account the optimum amount of profile modification. Several design parameters having an influence on the tooth stiffness function, including pressure angle, addendum and root fillet were not in the scope of this study.

Tooth thickness: for example, Hsu and Su [30] proposed a novel approach by using a modified adjustable tooth thickness hob to decrease the tooth flank twisting of a crowning gear with the same centre distance. The topologies of the tooth surface, static transmission error and contact ellipses were also investigated in this work using adjustable tooth thickness of the modified hob. For demonstration and verification of the competence of the proposed gear hobbing method (considering the longitudinal crowning), there examples were studied. While the methodology proposed is readily generalizable, it is e.g. not clear how well the results would hold if different tooth proportions and corresponding contact ratios would be used.

Cutter tip radius: for example, Spitas et al [43] proposed non-dimensional multi-parametric analytical model to determine corner contact and penetration at the root of the gear tooth to find the influence of the design parameters (i.e. number of teeth, cutter tip radius, dedendum, addendum and contact ratio) on the possibility of the interference. Based on this approach, novel design guidelines for nonstandard compact tooth (short dedendum, large root fillet) were presented.

Spitas and Spitas [45] applied finite element method to investigate the bending strength for two kinds of fillet, the circular fillet and the trochoidal fillet. The results showed that for the number of these higher than seventeen, the bending strength of both fillets are equivalent circular fillet can be used instead of trochoidal fillet. However, in both aforementioned studies the results can be expected to vary significantly if larger values for the pressure angle were used.

Pressure angle: for example, Lin [53] presented an analytical model for meshing of planar gears considering the typical geometry of the gear tooth profile. The angular displacement of gears was presented as a function of pressure angle. Different pressure angle functions could produce different gear tooth geometries. Although the new methodology can be used for any kind of gear mesh, nevertheless the possible variation of other tooth geometrical characteristics, such as addendum, was not in the scope of this study.

8.1.1.2. Application-driven parametric studies

Contact analysis: for example, Medvedev et al [55] presented an analytical modelling for contact analysis of multi-pair gear. The parabolic function of transmission errors was applied for contact pressure. The precise transmitted torque and force of each contact pair and the contact pressure of the multi pair contact were determined by means of a new algorithm. The algorithm can be used for any kinds of gears and an example of spiral bevel gear has been applied for demonstration.

Generation, contact and stress analysis: for example, Litvin et al [70] represented computerised improvements in generation, design, stress analysis and simulation of gear meshing. A modified algorithm of tooth contact analysis and a new parabolic function of transmission errors designed for noise simulation. The proposed developments have been demonstrated for the design and simulation of three kinds of gear drives (spiral bevel gear, face-gear, modified helical gear). While the approach is very general, it does not readily afford the correlation of specific design parameters to behaviours without a dedicated study.

Vibration: for example, Farshidianfar and Saghafi [75] applied Melnikov analytical analysis to investigate the chaotic performance of a gear system. The dynamic model of the gear system was included the time varying mesh stiffness, backlash, static transmission error and external excitation. The initial values of the control parameter for the happening of divergence and start of chaos were predicted by the proposed analysis. Moreover, for verification of the analytical approach, the numerical bifurcation analysis and numerical simulation of the system were applied. As typical in such studies, the focus was not on parametric analysis that could produce direct design insights without further study.

Dynamics: for example, Faggioni et al [83] developed a Random-Simplex optimization algorithm to find the optimum amount of profile modifications for vibration reduction of a gear system using a nonlinear dynamic model. The good results were achieved by using high contact ratio gear properties and the proposed optimisation methodology. The scope of this study did not cover variations in the pressure angle.

Cracking: With regards to tooth root cracking, for example, Pandya and Parey [92] studied the influence of the gear design parameters (such as: root fillet

radius, pressure angle, backup ratio) and the effect of crack path on time varying gear mesh stiffness. A cumulative reduction index has been proposed for investigating the crack propagation in a tooth root using 2D finite element analysis. The percentage change in time varying mesh stiffness has been determined by using variable crack intersection angle approach and a model of total potential energy. However the influence of addendum (or whole depth) was not in the scope of this study.

Lubrication: for example, Larsson [100] analysed the transient non-Newtonian elastohydrodynamic lubrication of an involute spur gear. With taking into the account the influence of fluid transition; the film thickness of lubricant and the pressure were calculated. In addition, considering the influence of shear strength restriction, it has been assumed that the model of the fluid was a non-Newtonian model and the film lubrication was isothermal. The results indicated that the influence of fluid transition was prominent at the transitions of the load. Once the load was increased (almost doubled), the minimum amount of film thickness was enlarged for a while because of the squeeze effect. At several points of contact, the stresses of subsurface and the factor of friction were evaluated. In this study, two types of oil (poly- α -olefin & paraffinic mineral) were used as lubricant. Effects of pressure angle and addendum were not considered.

Although all above mentioned examples of studies contribute significantly to the knowledge base that is relevant to gear design, each of them (justifiably) deals with interrelated design parameters in the separate contexts of their own focal areas- particularly the module, pressure angle and addendum seem to always be treated as decoupled design choices and there is little information about synergies (or conflicts) in the choice of these parameters. As such, they do not offer a comprehensive model that can account for interactions between these parameters. I.e. changing the module and the pressure angle of one gear at the same time may have synergistic or conflicting effects, when meshing with another gear, possibly leading to improved strength or interference; pressure angle and addendum choices can result in strength improvement, but also undercutting; the cutter tip radius choice for one gear may cause interference with the addendum choice for the mating gear [43, 44] etc. These types of couplings, which either affect *manufacturability* (for example undercutting) or *geometrical compatibility* (for example interference), have not so far been addressed comprehensively in the literature in a coupled sense.

In the presence of such overwhelming complexity, the predominant answer has been standardisation of gear design parameters and combinations thereof [8-12]. Traditional gear design is generally based on standardised cutting tools, which makes the design of gears simple and available for any application. The drawback is that standard gear designs are known to have less than optimum performance in a range of applications, such as very high power density, high power-to-weight ratios, metal-to-plastic replacement, low-cost, compact, and

low-vibration powertrains, which need to be designed with non-standard parameters. This becomes especially relevant as new production methods rely much less on standardised tooling, especially if non-generating processes are employed, for example, broaching, injection moulding, sintering etc.

This chapter aims to enable the multi-parametric design of gears in consideration of the major identified couplings between design parameters that limit or otherwise constrain the design space. Explicitly, the occurrence of undercutting and interference will be related to the combined values of the gear cutter pressure angle, module, number of teeth, cutter tip radius, dedendum, addendum, tooth thickness of each of two gears in a pair. The order of complexity is reduced by means of non-dimensionalisation with respect to the module, as well as the analytical coupling of some of these apparently independent parameters. The resulting model is both complete and computationally lightweight, to allow its use during the conceptual design and corresponding exploration of the design space.

As this chapter is focused on geometrical compatibility, the implications of parameter choices on stresses, load-carrying capacity, stiffness, dynamics etc are not considered herein. These will be the object of a subsequent study.

8.1.2. Manufacturability and geometrical compatibility as two considerations of gear design

8.1.2.1. Manufacturability (tip pointing, undercutting)

The first thing to be addressed in design is the matter of feasibility of a particular gear geometry choice: Can it be manufactured as intended? Except in the case of direct gear design [97-100], where gear geometry is directly and explicitly defined, typical design procedures define the gear geometry implicitly, based on basic gear rack parameters. In this sense, it can be that the gear produced by the manufacturing process deviates from the expected form due to the occurrence of secondary cutting action by the rack cutter, which manifests as either tip pointing or undercutting.

- 1) Tip pointing, which is essentially the elimination of the tooth top land and potentially the reduction of the tooth whole depth, can result from the use of a large pressure angle, and/ or addendum, or large positive profile shifting [2].
- 2) Undercutting is the condition where additional material is removed from the root of the tooth, potentially also removing part of the lower involute profile. It can result from the use of small numbers of teeth, small pressure angles, and/ or small cutter tip radii [2].

Tip pointing concerns the involute geometry exclusively and is as such very straightforward to calculate [1, 36,102]. On the other hand, undercutting prediction concerns both the involute flank and the non-involute root segments and as such requires a more involved calculation. A number of analytical models for undercutting have been proposed, of which the more accurate ones include

the effect of tip rounding, which introduces an additional parameter that in effect removes material from the cutter tip and lessens the propensity to undercut.

With regard to tip pointing in particular;

Litvin [1] studied the location of a tooth pointing area taking into the account that at the tooth top land, the two surfaces of the tooth had intersection. In order to solve this problem, a numerical programming has been presented. Different conditions were presented to avoid pointing tooth for modified involute gears, Novikov–Wildhaber helical gears and face-gear drives.

Townsend [2] presented a set of formulation for calculation to determine the maximum amount of tooth thickness in order to generate a tooth pointing. To compute the diameter of pointed tooth, an algorithm for testing the value of a gear tooth (with long and short addendum) was developed.

Kapelevich [102] showed that the pointed tooth of an asymmetric gear could be generated using the positive profile shift for number of teeth less than 17 resulting the increase of load capacity while the pressure angle and the maximum transverse contact ratio are the same of asymmetric and symmetric pointed tooth gear.

Marita [6] investigated the effect of positive profile shift modification on pointed tip. With increasing the amount of the positive correction, the tooth became more and more pointed. This phenomenon was termed as “Peaking”.

Rackov et al [103] applied generalized particle swarm optimization algorithm for high contact ratio gear. It was found the possibility if generation the pointed tooth would be increased with increasing the amount of addendum. To avoid this occurrence, all the constraints and equations were checked and the optimum amount of profile shift modification and addendum were calculated with the proposed optimisation methodology.

Arikan [104] studied on the determination of addendum modification coefficients for spur gears operating at non-standard centre distances considering avoiding pointed tooth and undercutting. The performance of gear were optimised with regard to addendum modification coefficients taking into the account the amount of dedendum, centre distance, clearance, backlash, gear ratio, contact stresses and root stresses.

Bair [105] investigated a three-dimensional geometric pointed tooth of crowned elliptical gear at major axis. The gear drive was designed to avoid edge contact while there was an axial misalignment. The rack cutter was used for developing an analytical model of the gear drive. Moreover, a numerical programming was computed for generation gear tooth without pointed teeth.

In the traditional theory of involute meshing, there is a minimum number of teeth to avoid the undercutting root by means of the tooling generating rack, i.e. for many 20 degree involute pinions this minimum number is 17. However, such

rules of thumb are of little use when dealing with non-standard designs, in which case more detailed models are appropriate:

Litvin [1] defined the limitation condition for tooth undercutting that the tooth has been generated by means of rack-cutter taking into the account the meshing between involute part of the gear and the straight line of the rack cutter.

Townsend [2] and Spotts [4] showed that for each pressure angle there is critical number of teeth that undercutting happens while the standard amount of addendum coefficient equals 1.0 and the amount of profile shift coefficient equals 0.0. I.e. for the pressure angle of $14\frac{1}{2}^\circ$, 20° , and 25° spur gears, the tooth root undercut occurs with a number of teeth lower than 32, 17 and 12, respectively.

The undercutting conditions for symmetric spur gears which have been designed directly are not constrained by the restrictions of the generating rack and its profile shift coefficient [36, 102].

Alipiev et al [106] proposed a generalized approach to describe the tooth undercutting. In this study, three kinds of boundary condition were defined for undercutting of spur gear tooth. The first one which was the traditional undercutting boundary condition called as “undercutting-type I”. The second and the third one were described as “undercutting-type IIa” and “undercutting-type IIb”. Based on this study, the type IIa and type IIb were made by means of the fillet of the rack cutter, whereas the type I was made by the straight line of the rack cutter profile. Moreover, the boundary condition for preventing undercutting of all the three typed were presented considering the amount of fillet radius of the rack cutter

He et al [107] presented a theoretical study and numerical simulation for undercutting occurrence. Minimum number of the involute gear teeth without undercutting was found in two different approaches as the traditional boundary condition and cutter tip radius limitation. The results indicated that the minimum number of teeth without undercutting considering traditional restriction is less than the cutter tip radius limitation.

Brauer [108] presented the analytical relations for a straight conical involute gear tooth surface and its offset surface to avoid undercutting occurrence. In this study, Merritt [5] formulation for undercutting restriction was applied for the modelling. A developed expression for undercutting check was presented considering the amount of addendum modification coefficient.

While the starting point of each of these models is the same, namely the geometrical simulation of gear to rack contact, the mathematical formulations present discrepancies in their predictions, as will be seen in section 8.2.2.

Based on these models the different undercutting conditions we calculate the minimum number of teeth to avoid undercutting as shown in Table 8.1.

Table 8.1: Comparison of undercutting equations for minimum number of teeth

Researcher(s)	Minimum number of teeth to avoid undercutting
Litvin[1], Kapelevich [102], Alipiev (type I) [106]	$N \geq \frac{2(c_k - c_m)}{\sin^2 \alpha_0}$
Townsend[2], Spotts [4]	$N \geq \frac{2c_k}{\sin^2 \alpha_0}$
He [107]	$N \geq \frac{2(c_k + c_c)}{\sin^2 \alpha_0}$
Alipiev (type II) [106]	$N \geq \frac{c_c}{\sin \alpha_0}$
Merritt [5], Brauer [108]	$N \geq \frac{2(c_k - c_m - c_c(1 - \sin \alpha_0))}{\sin^2 \alpha_0}$

In this chapter, we perform an independent investigation of the conditions that lead to tip pointing and undercutting, in the course of which we explain also the discrepancies observed between the existing models.

8.1.2.2. Geometrical compatibility (interference)

Even if a gear is manufacturable, as per section 8.1.1.1, it is not guaranteed that two gears configured in a pair and made to mesh will do so without geometrical interference. For this reason, there are guidelines in the standards, which steer parameter selection to subspaces in the design space where it is known a-priori that interference does not occur [101-102, 106-111]. However, interference becomes a concern when non-standard tooth forms with reduced radial clearance are employed, such as large-fillet short-dedendum gears [38]. These tooth forms have shorter involute working flanks and excess material at the root, which can lead to non-conjugate corner contact and penetration at the tooth root. Existing models for interference are unable to predict this, or rely on calculation-intensive simulations, which make them impractical for design.

As with undercutting, simple analytical models exist and are widely used to predict interference [1, 3]. However, these models have been proven recently to underestimate interference risk, and corner contact and penetration in particular, when small numbers of teeth are concerned, especially if compact low-dedendum gears produced with large cutter tip radii are concerned [38-39]. Interference for non-standard gears happens because of the penetration of the tip of the driven gear (gear number 2) at the tooth root of the driving gear (gear number 1). The new interference model has to cover the area of penetrating that

occurs at the corner-to-root contact region. Furthermore, interference due to module/ pressure angle compatibility, tooth width compatibility (backlash), and radial clearance compatibility are non-trivial factors that must be considered in non-standard gear design [112]. Thus in the case of non-standard and compact gear geometry, these new computational models have to be implemented in the context of multi-parametric design.

Based on these considerations, interference modelling can be categorised in four parts as:

1. Pitch compatibility: Normally the use of the same module and pressure angle for both gears in a mating pair, as dictated by all standards, is sufficient to guarantee pitch compatibility. In general, however, these may be assigned different values for each gear, as long as base pitch compatibility is maintained [112].
2. Thickness-wise interference: Negative backlash, i.e. due to errors in tooth thickness or centre distance, also leads to interference. It can be detected by observing only the conjugate parts of the profiles. Nonetheless, if the leading profiles are positioned in a compatible meshing position, seizure will manifest as corner penetration at the coast sides [49,112].
3. Radial interference: The concern here is that the radial clearance can be so small that the top land of one gear will contact the root of the mating gear [112].
4. Corner contact and penetration: While standards provide sufficient clearances to avoid interference for any selectable combination of the gear design parameters, this may not be the case in many non-standard and compact gear design configurations [38]. In those cases, it is possible that the corner of the tip of one gear tooth will contact and tend to penetrate the root of the mating gear tooth, causing interference.

Pitch compatibility, often taken for granted with standard mating gear pairs, is no longer guaranteed if module and pressure angle are free to vary between the gears. This is given special consideration in the present study, together with basic models for thickness-wise (backlash) and radial interference.

Furthermore, the well-known analytical solution which has been suggested by Litvin [1] is valid for studying interference occurring along the line of action only, which is a false premise in most non-standard and compact gear design configurations [38], where corner contact and penetration is a concern. In particular the necessary and sufficient condition for non-interference at the root of the reference gear (gear 1) proposed by Litvin [1] and elaborated by the authors as follows (re-writing equation (4.12)) [43]:

$$c_c \leq c_f \tan\left(\frac{\pi}{4} + \frac{\alpha_o}{2}\right) \sec\alpha_o - \left(\sqrt{\left(\frac{1}{2}N_2 + c_{k2}\right)^2 - \frac{1}{4}N_2^2\pi^2\cos^2\alpha_o - \frac{1}{2}N_2\pi\sin\alpha_o} \right) \tan\left(\frac{\pi}{4} + \frac{\alpha_o}{2}\right) \tan\alpha_o \quad (8.1)$$

In fact, equation (8.1) only predicts a tangent to the exact interference limit curve and is generally not valid, except at sufficiently high values of c_c and c_f of gear 1 (Figure 8.4). In this chapter equation (1) still provides a useful limit-tangent to the exact interference limit curves, which are calculated by the corner contact-and-penetration model [43]. In this work we perform a synthesis of appropriate models for the four different types of interference, providing a comprehensive set of accurate multi-parametric mathematical conditions for the geometrical compatibility of gear pairs.

8.1.3. Standards and computational resources for implicit and explicit/direct gear design

For the design of gear geometry, a number of established design solutions have been codified in standards for implicit gear design such as GOST 13755 [113], ISO 53[114], NF E 23-011[115], ISO TR 4467 [116], JIS B 1702 [117], DIN 867 [118], AGMA 201.02 [119], DIN 3972 [120]. These standards have been implemented in dedicated gear design software such as KISSSoft [8], HyGEARS [9] and Gear Design Pro [10].

Applicable standards also exist for explicit/ direct gear design, for instance ANSI/AGMA1006-A97 [121], as well as dedicated books [102] and software, for example Gear Tooth Root Fillet Optimization Software [122].

Given that the above sources are fundamentally implementations of the models discussed under section 1.1, they are also subject to the same critical considerations.

Where applicable throughout the chapter, a few selected standard solutions and de facto industry solutions ('best practices') are shown in context in the enlarged design space, allowing a quick assessment as to how close they are to naturally emerging design limits (which are often associated with local optima).

8.1.4. Current study

In this chapter, we start by introducing a non-dimensionalisation methodology (section 3.2.1.1) to produce an elegant generalised representation and reduce the order of the multi-parametric problem (sections 8.4.1-8.4.3). The basic principles are introduced to frame a comprehensive manufacturability (tip pointing, undercutting) and geometrical compatibility (interference) model for the parametric design of profile-generated involute gears (sections 8.2.1-8.2.4 and 8.2.1-8.2.5 respectively). The synthesised model simultaneously considers all applicable geometric and kinematical conditions and constraints to qualify each point in the design space (hence each combination of geometrical gear design parameters) in terms of manufacturability and geometrical compatibility. The design parameters considered include the module, pressure angle, tooth thickness, addendum, dedendum, cutter tip radius, and number of teeth of each

gear. While in principle the module and pressure angle may be varied between gears subject to specific constraints on pitch compatibility [113], in this study for simplicity the convention of choosing a common module and pressure angle for both gears in a mating pair is maintained. This reduces the considered design parameters from 14 to 12, all of which are in principle independent in the context of non-standard design. An extensive multi-parametric study is conducted over subsections 8.5.1.1-8.5.1.6, discussing the most notable effects of different choices for the considered design parameters.

To demonstrate the capabilities of the model, this chapter proposes two geometric metrics that function as indirect performance indicators, which are relevant to gear design: a) Compactness (associated with strength and stiffness) and b) Contact ratio (associated with dynamics and peak-to-peak dynamical transmission error). These are discussed in section 8.5.2. However useful, the proposed metrics are by no means exhaustive – they serve only to demonstrate the utility and additional insights obtainable by the developed multi-parametric model. For each performance indicator, given the multi-parametric nature of the problem, it is possible to dictate a-priori or restrict the range of certain parameters, thus limiting the search area for design space exploration (and the number of associated strength or dynamical simulations), or even suggest a global optimum at the boundary of the constrained design space.

Finally, design guidelines are extracted and multi-dimensional maps of the design space are given in terms of the aforementioned design parameters. Benchmarks against standards as well as known non-standard ‘best industry practices’ reveal significant potential in the less explored parts of the design space, especially with regard to a multitude of low-clearance, compact gear designs.

8.2. MANUFACTURABILITY MODELLING

8.2.1. Tip pointing

Tip pointing is the condition where the top land of the teeth disappears, leaving both sides of the working tooth profiles (drive and coast) to intersect.

The shape of the tooth becomes more peaked or pointed and the tooth flank becomes more curved as the pressure angle increases (Figure 8.1). Therefore, the top land becomes smaller and eventually results in pointed or peaked tip. Gear standards [113-121] recommended that the tip thickness should be greater than equal to 0.2 times the module for the hardened gears and this may be increased to 0.25 times the module in exceptional cases. The limitation of peaked or pointed tooth makes a boundary to the maximum amount of pressure angle. For a particular number of teeth there is a critical upper profile shift above which the teeth become pointed. With profile shifting, gear teeth generated by the same basic rack can be made to have different tooth thicknesses. In turn, the maximum attainable outside diameters of such gears are a function of tooth

thickness. For any given number of teeth, the tooth thickness can be increased such that the tip will become pointed at the outside diameter circle [2]. However, the resulting teeth do not have the correct whole depth because the involute curves cross over below the expected outside diameter (this phenomenon is termed ‘peaking’ [6]). The amount that the outside diameter of a gear is to be modified is usually a function of the tooth thickness desired. The maximum amount that the tooth thickness of a gear can be increased to just achieve a pointed tooth can be found already in Dudley’s Gear Handbook [2], reproduced here using an adapted notation:

$$c_k^{max} = \frac{N \left(\text{inv} \left(\cos^{-1} \frac{r_b}{r_k} \right) - \text{inv} \alpha_0 \right) - \frac{\pi}{2}}{2 \tan \alpha_0} \quad (8.2)$$

Where c_k^{max} is the maximum addendum coefficient at which a tooth having full working depth will come to a point, α_0 is standard pressure angle of the rack cutter and $\cos^{-1} \frac{r_b}{r_k}$ is pressure angle at tooth tip. To avoid pointed teeth and undercut root, it is needed to shorten the amount of addendum and working depth, however equation (8.2) cannot give us the condition of the avoidance of pointed tooth.

Buckingham [3] introduced a condition to avoid pointed tooth that the arc tooth thickness at outside radius (r_k) will be less than zero. With this regard, Figure 8.1 is presented to formulate this condition [3].

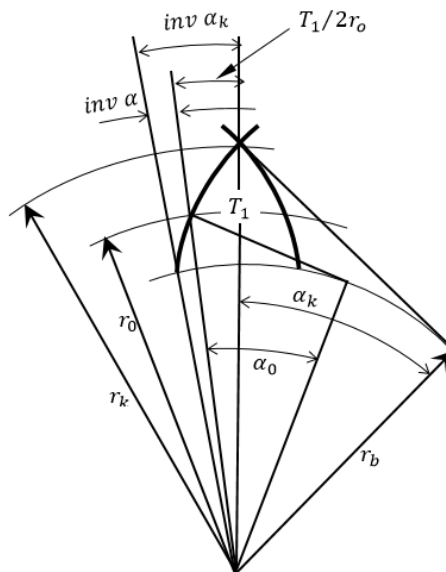


Figure 8.1: Pointed tooth model as per Buckingham [3]

Referring to Figure 8.1, T_1 is the tooth thickness at outside radius (r_k), $inv \alpha_k$ and $inv \alpha_0$ are the involute function of α_k (pressure angle at r_k) and α_0 (pressure angle at r_0), respectively.

From Figure 8.1, it can be obvious that:

$$\cos \alpha_0 = \frac{r_b}{r_o} \quad (8.3)$$

$$\cos \alpha_k = \frac{r_b}{r_k} \quad (8.4)$$

And

$$r_b = r_o + \cos \alpha_0 \quad (8.5)$$

$$r_k = r_o + mc_k \quad (8.6)$$

From equations (8.3) and (8.4), we have:

$$\frac{r_b}{r_k} = \frac{\frac{N}{2}m \cos \alpha_0}{\frac{N}{2}m + mc_k} \quad (8.7)$$

The arc tooth thickness at outside radius (r_k) can be presented as:

$$inv \alpha_k = (T_0/2r_o) + inv \alpha_0 \quad (8.8)$$

Which can be rewritten as:

$$inv \alpha_k = \left(\frac{\pi c_s}{N}\right) + inv \alpha_0 \quad (8.9)$$

With substituting equation (8.7) into equations (8.4) and then equations (8.9), the condition of avoiding pointed tooth can be presented as:

$$inv \left(\cos^{-1} \left(\frac{\frac{N}{2} \cos \alpha_0}{\frac{N}{2} + c_k} \right) \right) < \left(\frac{\pi c_s}{N}\right) + inv \alpha_0 \quad (8.10)$$

Illustration of equation (8.10) is presented in Figure 8.2. The grey area corresponds to tooth pointing, which is undesirable for gear design.

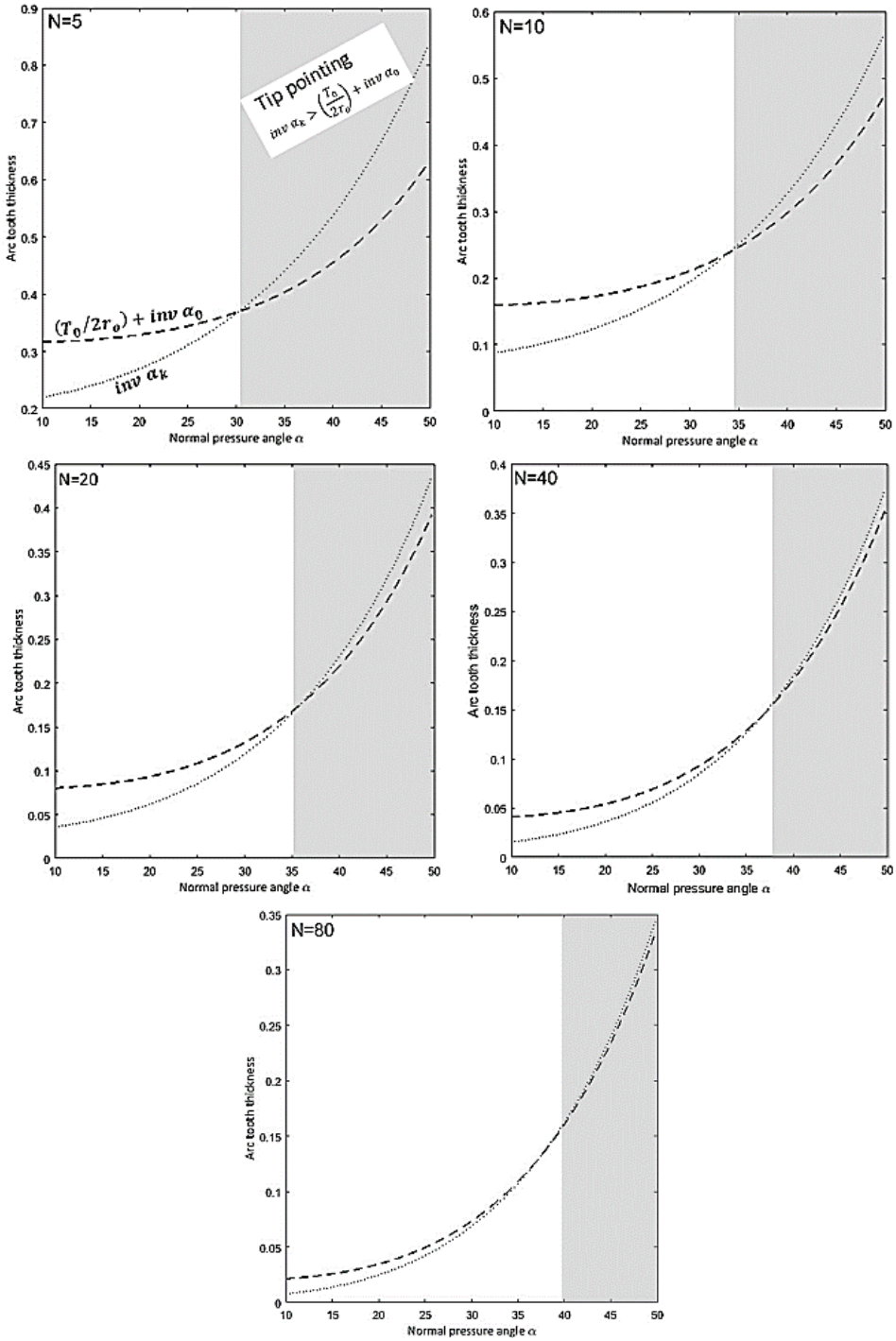


Figure 8.2: Illustration of tip pointing area design according to the condition of equation (8.10)

8.2.2. Undercutting

Conditions of non-undercutting by a rack-cutter may be determined by using the general approach presented based on simple geometric considerations has been introduced by Litvin [1]. The geometry of gear cutting at the tooth fillet (gear not shown, only rack cutter tooth shown for clarity) has been further elaborated by the authors [44] and is shown in Figure 8.3. According to this model the condition for non-undercutting is as follows:

$$\alpha_0 - \gamma \geq 0 \quad (8.11)$$

It follows from Figure 8.3 that:

$$\gamma = \tan^{-1} \frac{\frac{c_t}{\tan \alpha_0}}{(r_{o,u} - c_t)} \quad (8.12)$$

Further substituting some details of Figure 8.2 in equation (8.12) yields:

$$\alpha_0 - \tan^{-1} \frac{c_f \tan \left(45^\circ + \frac{\alpha_0}{2}\right) - c_c \cos \alpha_0}{\tan \alpha_0 \left[(r_{o,u} - c_f) \tan \left(45^\circ + \frac{\alpha_0}{2}\right) + c_c \cos \alpha_0 \right]} \geq 0 \quad (8.13)$$

According to research by He et al. [107], if the rack addendum extends inside the point of tangency of base circle and pressure line (Point C' in Figure 8.3), gear undercutting consequentially occurs. Therefore, the addendum of the rack must be under the theoretical contact point. The cutter centerline is tangent with the gears' reference circle. The requirement without undercutting for standard involute spur gears as follows:

$$GP \sin \alpha_0 \geq c_t \quad (8.14)$$

By substituting some details of Figure 8.3 in equation (8.14) we obtain:

$$(r_{o,u} \sin^2 \alpha_0 - c_f) \tan \left(45^\circ + \frac{\alpha_0}{2}\right) + c_c \cos \alpha_0 \geq 0 \quad (8.15)$$

On the other hand, according to Merritt [5], Brauer [108] and Alipiev et al. [106] (undercutting of type I) undercutting occurs (approximately) if the path of contact extends past the interference point. Therefore, a transverse plane of the tooth is not undercut if:

$$GP \geq C'P \quad (8.16)$$

And with same details of Figure 8.3 in equation (8.16), leading again to equation (8.15).

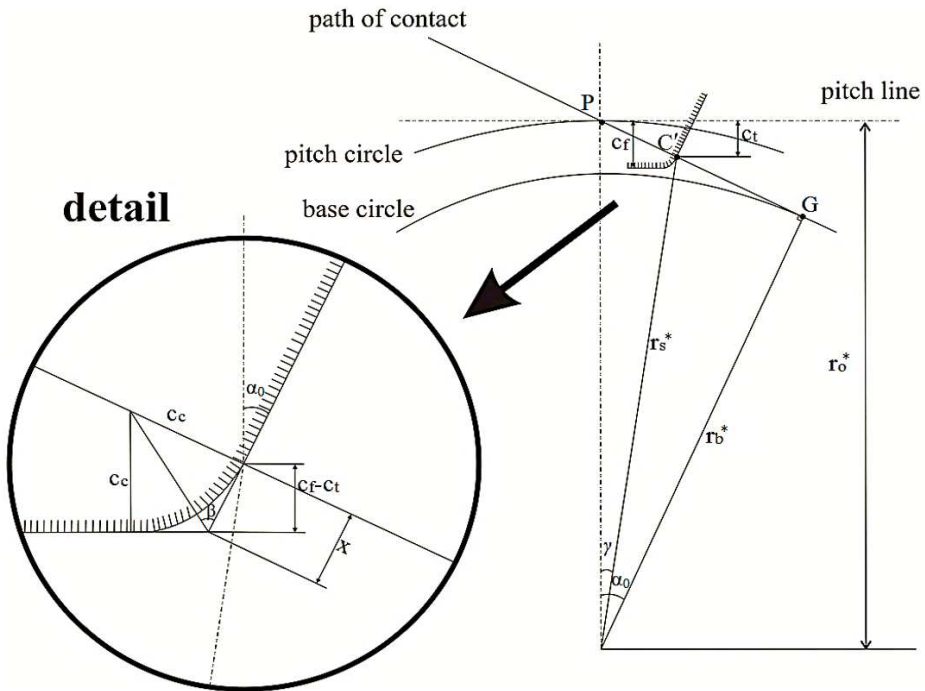


Figure 8.3: Geometry of gear cutting at the tooth fillet [44]

The predictions from the three undercutting models derived in equations (8.13), (8.15), (8.17) above are plotted and compared in Figure 8.4. According to Figure 7.4 the undercutting condition that has been introduced by Litvin [1], Merritt [5], Brauer [108] and Alipiev et al. [106] has same results for undercutting and non-undercutting parts of spur gears.

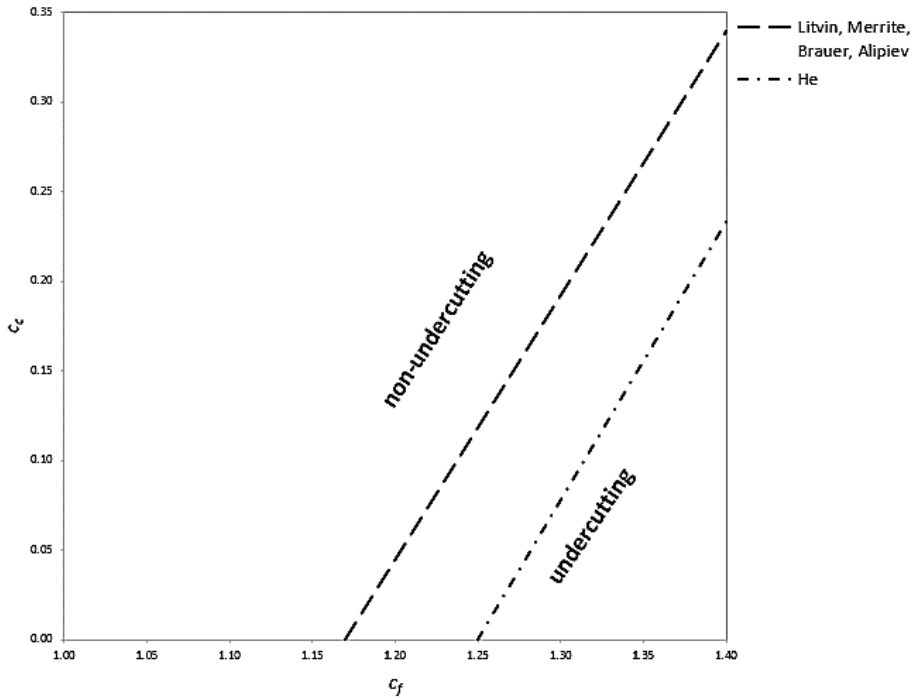


Figure 8.4: Comparison of undercutting phenomena for different theories

It is apparent that Litvin's condition, as per equation (8.11), and Merritt's condition, as per equation (8.16), produce identical predictions for interference, which are more conservative than the predictions based on He's condition (equation (8.14)), where the combined influence of the dedendum coefficient and the rack cutter tip radius coefficient has been considered.

8.2.3. Tooth thickness analysis

Figure 8.5 describes the case of maximum cutter tip radius $\max c_c$ [43-45, 123], where it can be observed that the tip thickness t'_u of a sharp tooth of the non-dimensional rack cutter relates to the pitch thickness $\pi(1 - c_s)$, the dedendum and the pressure angle according to equation (3.10) as follows:

$$\max\{c_c\} = \left[\frac{1}{2} \pi(1 - c_s) - c_f \tan \alpha_0 \right] \tan \left(\frac{\pi}{4} + \frac{\alpha_0}{2} \right)$$

Equations (3.10) and (3.11) are used for tooth thickness analysis to find the limitation of tooth thickness with regard to the cutter tip radius and dedendum coefficient. Notice that application of a larger radius than that calculated from equation (3.10) would result in an undercut cutter tooth, having a smaller whole depth and c_f value than intended.

8.2.4. Form radius analysis

By exploiting the symmetry of the rack cutter tooth as shown in Figure 8.3 (which has been introduced in Chapter 3, section 3.2.1.2), the following relationship can be deduced:

$$c_f - c_t = c_c \frac{\cos \alpha_0}{\tan \left(\frac{\pi}{4} + \frac{\alpha_0}{2} \right)}$$

And therefore,

$$r_s^* = \sqrt{\left(\frac{c_t}{\tan \alpha_0} \right)^2 + (r_o^* - c_t)^2}$$

8.3. GEOMETRICAL COMPATIBILITY (INTERFERENCE) MODELLING

8.3.1. Pitch compatibility

In this study, we use the conditions for pitch compatibility developed by Spitas [54, 112]. The underlying considerations and model are explained as follows.

Let us examine a pair of involute gears contacting at an arbitrary point A , as shown in Figure 8.5. Gear 1 can be uniquely defined by its base radius r_{g1} and number of teeth N_1 and gear 2 similarly by its base radius r_{g2} and number of teeth N_2 . It is possible to uniquely define point B as the intersection of the tooth profile of gear 1 with line GA , if point B is rotated by an angle $\frac{2\pi}{N_1}$. Correspondingly point Γ is defined as the intersection of the tooth profile of gear 2 with line GA , if Γ is rotated by an angle $\frac{2\pi}{N_2}$. By virtue of the properties of the involute:

$$AB = t_{g1} , \quad A\Gamma = t_{g2} \quad (8.17)$$

Clearly, to assure perfect contact of the next pair of rack-pinion teeth at A , the points B and Γ must coincide, hence the necessary condition for pitch compatibility is:

$$t_{g1} = t_{g2} \quad (8.18)$$

Let us examine a rack and an involute pinion (gear 1) in contact at an arbitrary point A , as shown in Figure 8.5. The rack can be uniquely defined by its pitch t_R and pressure angle α_0 and the pinion by its base radius r_g and number of teeth N . In this case point B is uniquely defined as the intersection of the tooth profile

of gear 1 with line GA , if the latter is rotated by an angle $\frac{2\pi}{N}$. Correspondingly, the rack must also travel a distance t_R ; hence the rack profile also intersects line GA at a new point Γ . By virtue of the properties of the involute:

$$AB = t_g \quad (8.19)$$

It can easily be verified from Figure 8.5 that:

$$A\Gamma = t_R \cos \alpha_0 \quad (8.20)$$

In order to assure perfect contact of the next pair of rack-pinion teeth at A , the points B and Γ must coincide, hence the necessary condition for pitch compatibility is:

$$t_g = t_R \cos \alpha_0 \quad (8.21)$$

From equation (8.21) we derive the following conclusion:

Two different racks defined by the pairs t_R, α_0 and t_R', α_0' generate gears of the same base pitch t_g if and only if:

$$t_R \cos \alpha_0 = t_R' \cos \alpha_0' \quad (8.22)$$

Because of equation (8.18) the generated gears can mesh perfectly, notwithstanding any tooth clearance restrictions, the racks that satisfy the condition of equation (8.22) are considered equivalent.

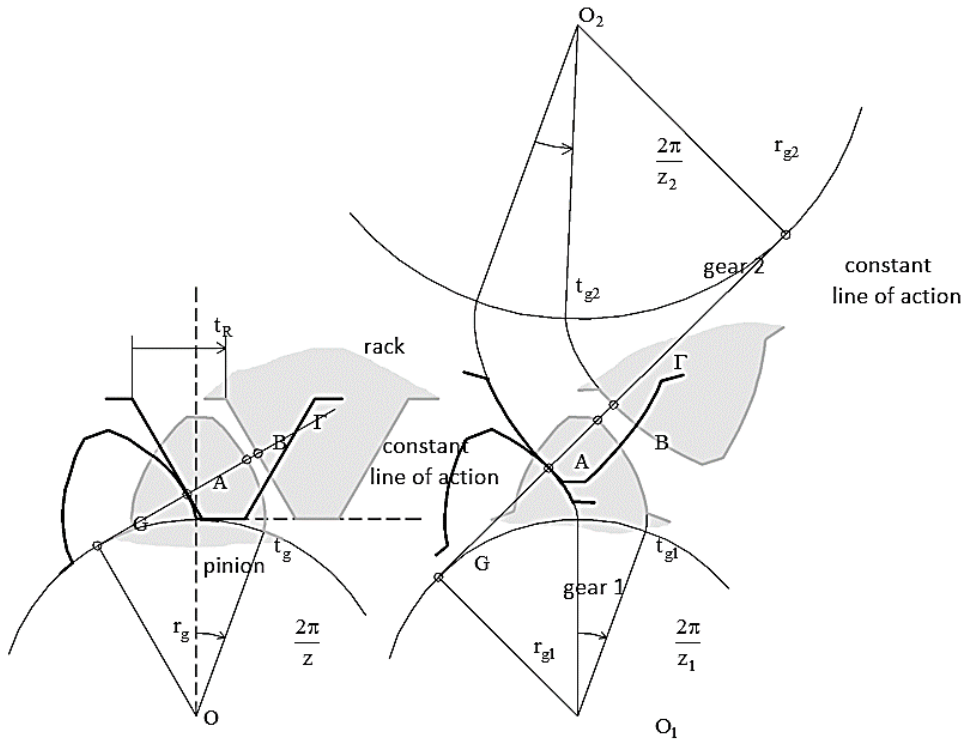


Figure 8.5: Pitch compatibility: pinion-rack (left), pinion-wheel (right) [54, 112]

8.3.2. Thickness-wise interference: Seizure

Let us examine the pair of involute gears illustrated in Figure 8.5. Besides the base radii r_{g1} and r_{g2} and numbers of teeth N_1 and N_2 , a sufficient geometrical definition of the gears must include the inside radii r_{f1} and r_{f2} , the outside radii r_{k1} and r_{k2} and the thickness coefficients at the base circles c_{sg1} and c_{sg2} respectively. The centre distance of the gear pair is a_{12} .

The general condition for sufficient tooth backlash is derived [54]:

$$\frac{N_1 + N_2}{\pi} (\alpha_c - \tan \alpha_c) \leq 1 - c_{sg1} - c_{sg2} \quad (8.23)$$

Where α_c is the operating pressure angle, c_{sg1} and c_{sg2} are the thickness coefficients at the base circles for gear 1 and 2, respectively.

8.3.3. Radial interference

One of the main constraints for fillet optimisation is a minimum radial clearance. Radial clearance results from the difference between addendum and dedendum of two mating gears, with standard radial clearance coefficients varying from 0.2

to 0.35. The minimal clearances must in any case be greater than zero to avoid the tooth tip/root interference. However, operating conditions, including temperature and humidity (especially with plastic gears), may reduce root clearances. Besides, low radial clearances may result in trapping lubricant in the tooth root area, increased hydraulic losses, and reduced gear efficiency, especially for relatively wide spur gears. This may require designing the tooth fillet with increased root clearances even with some compromise of bending stress reduction [54, 124].

In order to ensure that the conjugate gears operate without the risk of seizure, there should be a minimum allowable radial clearance.

To assure radial clearance the following relationships must be true:

$$r_{k1} + r_{f2} \leq a_{12} \quad (8.24)$$

$$r_{k2} + r_{f1} \leq a_{12} \quad (8.25)$$

That r_{f1} and r_{f2} are the inside radii of gear 1, 2, r_{k1} and r_{k2} are the outside radii of gear 1, 2, and a_{12} is the centre distance of the gear pair.

Furthermore, equation (8.25) can be reworked into the following form, considering that nominally $a_{12} = r_{o1} + r_{o2}$

$$c_{f1} - c_{k2} + 1 \geq 1 \quad (8.26)$$

and introducing the notation:

$$c_{f1eqv} = c_{f1} - c_{k2} + 1 \quad (8.27)$$

Equation (8.26) takes the form:

$$c_{f1eqv} \geq 1 \quad (8.28)$$

A similar condition can be formulated from equation (8.24) for gear 2. The significance of c_{f1eqv} will be revisited in section 8.3.5.

8.3.4. Corner contact and penetration

A detailed study of interference resulting from corner contact and penetration can be found in Chapter 4, section 4.3 (Figure 4.2). The points of the gear profile were generated using an in house computer programme in C++, using the algorithm presented in Figure 4.3. The algorithm has been used in this study for implementing the corner contact's model, is in accordance with equations (from (4.35) to (4.49)) which have been introduced in section 4.3.1.3.

8.3.5. Addendum and dedendum analysis

By means of the corner contact and penetration method from section 4.3, interference and non-interference design space for different combinations of the design parameters are presented in Figure 8.6. The design parameters are included as the number of teeth for gear 1 and 2, cutter tip radius coefficient of gear 1, dedendum coefficient of gear 1 and addendum coefficient of gear 2.

According to the results of Figure 8.6, there is a relation between dedendum coefficient of gear 1 (c_{f1}) and addendum coefficient of gear 2 (c_{k2}).

The relation is introduced as follows, same as in equation (8.27):

$$c_{f1eqv} = c_{f1} - c_{k2} + 1$$

Introducing this equivalent metric for c_f , which notably takes into account the mating gear as well, each family of curves is reduced to a single curve (coincident with each thick black line in Figure 8.6).

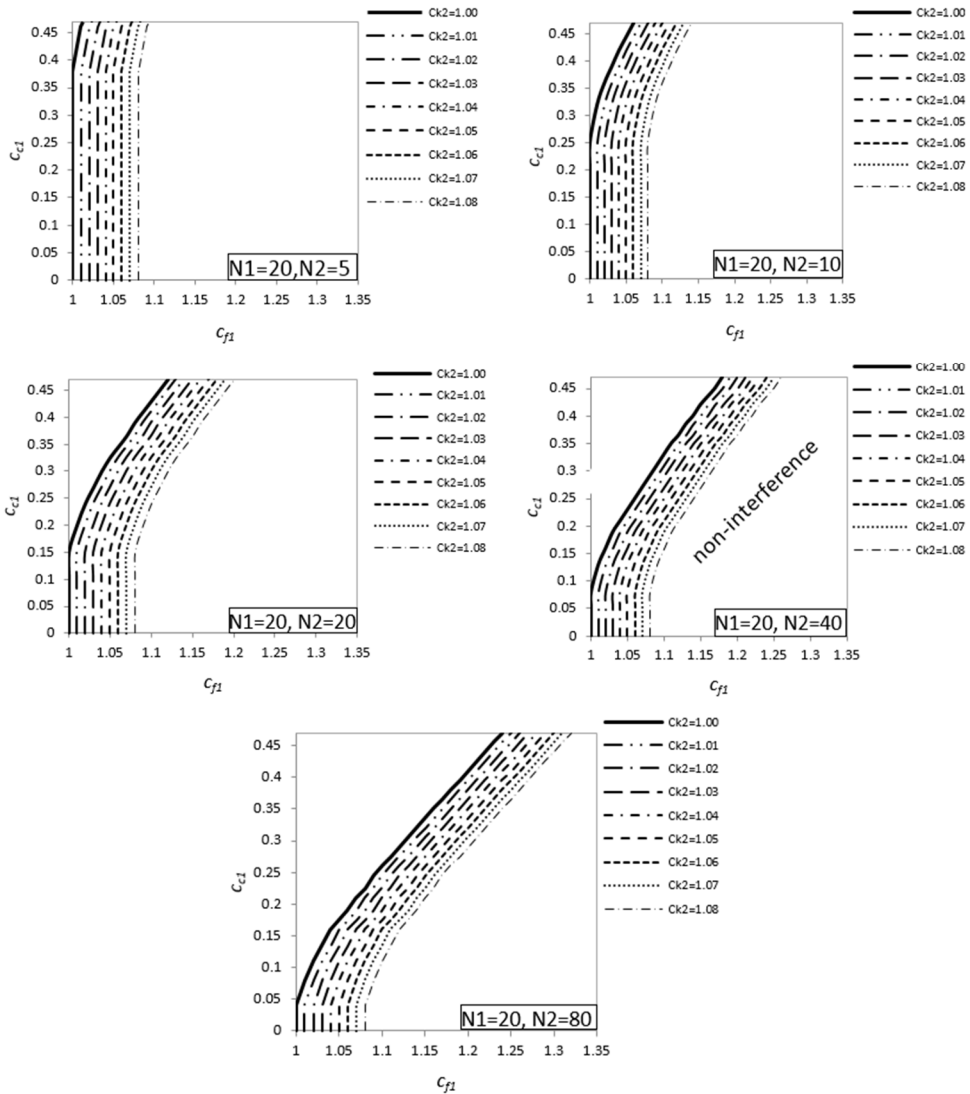


Figure 8.6: Detection of interference and non-interference are for different combination of the design parameters including addendum coefficient of gear 2 (c_{k2})

8.4. PARAMETRIC COUPLINGS AND SYNTHESIS OF GENERALISED MODEL

8.4.1. Parametric couplings

We notice the following important couplings between gear design parameters:

- Normally, it is considered that the pressure angle of two mating involute gears has to be the same, in order to allow them to mesh. However, it follows from basic geometry that any involute will fulfil the necessary tangency conditions when mating with any other involute, so the actual concern is pitch

compatibility: base pitch compatibility in particular. In fact, gears with different pressure angles may still mesh properly if they have the same base pitch, which can be obtained by a proper selection of the individual (non-standard) gear modules. In this sense, base pitch compatibility imposes a strong coupling between the pressure angle and module.

- Although in principle the addenda and dedenda of a pair of gears (4 parameters in total) may be selected arbitrarily, the predicted interference behaviour can be expected to depend on two distinct combinations involving the addendum of one gear and the dedendum of the other gear, as demonstrated in section 8.3.4. Clearly, increasing the amount of addendum of one gear will necessitate and increase in the dedendum of the mating gear.
- Tooth thickness and pressure angle are related with regard to tip pointing. With increasing the pressure angle it will be necessary to increase tooth width in order to avoid tip pointing. Addendum and dedendum (hence whole depth) are likewise coupled with tooth thickness and pressure angle in the same context, with shorter teeth being less prone to tip pointing even for large pressure angles and small tooth widths. This is shown in section 8.2.1.
- Dedendum, cutter tip radius and pressure angle can be expected to have a combined effect on the occurrence of undercutting, as shown in section 8.2.2.
- Thickness-wise interference between two gears can be expected to depend on tooth thickness, the operating pressure angle, and the numbers of teeth of both gears, all coupled as shown in section 8.3.2.
- Considering radial interference at the root of one gear mating with another gear, it has been shown in section 8.3.3 to depend on the relation between dedendum of the reference gear, the addendum of the mating gear, and the numbers of teeth of both gears. The same consideration is valid for radial interference at the root of the mating gear.
- Addendum, cutter tip radius, pressure angle and tooth thickness are in principle properties of the rack cutter (and cutting layout). As shown in section 8.2.3, not every combination is viable: i.e. a large cutter tip radius must be accommodated by correspondingly large thickness and/ or large pressure angle and/ or small addendum. While each one of these 4 parameters is in principle independent, the limits on each one are strongly coupled.

Thus hereinafter we shall consider the above couplings and the corresponding developed models to describe and support the relevant design choices.

8.4.2. Design parameters

Hereunder some of the considered parameters are discussed, summarising the main considerations typically at play in the context of gear design. This section, together with section 8.4.1, serves to support the condensed synthetic overview produced in section 8.4.3.

8.4.2.1. Pressure angle (α_0)

Pressure angle is the slope of the gear tooth at the pitch point. If the pressure angle were 0° , the tooth is parallel to the axis of the gear- and is really a spur-

gear tooth. Generally, gears can be manufactured with different type of pressure angles of 14.5°, 20° and 25° in industrial applications.

High pressure angles such as 22.5°, 25°, and 27.5° are in some cases used to increase bending strength [2]. Most designers prefer a 20° pressure angle for spur gears. In the past, the 14.5° pressure angle was widely used because it affords higher contact ratios. It is not popular today because it is more susceptible to undercutting when small numbers of pinion teeth are needed. Also, it lacks the load-carrying capacity of the 20° tooth form. Pressure angles above 20° give higher load capacity but may not run quite as smoothly or quietly because of reduced contact ratios.

In involute gear manufacturing, the 20° system has prevailed over the years [47-54] since it offers good pitting resistance along with acceptable bending strength, and good contact ratio without undercutting over 17 teeth, or 15 teeth if the maximum allowable rack cutter tip radius is used [1-7]. However, for tooth numbers less than 14 the only solution to avoid undercutting is to apply positive profile shifting of the cutting tool, resulting in long addendum teeth, decreased contact ratio, and increased sliding velocities at the ends of the path of contact [23-29]. The low tooth number region corresponds to the pinion designs that are reported to suffer more from bending than the mating gears [2]. Therefore, the selection of the fillet geometry is important for achieving adequate bending strength in low-tooth pinions if one wants to avoid applying profile modifications or changing the centre distance.

Gears generated with non-standard pressure angle have been demonstrated to achieve higher bending strength [54]. In fact, the same working flank can be cut by infinite combinations of pressure angles and modules [47-54], but with varying implication on the produced root shape and strength. Practical limitations to using high pressure angle values arise from unwanted tooth tipping (Figure 8.7) and corresponding addendum reduction, as well as increased radial force and bearing load components.

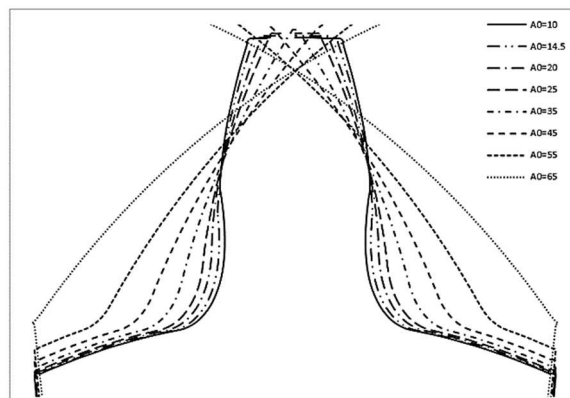


Figure 8.7: Tooth profile geometry with different pressure angle

Figure 8.7 shows the geometry of on tooth of a spur gear with different pressure angle. With different value of the pressure angle, a different part of the same involute will be produced (e.g. if applying profile shift), or possibly an entirely new involute. Increasing the pressure angle tends to increase the tooth root thickness, strength and consequently the load carrying capacity.

8.4.2.2. Module (m)

Geometrically speaking the module is just a scale factor for a gear. For instance all geometrical features of a spur gear with $m=2mm$ are two times bigger than the corresponding features of a $m=1mm$ gear, provided that the number of teeth, nominal pressure angle and the whole depth, fillet radius, backlash and profile shifting coefficients are the same. All linearly affected magnitudes (i.e. root stress including stress concentration, sliding velocity etc.) increase either proportional (sliding velocity) or inversely proportional to it (root stress), while others (i.e. contact stress) follow a non-linear relationship. Regarding the efficiency of a gear pair it is mainly dominated by the sliding velocities of the gears in mesh along their path of contact, therefore the bigger the module the higher the losses for a given angular velocity and transmission ratio.

8.4.2.3. Cutter tip radius (c_c)

The root fillet of a tooth is normally generated by the cutter tip trajectory. The root carries the maximum bending stress of the tooth, and therefore the value of the cutter tip radius has a significant effect on tooth bending strength. Increasing the cutter tip radius results in larger generated root fillet therefore reducing stress concentration and the value of the maximum root stress.

At the same time, a larger cutter tip radius tends to reduce the involute part of the tooth, thereby increasing the risk of interference with mating gears and limiting the values that may be applied practically.

Other considerations are:

- Small or zero radius has been known to cause localised tool wear, causing in turn poor surface quality and dimensional inaccuracy of the manufactured gear
- For a given whole depth, there is a practical limitation on the maximum radius that is obtainable; the larger radii will be incompatible with the designated whole depth for the 20° gear system, or the cutter teeth will be undercut, i.e. they cannot be realised unless the whole depth is reduced

8.4.2.4. Addendum (c_k)

With increasing the addendum, the number of simultaneously meshing teeth and the contact ratio can be increased, which can result in decreasing the operating transmission error and noise; long addendum gears are typically used to obtain transverse contact ratio of two or above (which is particularly useful in e.g. automotive spur gears). Contact ratio-induced load sharing and resulting gear tooth strength can also be regulated by judicious choice of addendum.

Other considerations include:

- The whole depth required to accommodate a long addendum is bigger, resulting in lower attainable stiffness per tooth.
- Long addendum pinion with short addendum gear pairs are in some cases utilised to strengthen the pinion and adjusting the tip sliding velocities [2]

8.4.2.5. Dedendum (c_f)

Addendum and dedendum together define the tooth whole depth and are such closely coupled with regard to geometrical compatibility and interference. The following considerations apply:

- Increasing the tooth whole depth to achieve higher contact ratio can reduce the load carrying capacity of individual teeth
- On the other hand, for high contact ratio spur gears (above two), where one expects the load-sharing between mating teeth to compensate for this reduction, a small pitch error or other error could neutralise this effect, making high contact ratio designs applicable only under precise accuracy (and cost) conditions
- With increasing dedendum coefficient the leverage of the applied load increases therefore leading to higher fillet stress values

8.4.2.6. Profile shifting

Profile shifting simultaneously affects the apparent addendum, dedendum, tooth thickness and pressure angle. As such, it can be modelled equivalently by means of these other parameters.

8.4.2.7. Tooth thickness (c_s)

Tooth thickness has a direct effect on the tooth root cross-section and corresponding bending stresses and strength, with higher thickness giving better results. However, the geometrical compatibility of mating gears imposes limits on the thickness of mating teeth, or interference will occur. Backlash can be controlled for a given centre distance by controlling the thickness of the mating gear teeth. Other applicable design considerations are that:

- Pinion tooth thicknesses are often increased at the expense of the mating gear to strengthen the pinion [2].
- The determination of tooth thickness depends on the amount of desired backlash and the desired addendum, for a minimum size of tooth top land [2]. The choice of tooth thickness can be used to mitigate tooth pointing.

8.4.2.8. Number of teeth (N)

The numbers of teeth of two mating gears combined dictate their transmission ratio and basic kinematics. Almost all other characteristics of the gear pair, including contact ratio, load sharing, strength etc are implicitly affected by this choice. The number of teeth of a gear together with its module dictate the gear size.

8.4.3. Generalised model

Base on the explanation in section 8.4.1, it can be concluded that the dependent design parameters can be reduced to independent design degree of freedoms only.

The design parameters that we discuss in this work are as: the number of teeth for gear 1 and 2, pressure angle, cutter tip radius, dedendum, addendum, tooth thickness.

With different formulations as explained in pervious sections, some of the design parameters are coupled and can be found from other formulations to be independent. Table 8.2 shows that how to use different formulas to reduce the design DOFs.

Table 8.2: Dependency of the design parameters

Design parameters (one per gear)	Dependency	Explanation
α_0	$\alpha_{01} = \alpha_{02} = \alpha_0$ or same base pitch	Pitch compatibility
c_k, α_0, c_s, N	Eq. (8.10)	Avoidance of tip pointing
c_f, c_c, α_0, N	Eq. (8.13)	Avoidance of undercutting
c_f, c_c, α_0, c_s	Eq. (3.10)	Cutter shape coupling/limitation
c_s, α_c, N	Eq. (8.23)	Avoidance of thickness-wise interference (backlash)
$c_f, c_k (c_{feqv})$	Eq. (8.28)	Avoidance of radial interference
$c_f, c_k (c_{feqv}), c_c, \alpha_0, N$	Eqs. (4.20)-(4.22)	Corner contact and interference

8.5. RESULTS AND DISCUSSION

8.5.1. Multi-parametric gear design maps and limit curves

Considering a pair of mating gears 1 and 2, in this section the relations between the design parameters such as the number of teeth for gear 1 and 2, pressure angle, cutter tip radius, dedendum, addendum, tooth thickness with regard to manufacturing feasibility (tip pointing/ non-pointing and undercutting/ non-undercutting) and geometrical compatibility (interference/ non-interference) are discussed. The corresponding design subspaces and limit curves are identified.

8.5.1.1. Influence of pressure angle on manufacturability

Figure 8.8 shows the manufacturing feasibility design space, according to equation (3.10), for different values of the pressure angle (10°, 14.5°, 20°, 25°, 30°, 35°, 40°, 45°, 50°, 60°) while the value of tooth thickness coefficient is given ($c_s = 0.5$). With increasing the pressure angle, the possibility of using larger c_f

will be increased and simultaneously the possibility of using larger cutter tip radius will be decreased.

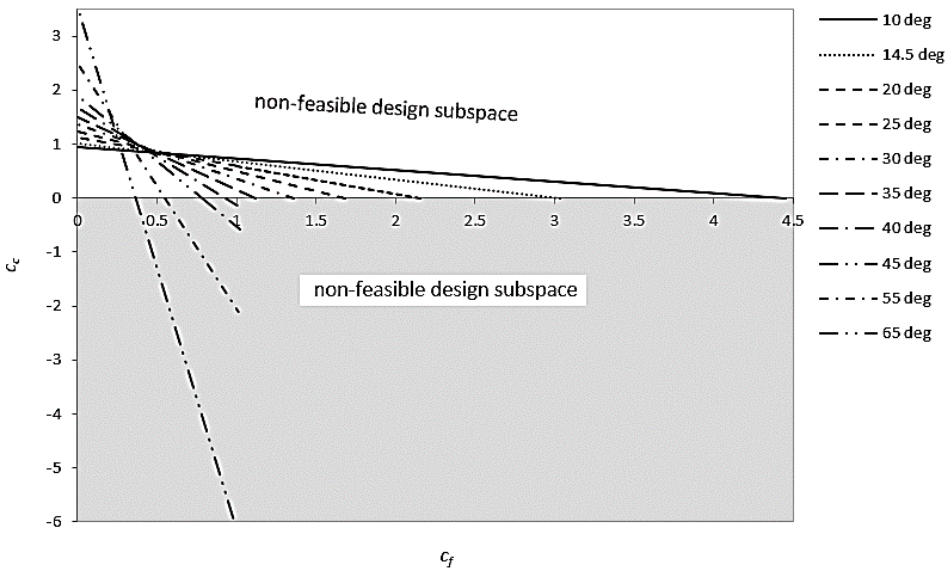
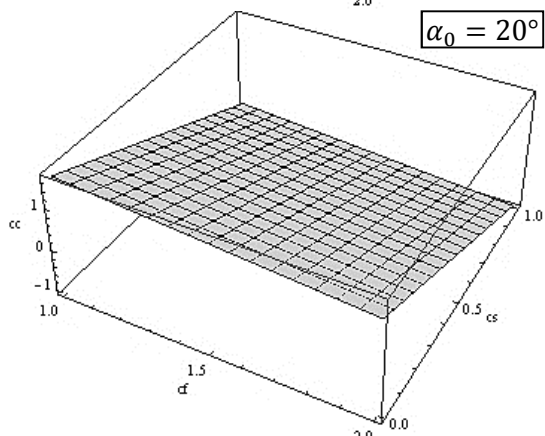
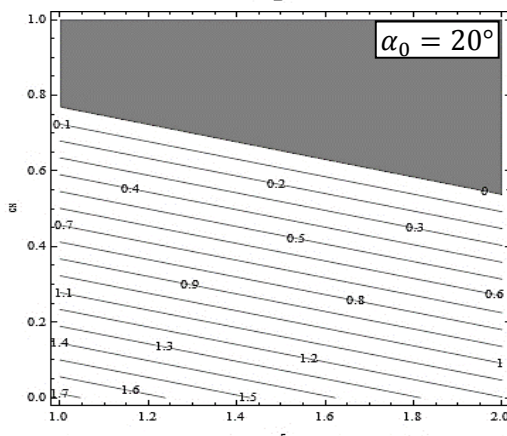
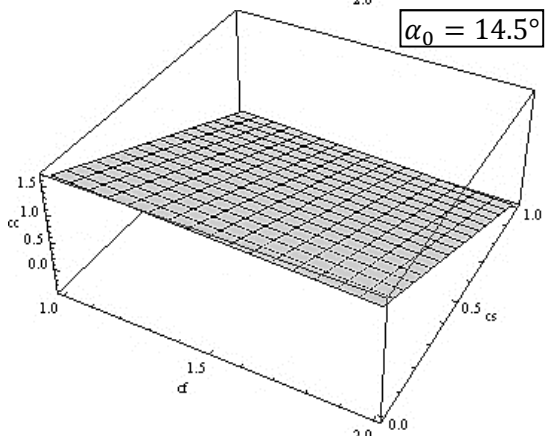
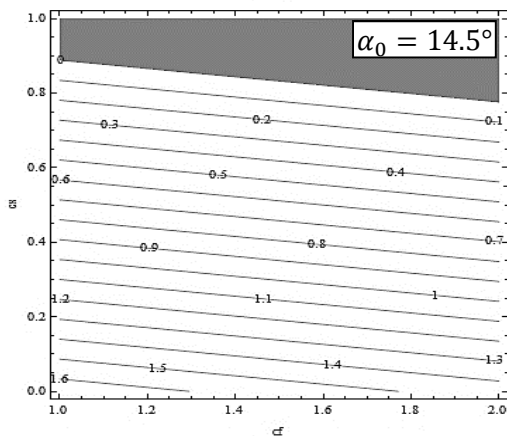
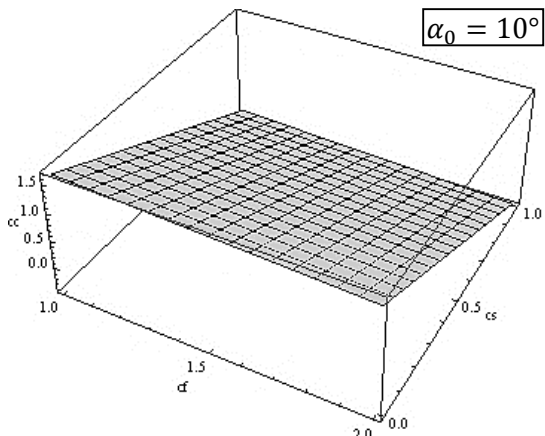
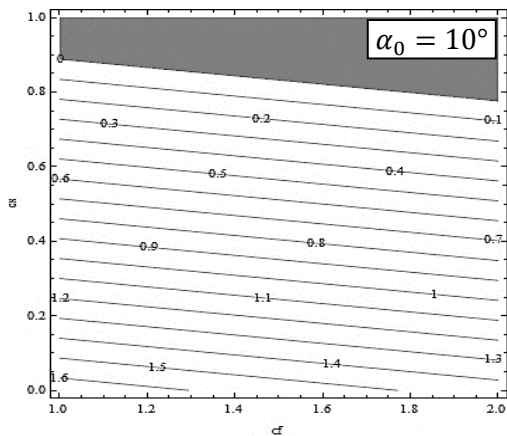


Figure 8.8: Influence of pressure angle on manufacturing feasibility with given amount of tooth thickness

Figure 8.9 reports the result of a more general study, according to equation (3.10), showing the complete relation between c_f , c_c , c_s and α_0 (10°, 14.5°, 20°, 25°, 30°, 35°).

In the left column, the diagonal lines present the amount of cutter tip radius coefficient (c_c) and the grey subspace corresponds to manufacturing non-feasibility. With smaller pressure angle, the feasible subspace will be bigger.

In the right column, a 3D plot is given of the relation between c_f , c_c , c_s for given amount of pressure angle. The subspace above the surface corresponds to non-feasible parameter combinations. With increasing the pressure angle, the feasible design space will be decreased.



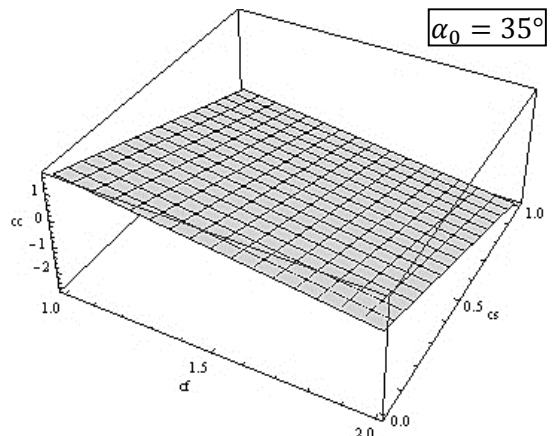
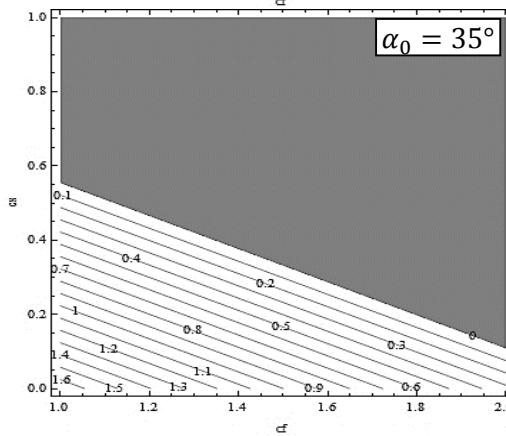
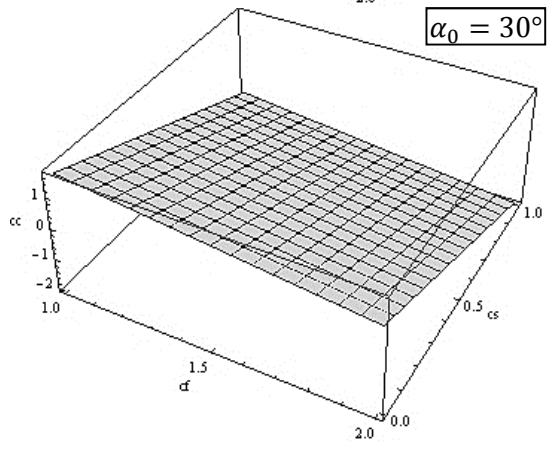
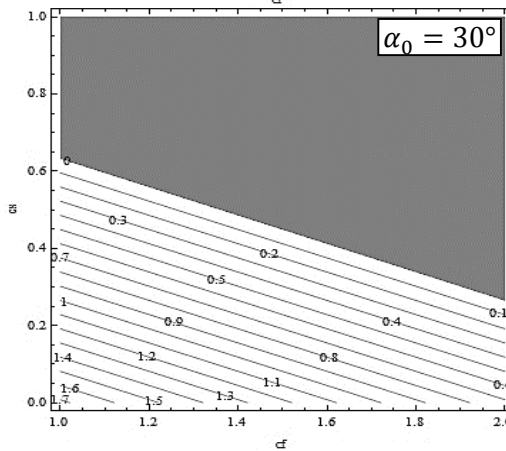
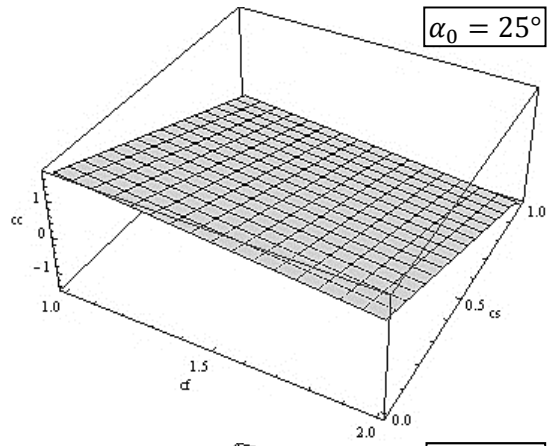
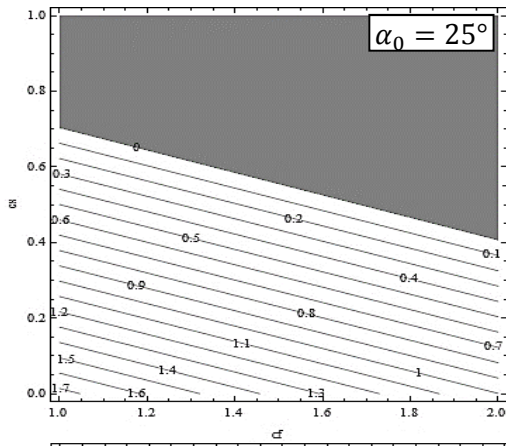


Figure 8.9: Feasibility of a gear design according to equation (3.10) (relation between c_f , c_c , c_s and α_0)

8.5.1.2. Tooth thickness limitation (cutter tooth undercutting)

Equation (3.10) presents the maximum value of c_c , with changing the amount of c_f while the value of c_s is given. In equation (3.10), different values for tooth thickness ($c_s=0.50, 0.52, 0.54, 0.56, 0.58, 0.60, 0.62, 0.64, 0.66, 0.68, 0.70$) present some limitations for different combinations of c_c and c_f . Figure 8.10 presents the feasible design space for different $c_c - c_f$ combinations in regard with tooth thickness limitations. With increasing the amount of tooth thickness, it is clear that the tolerance area for different values of c_c, c_f will be decreased.

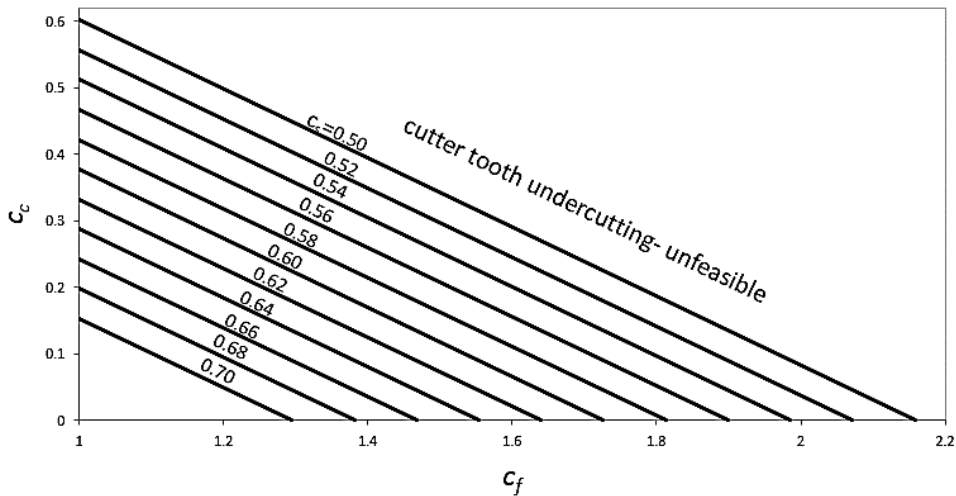


Figure 8.10: Tooth thickness limitation for different combinations of c_c, c_f

8.5.1.3. Interference limits in the design space

Figure 8.11 presents the limits to the design space imposed by interference for different combinations of the design parameters including N_1, N_2 (5, 10, 20, 40, 80), c_c, c_f, α_0 ($10^\circ, 14.5^\circ, 20^\circ, 25^\circ, 30^\circ, 35^\circ$). With regard to feasibility, equation (3.10) has been applied to find the maximum possible amount of tooth thickness coefficient. For calculating the interference subspace and corresponding limit curve the algorithm of corner contact and penetration method (section 8.3.4) has been implemented. Above the tooth thickness limitation line lies non-feasible design space. The non-interference subspace is bounded from the left by the family of curves depending on the pressure angle and the number of teeth of the mating gear.

With increasing pressure angle and the number of teeth for gear 2, the design subspace corresponding to manufacturing feasibility and non-interference will be smaller. Hence larger gears with bigger pressure angle are more at risk of manufacturing and interference problems.

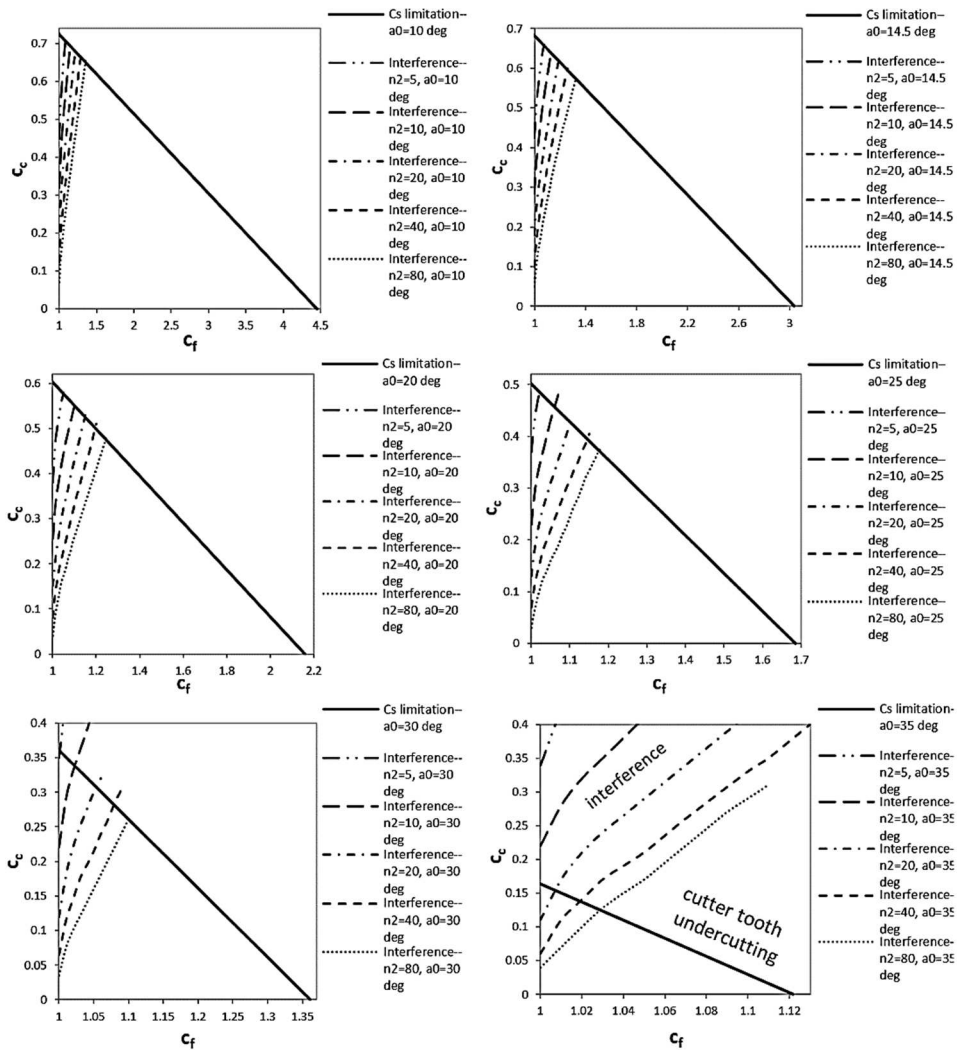


Figure 8.11: The design subspace corresponding to manufacturability and non-interference for different combinations of the design parameters including N_1 , N_2 , c_{c1} , c_{f1} , and α_0

8.5.1.4. Undercutting limitation

Using equation (8.13) for different numbers of teeth for gear 1 ($N_1=5, 10, 20, 40, 80$) allows to design a gear without undercut as shown in Figure 8.12, where the negative values for c_c are obviously not feasible. With increasing the number of gear teeth and the value of c_f , the safety of the design against undercutting will

be increased. Increasing the pressure angle also enlarges the design subspace that is free from undercutting.

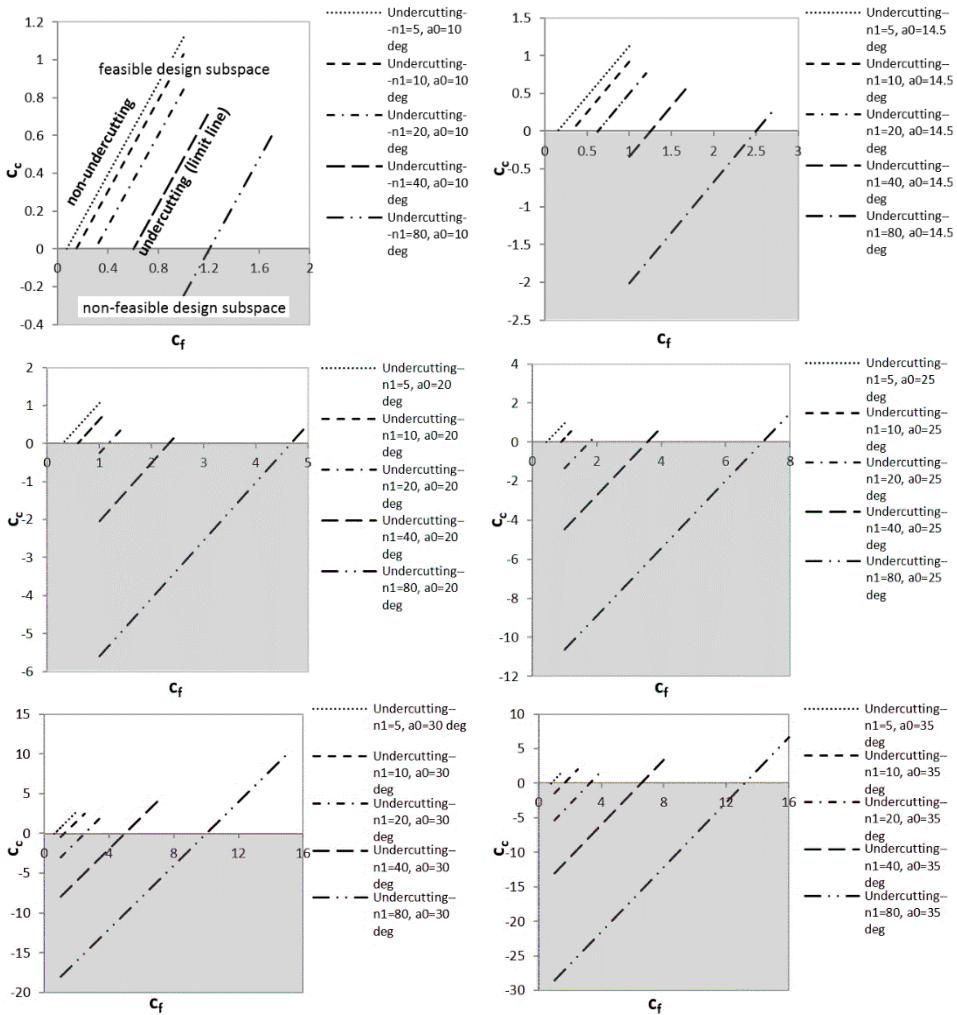


Figure 8.12: Undercutting and non-undercutting design subspaces for different combinations of N_1 , c_c , c_f , α_0 . The grey subspace corresponds to non-feasible designs

8.5.1.5. From radius limitation

Figure 8.13 shows the form radius for a 20-tooth pinion for an exhaustive array of dedendum and cutter tip radius combinations for undercut and non-undercut root tooth as calculated by equations (4.20), (4.21) and (4.22). Extreme combinations of dedendum and cutter tip radii that are impossible to attain have been filtered out by use of equation (8.13) and therefore no corresponding values exist at the far end of the chart, which is shown in Figure 8.14.

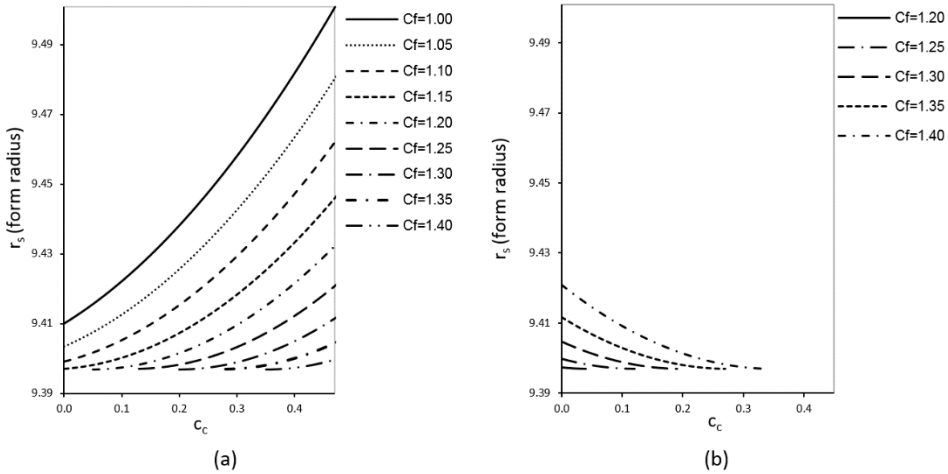


Figure 8.13: Form radius limitation for (a) non-undercut and (b) undercut root tooth ($N=20$)

It is easy to identify a region of dedendum and cutter tip radius combinations, where the form radius is minimised and therefore the involute portion of the teeth is maximised. As one moves away from that region, two different trends are to be identified: a) For combinations of relatively large values of dedendum and small values of cutter tip radius the form radius increases, suggesting the presence of a secondary cutting action (undercutting). b) For combinations of relatively small values of dedendum and large values of cutter tip radius the form radius increases also, which, depending on the mating gear geometry and the centre distance, presents an increasing risk of interference. As this is the region that produces the shallowest teeth with the stronger fillets, it is expected that this is the region where the optimal designs are to be sought.

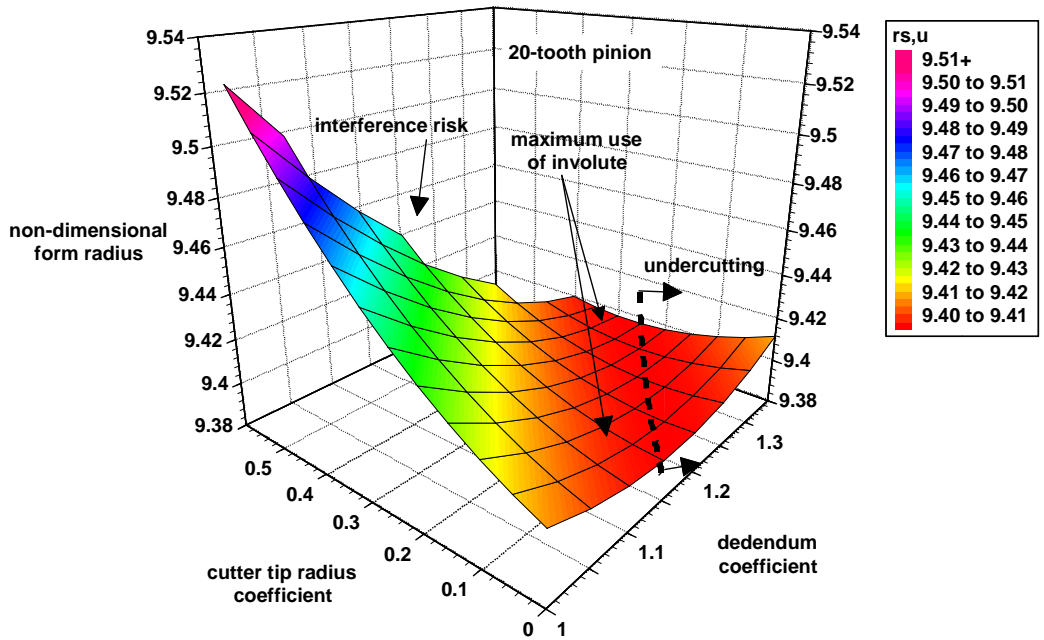


Figure 8.14: Calculated non-dimensional form radius for a 20-tooth pinion for the possible combinations of dedendum and cutter tip radius. Useful designs lie between the rightmost (undercutting) and leftmost (interference) extremes

It is also important to note that the iso- r_s curves are linear throughout the definition field; this means that any increase of cutter tip radius must be made at the expense of increasing the dedendum coefficient by an analogous amount. The ratio of this analogy is easily determined from equation (3.4) as:

$$\frac{\Delta c_f}{\Delta c_c} = \frac{\cos \alpha_0}{\tan \left(45^\circ + \frac{\alpha_0}{2} \right)} \quad (8.30)$$

For the 20° gears studied here, this means that $\Delta c_f / \Delta c_c = 0.658$.

8.5.1.6. Addendum limitation

From section 8.3.5 it can be concluded that instead of c_{f1} , we can use $c_{f1equivalent}$ as defined in equation (8.27), thereby incorporating the effect of the addendum in this new metric, which is always positive, since the addendum of the mating gear may not be larger than the dedendum of the reference gear. Figure 8.15 presents the interference limit curve calculations in consideration of N_1 , N_2 , c_{c1} , c_{f1} and c_{k2} .

These results show that the risk of interference will be increased with using smaller value of c_{f1eqv} , which can be the result of increasing the addendum of the mating gear, and/or bigger value of c_c .

The results show that the interference limit is not dependent on the number of teeth of gear 1 or the contact ratio, but only on the number of teeth of gear 2. Thus any combination of N_1, i_{12} , where $N_1 i_{12} = N_2$ is constant, produces an identical interference limit curve. This insight and in additional $c_{f1equivalent}$ allow reducing by two the dimensions of the parametric space, without loss of generality.

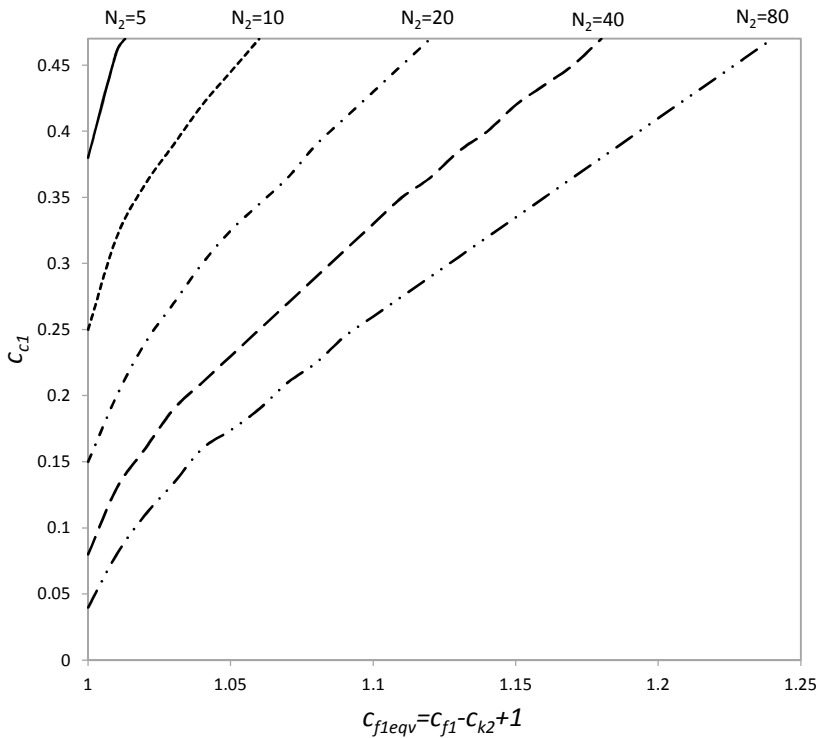


Figure 8.15: Reducing the five-parametric design space for interference limit curves to the three-parametric design space c_{f1eqv}, c_{c1}, N_2 after elimination of parameters N_1, i_{12} and c_{k2}

Considering the dedendum coefficient fixed, another relevant observation is that the contact ratio will be increased with decreasing the amount of equivalent dedendum coefficient, which is practically equivalent to increasing the addendum coefficient of the mating gear and is not affected by the dedendum or the cutter tip radius of the reference gear, as shown in Figure 8.16. The overall

contact ratio will depend of course on the addenda (or equivalent dedenda) of both gears.

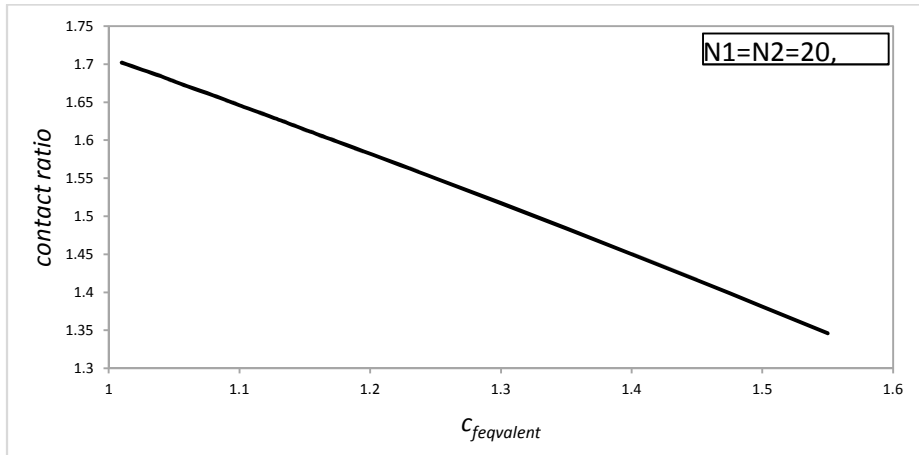


Figure 8.16: The relation between equivalent dedendum coefficient (c_{feqv}) and gear contact ratio

8.5.2. Compact and high contact ratio tooth forms

In section 8.5.1, a large family of combinable plots has been presented, from which the manufacturability and compatibility design subspaces can be delimited.

Compact tooth form can be designed with minimising the total volume of gear tooth. Besides reducing the module, this can be done by reducing the number of teeth and minimising the clearance between gear teeth [126-131]. Higher pressure angles, which are conducive to higher load carrying capacity and small modules and addenda, which are conducive to high scoring/ scuffing resistance, can also be chosen.

Likewise, while only pressure angle and the addenda of both gears affect the contact ratio, their feasible values when attempting to increase the contact ratio are affected by many other design parameters (including the limitation of form radius). The produced design spaces allows a fast assessment of these limits and corresponding attainable values.

Given that the design space, considering both gears in a pair, contains multiple parameters and the design goals vary from one application to another, from the provided analytical mapping of the design space limits the optimal (or Pareto-optimal) solutions can be found on a case by case basis. Figure 8.17 offers a qualitative summary of several of the plots presented in section 8.5.1 and can serve as a starting point and design guideline.

As the relations between the design parameters reduced to the independent design DOFs, selecting the design parameters can be easy and fast to find compact and/ or high contact ratio tooth forms.

Already, in high performance gear applications in the automotive and aerospace sectors the industry has moved away from the standard tooth proportions and many gear designs currently being developed or in use fall in the regions of the design space denoted by the thick arrows (left and top left part of the feasible design space). This is still largely based on trial-and-error. To the best knowledge of the authors, Figure 8.17 is the first representation to explain why such designs are optimal in the $c_c - c_f$ space, in terms of compactness and contact ratio (both of which are a function of c_{feqv}) allowing a better-informed design space exploration and design optimisation.

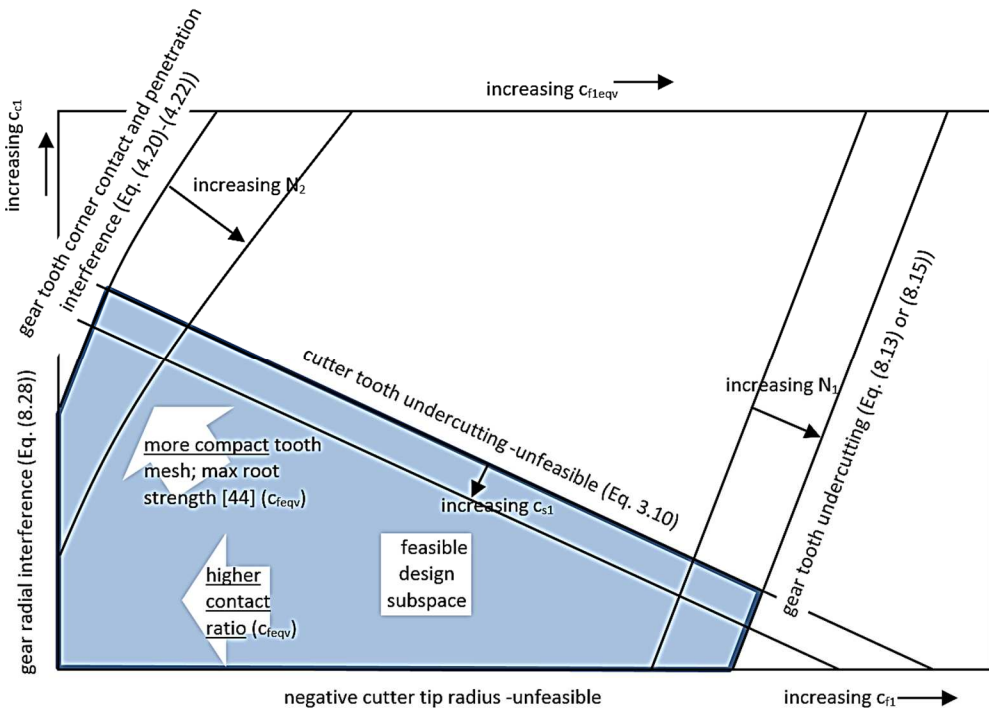


Figure 8.17: Overlay of different limit lines and delineation of feasible and non-feasible design subspaces on the multi-parametric non-dimensional design space ($c_f/c_{feqv}, c_c, c_s, N$). The limit lines corresponding to different values of α_0 are not shown for clarity

8.5.3. Implications of the choice of pressure angle

According to the results of section 8.5.1.2, the pressure angle plays an important role regarding not only gear performance, but also the size/extent of the design

subspace that is consistent with manufacturability and compatibility. Larger pressure angles are only feasible within limited design subspaces.

This means that for the large pressure angles that are used for special applications such as high capacity load carrying in heavy industry, the presented mapping can be used to precisely navigate the narrow design space in order to reach feasible designs.

8.6. CONCLUSION

This chapter presented a number of original and reworked mathematical models that are relevant to assessing the manufacturability and geometrical compatibility of gears, considering the multi-dimensional design space involving simultaneously the pressure angle, module, addendum, dedendum, cutter tip radius, thickness, and number of teeth of both gears in a pair. These models were synthesised into one comprehensive meta-model that supports fast assessment of gear design feasibility.

Various modes of interference were considered as well as the manufacturability of the individual gear teeth in terms of pointing and undercutting. Differences between different available models (e.g. with regard to undercutting were identified and discussed). Furthermore, models for pitch compatibility and corner contact and penetration were presented that provide new possibilities for non-standard and compact tooth form designs.

The resulting combined model serves to provide a complete analytical overview of the multi-parametric design space and is suitable for the fast assessment of existing designs, for implicit or explicit (direct) gear design, for extracting design guidelines, and for design optimisation. The model can be used to identify and explore highly promising under-used subspaces of the parametric design space, which are currently of significant interest to i.e. the automotive and aerospace industries.

REFERENCES

1. Litvin, F. L., 1994, *Gear geometry and applied theory*, Prentice Hall
2. Townsend, D. P., 1992, *Dudley's Gear Handbook*, McGraw Hill
3. Buckingham, E., 1988, *Analytical Mechanics of Gears*, Dover Publications Inc.
4. Spotts, M. F., 1985, *Design of Machine Elements*, 6nd Edition, Prentice hall, Englewood Cliffs
5. Merritt, H. E., 1954, *Gears*, 3rd Edition, Isaac Pitman & Sons
6. Maitra, G. M., 2001, *Handbook of Gear Design*, Tata McGraw-Hill Education, New Delhi
7. Prabhakaran, S., Ramachandran, S. ,2013, Comparison of bending stress of a spur gear for different materials and modules using AGMA standards in FEA, *Advanced Materials Research*,739:382-387

8. KISSsoft AG, version 03/2011, 2011
9. HyGEARS, Involute Simulation Software Inc., Version 4.0, 2014
10. Gear Design Pro 2011, Dontyne System, version 4.5.
11. GearTeq 2012, Camnetics Incorporated, version 20.32.341.
12. Geartrax 2012, Camnetics Incorporated, version 20.671 for SolidWorks 2012.
13. Nonaka, T., Satoh, D., Miyake, K., Kubo, A., 2002, Strength of spur gear teeth with small modules of the order of 0.1 mm: (1st report, nature of tooth failure), *Nippon Kikai Gakkai Ronbunshu, C Hen/Transactions of the Japan Society of Mechanical Engineers, Part C*, 68(8):2431-2437
14. Baglioni, S., Cianetti, F., Landi, L., 2012, Influence of the addendum modification on spur gear efficiency, *Mechanism and Machine Theory*, 49:216-233
15. Li, S., 2008, Effect of addendum on contact strength, bending strength and basic performance parameters of a pair of spur gears, *Mechanism and Machine Theory*, 43(12):1557-1584
16. Balambica, V., Prabhu, T. J., Venkatesh Babu, R., Deepak, E. V., 2013, Design and static analysis of an addendum modified helical gear tooth, *Applied Mechanics and Materials*, 391:132-138
17. Chen, T., Sun, W., Zhang, X., 2011, An analytical method to determine the addendum modification parameters of involute helical gears, *Proceedings of the Institution of Mechanical Engineers, Part C: Journal of Mechanical Engineering Science*, 225(11):2516-2524
18. Atanasiu, V., Iacob, M. R., 2010, Tooth wear effects on dynamic transmission error of spur gears with addendum modifications, *International Review of Mechanical Engineering*, 4(6):638-644
19. Antal, T. A., 2009, A new algorithm for helical gear design with addendum modification, *Mechanika*, 77(3):53-57
20. Imrek, H., Unuvar, A., 2009, Investigation of influence of load and velocity on scoring of addendum modified gear tooth profiles, *Mechanism and Machine Theory*, 44(5):938-948
21. Arikan, M. A. S., 2003, Determination of addendum modification coefficients for spur gears operating at non-standard center distances, *ASME International Design Engineering Technical Conferences and Computers and Information in Engineering Conference, DETC2003/PTG-48063*, 4:489-499
22. Pedrero, J. I., Artés, M., 1996, Approximate equation for the addendum modification factors for tooth gears with balanced specific sliding, *Mechanism and Machine Theory*, 31(7):925-935
23. Rockwell, P. D., 2001, Profile shift in external parallel-axis cylindrical involute gears, *Gear Technology*, 18(6):18-25
24. Wang, C., Liu, H., Xiang, C. -L., 2014, Influences of profile modification on dynamic characteristics of involute spur gears under a fluctuating torque, *Zhendong yu Chongji/Journal of Vibration and Shock*, 33(24):32-38
25. Barone, S., Borgianni, L., Forte, P., 2004, Evaluation of the effect of misalignment and profile modification in face gear drive by a finite element meshing simulation, *ASME Journal of Mechanical Design*, 126(5):916-924

26. Chen, Z., Shao, Y., 2013, Mesh stiffness calculation of a spur gear pair with tooth profile modification and tooth root crack, *Mechanism and Machine Theory*, 62:63-74
27. Bonori, G., Barbieri, M., Pellicano, F. 2008, Optimum profile modifications of spur gears by means of genetic algorithms, *Journal of Sound and Vibration*, 313(3-5):603-616
28. Lin, H. H., Oswald, F. B., Townsend, D. P., 1994, Dynamic loading of spur gears with linear or parabolic tooth profile modifications, *Mechanism and Machine Theory*, 29(8):1115-1129
29. Sankar, S., Nataraj, M., 2001, Profile modification-a design approach for increasing the tooth strength in spur gear, *International Journal of Advanced Manufacturing Technology*, 55(1):1-10
30. Hsu, R.-H., Su, H.-H., 2014, Tooth contact analysis for helical gear pairs generated by a modified hob with variable tooth thickness, *Mechanism and Machine Theory*, 71:40-51
31. Sharif, K. J., Evans, H. P., Snidle, R. W., 2006, Wear modelling in worm gears, *Solid Mechanics and Its Applications*, 134:371-383
32. Litvin, F. L., Hsiao, C.-L., Ziskind, M. D., 1998, Computerized overwire (ball) measurement of tooth thickness of worms, screws and gears, *Mechanism and Machine Theory*, 33(6):851-877
33. Li, S., Kahraman, A., 2010, Prediction of spur gear mechanical power losses using a transient elasto-hydrodynamic lubrication model, *Tribology Transactions*, 53(4):554-563
34. Höhn, B. R., Oster, P., Schrade, U., 2005, Studies on the micropitting resistance of case-carburised gears - Industrial application of the new calculation method, *VDI-Berichte*:1287-1307
35. Khoshnaw, F. M., Ahmed, N. M., 2008, Effect of the load location along the involute curve of spur gears on the applied stress at the fillet radius, *Materialwissenschaft und Werkstofftechnik*, 39(6):407-414
36. Kapelevich, A. L., Kleiss, R. E., 2002, Direct gear design for spur and helical involute gears, *Gear Technology*, 19(5):29-35
37. Hu, Y., Zhang, X.-C., Yang, Z.-J., Zhang, J., 2011, Precision cutting of spiral bevel gear with spherical involute tooth profile, *Beijing Gongye Daxue Xuebao / Journal of Beijing University of Technology*, 37(5):641-647
38. Jarchow, F., Yang, Q.J., 1990, Operational reliability of gear units with special consideration of the dedendum capacity, *Antriebstechnik*, 29:44-47
39. Sanders, A., Houser, D. R. , Kahraman, A., Harianto, J., Shon, S., 2011, An experimental investigation of the effect of tooth asymmetry and tooth root shape on root stresses and single tooth bending fatigue life of gear teeth, *ASME International Design Engineering Technical Conferences and Computers and Information in Engineering Conference*, DETC2011-48303, 8:297-305
40. Costopoulos, Th., Spitas, V., 2009, Reduction of gear fillet stresses by using one-sided involute asymmetric teeth, *Mechanism and Machine Theory*, 44(8):1524-1534

41. Chaphalkar, N., Hyatt, G., Bylund, N., 2013, Analysis of gear root forms: A review of designs, standards and manufacturing methods for root forms in cylindrical gears, *AGMA Fall Technical Meeting*,33-39
42. Brown, F. W., Davidson, S. R., Hanes, D. B., Weires, D. J., Kapelevich, A., 2010, Analysis and testing of gears with asymmetric involute tooth form and optimized fillet form for potential application in helicopter main drives, *AGMA Fall Technical Meeting*, 172-186.
43. Spitas, C., Spitas, V., Amani, A., 2015, Multi-parametric investigation of interference in non-standard spur gear teeth, *Mechanism and Machine Theory*, 88:105-124
44. Spitas, C., Spitas, V., Amani, A., Rajabalinejad, M., 2014, Parametric investigation of the combined effect of whole depth and cutter tip radius on the bending strength of 20 involute gear teeth, *Acta Mechanica*, 225(2):361-371
45. Spitas, C., Spitas, V., 2007, A FEM study of the bending strength of circular fillet gear teeth compared to trochoidal fillets produced with enlarged cutter tip radius, *Mechanics Based Design of Structures and Machines*, 35(1):59-73
46. Thirumurugan, R., Muthuveerappan, G., 2010, Maximum fillet stress analysis based on load sharing in normal contact ratio spur gear drives, *Mechanics Based Design of Structures and Machines*, 38(2):204-226
47. Marimuthu, P., Muthuveerappan, G., 2014, Influence of pressure angle on load sharing based stresses in asymmetric normal contact ratio spur gear drives, *Applied Mechanics and Materials*, 465-466:1229-1233
48. Xiao, J., Deng, X.L., He, J. N., Ma, W. X., Li, Y., Li, J. S., 2014, Simulation and analysis about different pressure angle in involute gears based on neural network, *Applied Mechanics and Materials*, 540:88-91
49. Sandooja, A., Jadhav, S., 2012, Analysis of gear geometry and durability with asymmetric pressure angle, *SAE International Journal of Commercial Vehicles*, 5(2):546-558
50. Kim, W., Lee, J. Y., Chung, J., 2012, Dynamic analysis for a planetary gear with time-varying pressure angles and contact ratios, *Journal of Sound and Vibration*, 331(4):883-901
51. Khoshnaw, F. M., Ahmed, N. M., 2009, The pressure angle effects of spur gears on stress concentration factor, *Engineering Computations*, 26(4):360-374
52. Danieli, G. A., 2000, Analytical description of meshing of constant pressure angle teeth profiles on a variable radius gear and its applications, *ASME Journal of Mechanical Design*, 122(1):123-129
53. Lin, J., 2009, A pressure angle function method for describing tooth profiles of planar gears, *ASME Journal of Mechanical Design*, 131(5):0510051-0510058
54. Spitas, C., Spitas, V. , 2008, Effect of cutter pressure angle on the undercutting risk and bending strength of 20° involute pinions cut with equivalent nonstandard cutters, *Mechanics Based Design of Structures and Machines*, 36(2):189-211

55. Medvedev, V. I., Volkov, A. E., Volosova, M. A., Zubelevich, O. E., 2015, Mathematical model and algorithm for contact stress analysis of gears with multi-pair contact, *Mechanism and Machine Theory*, 86:156-171
56. Chen, Y. -C., Lo, C. -C., 2015, Contact stress and transmission errors under load of a modified curvilinear gear set based on finite element analysis, *Proceedings of the Institution of Mechanical Engineers, Part C: Journal of Mechanical Engineering Science*, 229(2):191-204
57. Chen, B., Liang, D., Gao, Y., 2014, Geometry design and mathematical model of a new kind of gear transmission with circular arc tooth profiles based on curve contact analysis, *Proceedings of the Institution of Mechanical Engineers, Part C: Journal of Mechanical Engineering Science*, 228(17):3200-3208
58. Hsu, R. -H., Su, H. -H., 2014, Tooth contact analysis for helical gear pairs generated by a modified hob with variable tooth thickness, *Mechanism and Machine Theory*, 71:40-51
59. Tsuji, I., Kawasaki, K., Gunbara, H., Houjoh, H., Matsumura, S., 2013, Tooth contact analysis and manufacture on multitasking machine of large-sized straight bevel gears with equi-depth teeth, *ASME Journal of Mechanical Design*, 135(3), ID:34504
60. Spitas, C., Spitas, V., 2011, Fast unconditionally stable 2-D analysis of non-conjugate gear contacts using an explicit formulation of the meshing equations, *Mechanism and Machine Theory*, 46(7):869-879
61. Kolivand, M., Kahraman, A., 2010, An ease-off based method for loaded tooth contact analysis of hypoid gears having local and global surface deviations, *ASME Journal of Mechanical Design*, 132(7):0710041-0710048
62. Li, S., 2007, Finite element analyses for contact strength and bending strength of a pair of spur gears with machining errors, assembly errors and tooth modifications, *Mechanism and Machine Theory*, 42(1):88-114
63. Hwang, S. -C., Lee, J. -H., Lee, D. -H., Han, S. -H., Lee, K. -H., 2013, Contact stress analysis for a pair of mating gears, *Mathematical and Computer Modelling*, 57 (1-2):40-49
64. Imin, R., Geni, M., 2014, Stress analysis of gear meshing impact based on SPH method, *Mathematical Problems in Engineering*, ID: 328216
65. Naidoo Lingamanaik, S., Chen, B. K., Palanisamy, P., 2013, Finite element analysis on the formation and distribution of residual stresses during quenching of low carbon bainitic-martensitic large gears , *Computational Materials Science*, 79:627-633
66. Wang, S., Liu, G.R., Zhang, G.Y., Chen, L. , 2011, Design of asymmetric gear and accurate bending stress analysis using the es-pim with triangular mesh, *International Journal of Computational Methods*, 8(4):759-772
67. Gao, H., Li, Z., Deng, Z. ,2010, Sensitivity analysis of cup-shaped flexible gear parameters to its stress based on ANSYS , *Jixie Gongcheng Xuebao/Journal of Mechanical Engineering* ,46(5):1-7
68. Thirumurugan, R., Muthuveerappan, G., 2010 , Maximum fillet stress analysis based on load sharing in normal contact ratio spur gear drives, *Mechanics Based Design of Structures and Machines*, 38(2):204-226

69. Hassan, A. R., 2009, Contact stress analysis of spur gear teeth pair, *World Academy of Science, Engineering and Technology*, 58:611-616
70. Litvin, F. L., Vecchiato, D., Gurovich, E., Fuentes, A., Gonzalez-Perez, I., Hayasaka, K., Yukishima, K., 2005, Computerized developments in design, generation, simulation of meshing, and stress analysis of gear drives, *Meccanica*, 40(3):291-323
71. Chen, Y. -C., Tsay, C. -B., 2002, Stress analysis of a helical gear set with localized bearing contact, *Finite Elements in Analysis and Design*, 38(8):707-723
72. Tan, C. K., Irving, P., Mba, D., 2007, A comparative experimental study on the diagnostic and prognostic capabilities of acoustics emission, vibration and spectrometric oil analysis for spur gears, *Mechanical Systems and Signal Processing*, 21(1):208-233
73. Cai, Y., Hayashi, T., 1994, Linear approximated equation of vibration of a pair of spur gears (theory and experiment), *ASME Journal of Mechanical Design*, 116(2):558-564
74. Mohammed, O. D., Rantatalo, M., Aidanpää, J. -O., 2015, Dynamic modelling of a one-stage spur gear system and vibration-based tooth crack detection analysis, *Mechanical Systems and Signal Processing*, 54:293-305
75. Farshidianfar, A., Saghafi, A., 2014, Global bifurcation and chaos analysis in nonlinear vibration of spur gear systems, *Nonlinear Dynamics*, 75(4):783-806
76. Divandari, M., Aghdam, B. H., Barzamini, R., 2012, Tooth profile modification and its effect on spur gear pair vibration in presence of localized tooth defect, *Journal of Mechanics*, 28(2):373-381
77. Spitas, A., Costopoulo, Th. N., Spitas, V. A., 2002, Calculation of transmission errors, actual path of contact and actual contact ratio of non-conjugate gears, *VDI-Berichte*, 2(1665):981-994
78. Yurong, C., Hayashi, T., 1991, The estimation of vibration of a pair of spur gears due to their tooth profile errors. (2nd Report), The linear approximated formula of vibration in case of each contact ratio, *Seimitsu Kogaku Kaishi/Journal of the Japan Society for Precision Engineering*, 57(2):273-279
79. Spitas, C., Spitas, V., 2006, Calculation of overloads induced by indexing errors in spur gearboxes using multi-degree-of-freedom dynamical simulation, *Proceedings of the Institution of Mechanical Engineers, Part K: Journal of Multi-body Dynamics*, 220(4):273-282
80. Parker, R. G., Vijayakar, S. M., Imajo, T., 2000, Non-linear dynamic response of a spur gear pair: modelling and experimental comparisons, *Journal of Sound and Vibration*, 237(3):435-455
81. Howard, I., Jia, S., Wang, J., 2001, The dynamic modelling of a spur gear in mesh including friction and a crack, *Mechanical Systems and Signal Processing*, 15(5):831-853
82. Özgüven, H. N., 1991, A non-linear mathematical model for dynamic analysis of spur gears including shaft and bearing dynamics, *Journal of Sound and Vibration*, 145(2):239-260
83. Faggioni, M., Samani, F. S., Bertacchi, G., Pellicano, F., 2011, Dynamic optimization of spur gears, *Mechanism and Machine Theory*, 46(4):544-557

84. Osman, T., Velez, Ph., 2010, Static and dynamic simulations of mild abrasive wear in wide-faced solid spur and helical gears, *Mechanism and Machine Theory*, 45(6):911-924
85. Li, S., Kahraman, A., 2013, A tribo-dynamic model of a spur gear pair, *Journal of Sound and Vibration*, 332(20):4963-4978
86. Walha, L., Fakhfakh, T., Haddar, M., 2006, Backlash effect on dynamic analysis of a two-stage spur gear system, *Journal of Failure Analysis and Prevention*, 6(3):60-68
87. Huang, K. J., Wei, H. W., 2010, Approaches to parametric element constructions and dynamic analyses of spur/helical gears including modifications and undercutting, *Finite Elements in Analysis and Design*, 46(12):1106-1113
88. Khabou, M. T., Bouchaala, N., Chaari, F., Fakhfakh, T., Haddar, M., 2011, Study of a spur gear dynamic behavior in transient regime, *Mechanical Systems and Signal Processing*, 25(8):3089-3101
89. Chaari, F., Fakhfakh, T., Haddar, M., 2009, Analytical modelling of spur gear tooth crack and influence on gear mesh stiffness, *European Journal of Mechanics, A/Solids*, 28(3):461-468
90. Chen, Z., Shao, Y., 2011, Dynamic simulation of spur gear with tooth root crack propagating along tooth width and crack depth, *Engineering Failure Analysis*, 18(8):2149-2164
91. Chen, Z., Shao, Y., 2013, Mesh stiffness calculation of a spur gear pair with tooth profile modification and tooth root crack, *Mechanism and Machine Theory*, 62:63-74
92. Pandya, Y., Parey, A., 2013, Simulation of crack propagation in spur gear tooth for different gear parameter and its influence on mesh stiffness, *Engineering Failure Analysis*, 30:124-137
93. Guilbault, R., Lalonde, S., Thomas, M., 2015, Modeling and monitoring of tooth fillet crack growth in dynamic simulation of spur gear set, *Journal of Sound and Vibration*, 343:144-165
94. Li, S., Kahraman, A., 2010, A transient mixed elastohydrodynamic lubrication model for spur gear pairs, *Journal of Tribology*, 132(1):1-9
95. Wang, Y., Li, H., Tong, J., Yang, P., 2004, Transient thermoelastohydrodynamic lubrication analysis of an involute spur gear, *Tribology International*, 37(10):773-782
96. Kumar, P., Saini, P.K., Tandon, P., 2007, Transient elastohydrodynamic lubrication analysis of an involute spur gear using couple-stress fluid, *Proceedings of the Institution of Mechanical Engineers, Part J: Journal of Engineering Tribology*, 221(6):743-754
97. Wang, Y. -Q., Yi, X. -J., 2010, Non-Newtonian transient thermoelastohydrodynamic lubrication analysis of an involute spur gear, *Lubrication Science*, 22(10):465-478
98. Parsa, M., Akbarzadeh, S., 2014, A new load-sharing-based approach to model mixed-lubrication contact of spur gears, *Proceedings of the Institution of Mechanical Engineers, Part J: Journal of Engineering Tribology*, 228 (11):1319-1329

99. Li, S., Kahraman, A., Klein, M., 2012, A fatigue model for spur gear contacts operating under mixed elasto-hydrodynamic lubrication conditions, *ASME Journal of Mechanical Design*, 134(4), ID: 041007
100. Larsson, R., 1997, Transient non-Newtonian elasto-hydrodynamic lubrication analysis of an involute spur gear, *Wear*, 207(1-2):67-73
101. Amani A., Rajabalinejad M., Spitas C., 2011, Modelling of elasto-hydrodynamic lubrication problems in gears, *Proceedings of the 22nd International Symposium on Transport Phenomena (ISTP22)*, Delft, Netherlands, 8 pages.
102. Kapelevich, A. L., 2013, *Direct Gear Design*, CRC Press, *Taylor and Francis Group*
103. Rackov, M., Veres, M., Kanovic, Z., Kuzmanovic, S., 2013, HCR gearing and optimization of its geometry, *Advanced Materials Research*, 633:117-134
104. Bair, B. -W., 2009, Tooth profile generation and analysis of crowned elliptical gears, *ASME Journal of Mechanical Design*, 131(7):0745031-0745036
105. Arikan, M. A. S., 2003, Determination of addendum modification coefficients for spur gears operating at non-standard center distances, *ASME 2003 International Design Engineering Technical Conferences and Computers and Information in Engineering Conference*, DETC2003/PTG-48063, 4 A:489-499
106. Alipiev, O., Antonov, S., Grozeva, T., 2013, Generalized model of undercutting of involute spur gears generated by rack-cutters, *Mechanism and Machine Theory*, 64:39-52
107. He, J., Zhang, W., Zhang, H., Ma, W., Chen, S., Li, Q., Gao, Y., 2011, Study on minimum teeth without undercutting of standard involute gears, *Advanced Materials Research*, 199-200:329-336
108. Brauer, J., 2002, Analytical geometry of straight conical involute gears, *Mechanism and Machine Theory*, 37:127-141
109. Spitas, C., Spitas, V., 2008, Direct analytical solution of a modified form of the meshing equations in two dimensions for non-conjugate gear contact, *Applied Mathematical Modelling*, 32(10):2162-2171
110. Spitas, C., Costopoulos, Th., Spitas, V., 2008, Direct analytical solution of the inverse gear tooth contact analysis problem, *Inverse Problems in Science and Engineering*, 16(2):171-186
111. Vulgakov, E. B., 1995, *Theory of involute gears*, *Mashinostroenie*, Moscow (in Russian).
112. Spitas C., Spitas V., 2006, Can non-standard involute gears of different modules mesh?, *IMECE Journal of Mechanical Engineering Science*, 220(8):1305-1313.
113. GOST 13755-81, 1981, Basic requirements for interchangeability. Gearings cylindrical evolvent gears. Basic rack
114. ISO 53, 1974, Cylindrical gears for general and heavy engineering- Standard basic rack tooth profile
115. NF E 23-011, 1972, Cylindrical gears for general and heavy engineering - Basic rack and modules (similar to ISO 467 and ISO 53)
116. ISO/TR 4467, 1982, Addendum modification of the teeth of cylindrical gears for speed-reducing and speed increasing gear pairs

117. JIS B 1702-72, 1976, Accuracy for spur and helical gears
118. DIN 867, 1986, Basic rack tooth profiles for involute teeth of cylindrical gears for general engineering and heavy engineering
119. AGMA, 201.02 and 201.02A, 1968, Tooth proportions for coarse pitch involute spur gears. Alexandria VA: Gear Manufacturers Association (AGMA)
120. DIN 3972, 1952, Reference Profiles of Gear-cutting Tools for Involute Tooth Systems according to DIN 867
121. ANSI/AGMA 1006-A97, 1997, Tooth proportions for plastic gears, Appendix F "Generating Gear Geometry without Racks"
122. AKGears, Gear Tooth Root Fillet Optimization Software 2015
123. Amani, A., Spitas, V., Spitas, C., 2015, Influence of centre distance deviation on the interference of a spur gear pair, *International Journal of Powertrains*, 4(4):315-337
124. Rubtsov, V. N., 2008, Radial interference when cutting gears with internal teeth by means of a cutter with a rounded tip, *Russian Engineering Research*, 28(11):1151-1152
125. Jones, F. D., Ryffel, H. H., 1984, Gear design simplified (3rd ed.), *Industrial Press Inc.*, p. 20, ISBN 978-0-8311-1159-5
126. Savage, M., Coy, J. J., Townsend, D. P., 1982, Optimal tooth numbers for compact standard spur gear sets, *ASME Journal of Mechanical Design*, 104(4):749-758
127. Nguyen, T., Lin, H. H., 2011, Compact design for non-standard spur gears, *Journal of Mechanical, Aerospace and Industrial Engineering*, 2(1):1-15
128. Polder, J. W., Broekhuisen, H., 2003, Tip-fillet interference in cylindrical gears, *ASME Design Engineering Technical Conferences and Computers and Information in Engineering Conference*, 4A: 473-479
129. Smith, J. D., 2003, Gear Noise and Vibration, second edition, *Marcel Dekker Inc.*, New York Basel
130. Kleiss, R. E., Kapelevich, , Kleiss Jr., A. L., 2001, New Opportunities with Molded gears, *AGMA Fall Technical Meeting*, Detroit, October 3-5, (01FTM9)
131. Litvin, F. L., Kim, D. H., 1997, Computerized design, generation and simulation of meshing of modified involute spur gears with localized bearing contact and reduced level of transmission errors, *ASME Journal of Mechanical Design*, 119:96-100

9- Engineering gear tooth compliance

Summary

Design of powertrains involving compact, high-power-density and/or high precision gear transmissions need precise computational modelling of dynamics and compliance, over numerous calculation-intensive iterations. Another main concern, with regard to low-vibration systems in particular, is how to tailor the whole stiffness of a gear pair for limiting the amount of vibration in the gear system. However, current analytical/empirical methods for calculating gear compliance become inaccurate outside of the standard geometries for which they have been derived, whereas numerical, methods rely on complex finite element models, which are very resource intensive in order to be accurate. To address these shortcomings in this chapter, we develop a versatile hybrid analytical-numerical method and non-dimensional modelling framework for accurately calculating gear mesh compliance of arbitrary (including non-standard) tooth geometries. Finite element analysis is used for the calculation of bending & foundational compliance in conjunction with Saint-Venant's Principle, which has been used to allow accurate and fast numerical calculation whereas Hertzian compliance is calculated analytically with high accuracy for curved elastic body contact. The influence of different combinations of cutter tip radius, dedendum, number of teeth and gear transmission ratio on gear mesh compliance is investigated. By means of cubic Hermitian interpolation, the results of the hybrid analytical-numerical method have been mapped to a multi-parametric compliance function of the instantaneous position of two mating gears along the line of action and a large array of design parameters. The obtained compliance functions can be applied directly to gear dynamical simulations, parametric design and optimisation algorithms etc. The same functions can also provide powerful inverse solutions, which can be used for direct compliance-based gear design, i.e. to obtain optimised low-vibration powertrains.

8.1. INTRODUCTION

Achieving difficult goals in the design of powertrains regarding performance and reliability is more and more dependent on advanced computational models. The heuristic and often iterative nature of the design process means that accurate models must be sought that at the same time reduce complexity and computational cost and increase insight and versatility: i.e. non-dimensional

analytical formulation and multi-scale modelling (local meshing geometry/ physics versus drivetrain-scale system response) lend themselves well to this approach. These methods increase the capability of innovative non-standard (out-of-the-box) solutions in different aspects of the design. For strong, compact, efficient, vibration-free gears, the key challenge is to overcome the uncertainties imposed by a host of (chaotic and semi-chaotic) errors, external excitations and self-excitations. Ultimately, the sensitivity to each of these factors must be understood well, modelled, and then beyond-the-state-of-the-art technoeconomically appealing design solutions, guidelines and architectures must be formulated to minimise or eliminate such sensitivities.

As an example, low-vibration gear systems can be obtained in principle by tailoring the stiffness of the meshing gears [1-8], which requires methods for calculating compliance that are design- and iteration-friendly. The main problem for the design of high-accuracy low-vibration gear drives is the prediction of positional accuracy and vibration.

In the context of studying gear vibration, the main excitation happens during the transfer of the load from the driving gear to the driven gear across a varying number of simultaneous moving tooth contacts, each characterised by a different instantaneous stiffness. The resulting changes in stiffness and load sharing as well as external excitations can and do cause the direction and amplitude of the contact forces to change rapidly, producing vibration. While little can be done to alter this fundamental phenomenon, the following can be observed:

- Gear configuration design can be employed to simultaneously consider the effects of a host of parameters of the gear and drivetrain topology and geometry with the purpose of achieving desired low-vibration responses predictably and robustly. Of course, such configuration design requires obtaining a model for the prediction of gear vibration and an investigation of gear dynamics is needed.
- Low-vibration gear systems have to be controlled by tailoring the stiffness of the meshing gears. Modelling of the gear mesh compliance at multiple positions during a mesh cycle is essential to calculate the total gear stiffness, where typically more than one pairs of teeth are in mesh.
- Ultimately, a fast and accurate model for instantaneous mesh compliance is needed, that lends itself well to multiple calculations and iterations.

Investigations of gear mesh compliance and its effects on gear performance have been carried out over many years since the 1940's [9-29]. The basic premise is that two mating gears contact in the direction of the line of action and the displacements of the teeth happen along the line of action. The definition of tooth compliance is the ratio of the elastic deflection to the transmitted load- as such, compliance is the inverse of stiffness.

The computational modelling of gear mesh compliance is an essential requisite in any investigation pertaining to gear dynamics [30-34], also in consideration of errors and profile modifications [35-39] and is also important for quasi-static

calculations such as employed when dimensioning profile modifications [40-42]. Generally, stiffness tailoring for mating gears to limit the amount of vibration in the gear system can be important in the design of low-vibration drivetrains. Investigations of the magnitudes of elastic tooth deformations and also their effects on gear performance have been done by many researchers [11-27, 43]. There are some advantages in studying of the elastic deformations on a gear tooth such as I) measuring the total compliance of a gear pair in high precision control systems, II) calculation of the gear mesh compliance for dynamic analyses of compact gear drives and III) optimisation of the gear profile modification in heavily loaded compact gears, i.e. wind turbine gearing [1].

Whatever its application, however, it is obvious that the calculation of the mesh compliance should be both accurate and fast enough to fit into the computational resource constraints of a real-time dynamical simulation or an iterative optimisation algorithm. This is generally not the case with presently known models.

Computational models for compliance can generally be classified as either analytical, empirical and numerical (typically FEA-based). The analytical [15-21] and empirical models [22-27], although fast, present various shortcomings in terms of their calculation accuracy and (in)ability to analyse (optimised) non-standard tooth forms, whereas the numerical FEA-based models [28-29, 44-45] are typically intensive in terms of computational resources, slow, and impossible to apply efficiently during a dynamical simulation or a (multi-) parametric design optimisation process. Typical shortcomings of these models are as follows:

- (Quasi-) analytical/ empirical models: Use of simplified analytical or empirical quasi-analytical models for bending and foundational deflections produces results of limited accuracy, which are often only valid for certain standard geometries and cannot be generalised to new non-standard tooth forms [11-18,23-27].
- Numerical (FEA) models: Use of fine and complex finite element meshes, often also including contact elements, to account for generalised geometries, requiring large model preparation and computational time overheads [1,19-22]. These are too cumbersome to use effectively in a design and optimisation process.

To model compliance, two mating gears are considered to contact in the direction of the line of action, the displacements of the teeth taking place along said line of action. The compliance of one tooth (or the contacting tooth pair) is calculated from deflections due to bending- (Bending compliance), foundation- (Foundation compliance) and contact deflection (Hertzian compliance) [18, 25]. By dividing the deflection by the transmitted load, a compliance coefficient can be obtained as the inverse of stiffness.

The work presented in this chapter comprises two parts. Firstly, the development of an improved model for the instantaneous calculation of gear mesh compliance, which alleviates the shortcomings of previous models. Building on a

fundamental understanding of the tooth contact mechanics problem and making innovative use of Saint Venant's principle to combine different sub-models effectively, it features a hybrid analytical-numerical approach that combines fast computation with high accuracy. The model is intended for use in 1) evaluating the compliance of mating gears in high precision control systems, 2) calculating the gear mesh stiffness for dynamic analyses of compact gear systems, 3) optimising the profile modification in heavily loaded compact gears, for instance wind turbine gearing, and 4) recognising the performance of new type of gears as i.e. non-metallic gears. The overall deflection is calculated as the sum of bending deflection (bending compliance), foundation deflection (foundation compliance) and contact deflection (Hertzian compliance) as shown in Figure 9.1. Secondly, to further increase the speed of subsequent computations, the solutions are mapped via interpolation to multi-parametric analytical compliance functions using cubic Hermitian polynomials.

With regard to mapping the compliance computation results to analytical functions, a comprehensive look into the literature [1, 14, 16, 21, 27] already suggests that the relation between the gear mesh compliance and the position of two mating teeth along the line of action should be approximated well by third degree polynomial functions. Obviously using higher degree for the polynomial function could in theory provide for a more accurate function, but at the cost of calculation complexity- and possibly physicality: Polynomial interpolation is – after all– applied to determine possible values for an indicated function expressed at a distinct set of points. The geometric abilities of the interpolations are based on how well the interpolated curve replicates the inherent shape participated by means of the points [27]. For a truthful and perfect interpolation, special characters of the points i.e. concavity, convexity and monotonicity have to be considered. These mathematical properties can define a good fit in a geometric point of view. Finding a best fit curve is kind of an experimental choice based on human judgment [46].

A key consideration has been that the details or artefacts that cannot be established from the points must not be introduced. To obtain these specifications for an interpolated function, the function has to be established considering both geometric and algebraic properties [47, 48].

In this chapter, different gear design parameters are considered, including the number of teeth, contact ratio for different combinations of standard and non-standard tooth proportions (addendum, dedendum, root fillet/ cutter tip radius, thickness). The non-linear effect of varying transmitted load is also considered. Bending, foundation and Hertzian compliance are modelled using a hybrid analytical-numerical method, which achieves results of comparable accuracy to a fine-mesh-based numerical method using contact elements but at a speed comparable to simplified mesh finite elements.

Regarding the choice of spline interpolation method, Cubic Hermitian Interpolation (CHI) and its application to shape control was considered [48] among other alternatives. CHI is applied to solve a number of different test problems with two discrete points. The degree of convergence for the cubic Hermitian function is controlled by the order of accuracy of the expansion [46]. In the case of the present work, early comparative tests with other cubic interpolation forms showed that the Hermitian parameterisation produced a much higher physicality of the results, allowing meaningful regressions to be made connecting the polynomial coefficients to the gear design parameters. This has yielded a robust and powerful inverse solution for the compliance-based simulation and design of gear drives.

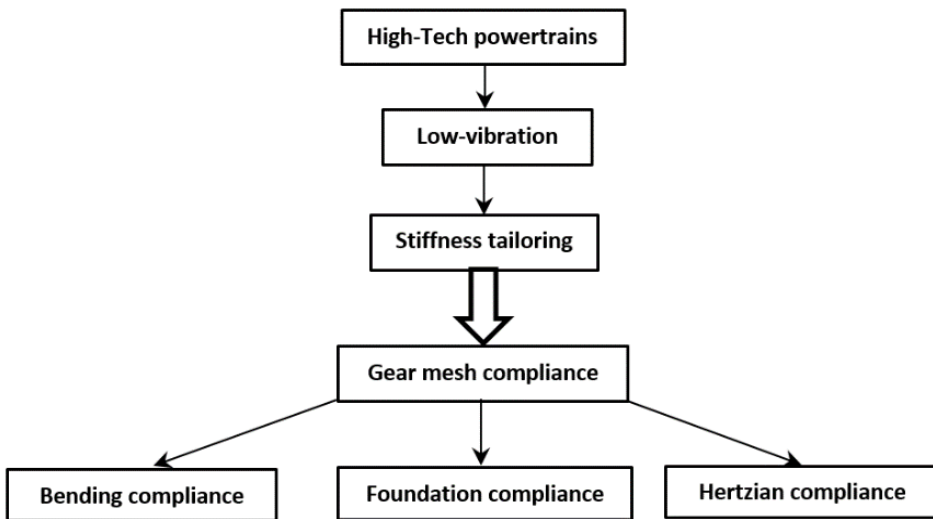


Figure 9.1: The relations between compliance of a gear pair and low-vibration system pertinent to the design of high-tech powertrains

9.2. NON-DIMENSIONALISATION OF GEOMETRY

Non-dimensionalisation is used in this study to provide greater generality to the results, without loss of accuracy [28-29, 44-45]. In this work geometrical features are non-dimensionalised in terms of the module. Hence any given feature f can be related to its non-dimensional correspondent f^* by equation (2.1) as:

$$f = mf^*$$

9.3. GENERALISED NON-DIMENSIONAL MODELLING OF GEAR MESH COMPLIANCE

The direction of displacements and of contact of two mating gears is considered along the line of action. As per standard practice, we define tooth compliance as the ratio of the elastic deflection to the transmitted load. Using the principle of superposition, the overall deflection is calculated as the sum of bending deflection (bending compliance), foundation deflection (foundation compliance) and contact deflection (Hertzian compliance).

The compliance coefficient is defined herewith by the following relationship:

$$C = \frac{\delta}{mP^*} \quad (9.1)$$

Where C is non-dimensional tooth compliance, δ is normal tooth deflection along the line of action, m is the module and P^* is non-dimensionalised force which defined as

$$P^* = \frac{P}{m \cdot b \cdot E} \quad (9.2)$$

Where b is face width of the gear, E is modulus of elasticity and P is normal tooth load along the line of action. The total tooth pair compliance C can be found as the summation of 'partial' compliances, thus:

$$C = (C_{B1} + C_{F1}) + C_H + (C_{B2} + C_{F2}) \quad (9.3)$$

Where C_B , C_F and C_H defined as bending-, foundation- and Hertzian compliance respectively. Subscript 1 and 2 related to the gear number 1 and the gear number 2, respectively.

We discuss the calculation of these components as follows.

9.3.1. Bending-Foundational Compliance

Traditionally for the calculation of bending deflection, a gear tooth is considered as a non-uniform cantilever beam with an effective length L_e [13-14], based on a rigid foundation, as shown in Figure 9.2.

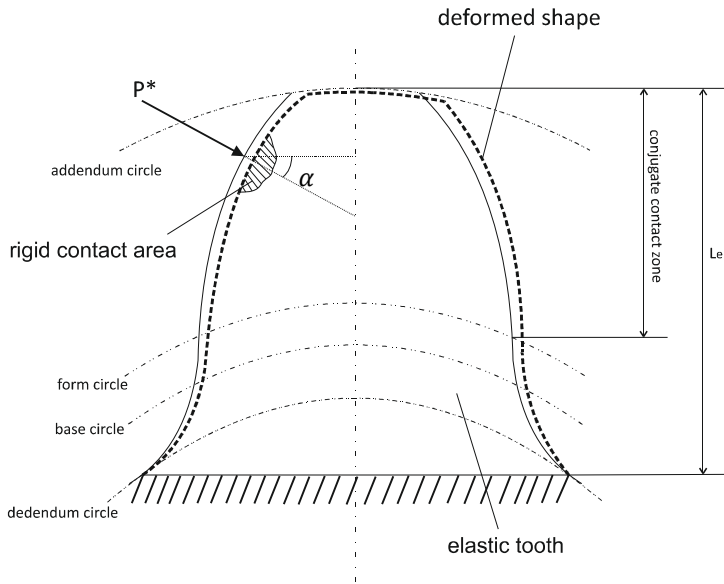


Figure 9.2: Modelling of a gear tooth as a non-uniform cantilever beam on a rigid foundation

Considering bending deflection δ_B and external load P^* , the bending compliance (C_B), will be introduced as:

$$C_B = \frac{\delta_B}{mP^*} \quad (9.4)$$

Due to fillet geometry and the flexibility of the tooth support material, we consider next that the foundation of the tooth is actually not rigid and will deform, this time with the tooth acting as a rotating rigid body (Figure 9.3). The foundation deflection is generally a function of fillet geometry, load position and direction. The analytical calculation of the foundation deflection of the gear tooth is based on the theory of Muskhelishvili [26] which applied to circular elastic rings [13-14], but in principle any method applying appropriate boundary conditions will be appropriate. The formulation of foundation compliance (C_F), as calculated from the foundation deflection (δ_F) and external load P^* is:

$$C_F = \frac{\delta_F}{mP^*} \quad (9.5)$$

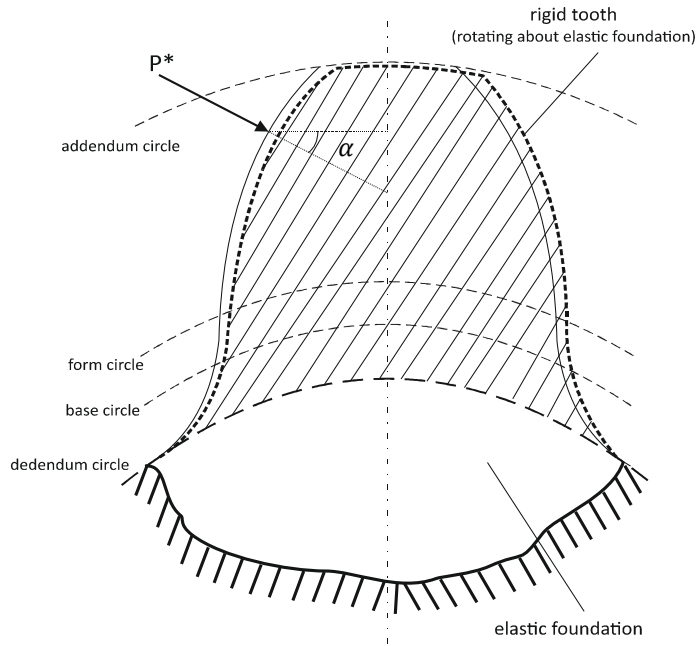


Figure 9.3: Deflection of tooth due to foundation flexibility

9.3.1.1. Calculation approach

For this work, the finite element method is applied for the calculation of bending and foundation compliance. Therefore, the bending and foundation compliance can be combined as follows:

$$C_{B+F} = C_B + C_F \quad (9.6)$$

And the total compliance as mentioned in equation (8.5) can be rewritten as:

$$C = C_{(B+F)1} + C_H + C_{(B+F)2} \quad (9.7)$$

The conceptual unification of bending and foundational compliance greatly simplifies the problem of identifying the boundary conditions, as making an accurate distinction between the tooth and its foundation would be largely arbitrary. It should be noted that, while this unification is typical for finite-element-based models, the Hertzian contact phenomenon is not included, marking a departure from all previous models.

9.3.1.2. Definition of (discrete) meshing points

In this research, the gear mesh compliance is calculated at several discrete points. Point 1 (Figure 9.4) is the initial point on the working line of action, where

the tip point of gear 1 is touching the lowest working point of the profile of gear 2, which must lie above its form circle, as it has been introduced in [28]. The pitch point is represented here as point 4. The distance from the initial point (point 1) to the pitch point (point 4) is divided by two for creation of point 3. With the same process, point 2 as a middle point between point 1 and point 3 will be created. The interval from point 4 to point 1 is assigned a positive position parameter ($+\xi$). With the same derivation method, points 5, 6, and 7 will be developed (Figure 9.4).

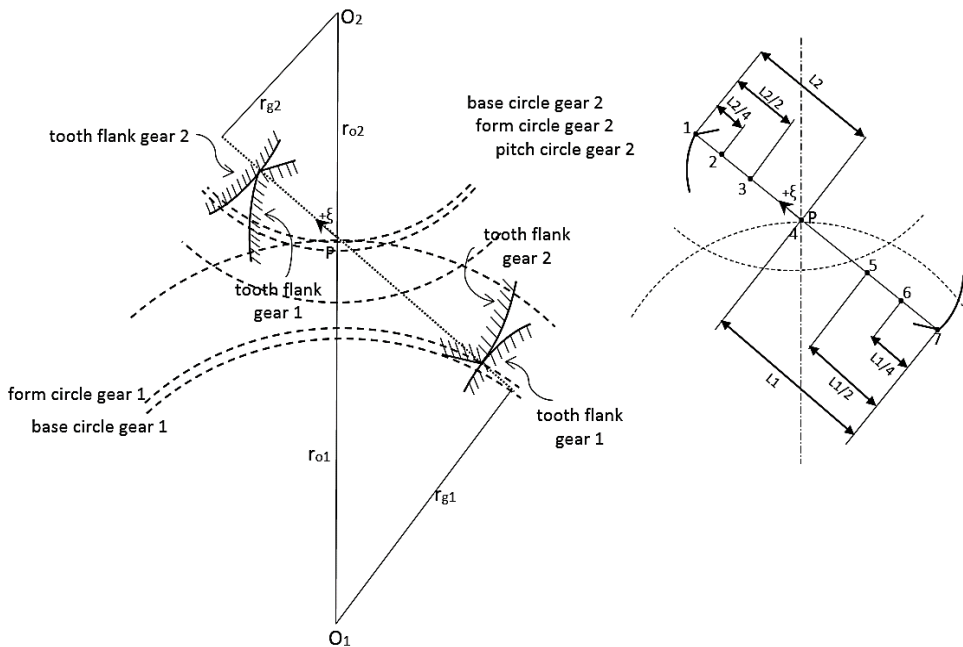


Figure 9.4: Developing isolated points on the line of action for bending & foundation compliance calculation

Unlike in all prior finite-element-based models, in this study the load is not applied at the contact point for calculation of bending & foundational deflection. The reason is that application of a point load at the contact surface of a tooth leads to an unrealistic local deformation/ singularity of the mesh (false penetration) and a corresponding error in predicting the tooth deflection. This penetration, as created by a normal force, can be seen in the finite element model of Figure 9.5. This error should obviously be avoided in the calculations.

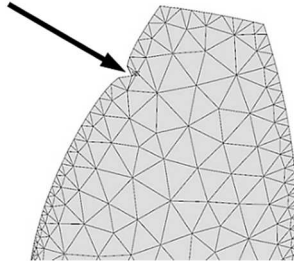


Figure 9.5: Penetration at the contact point of gear surface in finite element analysis software

In this chapter we eliminate this ‘false penetration’ error by applying an equivalent normal load to the loaded gear tooth at a location sufficiently far from the actual contact point, so as to separate the local singularity at the point of equivalent load application from the overall deflection field around the actual contact point due to the bending and foundation compliance. Defining such an equivalent load is possible by virtue of Saint Venant’s principle [49-54]. To obtain said equivalent load, we offset the normal tooth load along its line of action until the intersection of the line of action with the tooth centre axis. It is obvious from this geometrical construction that both the force and the bending moment applied to the tooth are maintained the same, which is sufficient for the required load equivalence. With this approach a singularity now appears near the centre of the tooth mesh, but this has been confirmed to have negligible influence on the overall simulated deflection and stress field, which is also proven in a subsequent sensitivity analysis in this chapter. This is illustrated in Figure 9.6. As an illustration, Figure 9.6 shows the application of Saint-Venant’s principle for a gear tooth. In case (a) the tooth replaces with a cantilever beam which is loaded at the contact point (point k). By means of Saint-Venant’s principle, the deflection at point k (Figure 9.6(b)) will be calculated at point \hat{k} (Figure 9.6(c)). The calculations will be on the correspondent point of the centre line of the gear tooth (Figure 9.7).

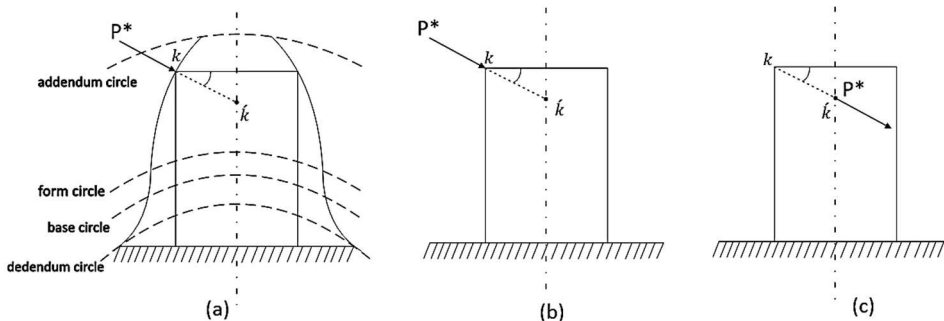


Figure 9.6: Implementation of Saint-Venant’s principle for a gear tooth in order to calculate bending & foundational compliance

ANSYS is used for the purposes of this investigation to calculate bending & foundation compliance. This software simulates the loading of different gear pairs with consistent boundary and loading conditions, namely point loading at isolated contact points (seven points in Figure 9.4) along the line of action. The iso-parametric element PLANE82 is used for modelling the gear tooth. This element provides accurate results for mixed (quadrilateral-triangular) automatic meshes and can tolerate shapes well-suited to model curved boundaries. This is illustrated in Figure 9.7.

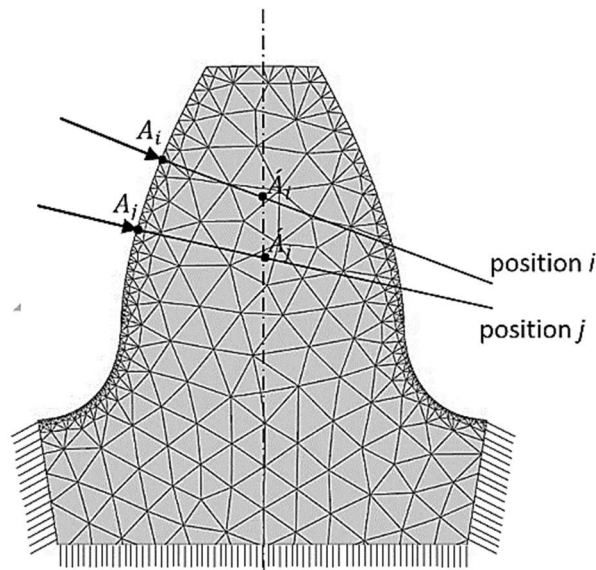


Figure 9.7: Calculation of bending & foundational compliance on the correspondent point in the centre line of gear tooth using finite element methods for two different contact positions

9.3.2. Hertzian compliance

Hertz's theory of elastic contact is utilised to account for local compressive deformation in the area of tooth contact. Though an approximation, the contact of two mating teeth can be taken to be equivalent to two cylinders having the same radius of curvature at the contact point. The radius of curvature changes continuously in case of an involute curve, and it changes sharply in the vicinity of the base circle.

In this work the accurate Roark's Formulas [27] for strain due to pressure on or between elastic bodies, will be used to find the Hertzian deflection between two teeth (Figure 9.8).

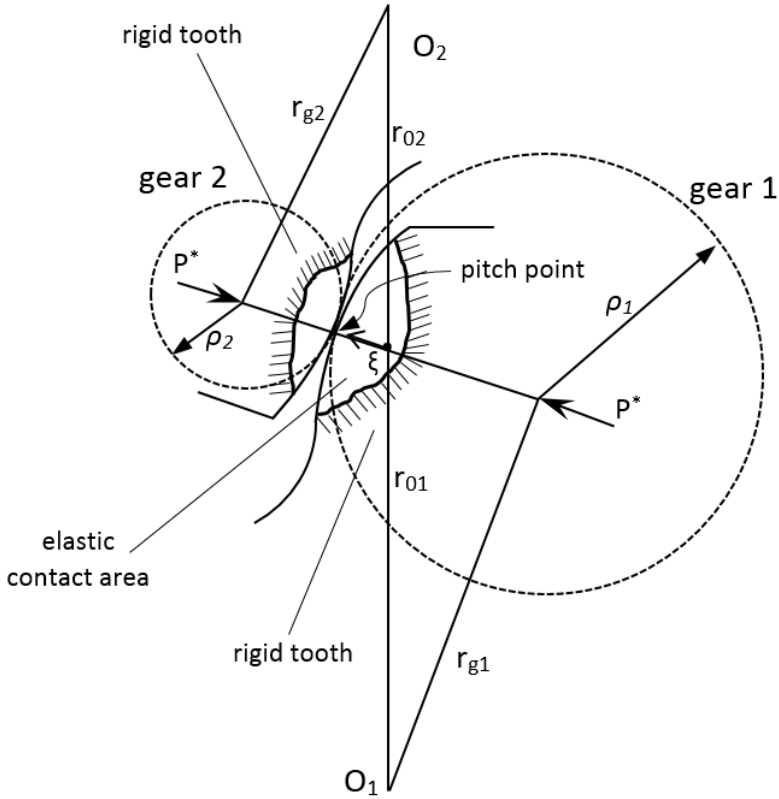


Figure 9.8: Contact of two mating teeth

Roark's handbook gives a summary of deflection formulas that are based on a Hertz pressure distribution. For the case of two cylinders pressed into contact, the distance between the cylinders is reduced by:

$$\delta_H = \frac{2 \left(\frac{P}{b}\right) (1 - \nu^2)}{\pi E} \left(\frac{2}{3} + \ln \frac{16\rho_1\rho_2}{L^2} \right) \quad (9.8)$$

Where P/b is load per unit length, ν is Poisson's ratio, E is Young's modulus, ρ_1, ρ_2 are the radius of curvature of the tooth of gear number 1 and 2, respectively, at the point of contact and L is total width of rectangular contact area for Hertzian deflection.

The total contact width L for the case of two gear teeth in contact with $\nu = 0.3$ is given by

$$L = 2.15 \sqrt{\frac{PK_D}{bE}} \quad (9.9)$$

Where

$$K_D = \frac{2\rho_1\rho_2}{\rho_1 + \rho_2} \quad (9.10)$$

9.3.2.1. Non-dimensionalisation in Hertzian compliance

In this study all geometrical features will be non-dimensionalised in terms of the module.

$$\rho^* = \frac{\rho}{m} \quad (9.11)$$

$$K_D^* = \frac{K_D}{m} = \frac{2\rho_1^*\rho_2^*}{\rho_1^* + \rho_2^*} \quad (9.12)$$

$$L^* = \frac{L}{m} = 2.15\sqrt{P^*K_D^*} \quad (9.13)$$

$$\delta_H^* = \frac{\delta_H}{m} \quad (9.14)$$

With this respect, the non-dimensional Hertzian deflection δ_H^* can be expressed as:

$$\delta_H^* = 2 \frac{P^*}{\pi} (1 - \nu^2) \left(\frac{2}{3} + \ln \frac{16\rho_1^*\rho_2^*}{(2.15)^2 P^* K_D^*} \right) \quad (9.15)$$

Substituting K_D^* from equation (9.12) into equation (9.15):

$$\delta_H^* = 2 \frac{P^*}{\pi} (1 - \nu^2) \left(\frac{2}{3} + \ln \frac{8(\rho_1^* + \rho_2^*)}{(2.15)^2 P^*} \right) \quad (9.16)$$

Replacing ρ_1^*, ρ_2^* with following relations as shown in Figure 9.8:

$$\rho_1^* = \sqrt{r_{o1}^{2*} - r_{g1}^{2*}} - \xi \quad (9.17)$$

$$\rho_2^* = \sqrt{r_{o2}^{2*} - r_{g2}^{2*}} + \xi \quad (9.18)$$

In equation (9.16), δ_H^* can be rewritten as:

$$\delta_H^* = 2 \frac{P^*}{\pi} (1 - \vartheta^2) \left(\frac{2}{3} + \ln \frac{8 \left(\sqrt{r_{o1}^{2*} - r_{g1}^{2*}} + \sqrt{r_{o2}^{2*} - r_{g2}^{2*}} \right)}{(2.15)^2 P^*} \right) \quad (9.19)$$

However:

$$\sqrt{r_{o1}^{2*} - r_{g1}^{2*}} = r_{g1}^* \tan(\alpha) \quad (9.20)$$

$$\sqrt{r_{o2}^{2*} - r_{g2}^{2*}} = r_{g2}^* \tan(\alpha) \quad (9.21)$$

Where r_o and r_g are pitch radius and base radius respectively.
Eventually non-dimensional Hertzian deflection can be obtained as:

$$\delta_H^* = 2 \frac{P^*}{\pi} (1 - \vartheta^2) \left(\frac{2}{3} + \ln \frac{8(r_{g1}^* + r_{g2}^*) \tan(\alpha)}{(2.15)^2 P^*} \right) \quad (9.22)$$

This means that for a given load the Hertzian deflection only depends on pressure angle and base radius of gear number 1 and 2.

Considering equation (9.22), the Hertzian compliance C_H will be calculated as:

$$C_H = \frac{\delta_F^*}{P^*} \quad (9.23)$$

9.4. MULTI-PARAMETRIC TOOTH MODELLING

For the purposes of this study a set of relevant independent design parameters was considered (dependent ones are shown in parentheses), as shown in Table 9.1.

Table 9.1: Design parameters and ranges explored in the study

Gear	α	N	i_{12}	c_f	c_c	c_k	c_s	c_m
Ref. (1)	20°	10, 20, 40		1.00-2.20	0.00-0.62	1.0	0.50-0.70	0.0
Mating (2)	(20°)	(5, 10, 20, 40, 80)	0.5, 1.0, 2.0	1.25	0.30	1.0	0.5	0.0

For the generation of the tooth model, a computer programme was developed based on discrete representation of the tooth flank by infinitesimal involute segments [55].

9.5. RESULTS AND DISCUSSION

The results obtained from the developed model are presented in the context of two different investigations. The first investigation (section 9.5.1.1) calculates the compliance function in terms of the meshing position along the path of contact (line of action) in consideration of the non-linear influence of the load magnitude on compliance due to Hertzian effects. The second one (section 9.5.1.3) is the influence of gear geometry on compliance. The computed compliance values are presented in the form of parametric graphs for different numbers of teeth of the mating gear and tooth form design parameters, as a function of the position of a gear pair along the line of action.

9.5.1. Model validation, sensitivity analysis and benchmarking

A fully numerical calculation approach was also developed in the context of this work, similar to [56-57], to serve as a benchmark and help validate the developed hybrid model.

The analysis is carried out with the help of ANSYS WORKBENCH 14.5 [58] for the calculation of total compliance and the customized APDL (ANSYS Parametric Design Language) looping program for the calculation of Hertzian compliance.

Two conditions have been assumed in advance for this study as: a) there is no sliding in the contact zone between the teeth (no shear force considered, this is reasonably accurate considering that shear forces are typically less than 1% of the normal contact forces); b) the contact surface is continuous and smooth. For these purposes ANSYS can solve the contact problem and not be limited by the above two conditions. A two-dimensional contact model was modelled. First, parameter definitions are given and then cloud points of the profile (involute-trochoid) of the gear 1 and 2 are calculated (according to Table 9.1) to plot gear geometry.

9.5.1.1. Modelling of Spur Gear

In this study, total compliance is determined, during the transmission of dimensionless torque of 9.3969 by steel spur gears, using finite element analysis. The value of dimensionless torque is the multiplication of non-dimensionalised force (P^*) along the line of action at pitch point and base radius ($r_o \cos \alpha$). The non-dimensionalised force in this particular example is 0.005. The spur gear is sketched and modelled in SolidWorks 2013. Gear 1 is non-standard gear with $N_1=20$, $c_{c1} = 0.10$, $c_{f1} = 1.10$ and gear 2 is 20 teeth standard gear with $c_{c2} = 0.30$, $c_{f2} = 1.25$. The value of c_s is given as 0.5 for both gears.

9.5.1.2. Finite Element Analysis

In this section, finite element analysis is carried out in ANSYS Workbench 14.5 [58] to determine the maximum deformation at the pitch point for gear 1 (Figure 9.9).

Three contact models, namely node-to-node, node-to-surface, and surface-to-surface [56], are supported by ANSYS. For different problem different types of model is used and in the present work the surface-to-surface model was selected. The finite element model recognises possible contact pairs by the presence of specific contact elements. These contact elements are then interpreted with the model exactly where they are being analysed for interaction. The contact conditions of gear teeth are sensitive to the geometry of the contacting surfaces, which means that the elements near the contact zone need to be refined. Accordingly, the mesh density was increased locally around the contact points, in order to achieve high accuracy while maintaining reasonably low computational requirements for the entire model. An eight noded iso-parametric plane strain quadratic quadrilateral element was used to make the finite element models of the two mating teeth. The target surface was chosen in the tooth of gear 1 and meshed by 2D target element. The contact surface was chosen in the tooth of gear 2 with 2D contact element Conta175 and the target surface was chosen in the tooth of gear 2 with 2D contact element Targe169 [58].

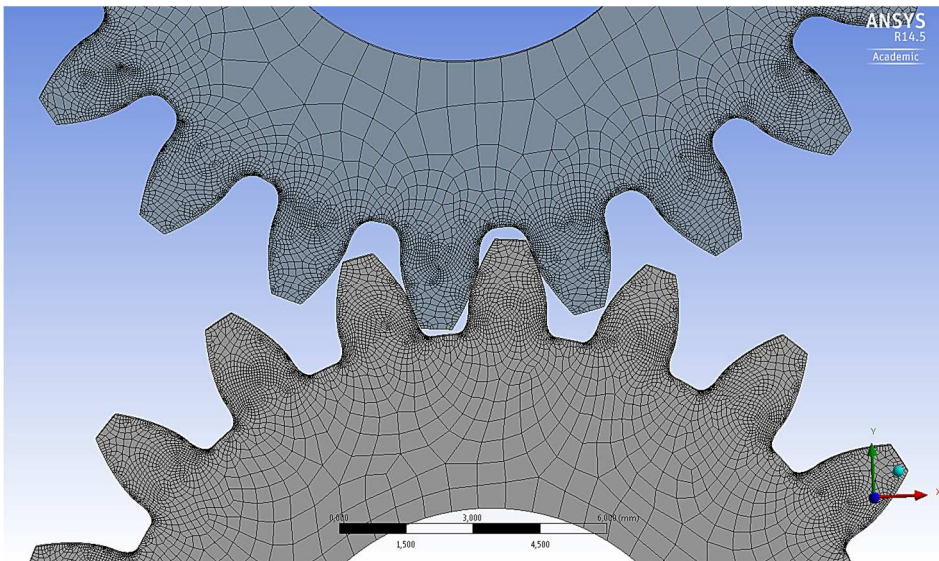


Figure 9.9: Meshing of a gear pair, lower gear is non-standard gear $N_1=20$, $c_{f1}=1.10$, $c_{c1}=0.10$, upper gear is standard gear $N_2=20$, $c_{f2}=1.25$, $c_{c2}=0.25$

8.5.1.3. Boundary Condition

Fixed support is applied to the inner rim of the gear 1. Frictionless support is applied on the inner rim of gear 2 to allow its tangential rotation but restrict from radial translation. Non-dimensionalised moment of 9.3969 is applied on the inner rim of upper gear in counter clockwise direction as a driving torque (Figure

9.10). This is the moment which has been created by the unitary force at the pitch point.

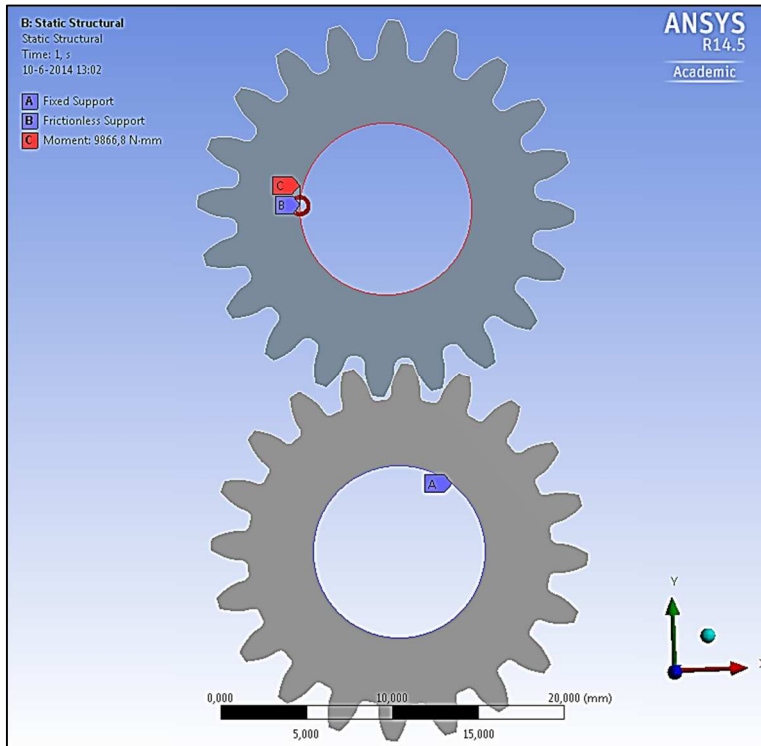


Figure 9.10: Boundary condition of two mating gears, lower gear is non-standard gear $N_1=20$, $c_{f1}=1.10$, $c_{c1}=0.10$, upper gear is standard gear $N_2=20$, $c_{f2}=1.25$, $c_{c2}=0.25$

9.5.1.4. Deformation Analysis

To find the maximum deflection at the pitch point, two different types of smart mesh density (coarse and fine) have been used in ANSYS, where 'smart' denotes that the mesh density is locally variable. The smart fine mesh is five times smaller than the smart coarse mesh (average area for a single element is 0.032439) at the contact area. The accuracy of solution increases with the number of elements taken. However, a higher number of elements will result in increased computational cost. Hence optimum number of divisions should be taken. The deflection result calculated with a coarse and a fine mesh is 0.04485 and 0.04569, respectively (Figure 9.11).

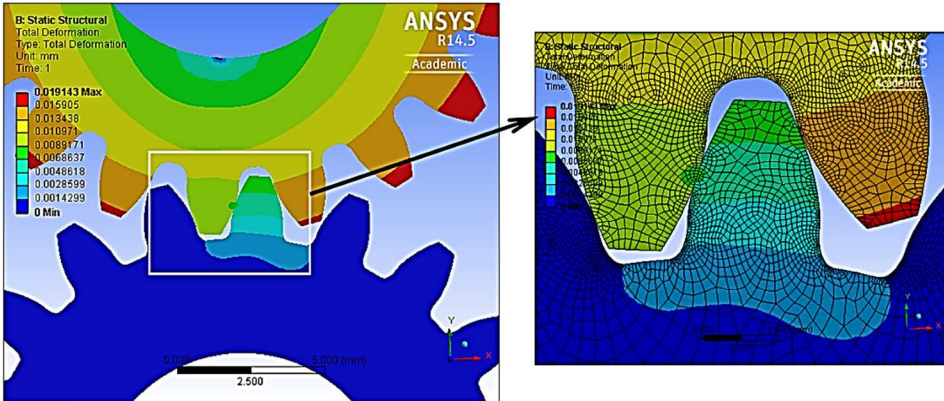


Figure 9.11: Deformation pattern of a gear pair, lower gear is non-standard gear $N_1=20$, $c_{f1}=1.10$, $c_{c1}=0.10$, upper gear is standard gear $N_2=20$, $c_{f2}=1.25$, $c_{c2}=0.25$

The total compliance for this case study, as per the hybrid model, is 9.21317. By means of equation (9.1) the total deflection will be 0.04606. The calculation time for coarse and adaptive fine mesh is 244s and 383s seconds, respectively.

A comparison between the developed hybrid solution and the results of ANSYS for different mesh size is given in Table 9.2. By comparing these results, it can be found that the results of hybrid calculation and finite element analysis are comparable and validated. With using smart fine mesh, the error percentage will be decreased. Although by using coarse mesh the calculation time will be 1.57 times faster, the result of using fine mesh is 3.3 times more accurate, using the hybrid calculation as the benchmark.

Table 9.2: Comparison of total deflection obtained from hybrid calculation (equation (9.2)) and ANSYS WORKBENCH 14.5, (average area for a single element of adaptive coarse mesh: 0.162195, average area for a single element of adaptive fine mesh: 0.032439 at contact area)

Total deflection (hybrid)	Total deflection (numerical)		Deviation percentage (%)
0.04606	adaptive coarse mesh (calculation time:244 s)	0.04485	2.63
	adaptive fine mesh (calculation time:383 s)	0.04569	0.80

The result of Table 9.2 shows the accuracy of the hybrid approach for the total compliance. To (indirectly) assess the accuracy of using Saint-Venant's Principle for the calculation of the combined bending and foundational compliance, the accuracy of the Hertzian compliance calculation is also investigated by finite element analysis, as follows.

In order to verify the FEM contact model procedure, contact between two cylinders was modelled [56]. Half-cylinders were meshed in the model as shown in Figure 9.12(a), the radius of each cylinder being ρ_1 and ρ_2 respectively, i.e. the local radii of curvature of the teeth of gear 1 and 2 at the point of contact. The smart fine meshed rectangular shaped elements were generated near contact areas as shown in Figure 9.12(a). The dimensions of the elements are based on the half-width of the contact area. The mesh near the contact zone needs to be highly refined because of the sensitivity of the geometry. Finer meshing generally leads to a more accurate solution, but requires more time and system resources. The normal contact deflection along the contact surface from the ANSYS solution is presented in Figure 9.12(b). This figure shows the distribution of the contact deflection along the contact area.

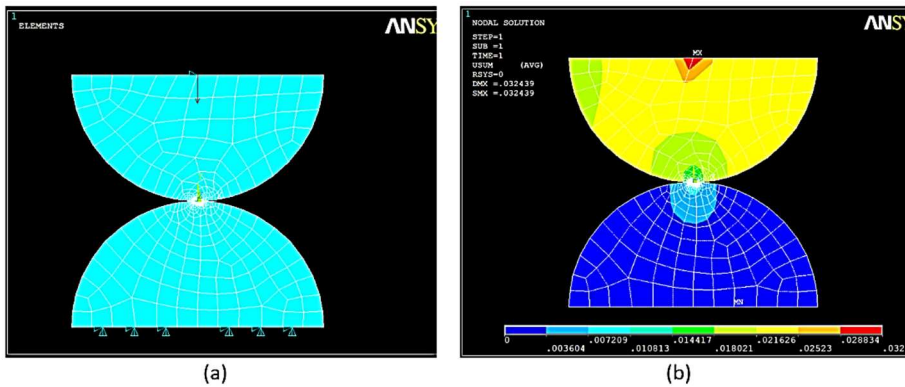


Figure 9.12: (a) adaptive rectangular shaped elements generated near contact areas for two half equivalent cylinders of two mating teeth, (b) Normal contact deflection along the contact surface

The comparison of maximum contact deflection, obtained from Hertz equation and ANSYS 14.5 is given in Table 9.3. With smart fine-meshed model the results are somewhat more accurate, considering the analytical calculation as the benchmark.

Table 9.3: Comparison of accuracy between Hertzian equation (equation (9.22)) and ANSYS results (average area for a single element of adaptivecoarse mesh: 0.162195, average area for a single element of adaptive fine mesh: 0.032439 at contact area)

Analytical deflection (Eq. (9.23))	Numerical deflection (ANSYS)		Deviation percentage (%) (error)
0.024437	adaptive coarse mesh	0.024036	1.64
	adaptive fine mesh	0.024068	1.51

Since the total compliance is the combination of bending and foundational compliance and Hertzian compliance, the bending and foundational compliance

accuracy of the hybrid model can be assessed indirectly from the information in Tables 9.2 and 9.3. The deviations of the full-finite-element model results (for coarse and fine meshes) from the hybrid model are summarised in Table 9.4. The results of Table 9.4 are the subtraction of the results of Table 9.3 from Table 9.2 according to the following relation:

$$C_{B+F+H} - C_H = C_{B+F} \quad (9.24)$$

Table 9.4: Deviations of the full-finite-element model (using coarse and fine mesh) from the hybrid model

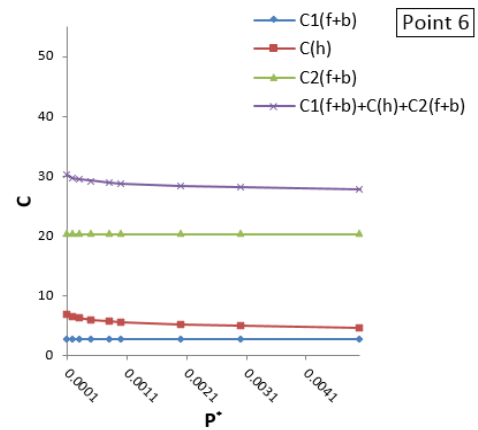
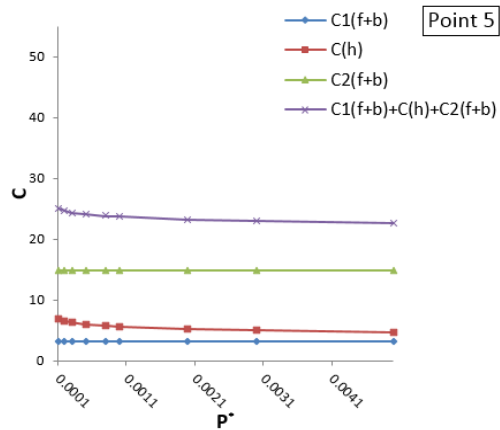
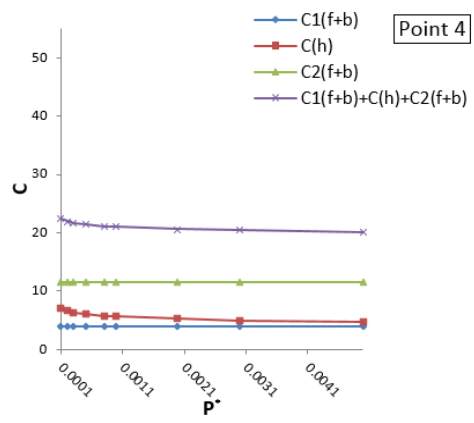
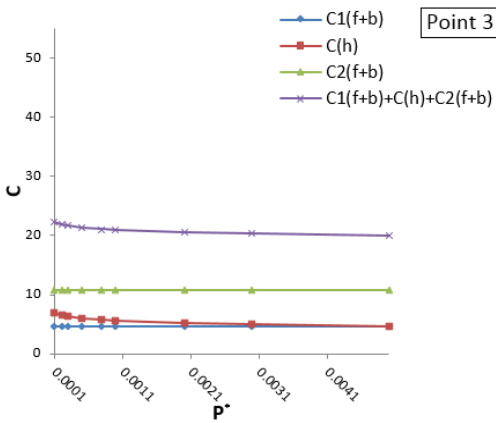
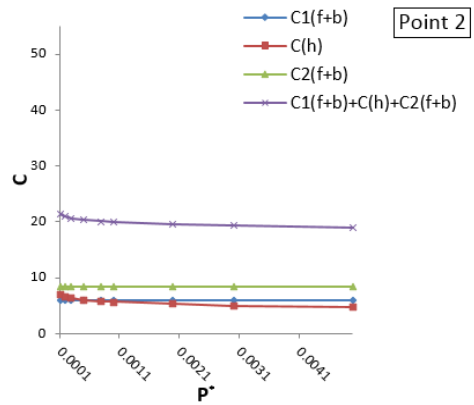
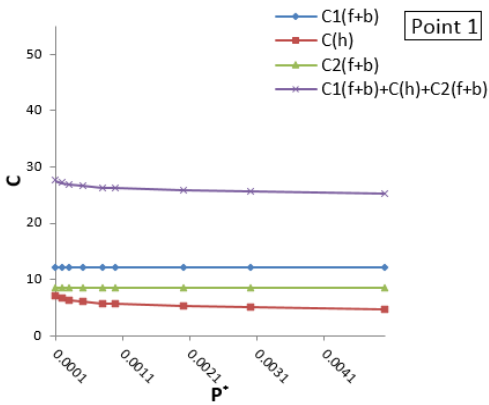
Mesh size	Total compliance deviation (%)	Hertzian compliance deviation (%)	Bending & foundational compliance deviation (%)
coarse	2.63	1.64	3.74
fine	0.8	1.51	0.0046

As can be seen, the hybrid model is quite accurate and potentially more accurate than the finely-meshed full-finite-element model, given that the latter's predictions converge to the former's with increasing mesh density. Notably, the deviation in the calculation of bending & foundational compliance is practically zero for adaptive fine mesh, which further suggests that the use of Saint Venant's principle in the hybrid model produces accurate results.

9.5.2. Influence of Loads on Gear Mesh Compliance

The calculated non-linear influence of load on deflection and therefore compliance is presented in Figures 9.13, 9.14, 9.15 and 9.16.

In particular, the influence of load on non-dimensional compliance has been investigated for one pair of mating teeth considering different gear transmission ratios ($i_{12}=0.5, 1, 2, 4$), obtained by meshing a non-standard gear (gear 1, $N_1=20$) with different amount of cutter tip radius ($c_c= 0.545, 0.515, 0.485, 0.460$) and dedendum coefficient ($c_f=1.0917, 1.1417, 1.1917, 1.2333$) and standard gear (gear 2, $N_2=10, 20, 40, 80$) with $c_c = 0.30, c_f = 1.25$. Figures 9.13, 9.14, 9.15 and 9.16 show that the amount of Hertzian compliance on point 7 as the final point along the line of action has the maximum compliance for a given normal load for different combinations of a gear pair and different amounts of cutter tip radius and dedendum coefficient. Furthermore the total gear mesh compliance is maximum, at point 7. With increasing the number of teeth for the mating gear, the total gear mesh compliance will be increased for point 7.



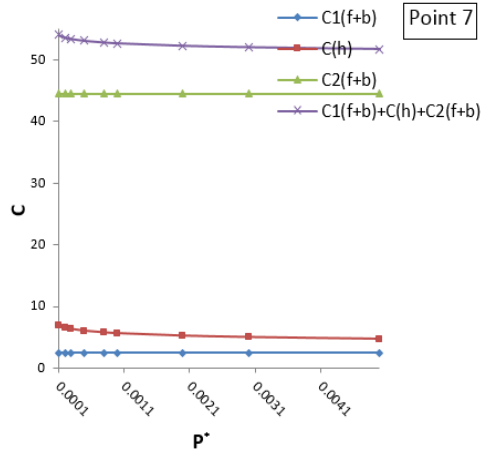
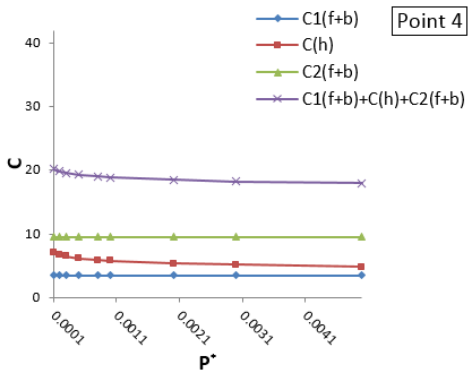
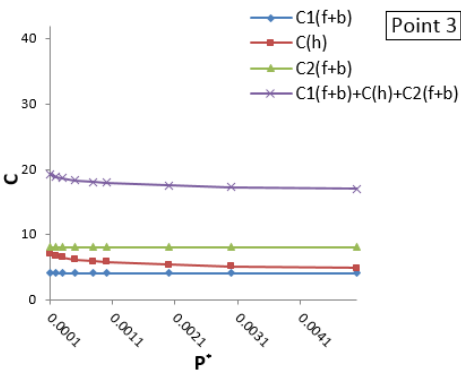
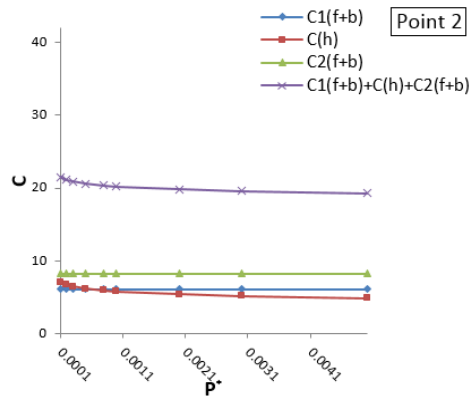
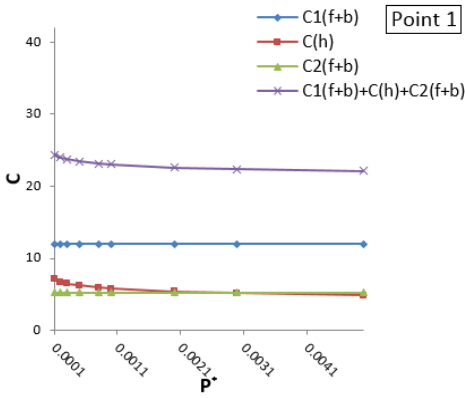


Figure 9.13: Influence of the position of different loads location on the tooth profile along the line of action for calculation of total gear mesh compliance, $N_1=20$, $N_2=10$, $c_f=1.0917$, $c_c=0.545$, (point number refers to Figure 9.4)



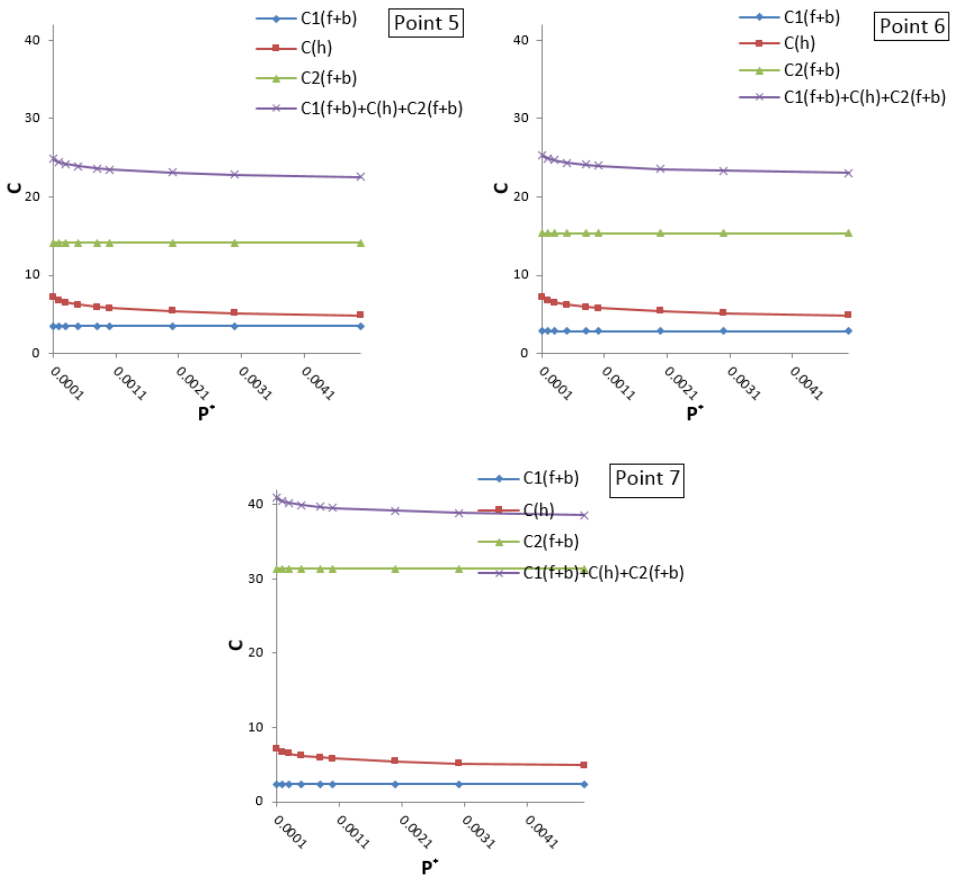
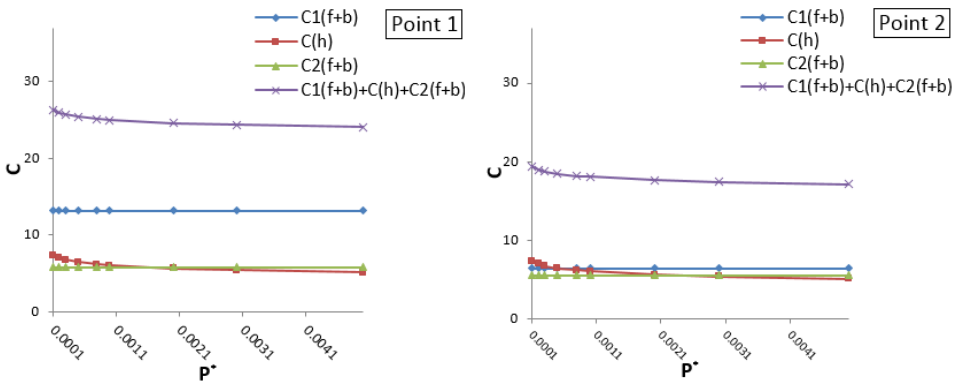


Figure 9.14: Influence of the position of different loads location on the tooth profile along the line of action for calculation of total gear mesh compliance, $N_1=20$, $N_2=20$, $c_f=1.1417$, $c_c=0.515$, (point number refers to Figure 9.4)



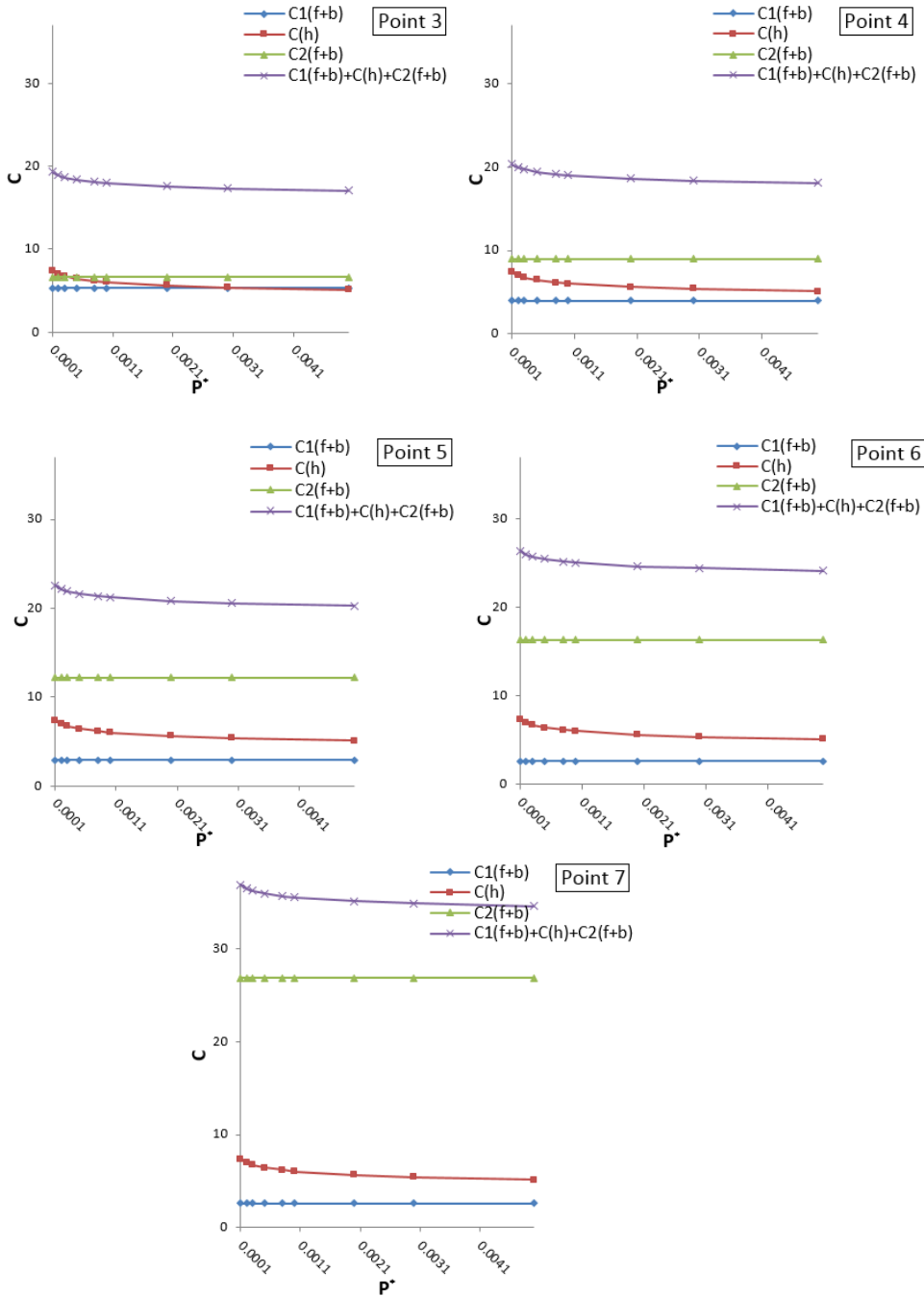
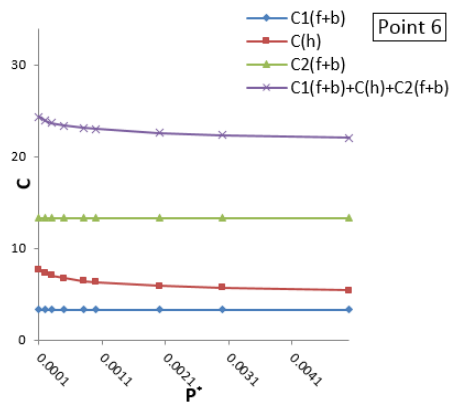
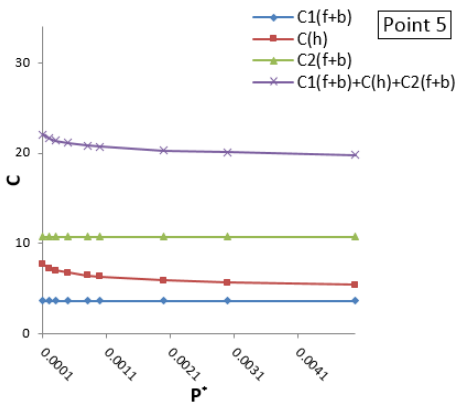
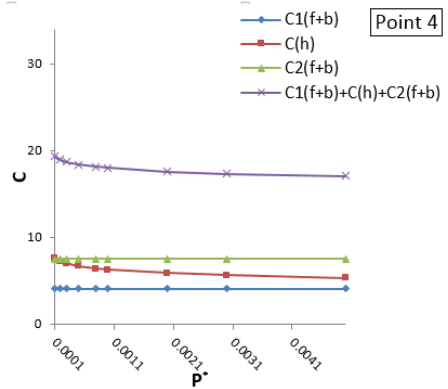
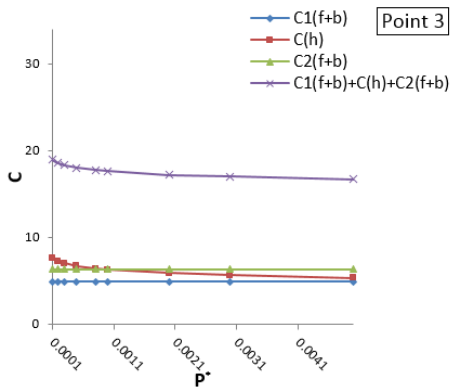
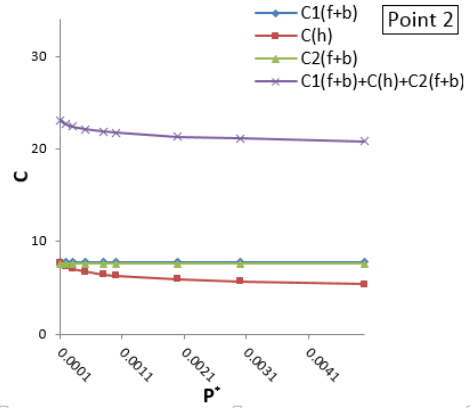
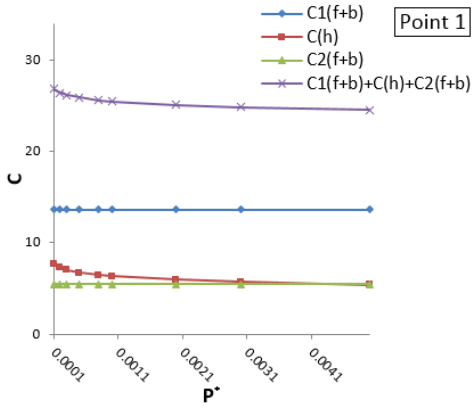


Figure 9.15: Influence of the position of different loads location on the tooth profile along the line of action for calculation of total gear mesh compliance, $N_1=20$, $N_2=40$, $c_f=1.1917$, $c_c=0.485$, (point number refers to Figure 9.4)



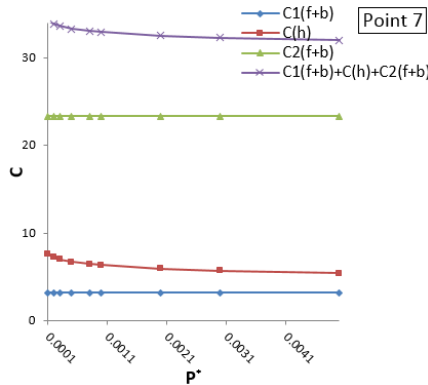


Figure 9.16: Influence of the position of different loads location on the tooth profile along the line of action for calculation of total gear mesh compliance, $N_1=20$, $N_2=80$, $c_f=1.2333$, $c_c=0.460$, (point number refers to Figure 9.4)

Three different combinations for c_c and c_f for different respective combinations of a non-standard gear ($N_1=20$) and a standard gear ($N_2= 10, 20, 40, 80$) were used for the calculation of bending and foundational compliance. The pressure angle is 20° . The coefficient values were picked from across the parametric boundary (family of rising curves) of interference and non-interference area which has been investigated with using the corner contact-and- penetration method (Chapter 4), as presented in Figure 9.17. The area has an upper boundary at the tooth thickness limit line (straight descending line) [29]. The third point of each set is located exactly at the intersection of the parametric interference limit curve and the tooth thickness limit line. The (c_c, c_f) coordinates of the selected points are overlaid on Figure 9.17.

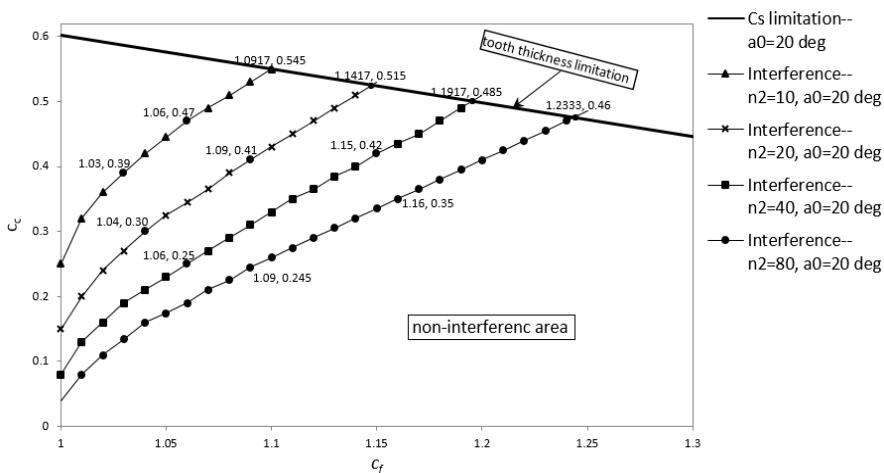


Figure 9.17: Interference limit curves in the three-parametric design space c_{f1} , c_{c1} , N_2 (Chapter 4)

Figure 9.18 presents a comparison between different combinations of cutter tip radius and dedendum coefficient for different combinations of non-standard gear ($N_1=20$) and standard gear ($N_2= 10, 20, 40, 80$) for calculation of bending & foundational compliance.

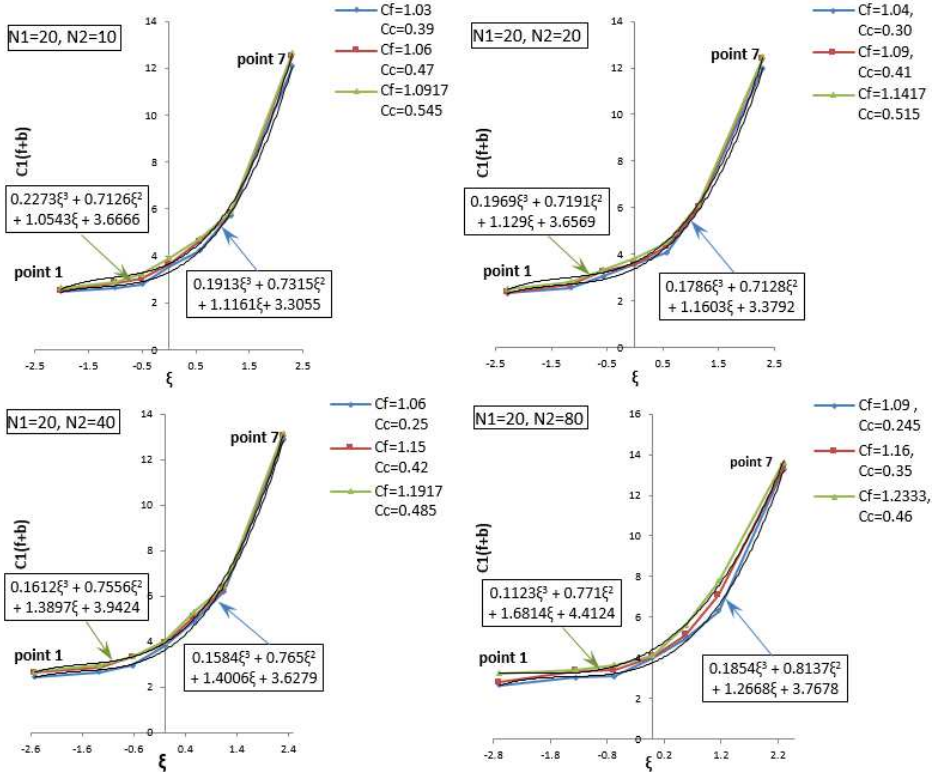


Figure 9.18: Comparison the amount of bending & foundational compliance between different combinations of cutter tip radius and dedendum coefficient for different combinations of gear pair, reference gear ($N_1=20$) in non-standard gear, mating gear ($N_2= 10, 20, 40, 80$) is standard gear with $c_c=0.30, c_f=1.25$ (point number refers to Figure 9.4)

According to the results, it can be found that:

- 1) Points on the interference limit curves are characterised by the same compliance, thus the interference limit curves are the iso-compliance curves;
- 2) With increasing the value of cutter tip radius and dedendum coefficient at the same time, the amount of bending & foundational compliance will be increased; and
- 3) Initial contact point (point 1) on the line of action has minimum and final point (point 7) has maximum value of bending & foundational compliance.

While points 2-3 are well-anticipated from basic principles, point 1 is particularly non-obvious and interesting: Apparently all gear geometries on the same interference limit curve share a mechanical similarity.

9.5.3. Influence of design parameters on gear mesh compliance

In this section, the influences of the design parameters of gear geometry have been investigated. The reference gear (gear 1) is a non-standard gear and gear 2 is a standard gear, both with 20 teeth. The value of non-dimensional force is 1 ($P^* = 1$).

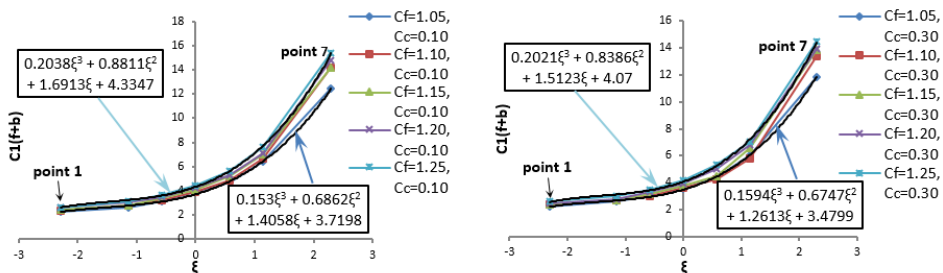
The total compliance of mating tooth pair is calculated through summation of the compliance curves corresponding to the one pair of mating teeth.

As the results shown in Figures 9.19, 9.20, 9.21 and 9.22, it can be concluded that:

- 1) With increasing the value of dedendum coefficient (c_f) with given value of cutter tip radius coefficient (c_c), the bending & foundation compliance will be increased and also the total gear mesh compliance of each point along the line of action will be increased;
- 2) The bending & foundation compliance will be decreased with increasing the value of cutter tip radius coefficient, whereas the value of dedendum coefficient is given; and
- 3) The total gear mesh compliance at pitch point (point 4 in Figure 9.4), where $\xi=0$, has a minimum value compared to all other meshing positions.

It can be concluded that the design parameters pertaining to the gear geometry have a significant influence on gear mesh compliance, which can now be taken systematically into account.

This conclusion gives us this vision that the design parameters of gear geometry play a significant role in gear mesh compliance, which should be taken into account.



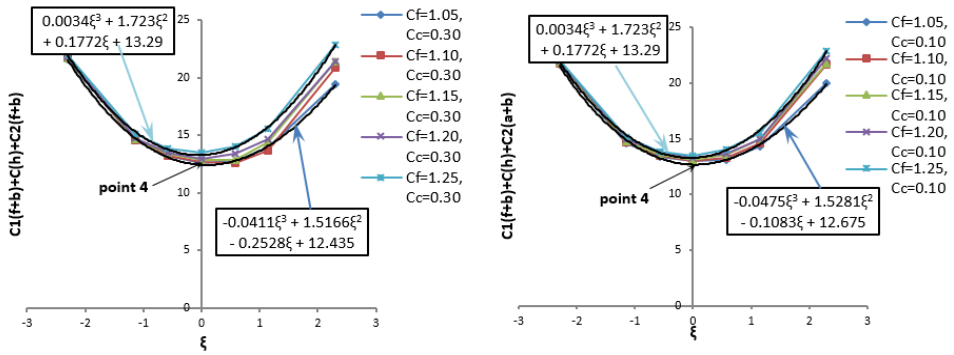
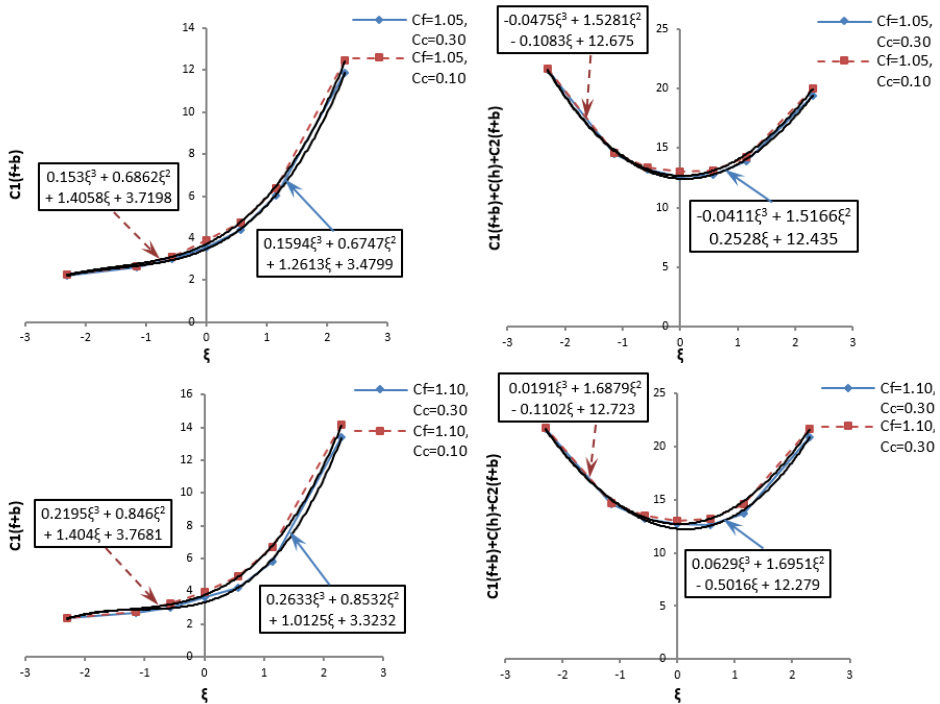


Figure 9.19: Influence of dedendum coefficient on gear mesh compliance ($N_1=20$ nonstandard, $N_2=20$ standard, $P^*=1$) (point number refers to Figure 9.4)



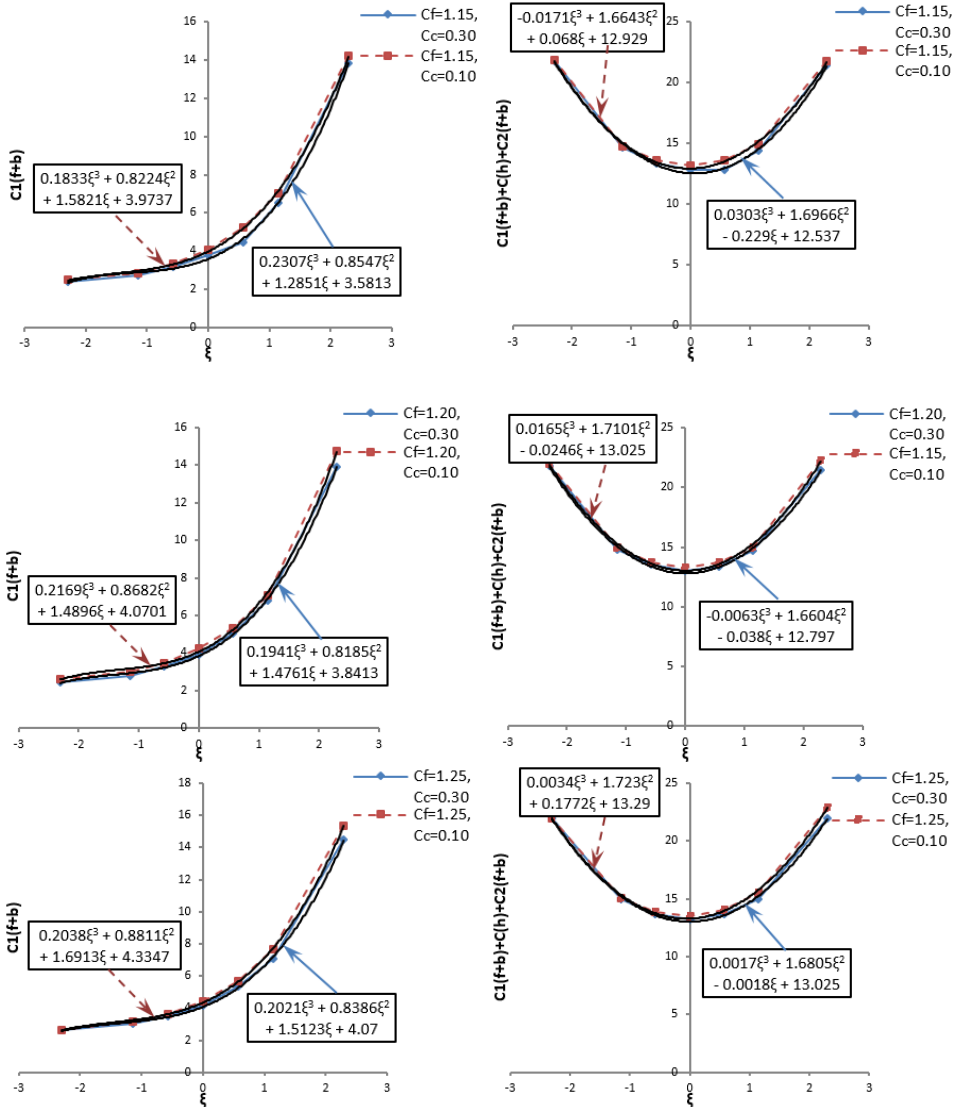
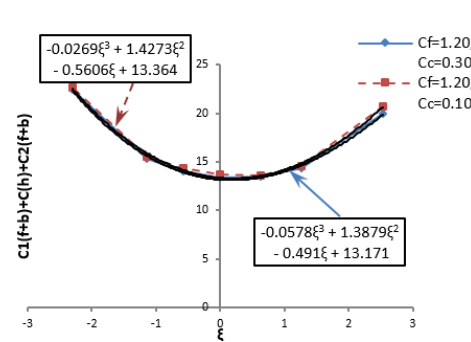
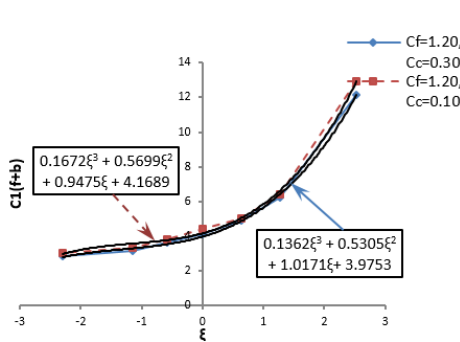
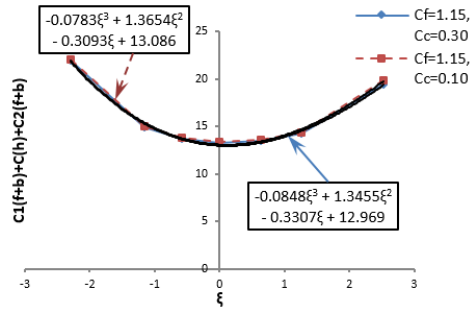
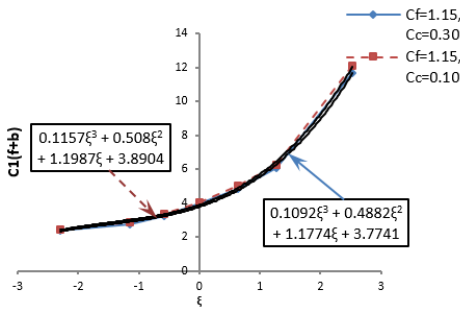
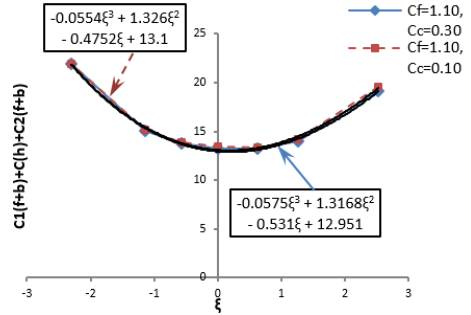
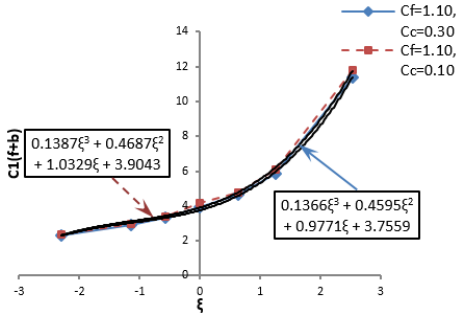
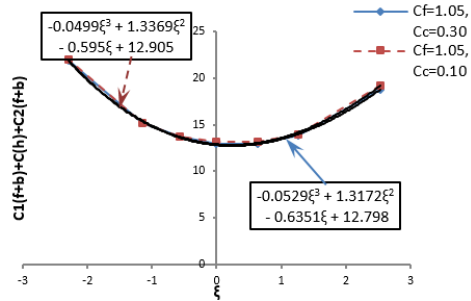
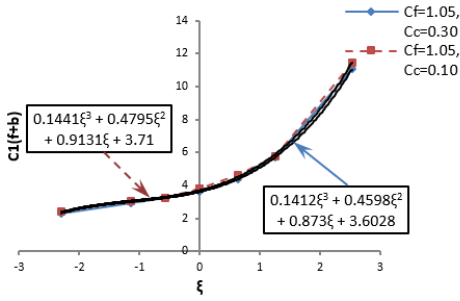


Figure 9.20: Influence of cutter tip radius coefficient on gear mesh compliance ($N_1=20$ nonstandard, $N_2=20$ standard, $P^*=1$)



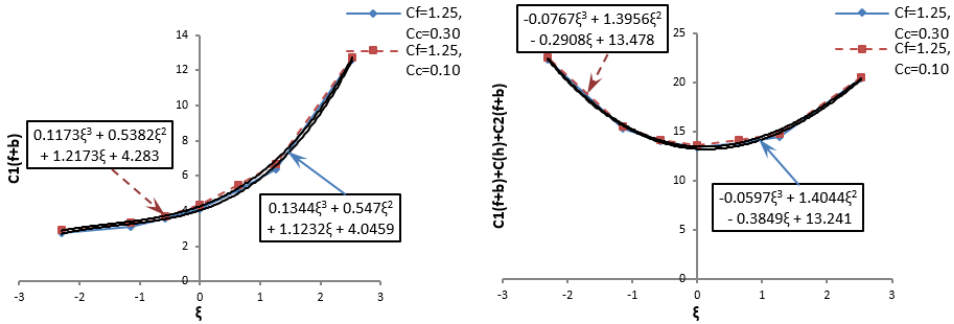
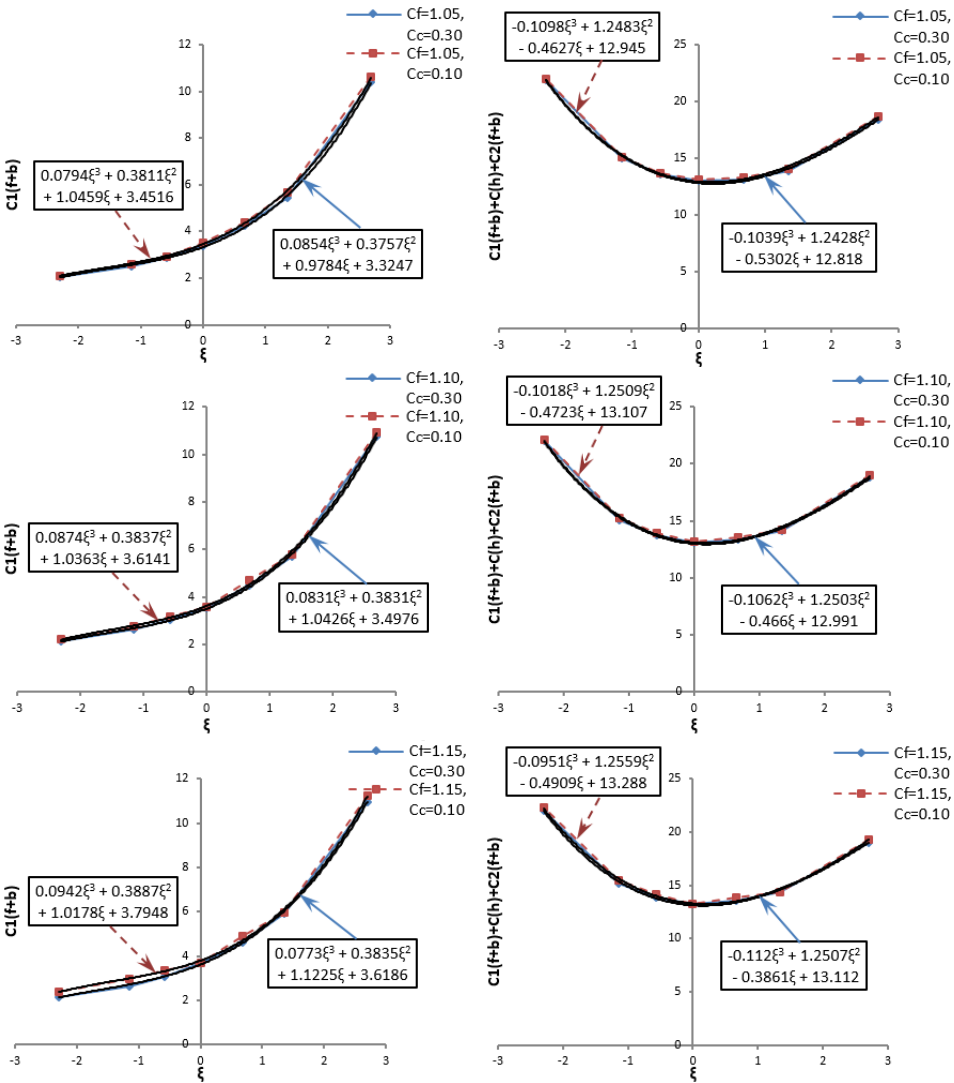


Figure 9.21: Influence of cutter tip radius coefficient on gear mesh compliance ($N_1=20$ nonstandard, $N_2=40$ standard, $P^*=1$)



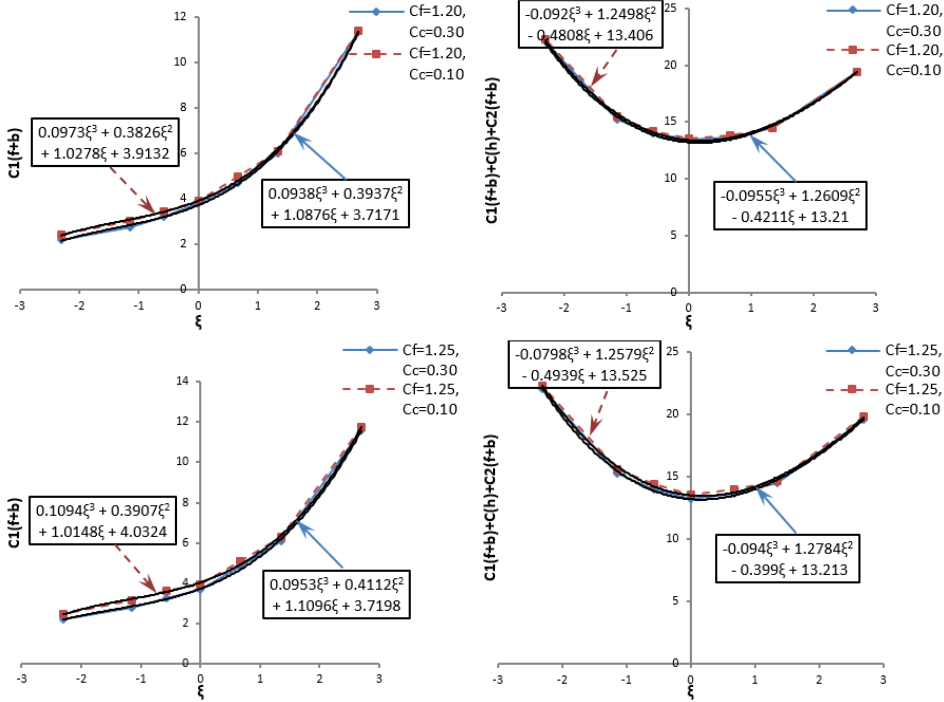


Figure 9.22: Influence of cutter tip radius coefficient on gear mesh compliance ($N_1=20$ nonstandard, $N_2=80$ standard, $P^*=1$)

As Figures 9.19 , 9.20, 9.21 and 9.22 show, there are some clear relationships between the gear mesh compliance (C) function along the line of action, the position of two mating teeth (ξ), design parameters (c_c , c_f) for every combination of different numbers of teeth for a gear pair. The differences are more pronounced at the part of the path of contact corresponding to the positive ξ values; conversely, the compliance values converge at the extreme negative ξ values. Finding the analytical relations between these four parameters is complex and will be the subject of next step.

The results allow us to use a function as the polynomial of degree 3 for compliance as follows:

$$C = \beta_3 \xi^3 + \beta_2 \xi^2 + \beta_1 \xi + \beta_0 \quad (9.25)$$

where β_3 , β_2 , β_1 and β_0 all must be a function of the design parameters which in this case are cutter tip radius coefficient (c_c), dedendum coefficient (c_f) and number of teeth (N).

To find the function of β in equation (9.25) a well-known mathematical methodology called as cubic Hermitian interpolation [46-48, 59-62] on the unit interval will be used.

9.6. CUBIC HERMITIAN INTERPOLATION (CHI)

Computational modelling involves the geometrical consideration of the solution domain [46-48, 59-62]. Linear interpolation functions are the most common choice considering in this respect because of obtainability and theoretical simplicity of tools for generation the functions.

Polynomial interpolation is applied at a discrete set of points or a cloud point to drive feasible values for approximate functions. For interpolation the continuity properties of the data such as convexity, concavity and monotonicity have to be remained. Thus the interpolation has to be presented in terms of algebraic and geometric characters.

Cubic Hermitian interpolation (CHI) presents a strong technique for solving two-point boundary value problems. CHI is a strong and powerful tool for the design of curves. In recent years, cubic hermite spline, especially and its application to shape control have been considered [63-71].

The standard one-dimensional linear Lagrange basis functions are

$$\varphi_1(\xi) = 1 - \xi ; \quad \varphi_2(\xi) = \xi \quad (9.26)$$

Where ξ is a local coordinate on the element (varying from 0 at local point 1 to 1 at local point 2). The linear interpolation formula for this case is

$$\phi(\xi) = \varphi_x(\xi)\phi_x \quad (x = 1, 2) \equiv \varphi_1(\xi)\phi_1 + \varphi_2(\xi)\phi_2 \quad (9.27)$$

Where ϕ_x is the value of ϕ at point x . Such an interpolation preserves continuity between elements, but fails to preserve slope continuity. Extension of this idea to more than one variable is afforded by using a local ξ variable in each direction. In contrast to this, the one-dimensional four Hermitian interpolation basis functions Ψ_x^i in with local coordinate $\xi \in [0,1]$ are [60]:

$$\begin{aligned} \Psi_1^0(\xi) &= 2\xi^3 - 3\xi^2 + 1 \\ \Psi_1^1(\xi) &= \xi^3 - 2\xi^2 + \xi \\ \Psi_2^0(\xi) &= -2\xi^3 + 3\xi^2 \\ \Psi_2^1(\xi) &= \xi^3 - \xi^2 \end{aligned} \quad (9.28)$$

The Hermitian basic function of equation (9.28) is presented in Figure 9.23

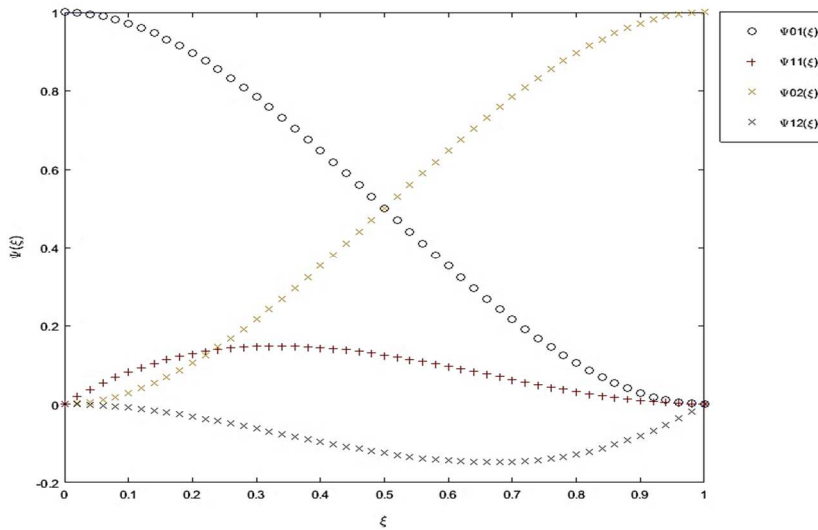


Figure 9.23: Hermitian interpolation basis functions

Where index x indicates to each of the two local points of a 1D element, and index i refers to the kind of continuity the basis is responsible for at that point. Interpolation of an arbitrary field ϕ in a 1D element is given by a linear combination of these four basis functions as follows:

$$\begin{aligned} \phi(\xi) &= \Psi_x^i(\xi)\phi_i^x \quad (i = 0, 1; x = 1, 2) \\ &\equiv \Psi_1^0(\xi)\phi_1 + \Psi_1^1(\xi)\left.\frac{\partial\phi}{\partial\xi}\right|_1 + \Psi_2^0(\xi)\phi_2 + \Psi_2^1(\xi)\left.\frac{\partial\phi}{\partial\xi}\right|_2 \end{aligned} \quad (9.29)$$

Equation (9.29) is an interpolation of ϕ that preserves continuity of function and derivative across element boundaries. Here ϕ_x^x is the value of ϕ at point x and $\phi_{,1}^x = \frac{\partial\phi}{\partial\xi}$ at point x , $x=1, 2$.

A further step is required to apply the cubic Hermitian interpolation in practice. The derivative $\left.\frac{\partial\phi}{\partial\xi}\right|_x$ defined at point x is dependent upon the local element ξ -coordinate.

The cubic Hermite polynomial $p(x)$ has the interpolative properties:

$$\begin{aligned} p(0) &= f(x_0), \quad p(1) = f(x_1) \\ \dot{p}(0) &= \dot{f}(x_0), \quad \dot{p}(1) = \dot{f}(x_1) \end{aligned} \quad (9.30)$$

Where $p(0)$ is the start point of the curve, $\dot{p}(0)$ is the tangent at the start point describing how the curve leaves point, $p(1)$ is the endpoint of the curve and

$\dot{p}(1)$ is the tangent at the endpoint of the curve. Both the function values and their derivatives are known at the endpoints of the interval $[x_0, x_1]$. This situation is illustrated in Figure 9.24.

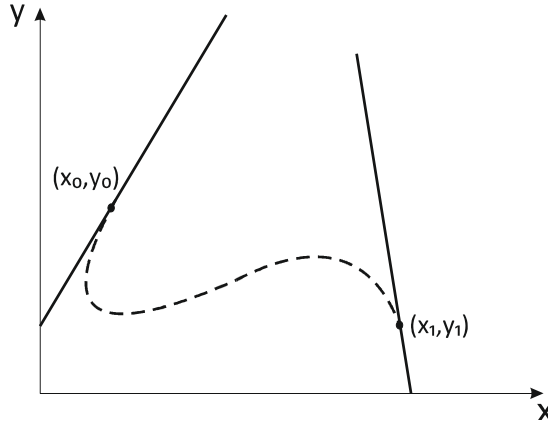


Figure 9.24: Cubic Hermite Polynomial

On the unit interval $(0,1)$, a starting point C_0 at $\xi = 0$ and an ending point C_1 at $\xi=1$ with starting tangent \dot{C}_0 at $\xi=0$ and ending tangent \dot{C}_1 at $\xi=1$, the polynomial can be defined by:

$$C(\xi) = (2\xi^3 - 3\xi^2 + 1)C_0 + (\xi^3 - 2\xi^2 + \xi)\dot{C}_0 + (-2\xi^3 + 3\xi^2)C_1 + (\xi^3 - \xi^2)\dot{C}_1 \quad (9.31)$$

Where $\xi \in [0,1]$ and C_0, C_1, \dot{C}_0 and \dot{C}_1 are kinds of a polynomial function of degree 3 of c_c, c_f and N with the following conditions:

$$\begin{aligned} C_0|_{t=0} &= C_0|_{x_0} \\ \dot{C}_0|_{t=0} &= \dot{C}_0|_{x_0} \\ C_1|_{t=1} &= C_1|_{x_1} \\ \dot{C}_1|_{t=1} &= \dot{C}_1|_{x_1} \end{aligned} \quad (9.32)$$

Where x_0 and x_1 are starting point and ending point on the contact line respectively, that for the different gear transmission ratio ($i_{12}=1, 2, 3$) are not the same.

The results of Cubic Hermitian interpolation for the different gear transmission ratio are presented in Figures 9.25 and 9.26. In all combinations, the first gear is non-standard gear with 20 teeth, and the gear number 2 is a standard gear.

Figure 9.25 presents the sub-functions of each gear transmission ratio and Figure 9.26 is a comparison of each one of the non-dimensionlised sub-function for the different gear transmission ratio ($i_{12}=1,2,3$).

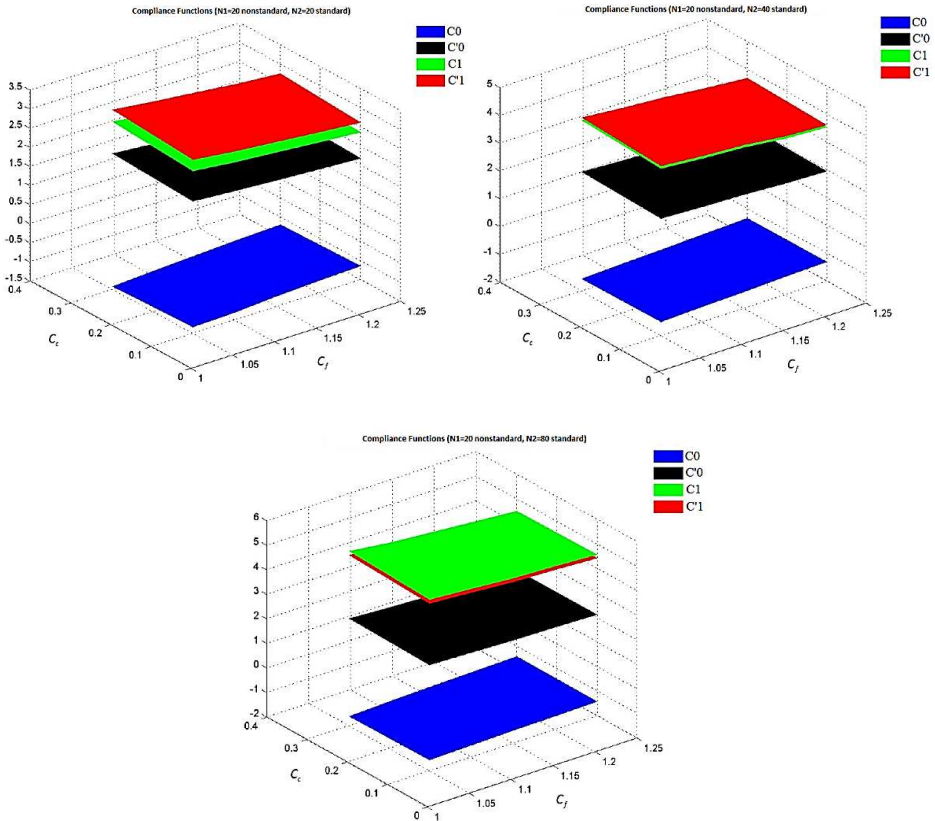
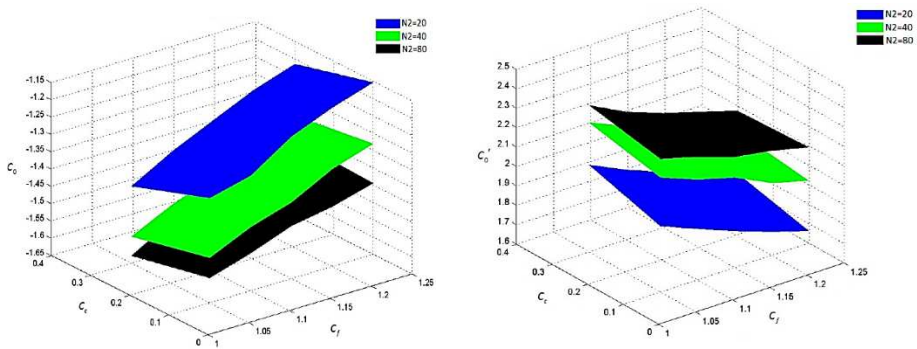


Figure 9.25: Results of Cubic Hermitian interpolation sub-functions of a pair of mating teeth (non-standard and standard gear) with different gear transmission ration ($i_{12}=1, 2, 3$)



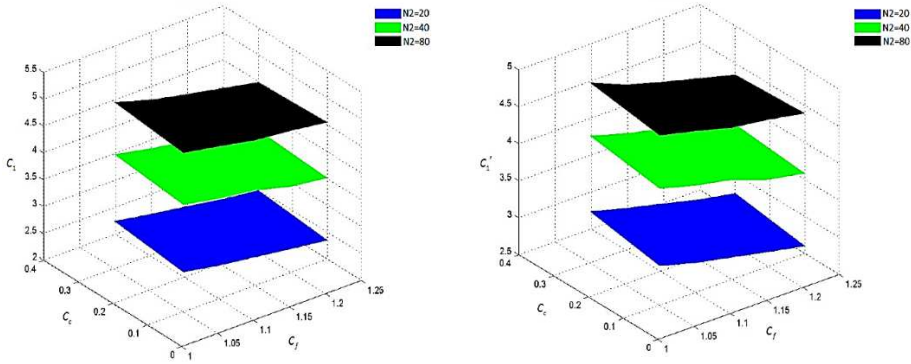


Figure 9.26: Comparison of each sub-function of non-dimensionalised compliance for different gear transmission ratio ($i_{12}=1, 2, 3$) using Cubic Hermitian interpolation

With the result of CHI for the combinations between a non-standard gear with 20 teeth and standard gear with 20 teeth, we will have:

$$\begin{aligned}
 C_0 &= -2.422 - 0.3165c_c + 1.045c_f & (9.33) \\
 \dot{C}_0 &= -3.404 + 0.4807c_c - 1.443c_f \\
 \dot{C}_1 &= 4.753 + 0.6905c_c - 1.996c_f \\
 \dot{C}_1 &= 5.281 + 0.7591c_c - 2.223c_f
 \end{aligned}$$

For the total compliance function for combination between $N_1=20$ (non-standard) and $N_2=20$ (standard) the equation (9.31) can be rewritten as follows:

$$\begin{aligned}
 C(\xi, c_c, c_f) &= (2\xi^3 - 3\xi^2 + 1)(-2.422 - 0.3165c_c + 1.045c_f) & (9.34) \\
 &+ (\xi^3 - 2\xi^2 + \xi)(-3.404 + 0.4807c_c - 1.443c_f) \\
 &+ (-2\xi^3 + 3\xi^2)(4.753 + 0.6905c_c - 1.996c_f) \\
 &+ (\xi^3 - \xi^2)(5.281 + 0.7591c_c - 2.223c_f)
 \end{aligned}$$

And with the combination between $N_1=20$ (non-standard) and $N_2=40$ (standard) with CHS interpolation, we will have:

$$\begin{aligned}
 C_0 &= -2.548 - 0.2204c_c + 0.9962c_f & (9.35) \\
 \dot{C}_0 &= 3.658 + 0.3248c_c - 1.427c_f \\
 C_1 &= 6.613 + 0.6094c_c - 2.556c_f \\
 \dot{C}_1 &= 6.784 + 0.6144c_c - 2.823c_f
 \end{aligned}$$

The compliance function of this combination ($N_1=20$ non-standard and $N_2=40$ standard) whereas $i_{12}=2$ will be as:

$$\begin{aligned}
C(\xi, c_c, c_f) = & (2\xi^3 - 3\xi^2 + 1)(-2.548 - 0.2204c_c + 0.9962c_f) \quad (9.36) \\
& + (\xi^3 - 2\xi^2 + \xi)(3.658 + 0.3248c_c - 1.427c_f) \\
& + (-2\xi^3 + 3\xi^2)(6.613 + 0.6094c_c - 2.556c_f) \\
& + (\xi^3 - \xi^2)(6.784 + 0.6144c_c - 2.823c_f)
\end{aligned}$$

And for mating gear teeth with $i_{12}=3$ ($N_1=20$ non-standard, $N_2=80$ standard), the sub-functions of compliance present as follows:

$$\begin{aligned}
C_0 = & -2.427 - 0.06702c_c + 0.8043c_f \quad (9.37) \\
\dot{C}_0 = & 3.521 + 0.09184c_c - 1.173c_f \\
C_1 = & 7.619 + 0.1875c_c - 2.535c_f \\
\dot{C}_1 = & 7.388 + 0.177c_c - 2.463c_f
\end{aligned}$$

And eventually the compliance as a function of ξ , c_c and c_f for this pair of gear can be rewritten as:

$$\begin{aligned}
C(\xi, c_c, c_f) = & (2\xi^3 - 3\xi^2 + 1)(-2.427 - 0.06702c_c + 0.8043c_f) \quad (9.38) \\
& + (\xi^3 - 2\xi^2 + \xi)(3.521 + 0.09184c_c - 1.173c_f) \\
& + (-2\xi^3 + 3\xi^2)(7.619 + 0.1875c_c - 2.535c_f) \\
& + (\xi^3 - \xi^2)(7.388 + 0.177c_c - 2.463c_f)
\end{aligned}$$

It can be concluded that the different gear transmission ratio of different pairs of mating teeth have own gear mesh compliance function.

Equations (9.34), (9.36) and (9.38), if solved inversely in terms of the design parameters, can provide a powerful inverse solution, which can be used for direct compliance-based design, i.e. to obtain optimised low-vibration powertrains.

Clearly, the same approach can be extended to parametric models of three-dimensional gear configurations, cracked teeth etc geometries admitting suitable parametric descriptions.

9.7. CONCLUSION

In the first part of this work a versatile hybrid analytical-numerical method and non-dimensional modelling framework for accurately calculating gear mesh compliance of arbitrary (including non-standard) tooth geometries has been developed. Finite element analysis has been used for the calculation of bending & foundational compliance simultaneously. Saint-Venant's Principle has been applied to the numerical method to make the calculations accurate and fast, producing a practically zero (0.0046%) deviation compared to much more complex full-finite-element models using smart fine meshes. The calculation of

Hertzian compliance has been accomplished by means of a robust analytical method (Roark's formula for strain due to pressure between elastic bodies) with computational speed than contact-element-based FEA of similar accuracy.

Non-dimensional modelling has been utilised to obtain results for whole multi-parametric gear families, including non-standard tooth proportions, lending wide generality to the results. The influences of different combination of the design parameters i.e. cutter tip radius, dedendum, number of teeth and gear transmission ratio for the calculation of gear mesh compliance have been studied. It has been found that the boundary between interference and non-interference area for different combinations of a gear pair is the iso-compliance curve. The accurate calculation of gear mesh compliance can be used in different aspects of gear design i.e. dynamical simulation and optimisation, vibration reduction, and (quasi-static) load sharing, failure modelling and crack propagation studies.

In the second part, the results of compliance functions have been formulised into a function by means of Cubic Hermitian interpolation. This is a hybrid analytical-numerical function of i) cutter tip radius coefficient, ii) dedendum coefficient, iii) number of teeth and iv) the position of two mating gear teeth on the line of action. The obtained compliance functions can be applied directly to gear dynamical simulations, parametric design and optimisation algorithms etc.

REFERENCE

1. Arafa, M. H., Megahed, M. M., 1999, Evaluation of spur gear mesh compliance using the finite element method, *Proceedings of the Institution of Mechanical Engineers, Part C: Journal of Mechanical Engineering*, 213(6):569-579
2. Lin, J., Parker, R. G., 2001, Mesh stiffness variation instabilities in two-stage gear systems, *Journal of Vibration and Acoustics*, 124(1):68-76
3. Cai, Y., 1995, Simulation on the rotational vibration of helical gears in consideration of the tooth separation phenomenon (A new stiffness function of helical involute tooth pair), *ASME Journal of Mechanical Design*, 117(3):460-469
4. Chen, Y. C., Kang, C. H., Choi, S. T., 2012, Vibration analysis of geared rotor system under time varying mesh stiffness effects, *Journal of Vibroengineering*, 14(3):1141-1150
5. Aida, T., 1969, Fundamental research on gear noise and vibration, *Transaction of the Japanese Society of Mechanical Engineering*, 35:2113-2119
6. Tavakoli, M. S., Houser, D. R., 1986, Optimum profile modifications for the minimization of static transmission errors of spur gears, *Journal of Mechanisms, Transmissions and Automation in Design*, 108(1):86-94

7. Choy, F. K., 1989, Experimental and analytical evaluation of dynamic load and vibration of a 2240-kw (3000-hp) rotorcraft transmission, *Journal of the Franklin Institute*, 326(5):721-735
8. Fonseca, D. J., Shishoo, S., Lim, T. C., Chen, D. S., 2005, A genetic algorithm approach to minimize transmission error of automotive spur gear sets, *Applied Artificial Intelligence: An International Journal*, 19(2):153-179
9. Nevzat Özgüven, H., Houser, D. R., 1988, Mathematical models used in gear dynamics-A review, *Journal of Sound and Vibration*, 121(3):383-411
10. Wei, Z., 2004, Stresses and deformations in involute spur gears by finite element method, *Master Thesis*, University of Saskatchewan.
11. Sainsot, P., Duverger, O., Velex, P., 2004, Contribution of gear body to tooth deflections-a new bidimensional analytical formula, *ASME Journal of Mechanical Design*, 126(4):748-752
12. Fonseca, D. J., Shishoo, S., Lim, T. C., Chen, D. S., 2005, A genetic algorithm approach to minimize transmission error of automotive spur gear sets, *Applied Artificial Intelligence: An International Journal*, 19(2):153-179
13. Chaari, F., Fakhfakh, T., Haddar, M., 2006, Analytical investigation on the effect of gear teeth faults on the dynamic response of a planetary gear set, *Noise & Vibration Worldwide*, 37(8):9-15
14. Chaari, F., Fakhfakh, T., Had, M., 2009, Analytical modelling of spur gear tooth crack and influence on gear mesh stiffness, *European Journal of Mechanics- A/Solids*, 28(3):461-468
15. Meagher, J., Wu, X., Kong, D., Lee, C. H., 2010, A comparison of gear mesh stiffness modelling strategies, *Conference Proceedings of the Society for Experimental Mechanics Series 2010*, 255-263
16. Thirumurugan, R., Muthuveerappan, G., 2010, Maximum fillet stress analysis based on load sharing in normal contact ratio spur gear drives, *Mechanics Based Design of Structures and Machines: An International Journal*, 38(2):204-226
17. Bouchaala, N., Chaari, F., Khabou, M. T., Fakhfakh, T., Haddar, M., 2011, Influence of the non-linear Hertzian stiffness on the dynamics of a spur gear system under transient regime and tooth defects, *International Journal of Vehicle Noise and Vibration*, 7(2):149-177
18. Liu, H., Mao, K., Zhu, C., Chen, S., Xu, X., Liu, M., 2013, *Spur gear lubrication analysis with dynamic loads*, *Tribology Transactions*, 56(1):41-48
19. Chabert, G., Tran, T. D., Mathis, R., 1974, An evaluation of stresses and deflection of spur gear teeth under strain, *Journal of Engineering for Industry*, 96(1):85-93
20. Coy, J. J., Chao, C. H., 1982, A method of selecting grid size to account for Hertz deformation in finite element analysis of spur gears, *ASME Journal of Mechanical Design*, 104(4):759-764
21. Pimsarn, M., Kazerounian, K., 2002, Efficient evaluation of spur gear tooth mesh load using pseudo-interference stiffness estimation method, *Mechanism and Machine Theory*, 37(8):769-786
22. Li, S., Kahraman, A., 2010, A transient mixed elastohydrodynamic lubrication model for spur gear pairs, *Journal of Tribology*, 132(1): 011501

23. Walker, H., 1938, Gear tooth deflection and profile modification: Part I., *The Engineer*, 166:409-412
24. Walker, H., 1938, Gear tooth deflection and profile modification: Part II., *The Engineer*, 166:434-436
25. Steward, J. H., 1990, The compliance of solid, wide-faced spur gears, *ASME Journal of Mechanical Design*, 112(4):590-595
26. Muskhelishvili, N. L., 1975, Some Basic Problems of the Mathematical Theory of Elasticity, second ed., English ed. *P. Noordhoff Limited*, Netherlands
27. Young, W. C., 2002, Budynas, R. G. Roark's Formulas for Stress and Strain, 7th ed., *McGraw-Hill*, New York
28. Spitas, C., Spitas, V., 2007, A FEM study of the bending strength of circular fillet gear teeth compared to trochoidal fillets produced with enlarged cutter tip radius, *Mechanics Based Design of Structures and Machines*, 35(1):59-73
29. Spitas, C., Spitas, V., 2007, Four parametric design study of the bending strength of circular-fillet versus trochoidal-fillet in gear tooth design using BEM, *Mechanics Based Design of Structures and Machines*, 35(2):163-178
30. Osman, T., Velex, P., 2012, A model for the simulation of the interactions between dynamic tooth loads and contact fatigue in spur gears, *Tribology International*, 46(1):84-96
31. Hotait, M., Kahraman, A., 2013, Experiments on the relationship between the dynamic transmission error and the dynamic stress factor of spur gear pairs, *Mechanism and Machine Theory*, 70:116-128
32. Fakhfakh, H., Bruyère, J., Velex, P., Becquerelle, S., 2014, A torsional dynamic model of multi-stage geared systems submitted to internal and external excitations, *International Gear Conference*, Lyon, France, 576-585
33. Ozturk, V. Y., Cigeroglu, E., Özgüven, H. N., 2014, Optimum profile modifications for the minimization of dynamic transmission error, *International Gear Conference*, Lyon, France, 596-605
34. Sankar, S., Nataraj, M., 2011, Profile modification-a design approach for increasing the tooth strength in spur gear, *International Journal of Advanced Manufacturing Technology*, 55(1-4): 1-10
35. Spitas, C., Spitas, V., 2006, Non-linear dynamical simulation of spur gears with indexing errors and profile modifications, *Proceedings of the 25th IASTED International Conference on Modelling, Identification, and Control*, Lanzarote, Canary Islands, 354-359
36. Liou, C.-H., Lin, H. H., Oswald, F. B., Townsend, D. P., 1996, Effect of contact ratio on spur gear dynamic load with no tooth profile modifications, *ASME Journal of Mechanical Design*, 118(3):439-443
37. Bruyère, J., Velex, P., 2014, A simplified multi-objective analysis of optimum profile modifications in spur and helical gears, *Mechanism and Machine Theory*, 80:70-83
38. Özgüven, H. N., 1991, A non-linear mathematical model for dynamic analysis of spur gears including shaft and bearing dynamics, *Journal of Sound and Vibration*, 145(2):239-260
39. Kapelevich, A., Shekhtman, Y., 2008, Tooth fillet profile optimization for gears with symmetric and asymmetric teeth, *AGMA Fall Technical Meeting*, 73-83

40. DIN 3993, 1981, Pt 3 08.81- Geometrical design of cylindrical internal involute gear pairs - Diagrams for the determination of addendum modification coefficients
41. ISO/TR 4467, 1982, Addendum modification of the teeth of cylindrical gears for speed-reducing and speed increasing gear pairs
42. BS ISO 6336-1, 2006, Calculation of load capacity of spur and helical gears. Basic principles, introduction and general influence factors.
43. Costopoulos, Th., Spyropoulou, M., 1994, Tooth compliance and load distribution of spur gears, *Modelling, Measurement & Control B*, 54(4):23-30
44. Spitas, C., Spitas, V., 2008, Effect of cutter pressure angle on the undercutting risk and bending strength of 20° involute pinions cut with equivalent nonstandard cutters, *Mechanics Based Design of Structures and Machines*, 36(2):189-211
45. Spitas, C., Spitas, V., 2006, Generating standard 20° involute pinions with increased fillet strength by using 25° rack cutters with non-standard module, *Proceedings of the Institution of Mechanical Engineers, Part C: Journal of Mechanical Engineering Science*, 220(8):1297-1304
46. Peirce, A., 2010, A Hermite cubic collocation scheme for plane strain hydraulic fractures, *Computer Methods in Applied Mechanics and Engineering*, 199:1949-1962
47. Hyman, J. M., 1983, Accurate monotonicity preserving cubic interpolation, *SIAM Journal on Scientific and Statistical Computing*, 4(4):645-654
48. Duan, Q., Djidjeli, K., Price, W. G., Twizell, E. H., 1999, The approximation properties of some rational cubic splines, *International Journal of Computer Mathematics*, 72(2):155-166
49. Karp, B., Durban, D., 2011, Saint-venant's principle in dynamics of structures, *Applied Mechanics Reviews*, 64(2):20801.
50. D'Apice, C., Chirita, S., 2010, On Saint-Venant's principle for a linear poroelastic material in plane strain, *Journal of Mathematical Analysis and Applications*, 363(2):454-467
51. Knops, R. J., Villaggio, P., 2009, On Saint-Venant's principle for elasto-plastic bodies, *Mathematics and Mechanics of Solids*, 14(7):601-621
52. Babenkova, Ye. V., Kaplunov, Yu. D., Ustinov, Yu. A., 2005, Saint-venant's principle in the case of the low-frequency oscillations of a half-strip, *Journal of Applied Mathematics and Mechanics*, 69(3):405-416
53. Kalashnikov, V. V., Karyakin, M. I., 2006, Second-order effects and Saint Venant's principle in the torsion problem of a nonlinear elastic rod, *Journal of Applied Mechanics and Technical Physics*, 47(6):879-885
54. Chirita, S., 2005, On Saint-Venant's principle for a homogeneous elastic arch-like region, *Journal of Elasticity*, 81(2):115-127
55. Spitas, V., Costopoulos, T., Spitas, C., 2007, Fast modelling of conjugate gear tooth profiles using discrete presentation by involute segments, *Mechanism and Machine Theory*, 42(6):751-762
56. Hassan, A. R., 2009, Contact Stress Analysis of Spur Gear Teeth pair, *World academy of Science, Engineering and Technology*, 34:611-616

57. Zeping, W., 2004, Stresses and deformations in involute spur gears by finite element method, Master thesis, Department of Mechanical Engineering, University of Saskatchewan, Saskatchewan, Canada.
58. ANSYS (2014), Release 14.5, SAS IP, ANSYS Inc. U.S.A.
59. Ganaie, I. A., Kukreja, V. K., 2014, Numerical solution of Burgers' equation by cubic Hermite collocation method, *Applied Mathematics and Computation*, 237:571-581
60. Lamata, P. , Niederer, S., Nordsletten, D., Barber, D. C., Roy, I., Rod Hose, D., Smith, N., 2011, An accurate, fast and robust method to generate patient-specific cubic Hermite meshes, *Medical Image Analysis*, 15:801-813
61. Pullan, A. J., Bradley, C. P., 1996, A coupled cubic hermite finite element boundary element procedure for electrocardiographic problems, *Computational Mechanics*, 18:356-368
62. Sarfraz, M., 1992, Interpolatory rational cubic spline with biased, Point and Interval Tension, *Computers & Graphics*, 16(4):427-430
63. Yousefi, M., Gherjalar, H. -A. D., Arzhang, A., 2011, Numerical solution of the two point boundary value problems by using wavelet bases of Hermite cubic spline wavelets, *Australian Journal of Basic and Applied Sciences*, 5(12):2098-2105
64. Bica, A. M., 2012, Fitting data using optimal Hermite type cubic interpolating splines, *Applied Mathematics Letters*, 25(12):2047-2051
65. Xiang, J., Wang, Y., Jiang, Z., Long, J., Ma, G., 2012, Numerical simulation of plane crack using Hermite cubic spline wavelet, *CMES - Computer Modeling in Engineering and Sciences*, 88(1):1-16
66. Kulkarni, P. G., Sahasrabudhe, A. D., 2014, A dynamic model of ball bearing for simulating localized defects on outer race using cubic hermite spline, *Journal of Mechanical Science and Technology*, 28(9):3433-3442
67. Mohammadzadeh, R., Lakestani, M., Dehghan, M., 2014, Collocation method for the numerical solutions of Lane-Emden type equations using cubic Hermite spline functions, *Mathematical Methods in the Applied Sciences*, 37(9):1303-1317
68. Schneider, A., 2009, Biorthogonal cubic hermite spline multiwavelets on the interval with complementary boundary conditions, *Results in Mathematics*, 53(3-4):407-416
69. Krajnc, M., 2009, Geometric Hermite interpolation by cubic G1 splines, Nonlinear Analysis, Theory, *Methods and Applications*, 70(7):2614-2626
70. Maleknejad, K., Yousefi, M., 2006, Numerical solution of the integral equation of the second kind by using wavelet bases of Hermite cubic splines, *Applied Mathematics and Computation*, 183(1):134-141
71. Zhu, J., Duan, Q., Tian, M., Zhang, Y., 2005, Cubic geometric Hermite interpolation spline with minimum strain energy, *Journal of Information and Computational Science*, 2(3):625-629

10- Conclusion and recommendation

Conclusion of Chapter 3

This work presented a unified multi-parametric model considering design-relevant coupling, that in Chapter 3, a parametric study of the combined effect of whole depth and cutter tip radius on tooth strength and compliance for the 20° involute gear system was presented. Standard 20° spur gears are typically generated with a whole depth of 2.2 to 2.25 times the module. At the nominal centre distance, this leaves a radial clearance, which is in itself redundant from a functional point of view. However, the intrinsic geometry of the cutting process always results in a non-involute root profile (the trochoid), which is even more pronounced in the case of using a rounded cutter tip in order to increase the strength of the cutting edge. Larger tip radii produce stronger tooth fillets, potentially increasing the bending strength, but reducing the involute part of the tooth. Thereby they increase the risk of interference with mating gears. Chapter 3 performed a parametric investigation of the combined effect of the cutter radius and the dedendum on the clearance and the resulting tooth bending strength using analytical calculations, computerised generation and finite element simulations to determine the exact tooth geometry in search of stronger tooth forms. Non-dimensional modelling was used to reduce the number of independent parameters and obtain results applicable to entire gear families.

Conclusion of Chapter 4

In Chapter 4, multi-parametric investigation of interference in non-standard spur gear teeth was studied. Tooth interference, normally avoided altogether by adhering to standard design guidelines, becomes a concern when non-standard tooth forms with reduced radial clearance are employed, such as large-fillet short-dedendum gears. These tooth forms have shorter involute working flanks and excess material at the root, which can lead to non-conjugate corner contact and penetration at the tooth root. Existing models for interference are unable to predict this, or rely on calculation-intensive simulations, which make them impractical for design. This chapter proposed a general and fast mathematical model for calculating corner penetration at the tooth root, which is applicable to both analytically expressed and discretised tooth geometries. Based thereupon a non-dimensional multi-parametric investigation was carried out to quantify the effect of addendum and dedendum length, cutter tip radius, number of teeth and contact ratio on the interference risk. On this basis generalised guidelines were produced for the design of compact nonstandard large fillet short

dedendum 20° involute gears, including a method using standard cutters with indexing offsets. Prior analytical and numerical interference models in the literature were shown to be limited subcases of this model.

Conclusion of Chapter 5

In Chapter 5, the influence of centre distance deviation on the interference of a spur gear pair were performed. Gear design generally considers global geometry like tooth profile shape and centre distance, however, it needs also to consider the tolerances introduced in the manufacturing and assembly of two mating gears. The influence of these tolerances can be predicted better by understanding the behaviour of such manufacturing and assembly errors in conjunction with the gear geometry design process. To address this, in this chapter, the influence of the centre distance deviation and of the design parameters (i.e., cutter tip radius, dedendum, and tooth thickness) of the tooth profiles on interference were investigated. An analytical modelling framework for interference of a gear pair were developed, which were used to characterise a structurally well-defined gear meshing system. The tolerance zone were evaluated, with regard to cutter tip radius, dedendum, tooth thickness and centre distance deviation for a structurally well-defined gear mesh model. Different gear transmission ratio, contact ratio and a pressure angle of 20° have been considered. The results of this chapter can be used as a guideline for the tolerance design of a gear pair.

Conclusion of Chapter 6

In Chapter 6, design of profile-generated involute gears to maximise compactness and bending strength using non-standard equivalent rack dedendum and tip radius were studied. A methodology were developed to design non-standard involute gear geometries generated by cutting tools with standard and non-standard proportions, such as to produce compact tooth meshes by minimising the unused radial clearance, while at the same time avoiding detrimental corner contact at the tooth root. It was shown under which parametric combinations of dedendum and tip radius of the equivalent rack (cutter) the feasible design solutions for different tooth numbers and transmission ratios produce lower tensile bending stresses at the root, thus leading to optimal solutions for compact gears and allowing the identification of a global optimum. The analysis leads to a comprehensive mapping of the four-parametric design space in consideration of interference and undercutting and the discovered optima were compared to the design solutions found in current ISO, AGMA, GOST and JIS standards.

Conclusion of Chapter 7

In Chapter 7, the effect of cutter tip radius coefficient on the maximum root bending stress of spur involute gears with comparative evaluation of different standards were investigated. A parametric investigation of the cutter radius coefficient on the maximum bending stress at the root for spur involute gears were performed. The approach of this chapter were to apply unitary force at the highest point of single tooth contact (HPSTC) and then calculation the stress at the root using FEA. The results of FEM were compared with stresses calculated based on the ISO 6336-Method B. A comprehensive comparison with the popular existing gear standards such as DIN, AGAM, ANSI, JIS and GOST were performed. It was shown under which value of the cutter tip radius, the feasible design solutions for different tooth numbers and transmission ratios produce lower bending stresses at the root, consequently leading to design a stronger gear. The analysis leads to the analytical relation between the cutter tip radius and maximum bending stress at the root as a function of the number of teeth (for gear 1) and gear transmission ratios, which can be used non-standard involute gears as well.

Conclusion of Chapter 8

In Chapter 8, a generalised non-dimensional multi-parametric involute spur gear design model considering manufacturability and geometrical compatibility were performed. An accurate generalised model for various modes of interference present as corner contact-and- penetration (CCP) model were presented in consideration of the module, pressure angle, tooth addendum, dedendum, cutter tip radius, and the numbers of teeth of a pair of mating gears. The effect of the same parameters together with tooth thickness on the manufacturability of the individual gear teeth were also modelled in terms of pointing and undercutting. The study of this chapter serves to provide a complete analytical overview of the multi-parametric design space and is suitable for the fast assessment of existing designs, for implicit or explicit (direct) gear design, and for design optimisation. The model can be used to identify and explore highly promising under-used areas of the parametric design space, which are currently of significant interest to i.e. the automotive and aerospace industries.

Conclusion of Chapter 9

In Chapter 9, a versatile analytical-numerical method for accurate calculation of instantaneous gear mesh compliance in real time were studied. Design of powertrains involving compact, high-power-density and/or high precision gear transmissions need precise computational modelling of dynamics and compliance, over numerous calculation-intensive iterations. Another main concern, with regard to low-vibration systems in particular, is how to tailor the whole stiffness of a gear pair for limiting the amount of vibration in the gear system. However, current analytical/empirical methods for calculating gear

compliance become inaccurate outside of the standard geometries for which they have been derived, whereas numerical, methods rely on complex finite element models, which are very resource intensive in order to be accurate. To address these shortcomings in this chapter, we develop a versatile hybrid analytical-numerical method for accurately calculating gear mesh compliance of arbitrary (including non-standard) tooth geometries. Finite element analysis were used for the calculation of bending & foundational compliance in conjunction with Saint-Venant's Principle, which has been used to allow accurate and fast numerical calculation whereas Hertzian compliance were calculated analytically with high accuracy for curved elastic body contact. The influence of different combinations of cutter tip radius, dedendum, number of teeth and gear transmission ratio on gear mesh compliance has been investigated. Non-linear effects of load have also been considered. The results of this chapter are particularly well-suited for complex iterative tasks, such as dynamical simulation and gear design.

In addition, engineering gear tooth compliance using an interpolated multi-parametric cubic Hermitian function map based on a hybrid analytical-numerical contact mechanics model were presented in this chapter. A versatile non-dimensional model were developed for the fast and accurate calculation of gear mesh compliance in any position along the path of contact. By means of cubic Hermitian interpolation, the results of the hybrid analytical-numerical method have been mapped to a multi-parametric compliance function of the instantaneous position of two mating gears along the line of action and a large array of design parameters. The obtained compliance functions can be applied directly to gear dynamical simulations, parametric design and optimisation algorithms etc. The same functions can also provide powerful inverse solutions, which can be used for direct compliance-based gear design, i.e. to obtain optimised low-vibration powertrains.

Recommendations

Given the main hypothesis that gear design can be optimized by manipulating interference and compliance to produce low-vibration gears allowing to do the dynamical simulation is essential to bring together the whole PhD as meaningful, defendable piece of research that has impact. The following opportunities have been found during the research for further research:

- Programming via numerical analysis software to find directly the multi-parametric design space for the fast assessment of existing designs, for implicit or explicit (direct) gear design, for extracting design guidelines, and for design optimisation.
- Using the comprehensive and consistent meta-model to identify and explore highly promising under-used subspaces of the parametric design space, which

are currently of significant interest to i.e. the automotive and aerospace industries.

- The accurate calculation of gear mesh compliance can be used in different aspects of gear design i.e. dynamical simulation and optimisation, vibration reduction, and (quasi-static) load sharing, failure modelling and crack propagation studies.
- The obtained compliance functions can be applied directly to gear dynamical simulations, parametric design and optimisation algorithms etc.
- Control of high precision compact compliant gear mechanisms using test-rig can be investigated.
- The hybrid analytical-numerical formulation of the gear mesh compliance can be implemented into the vibration equations of the gear system to investigate the behaviour the system dynamic
- Multi-parametric design implementation of ultra-high pressure angle gear transmissions can be analysed.
- Design of high-ratio high-efficiency high-power gear transmission topologies can be studied.

Nomenclature

Symbol	Definition	Symbol	Definition
α_0	pressure angle	$r_b(r_{bi})$	base circle radius (of gear i)
α_{12}	nominal centre distance	$r_o(r_{oi})$	radius of pitch circle (of gear i)
α_c	operating pressure angle	$r_g(r_{gi})$	involute base radius (of gear i)
b	tooth width	$r_f(r_{fi})$	inside radius (of gear i)
$c_c(c_{ci})$	cutter tip radius coefficient (of gear i)	$r_k(r_{ki})$	outside radius
$c_f(c_{fi})$	dedendum coefficient (of gear i)	σ	bending stress at tooth critical cross-section
$c_k(c_{ki})$	addendum coefficient (of gear i)	ε	contact ratio
$c_s(c_{si})$	tooth thickness coefficient (of gear i)	t_b	base pitch (ref. to involute)
$c_m(c_{mi})$	profile shift coefficient (of gear i)	t_R	circular pitch
$c_{sg}(c_{sgi})$	thickness coefficients at the base circles (of gear i)	*	(as subscript) ref. to non-dimensional gear
r_s	form circle radius	i	ref. to gear no. i
\hat{t}	trochoid tip thickness of the generating rack tooth (sharp tooth)	x	addendum modification coefficient
P_N	normal force	N_i	number of teeth (of gear i)
m	module	A_i	point on profile of gear i
$\overline{O_iR}$	vector from centre of gear i to intersection point	$\overline{O_iO_j}$	vector from the centre of gear i to the centre of gear j
$\overline{A_1^{(n)}A_1^{(n+1)}}$	vector from two consecutive points on the tooth profile geometry of the gear number one	$\overline{O_iK_j}$	vector from the centre of gear i to the tip point of gear j
R	intersection point of tooth profiles	O_i	centre of gear i
$\vec{t}_i(r_i)$	tooth flank vector equation of gear no. i	ξ_1	unitary vector of $\overline{A_1^{(n)}A_1^{(n+1)}}$
$i_{1,2}$	gear transmission ratio	ξ_2	unitary vector of $\overline{O_1K_2}$
O	centre of reference coordinate system	K_i	single ref. point at the corner of gear no. i
θ_i	angular position (of gear i)	φ_{si}	angle corresponding to the tooth pitch thickness of gear i
$d\theta_i$	angular velocity (of gear i)	P	tooth load along the line of action
a_{12}	nominal centre distance	L_e	effective length of gear tooth
Δa_{12}	centre distance deviation	δ_B	bending deflection
δ	total deflection	δ_F	foundation deflection
b	tooth width	δ_H	Hertzian deflection
E	modulus of elasticity	ϑ	Poisson's ratio
C	total gear mesh compliance	ρ_i	radii of curvature at the point of contact of gear i
C_B	bending compliance	K_D	equivalent radius of curvature
C_F	foundation compliance	ξ	length along the working line of action from start point of contact
C_H	Hertzian compliance	L	width of rectangular contact area for Hertzian deflection
C_{B+F}	bending & foundation compliance		

List of Figures

Figure 1.1: The layout of the thesis 7

Figure 3.1: Tooth geometry and identification of different functional regions..... 30

Figure 3.2: Analysis of gear cutting at the tooth fillet (gear not shown, only rack cutter tooth shown for clarity) 32

Figure 3.3: Calculation of the maximum cutter tip radius for a given dedendum..... 34

Figure 3.4: Calculated tooth profiles of a 20-tooth pinion for some of the dedendum-cutter tip radius combinations, including maximum tip radius, as calculated by equation (3.10). Notice the shift of the form radius 35

Figure 3.5: Interference simulations a pinion defined by equations (3.4) and (3.11) in mesh with AGMA standard gears 36

Figure 3.6: Two parametric c_c vs. c_f map of gear tooth proportions into the interference space. The “S” numbers stand for different standards..... 38

Figure 3.7: Single-tooth finite element model for $c_f=1.25$, $c_c=0.30$ as per AGMA 201.02, a) Non-dimensional bending stress, b) Detail: Maximum non-dimensional bending stress at the critical section..... 39

Figure 3.8: Topological graph of finite element analysis results for maximum tensile stress at tooth root with different combination of cutter tip radius and dedendum coefficient. The “S” numbers (S1-S9) stand for different standards..... 40

Figure 4.1: Gear tooth (bottom gear) in mesh with generating rack and mating tooth (top gear), showing (a) an assumed noninterfering configuration and (b) an assumed interfering configuration..... 48

Figure 4.2: Model of gear meshing and corner contact and penetration. Right: Detail showing contact discretisation around point **R**..... 54

Figure 4.3: Algorithm for the discrete first order model for detecting corner interference 59

Figure 4.4: Interference limit curves in the three-parametric design space c_{f1}, c_{c1}, N_2 after elimination of parameters N_1, i_{12} 64

Figure 4.5: Interference limit curves as predicted by equation (4.13) (thin straight lines) versus the corner penetration model (thick lines) on the $c_c - c_f$ plane 65

Figure 4.6: Contact simulation showing corner penetration at the tooth root of three reference gears having different numbers of teeth, but otherwise being identical, meshing with the same gear. $N_2=20, N_1=10, 20, 40$	68
Figure 4.7: Contact simulation showing marginal non-interference at the tooth root of three reference gears having different numbers of teeth, but otherwise being identical, meshing with the same gear. $N_2=20, N_1=10, 20, 40$	68
Figure 4.8: Cubic spline approximations of interference limit curves on the $c_f - N_2$ plane	70
Figure 4.9: Cubic spline approximations of interference limit curves on the $N_2 - c_c$ plane	70
Figure 5.1: Qualitative relations between different parameters on the design of tolerance	75
Figure 5.2: The limitation of $c_{c1}-c_{f1}$ combination for different values of tooth thickness (c_{s1}). (c_{s2} assumed to be compatible)	79
Figure 5.3: Influence of centre distance deviation on interference risk for different gear tooth combinations & transmission ratios.....	80
Figure 5.4: Influence of different design parameters on the tolerance zone	81
Figure 6.1: Undercutting limitation of $c_{c1} - c_{f1}$ combination for different number of teeth. The grey area is non-feasible design area	90
Figure 6.2: Maximum non-dimensional root stress corresponding to the corner contact (CCP) limit curve as a function of c_{f1} (left column) or c_{c1} (right column), N_1 and N_2	92
Figure 6.3: Depiction of four-dimensional design space c_{f1}, c_{c1}, N_1, N_2 , showing the locus of feasible designs as bounded by the various interference and undercutting limits, as well as the compact designs that produce the minimal stresses.....	93
Figure 7.1: Determination of the critical section location according to the AGMA standard [13]	106
Figure 7.2: Determination of normal chordal dimensions of tooth root critical section according the ISO standard (ISO 6336-3 Method B) [11].....	106
Figure 7.3: Tooth geometry for stress calculations using modified Heywood formula [40]	107

Figure 7.4: Non-dimensional gear modelling of a single teeth contact, Point B' is the highest point of single tooth contact (HPSTC) for gear 1 [22, 44].....	110
Figure 7.5: The maximum bending stress at tooth root with different amount of cutter tip radius and gear contact ratio.....	113
Figure 7.6: Influence of the number of teeth for gear 1, while the value of cutter tip radius is given	114
Figure 8.1: Pointed tooth model as per Buckingham [3]	131
Figure 8.2: Illustration of tip pointing area design according to the condition of equation (8.10)	133
Figure 8.3: Geometry of gear cutting at the tooth fillet [44]	135
Figure 8.4: Comparison of undercutting phenomena for different theories.....	136
Figure 8.5: Pitch compatibility: pinion-rack (left), pinion-wheel (right) [54, 112]	139
Figure 8.6: Detection of interference and non-interference are for different combination of the design parameters including addendum coefficient of gear 2 (c_{k2}).....	142
Figure 8.7: Tooth profile geometry with different pressure angle	144
Figure 8.8: Influence of pressure angle on manufacturing feasibility with given amount of tooth thickness	148
Figure 8.9: Feasibility of a gear design according to equation (3.10) (relation between c_f , c_c , c_s and α_0)	150
Figure 8.10: Tooth thickness limitation for different combinations of c_c , c_f	151
Figure 8.11: The design subspace corresponding to manufacturability and non-interference for different combinations of the design parameters including N_1 , N_2 , c_{c1} , c_{f1} , and α_0	152
Figure 8.12: Undercutting and non-undercutting design subspaces for different combinations of N_1 , cc , cf , α_0 . The grey subspace corresponds to non-feasible designs	153
Figure 8.13: Form radius limitation for (a) non-undercut and (b) undercut root tooth ($N=20$)	154

Figure 8.14: Calculated non-dimensional form radius for a 20-tooth pinion for the possible combinations of dedendum and cutter tip radius. Useful designs lie between the rightmost (undercutting) and leftmost (interference) extremes.....	155
Figure 8.15: Reducing the five-parametric design space for interference limit curves to the three-parametric design space c_{f1eqv} , c_{c1} , N_2 after elimination of parameters N_1 , i_{12} and c_{k2}	156
Figure 8.16: The relation between equivalent dedendum coefficient (c_{feqv}) and gear contact ratio.....	157
Figure 8.17: Overlay of different limit lines and delineation of feasible and non-feasible design subspaces on the multi-parametric non-dimensional design space (c_c/c_{feqv} , c_c , c_s , N). The limit lines corresponding to different values of α_0 are not shown for clarity	158
Figure 9.1: The relations between compliance of a gear pair and low-vibration system pertinent to the design of high-tech powertrains.....	172
Figure 9.2: Modelling of a gear tooth as a non-uniform cantilever beam on a rigid foundation.....	174
Figure 9.3: Deflection of tooth due to foundation flexibility.....	175
Figure 9.4: Developing isolated points on the line of action for bending & foundation compliance calculation.....	176
Figure 9.5: Penetration at the contact point of gear surface in finite element analysis software	177
Figure 9.6: Implementation of Saint-Venant's principle for a gear tooth in order to calculate bending & foundational compliance	177
Figure 9.7: Calculation of bending & foundational compliance on the correspondent point in the centre line of gear tooth using finite element methods for two different contact positions.....	178
Figure 9.8: Contact of tow mating teeth.....	179
Figure 9.9: Meshing of a gear pair, lower gear is non-standard gear $N_1=20$, $c_{f1}=1.10$, $c_{c1}=0.10$, upper gear is standard gear $N_2=20$, $c_{f2}=1.25$, $c_{c2}=0.25$	183
Figure 9.10: Boundary condition of two mating gears, lower gear is non-standard gear $N_1=20$, $c_{f1}=1.10$, $c_{c1}=0.10$, upper gear is standard gear $N_2=20$, $c_{f2}=1.25$, $c_{c2}=0.25$	184

Figure 9.11: Deformation pattern of a gear pair, lower gear is non-standard gear $N_1=20$, $c_{f1}=1.10$, $c_{c1}=0.10$, upper gear is standard gear $N_2=20$, $c_{f2}=1.25$, $c_{c2}=0.25$ 185

Figure 9.12: (a) adaptive rectangular shaped elements generated near contact areas for two half equivalent cylinders of two mating teeth, (b) Normal contact deflection along the contact surface 186

Figure 9.13: Influence of the position of different loads location on the tooth profile along the line of action for calculation of total gear mesh compliance, $N_1=20$, $N_2=10$, $c_f=1.0917$, $c_c=0.545$, (point number refers to Figure 9.4) 189

Figure 9.14: Influence of the position of different loads location on the tooth profile along the line of action for calculation of total gear mesh compliance, $N_1=20$, $N_2=20$, $c_f=1.1417$, $c_c=0.515$, (point number refers to Figure 9.4) 189

Figure 9.15: Influence of the position of different loads location on the tooth profile along the line of action for calculation of total gear mesh compliance, $N_1=20$, $N_2=40$, $c_f=1.1917$, $c_c=0.485$, (point number refers to Figure 9.4) 191

Figure 9.16: Influence of the position of different loads location on the tooth profile along the line of action for calculation of total gear mesh compliance, $N_1=20$, $N_2=80$, $c_f=1.2333$, $c_c=0.460$, (point number refers to Figure 9.4) 193

Figure 9.17: Interference limit curves in the three-parametric design space c_{f1} , c_{c1} , N_2 (Chapter 3) 193

Figure 9.18: Comparison the amount of bending & foundational compliance between different combinations of cutter tip radius and dedendum coefficient for different combinations of gear pair, reference gear ($N_1=20$) in non-standard gear, mating gear ($N_2= 10, 20, 40, 80$) is standard gear with $c_c=0.30$, $c_f=1.25$ (point number refers to Figure 9.4) 194

Figure 9.19: Influence of dedendum coefficient on gear mesh compliance ($N_1=20$ nonstandard, $N_2=20$ standard, $P^*=1$) (point number refers to Figure 9.4) 196

Figure 9.20: Influence of cutter tip radius coefficient on gear mesh compliance ($N_1=20$ nonstandard, $N_2=20$ standard, $P^*=1$) 197

Figure 9.21: Influence of cutter tip radius coefficient on gear mesh compliance ($N_1=20$ nonstandard, $N_2=40$ standard, $P^*=1$) 199

Figure 9.22: Influence of cutter tip radius coefficient on gear mesh compliance ($N_1=20$ nonstandard, $N_2=80$ standard, $P^*=1$) 200

Figure 9.23: Hermitian interpolation basis functions 202

Figure 9.24: Cubic Hermite Polynomial 203

Figure 9.25: Results of Cubic Hermitian interpolation sub-functions of a pair of mating teeth (non-standard and standard gear) with different gear transmission ration ($i_{12}=1, 2, 3$) 204

Figure 9.26: Comparison of each sub-function of non-dimensionlised compliance for different gear transmission ratio ($i_{12}=1, 2, 3$) using Cubic Hermitian interpolation..... 205

List of Tables

Table 2.1: Summary of literature review	21
Table 3.1: The boundaries of non-interference area.....	37
Table 3.2: Comparison of different standards and optimal design for rack cutter proportions. Stress related to the non-dimensional maximum tensile stress at tooth root	41
Table 4.1: Interference calculations by KISSsoft v03-2011 [5] vs. simulation results for two pinions in mesh ($N_1 = N_2 = 20$, $c_{k1} = c_{k2} = 1.0$, $c_{s1} = c_{s2}$ as per DIN3967 cd25 [12]).....	52
Table 4.2: Design parameters and ranges explored in the study	61
Table 4.3: Gear pair macro-geometries computed in the parametric study, scanning the N_1 - i_{12} space. For clarity the root shape variations due to c_c , c_f are not shown here and nominal values are used ($c_c = 0.30$, $c_f = 1.25$).....	62
Table 4.4: Interference limit curves in the four-parametric design space c_{f1} , c_{c1} , N_1 , i_{12} . Boundaries on the iso- N_2 combinations (same-colour-coded diagonals) are identical. The results in this table correspond 1-1 to the configurations in Table 4.3	63
Table 4.5: Simulated overlays of reference gears (gear 1, bottom) with different numbers of teeth, producing identical interference patterns when meshing with the same gear (gear 2, top).....	67
Table 5.1: Interference limit curves as predicted by equation (4.13) (grey lines) versus the corner contact-and-penetration model (points & black lines) on the $c_{c1} - c_{f1}$ plane...	78
Table 6.1: Design parameters and ranges explored in the study	89
Table 6.2: Maximum root stress obtained by different designs	95
Table 7.1: Comparison of different standards; different cutter tip radius (c_c) and given dedendum ($c_f=1.25$). The addendum coefficients is constant ($c_k=1.0$).....	111
Table 8.1: Comparison of undercutting equations for minimum number of teeth.....	127
Table 8.2: Dependency of the design parameters.....	147
Table 9.1: Design parameters and ranges explored in the study	181

Table 9.2: Comparison of total deflection obtained from hybrid calculation (equation (9.2)) and ANSYS WORKBENCH 14.5, (average area for a single element of adaptive coarse mesh: 0.162195, average area for a single element of adaptive fine mesh: 0.032439 at contact area) 185

Table 9. 3: Comparison of accuracy between Hertzian equation (equation (9.22)) and ANSYS results (average area for a single element of adaptivecoarse mesh: 0.162195, average area for a single element of adaptive fine mesh: 0.032439 at contact area) . 186

Table 9.4: Deviations of the full-finite-element model (using coarse and fine mesh) from the hybrid model..... 187

Curriculum Vitae

Amin Amani was born on the 21st of September 1984 in Amol, Iran. After finishing his high school and a pre-university education at Nemouneh, in 2002, he pursued his undergraduate studies at University of Mazandaran. Focusing on “stress analysis of a cylindrical pressure vessel”, he obtained his B.Sc. in mechanical engineering - solid mechanics.



After completion of B.Sc. in 2006, he started his M.Sc. at Imam Hossein University (IHU), where he developed “design and kinematic-dynamic analysis of a 3DOF parallel platform (Stewart robot) with moving base”. In 2010, he received his M.Sc. in mechanical engineering - applied design with specialization in kinematic of parallel robots.

Subsequent to graduation from IHU, he started to work as a junior research engineer at Marine Research Centre of Imam Hossein University and lecture at Islamic Azad University.

In November 2010, he started his new carrier as lecturer/ Ph.D. researcher at Industrial Design Engineering (IDE) Faculty of Delft University of Technology under the supervision of Prof. dr. ir. Christos Spitas and Prof. dr. ir. Vasilios Spitas. His topic of research was the multi-parametric design of compact high-power low-vibration geared powertrains in consideration of compliance and interference. The results of his Ph.D. research on the “Computationally efficient analysis & design of optimally compact gear pairs and assessment of gear compliance” are presented in this thesis.

List of Publications

Journal Papers (published)

1. Spitas, C., Amani, A., Spitas, V., 2015, A review of emerging computational models for the design of smart structures and powertrains, *Journal of Coupled Systems and Multiscale Dynamics*, 3(4):279-332
2. Amani, A., Spitas, C., Spitas, V., 2015, Influence of centre distance deviation on the interference of a spur gear pair, *International Journal of Powertrains*, 4(4):315-337
3. Spitas, C., Spitas, V., Amani, A., 2015, Multi-parametric investigation of interference in non-standard spur gear teeth, *Mechanism and Machine Theory*, 88:105-124
4. Spitas, C., Spitas, V., Amani, A., Rajabalinejad, M., 2014, Parametric investigation of the combined effect of whole depth and cutter tip radius on tooth strength and compliance for the 20° involute gear system, *Acta Mechanica*, 225(2):361-371

Journal Papers (under review/ in preparation)

5. Amani, A., Spitas, C., Spitas, V., "Generalised non-dimensional multi-parametric involute spur gear design model considering existence and interference", under review, *Mechanism and Machine Theory*
6. Amani, A., Spitas, C., Spitas, V., "A versatile analytical- numerical method for accurate calculation of instantaneous tooth compliance in real time", in preparation for *Mechanism and Machine Theory*
7. Amani, A., Spitas, C., Spitas, V., "Designing gear tooth compliance using a hybrid analytical-Hermitian cubic spline interpolation method: A multi-parametric map of the solution space", in preparation for *Mechanism and Machine Theory*
8. Amani, A., Spitas, C., Spitas, V., "Design of profile-generated involute gears to maximise compactness and bending strength using non-standard equivalent rack dedendum and tip radius", in preparation for *ASME Journal of Mechanical Design*
9. Amani, A., Spitas, C., Spitas, V., "Effect of cutter tip radius coefficient on the maximum bending stress of spur involute gears: comparative evaluation of different standards", in preparation for *ASME Journal of Mechanical Design*

Conference papers

10. Spitas, C., Amani, A., Tsolakis, S., Spitas, V., 2016, Multi-parametric design implementation of ultra-high pressure angle gear transmissions, *3rd Biennial International Conference on Powertrain Modelling and Control (PMC2016)*, Loughborough University, UK
11. Amani, A., Spitas, C., 2014, Computational modelling of compact gear drives in consideration of interference and compliance, *The 10th International Conference of Computational Methods in Sciences and Engineering (ICCMSE 2014)*, Athens, Greece